Application of *in-situ* cosmogenic nuclide analysis to landform evolution in Dartmoor, south-west Britain

Joseph Hunter Hägg

PhD
The University of Edinburgh
2009

I attest that this document has been composed entirely by myself and it represents my own research. It has not been submitted for any other degree or professional qualification.

Joseph Hunter Hägg

Abstract

Located beyond the southern limit of glaciation in Britain, the upland granitic terrain of Dartmoor, south-west England, has been exposed to long intervals of intense periglacial activity during the Pleistocene. This region has been significant in debates about appropriate models of long-term landscape change, most notably two-phase versus single-phase models of landform evolution, and the development of tors. However, given the previous lack of quantitative techniques capable of constraining denudation and specific process rates, and thereby testing developmental models for these features, there remains much uncertainty in the interpretation of the classic landforms of the region. This study measures concentrations of the cosmogenic nuclide ^{10}Be produced in-situ in quartz within the upper few metres of the Earth surface. These reflect the history of near-surface exposure to cosmic radiation of sampled material, and allow for the interpretation of exposure age and/or erosion rates of the land surface. This research utilises these cosmogenic nuclide values to evaluate geomorphological processes and investigate key aspects of landform development. These include the formation of tors in non-glaciated regions, the development of regolith and boulderfields under periglacial conditions, and the derivation of catchment-averaged denudation rates. This study provides the first quantitative measurement of erosion on tor surfaces in Dartmoor, with typical rates of 14-45 mm ka^{-1}. These are relatively high and comparable to other components of the landscape. In addition, there is no clear relationship of cosmogenic nuclide concentration to tor dimensions. It is shown that the tors are dynamic landforms and simple, two-stage development is an inappropriate model. Catchment-averaged denudation rates are derived and these long-term rates of 20-94 mm ka^{-1} are significantly higher than modern, short-term values. Finally, downslope transport in a palaeo-periglacial blockslope is investigated using ^{10}Be concentrations. This variety of landforms and scale of investigation facilitates an integrated approach to the understanding of catchment-scale erosional dynamics. In addition, the complex nature of landform development that is evident in the area provides challenges to the application of in-situ cosmogenic nuclides and highlights both the potential and limitations of the technique.

Acknowledgements

I would like to thank Mike Summerfield, for supervision of this research, and his patience and encouragement during the arduous task of compiling this thesis. I would also like to thank Cristoph Schnabel and Bill Phillips for their guidance in aspects of this research. Steve Binnie provided absolutely vital assistance, and taught me most of what I know about lab work. I'd also like to thank Elaine McDougall, who had the lab running smoothly when my research needed it most. Cosmogenic nuclide research relies on the AMS facility, and I was fortunate to not only be provided with excellent access, but to have a friendly and patient assistance of the SUERC team, especially Stewart Freeman, Colin Maden and Sheng Xu. Permission to conduct field work in Dartmoor was kindly granted by the Dartmoor National Park Authority, English Nature, the Duchy of Cornwall, and the Ministry of Defence, for whom Lt. Col. Tony Clarke was a most approachable and enthusiastic liaison. I am also indebted to those who helped in the field, braving the hardships of rural Devonshire, thank you to Jon Butler, Nick Cutler, Iain Cameron, Dan Burton, and Kate Dunlop. I'd also like to acknowledge, the too many to name, who made my time in Edinburgh so memorable. But especially my great friends Neelu Sarkar and Trina Clarke, who (hopefully) printed this from afar. My family were always supportive, even from the other side of the world. And finally, to Angela, whose love, persistence and endless patience got me through this ordeal in the end.

I was supported in this research by a Top Achiever Doctoral Scholarship, from the Tertiary Education Commission (TEC), New Zealand. Funding for research was kindly granted by the School of Geosciences and a SUERC AMS analysis grant.

Table of Contents

1: Introduction 1
- 1.1 Research Overview 1
- 1.2 The Pleistocene Climate of Dartmoor 2
- 1.3 Geology of Dartmoor 2
- 1.4 Previous Research on Dartmoor 5
- 1.5 Thesis Organisation 7
- 1.6 Notes on Terminology 8

2: Cosmogenic Nuclide Production Systematics and Analysis 9
- 2.1 Introduction 9
- 2.2 Spatial and Temporal Variability of Cosmic Radiation 9
  - 2.2.1 Modulation and Attenuation of Cosmic Radiation 10
  - 2.2.2 Spatial Scaling Factors for Cosmogenic Nuclide Production Rates 11
  - 2.2.3 Geometric Shielding of a Surface 14
    - 2.2.3.1 Shielding by Topographic Obstruction 15
    - 2.2.3.2 Shielding of a Sloping Surface 15
    - 2.2.3.3 Shape Effects 17
- 2.3 In Situ Production of Cosmogenic Nuclides 18
  - 2.3.1 Spallation 18
  - 2.3.2 Muonic Production 19
  - 2.3.3 Overview – Cosmogenic Nuclide Production 19
  - 2.3.4 Correction for Sample Thickness 20
- 2.4 Exposure Age and Erosion Rate Models 21
  - 2.4.1 Exposure Age Model 22
  - 2.4.2 Erosion Rate Model 23
    - 2.4.2.1 Contribution from Muons 25
    - 2.4.2.2 Averaging Time Scales 25
    - 2.4.2.3 Episodic Erosion 27
    - 2.4.2.4 Mixed Soil/Regolith Profiles 31
    - 2.4.3 Catchment-Averaged Denudation Rates 32
- 2.5 Cosmogenic Nuclide Sample Analysis and Calculations 35
  - 2.5.1 ^{10}Be Target Preparation 35
  - 2.5.2 Accelerator Mass Spectrometry 37
  - 2.5.3 Calculation of 10Be Concentration 38
  - 2.5.4 Exposure Age and Erosion Rate Calculations 39
    - 2.5.4.1 Input to the Calculator 39
    - 2.5.4.2 Calculations in the Program 42
    - 2.5.4.3 Output from the Calculator 43
- 2.6 Conclusion 43

3: The Formation of Tors 45
- 3.1 Introduction 45
- 3.2 Geomorphological Context 46

3.2.1 Dartmoor Tors....46
3.2.2 Two-Stage Development....52
3.2.3 Single-Phase / Dynamic Model of Development....57
3.3 Research Strategy....63
3.3.1 Overview of Study Sites....63
3.3.2 Interpretation of 10Be Concentration....64
3.3.2.1 Exposure Age for Tor Surfaces....65
3.3.2.2 Tor Surface Erosion Rates....68
3.3.2.3 Regolith Erosion Rates....70
3.4 High Willhays....72
3.4.1 Study Site....72
3.4.2 Regolith at High Willhays....72
3.4.2.1 Observations of the Summit....74
3.4.2.2 Sub-surface Excavations....74
3.4.2.3 Regolith Characteristics....74
3.4.3 Tors at High Willhays....80
3.4.3.1 High Willhays Tor Group....80
3.4.3.2 Tor HW1....81
3.4.3.3 Tor HW2....81
3.4.3.4 Tor HW5....85
3.4.3.5 Summary....86
3.4.4 Cosmogenic Nuclide Results....90
3.4.4.1 Regolith & Bedrock Surfaces....91
3.4.4.2 Tors....94
3.5 Great Links Tor....98
3.5.1 Study Site....98
3.5.1.1 Tor GLT1....100
3.5.1.2 Tor GLT2....100
3.5.1.3 Tor GLT3....100
3.5.1.4 Tor GLT4....107
3.5.1.5 Tor GLT5....107
3.5.2 Cosmogenic Nuclide Results....107
3.6 Other Tors in West Okement Valley....110
3.6.1 Black Tor....112
3.6.2 Lints Tor....116
3.6.3 Dinger Tor....121
3.6.4 Steng-a-Tor....124
3.6.5 Summary....126
3.7 Discussion....126
3.7.1 Erosion of Tor Surfaces....126
3.7.1.1 Granular Disintegration....127
3.7.1.2 Episodic Block Removal....131
3.7.1.3 Cosmogenic Nuclide Erosion Rates....134
3.7.2 Emergence of Tor Landforms....137
3.7.3 Implications for Landscape Development....141
3.8 Conclusion....142

4: The Development of Blockslopes 144
4.1 Introduction 144
4.2 Geomorphological Context 144
4.2.1 Blockslope Terminology 144
4.2.2 Dartmoor Blockslopes 145
4.2.3 Development of Blockslopes 147
4.3 Research Design 149
4.3.1 Study Objectives 149
4.3.2 Study Site - Yes Tor Blockslope 152
4.3.3 Sample Collection 153
4.4 Results 153
4.4.1 Measured 10Be Concentrations 153
4.4.2 Block Exposure to Cosmic Radiation 154
4.4.2.1 Exposure Age Model 154
4.4.2.2 Block Origin – Nuclide Inheritance 155
4.4.2.3 Exposure in the Surface Layer 157
4.4.2.4 Block Geometry 157
4.4.2.5 Block Erosion 158
4.4.2.6 Summary 159
4.4.3 Yes Tor Blockslope Exposure Ages 159
4.5 Discussion 161
4.5.1 Timescale of Blockslope Development 161
4.5.2 Downslope Block Transportation 163
4.5.3 Implications for Landscape Evolution 166
4.5.4 Limitations of Study 168
4.6 Conclusions 169

5: Spatially-Averaged Denudation in the Dartmoor Landscape 170
5.1 Introduction 170
5.2 The Dartmoor Landscape 171
5.3 Research Strategy 180
5.3.1 Sampling Strategy 180
5.3.2 Sample Collection 182
5.3.3 Interpretation of 10Be concentration 182
5.4 River Dart and Sub-Catchments 185
5.4.1 Study Catchments 186
5.4.1.1 East Dart River (ED01) 186
5.4.1.2 West Dart River (WD01) 186
5.4.1.3 Two Bridges (TB01) 187
5.4.1.4 Upper Cherry Brook (UCB01) 189
5.4.1.5 Foxton Mires (SM01) 189
5.4.2 Cosmogenic Nuclide Results 191
5.4.3 Summary 193
5.5 River Walkham and East Okement River 193
5.5.1 Study Catchments 193
5.5.1.1 River Walkham (WB01) 193
5.5.1.2 East Okement River (EO01) 195

5.5.2 Cosmogenic Nuclide Results 197
5.6 West Okement River 198
5.6.1 West Okement River Catchment 198
5.6.2 Cosmogenic Nuclide Results 204
5.6.2.1 M0/M1 204
5.6.2.2 M2/M3 206
5.6.2.3 M5 209
5.6.3 Summary 209
5.7 Discussion 212
5.7.1 Validity of Catchment-Averaged Denudation Rates 212
5.7.2 Interpreting Denudation of the Dartmoor Landscape 217
5.7.2.1 Variability of Denudation Rates 217
5.7.2.2 Comparison of Catchment Denudation Rates 218
5.7.2.3 Changes In Denudation Rate Over Time 220
5.7.2.4 The Denudation of Dartmoor in a Global Context 212
5.8 Conclusion 224

6: Implications for Landscape Evolution in Dartmoor 225
6.1 Introduction 225
6.2 The Weathering of Granite 225
6.3 Periglacial Hillslope and Landform Development 227
6.4 Evaluating Potential Glaciation of Dartmoor 230
6.5 Conclusion 232

7: Conclusion 233

References 239
Appendix I 251
Appendix II 258
Appendix III 262

1: Introduction

1.1 Research Overview

Located beyond the southern limit of glaciation in Britain, the upland granitic terrain of Dartmoor, south-west England, has been exposed to long intervals of intense periglacial activity during the Pleistocene. The region has been significant in debates about the long-term development of landscape, most notably with the contribution of a seminal paper on two-stage landform development (Linton, 1955) and the counter-argument that favoured a single-phase of periglacial weathering (Palmer & Neilson, 1962). This spurred ongoing research into the origins of widespread *in situ* altered granite (e.g. Eden & Green, 1971; Doornkamp, 1974; and Dearman & Baynes, 1978), the development of periglacial landforms (e.g. Waters, 1964; Green & Eden, 1973; Gerrard, 1988), and the role of joint structure in tor formation and landscape evolution (Gerrard, 1978; and Ehlen, 1991; 1992). However, there have been no methods available to provide age constraints on the development of landforms, or with which to assess long-term rates of landscape denudation. Without these, the development of the landscape remains open to interpretation, and there is no way to resolve the many outstanding issues relating to the Dartmoor landscape.

By measuring the concentration of ^{10}Be produced *in situ* in quartz minerals, it is possible to determine residence time within the upper few metres of the Earth's surface. The development of the cosmogenic nuclide approach has allowed for the calculation of exposure age or denudation rate of rock surfaces (or even landscapes) and has opened up a diverse range of geomorphological applications (Cockburn & Summerfield, 2004). This research utilises the measurement of ^{10}Be concentrations to evaluate three key aspects of the Dartmoor landscape: (1) the formation of tors, the subject of an ongoing and unresolved debate; (2) the development and timescale of blockslopes, a widespread periglacial landform; and (3) the calculation of spatially-averaged denudation rates from alluvial sediments, which allows for an assessment of long-term landscape denudation. These results provide a first quantitative measurement of the rates at which landforms develop in Dartmoor, and in doing so, they allow for a reassessment of fundamental models of its landscape evolution.

1.2 The Pleistocene Climate of Dartmoor

The present day climate of Dartmoor is cool and wet; with prevailing south-westerly winds, a strong Atlantic maritime influence, and annual rainfall of ~1900 mm (Williams *et al.*, 1986). During the Devensian (last) glacial maximum, mean annual air temperatures were depressed by as much as 25°C, while July temperatures were up to 10°C lower than present (Watson, 1977). This lead to the development of discontinuous permafrost across south-west England, although the severity of conditions was moderated by snow cover and the continued maritime influence (Williams, 1975; Watson, 1977; Gerrard, 1988). The Dartmoor uplands were exposed to intense cold conditions in the region, leading to the development of widespread periglacial landforms, such as blockslopes, hummocky ground, frost wedges, and altiplanation terraces (e.g. Te Punga, 1957; Waters, 1964; Gerrard, 1988). It has generally been argued that south-west England remained beyond the limit of glaciation during the Quaternary (Figure 1.1), with a permanent snow-line estimated some 30 m above the highest summits in Dartmoor (Gerrard, 1988). The geomorphological evidence given for glaciation on Dartmoor can often be better explained by other processes (Gerrard, 1988), although there continues to be an speculation on some form of glaciation on Dartmoor (Harrison, 2001). As the region is (at best) marginal for glacier formation, many of the distinctive forms normally associated with glaciation are not present, and interpretation remains equivocal.

1.3 Geology of Dartmoor

The Cornubian Batholith underlies south-west England extending from Dartmoor to the Isles of Scilly and some 100 miles beyond. It is exposed in five major mainland plutons at Dartmoor, Bodmin Moor, St Austell, Carnmenellis, and Land's End (Figure 1.2; LeBoutllier, 2002). The batholith is a granitic intrusion related to a large-scale tectonic episode during the Variscan or Hercynian Orogeny (Campbell *et al.*, 1998). The intrusion of the granite into the surrounding Devonian and Carboniferous 'country' rock has led to this becoming folded, faulted and metamorphosed to varying degrees within 1-3 km of the pluton (Campbell *et al.*, 1998). Following the emplacement of the batholith, the denudation of surrounding

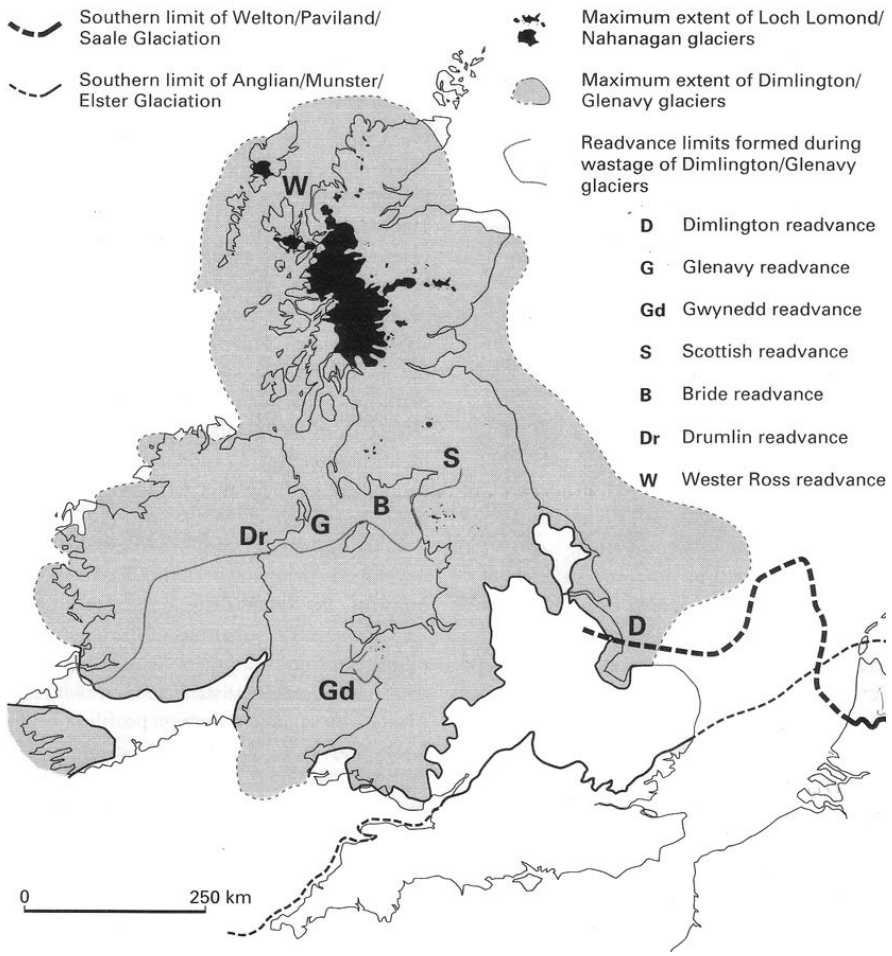

Figure 1.1 Limits of glaciation in Britain and Ireland during the Devensian (the last) and Anglian (maximum extent) glacial stages. Source: Lowe & Walker (1997); after Bowen *et al.* (1986)

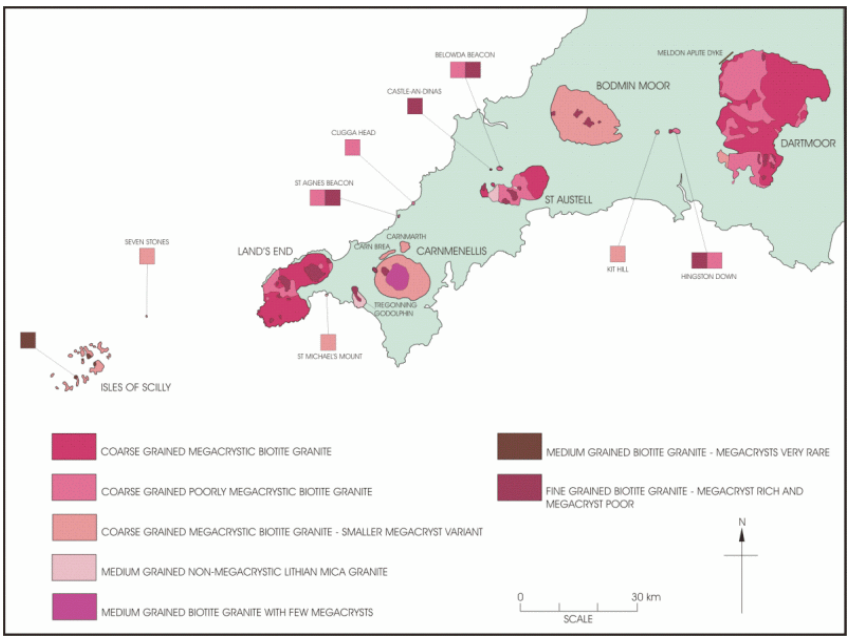

Figure 1.2 Exposures of the Cornubian Batholigh across south-west England; with the distribution of granite types.

Source: LeBoutllier (2002); after Hawkes *et al.* (1987)

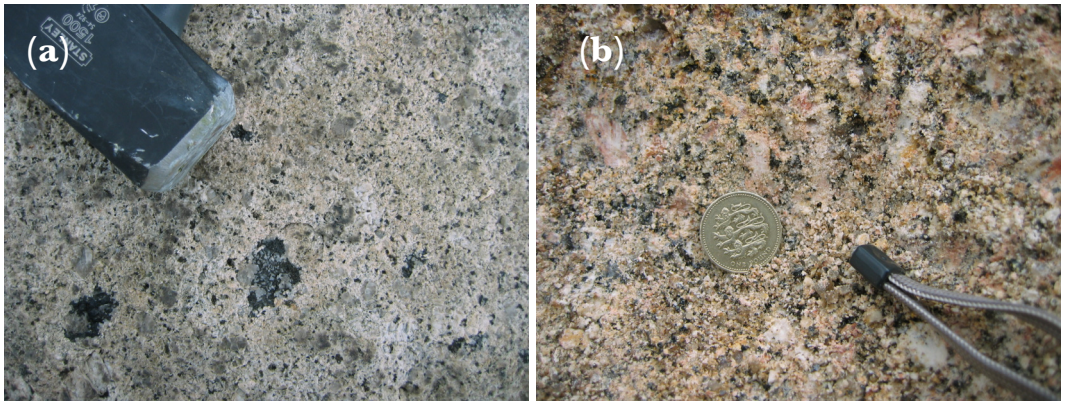

Figure 1.3 The coarse-grained megacrystic biotite granite of Dartmoor; (a) solid bedrock at the High Willhays; and (b) *in situ* altered granite, or growan, at the Two Bridges Quarry.

sedimentary 'country' rock has resulted in the unroofing of the Dartmoor pluton, which now forms an extruded upland in the region with elevations up to 621 m.

Classification schemes for the Cornubian Batholith have been devised by Exley & Stone (1982) and Dangerfield & Hawkes (1981); both of which classify the Dartmoor granite as a coarse-grained megacrystic biotite granite. Dangerfield & Hawkes (1981) identifies two categories on Dartmoor: Type 1A features feldspar megacrysts >15 mm long, and >5-9% by volume; while in Type 1B these are <5% by volume. In both, biotite is more common than muscovite; distribution shown in Figure 1.2. It is considered that type 1A granites form a relatively thin carapace that extends across the top of the pluton, and downgrades to type 1B at a few hundred metres depth (LeBoutllier, 2002). These differences are largely inconsequential to cosmogenic nuclide sampling, as there is a similarity of both texture and quartz content. The mineralogy of the granite is described in detail by Exley & Stone (1964; 1982); it is also summarised by LeBoutllier (2002). The granite has a quartz content of ~34%. The quartz tends to be equigranular, though irregular in shape, and will occasionally form an aggregate 'grain' of interlocking crystals, which may reach up to 40 mm in size. Quartz grains may also contain tiny inclusions, and are frequently strained. There are outcrops of unweathered granite across Dartmoor, most conspicuously in the form of tors. There is also widespread *in situ* altered granite (locally known as growan), the alteration of which has varyingly been ascribed to chemical weathering (e.g. Linton, 1955; Eden & Green, 1971), hydrothermal alteration (Palmer & Neilson, 1962; Exley & Stone, 1964), and frost action (Te Punga, 1957; Palmer & Neilson, 1962), or a combination of these processes (Figure 1.3).

1.4 Previous Research on Dartmoor

Campbell *et al.* (1998) provide a comprehensive review of previous geomorphological research in Dartmoor in a section of *Quaternary of South-West England*, part of a Geoconservation series. It documents the development of ideas in understanding the landscape, and spans the two centuries leading up to its publication, after which there has been little further research published. Given the detail presented in this review, it seems unnecessary to reproduce much of the detail here. Instead, this section

provides a brief overview of the key works that relate to this research. Further detail is provided where relevant in the main sections of this thesis, i.e. tors (Chapter 3), blockslopes (Chapter 4), and landscape (Chapter 5).

The granite landforms of Dartmoor have attracted researchers since the 1830s. In particular, the origin of tors has received attention, with many early investigators identifying key concepts of differential subsurface weathering and periglacial processes, as well as discounted notions of tors as relict sea stacks or formed by wind-blown sand (Campbell *et al.*, 1998). However, it was work in the mid-20th century that formed the conceptual basis for most subsequent research. Linton's (1955) paper on 'the problem of tors' is widely considered a 'classic' paper in geomorphology, mainly due to its formalisation of the two-stage landform development model (Gerrard, 1994). This work drew an immediate rebuttal from many other geomorphologists at the time (see comments in Linton, 1955), which most notably lead to the work of Palmer & Neilson (1962) who proposed that a single-phase of periglacial weathering was responsible for tor formation. The investigation of the tor outcrops was renewed by the work of Gerrard (1978) and later Ehlen (1991; 1992), who investigated relationships between joint structure, petrology, and landscape position.

In these models, the presence and origin of *in situ* altered granite (or growan) became an issue of importance. Linton (1955) argued for deep chemical weathering during warmer conditions in the Tertiary; while Palmer & Neilson (1962) and Exley & Stone (1964) suggested that it was mostly due to hydrothermal alteration of the granite; and Te Punga (1957) and Palmer & Neilson (1962) ascribed physical weathering (i.e. intergranular frost-shattering). Subsequent work has continued to investigate the relative importance of these three main sets of processes, which may all have a role to play in growan development. Most notable is work by Brunsden (1964), Eden & Green (1971), Doornkamp (1974), and Dearman & Baynes (1978).

Many of Dartmoor's most distinctive landforms have been associated with periglacial conditions. In addition to a periglacial origin of tors suggested by Palmer & Neilson

(1962), there has been geomorphological investigation of solifluction (or head) deposits, clitter and blockslopes, earth hummocks, and altiplanation terraces (Waters, 1964; Brunsden, 1968; Green & Eden, 1973; Gerrard, 1989).

At the larger scale, the early work of Worth (1930: cited in Campbell *et al.*. 1998) divided the Dartmoor landscape based on elevation and relief, an approach continued by Waters (1960) and Brunsden (1963; 1964) to determine erosion surfaces and a denudation chronology. Furthermore, Gregory (1969) and Gerrard (1993) investigated patterns of valley-interfluve formation across the landscape.

1.5 Thesis Organisation

This research is based upon the interpretation of ^{10}Be concentrations measured in samples taken from landforms across the Dartmoor landscape. The conceptual underpinning of this approach is summarised in *Chapter 2 – Cosmogenic Nuclide Production Systematics and Analysis*. This covers the *in situ* production of ^{10}Be within the Earth's surface, the modelling of scaling factors for estimation of nuclide production rates, and models for geomorphological interpretation of measured ^{10}Be concentrations (i.e. exposure age and erosion rate for both surface and catchment-averaged approaches). In doing so, it provides the basis for interpretations in later sections, although these also provide further discussion of the application of cosmogenic nuclides to the specific landform. The main body of the research is divided into three sections related to the specific landform being investigated; each is mostly self-contained presenting the background, an interpretative methodology, results, and a discussion. *Chapter 3 – The Formation of Tors* is a study of the most distinctive landform in the Dartmoor landscape, which has attracted geomorphological interpretation for the last two centuries. These have been used to formulate important geomorphological theory (i.e. two-stage landform development), with ensuing controversy. This chapter provides an evaluation of tor formation using ^{10}Be measurements from tor surfaces and regolith. *Chapter 4 – The Development of Blockslopes* investigates these classic periglacial features of the Dartmoor landscape that have been preserved since the termination of the Devensian cold stage.

Cosmogenic nuclides are used to provide long-term constraints on blockslope development of these dynamic landforms. *Chapter 5 – Spatially-Averaged Denudation in the Dartmoor Landscape* interprets the ^{10}Be concentration measured in samples of alluvial sediments to provide spatially-averaged denudation rates across the landscape, which are also averaged over a time span that includes both Holocene and periglacial conditions. Following these core sections, *Chapter 6 – Implications for Landscape Evolution in Dartmoor* provides a brief synthesis that ties together the key findings from each of the studied landforms, and highlights the main implications for our understanding of landscape evolution in Dartmoor.

1.6 Notes on Terminology

Use of Erosion and Denudation:

The term denudation refers to the stripping of material from Earth's surface, and includes the removal of mass through both physical and chemical processes. As the cosmogenic nuclide signal is a reflection of the removal of overlying mass, strictly it is always denudation rate. The term erosion refers to the mechanical process of removal of material from a surface. However, it is common in the cosmogenic nuclide literature to refer to derived denudation rates as an "erosion rate", which is only a valid approximation when chemical weathering is negligible (von Blanckenburg, 2005).

In this thesis, the term 'denudation' rate is used when the context is the lowering of the landscape or spatially averaged elements within it. However, given the widespread use of 'erosion' rate when referring to tor surfaces elsewhere in the cosmogenic nuclide literature, and in the wider geomorphological community, the term is often used here. It is likely that the majority of mass removal from exposed tor surfaces is by mechanical erosion, although features like weathering pits suggest that this is not exclusively the case. It is hoped that the (mis)use of the term 'erosion' in this context does not cause confusion, but instead makes the text more easily compared to those elsewhere.

2: Cosmogenic Nuclide Production Systematics and Analysis

2.1 Introduction

The analysis of cosmogenic nuclides is the principal method utilised in this research. It allows for the evaluation of near-surface exposure of quartz within granite to cosmic radiation, thereby, allowing for interpretation of geomorphological processes and landscape evolution. This chapter details the production systematics of *in situ* cosmogenic nuclides that forms the basis of the technique. This includes spatial variability in production rates that is dependent on location of the sampling site on the Earth's surface, due to geomagnetic modulation and atmospheric attenuation of incoming radiation. It also outlines the *in situ* production of cosmogenic nuclides within the near surface of the Earth and provides case specific context for the main geomorphic features studied in this research.

2.2 Spatial and Temporal Variability of Cosmic Radiation

The Earth is exposed to a constant bombardment of galactic cosmic radiation, which consists of highly energetic particles (the vast majority between ~0.1 and 10 GeV) with 87% protons, 12% α-particles, and 1% heavy nuclei (Pigati & Lifton, 2004), which are capable of generating nuclear disintegrations. The initial interaction of this primary cosmic radiation with atomic nuclei occurs in the upper atmosphere and generates a cascade of secondary particles, some of which will propagate through the atmosphere and ultimately reach the Earth's surface (Tuniz et al., 1998; Gosse & Phillips, 2001).

The flux of cosmogenic nuclide producing radiation received at any specific location on the Earth's surface will be determined by: (i) the modulation of incoming cosmic rays by solar and terrestrial magnetic fields; (ii) the atmospheric mass length through which the secondary particle cascade must pass; and (iii) the shielding geometry of the sampling site. For any interpretation of cosmogenic nuclide concentrations from a sample, these influences must be modelled and an appropriate production rate calculated for the site-specific surface.

2.2.1 Modulation and Attenuation of Cosmic Radiation

The high-energy cosmic radiation required for the nuclear interactions that generate *in situ* cosmogenic nuclides originates from outside the solar system. The source of these particles is uncertain, although they are believed to be produced and accelerated as a consequence of stellar flares, supernovae, pulsars and the explosion of galactic nuclei (Ziegler, 1996). Because cosmic rays are charged particles they interact with galaxies' magnetic field and this changes their trajectories from that of their original source. Consequently, from the perspective of the solar system, primary galactic cosmic rays are isotropic with no particular source (Ziegler, 1996). There may be variations in the galactic cosmic ray intensity over timescales of 10^4 to 10^7 ka (Reedy *et al.*, 1983) related to the passage of the solar system in relation to interstellar medium or the effects of nearby supernovae (Gosse & Phillips, 2001), although these changes are not easily quantified and are likely to be averaged over the timescales of investigation. The magnitude of these changes is also likely to be significantly less than those due to solar and geomagnetic modulation.

The first filtering of incoming primary galactic cosmic radiation occurs in the heliosphere, where the ionized particles of the solar wind project solar-magnetic fields outward from the sun (Lal, 2000; Lifton et al., 2005). The intensity of this modulation will vary temporally with fluctuations in solar activity, and is thus influenced by solar cycles (e.g. 11, 22, 88, 208, and possibly 2300yrs) and long-term variability over time-scales of $10^4 - 10^7$ years (Reedy et al., 1983; Lifton et al., 2005). However, as this solar modulation primarily effects low-energy cosmic radiation (<1 GeV), these variations will only be significant in terrestrial locations with low cut-off rigidity (R_c) (i.e. high latitude polar regions) where low-energy particles are not excluded by the geomagnetic field (Lifton et al., 2005).

Of greater importance in the determination of the intensity of cosmic radiation reaching the Earth's surface is the influence of the geomagnetic field on trajectories of incoming charged primary particles. These charged particles are admitted or deflected by the geomagnetic field depending on their rigidity (momentum per unit charge) and angle of incidence (Pigati & Lifton, 2004). For any given location, the

particle rigidity must exceed the cutoff rigidity (R_c) to penetrate the Earth's magnetic field, or it will be deflected back into space or towards higher latitudes (Pigati & Lifton, 2004). In the Earth's magnetic field, R_c is greatest in equatorial regions, where field lines are perpendicular to the trajectory of incoming radiation, and decreases towards the geomagnetic poles as field lines become more vertical (Gosse & Phillips, 2001). At latitudes greater than ~55° the R_c is below the minimum rigidity of the galactic cosmic ray flux and all primary particles are admitted (Pigati & Lifton, 2004).

The other primary determinant of cosmic ray intensity at a given location is the mass of atmosphere through which it must pass. The propagation of the secondary particle cascade through the atmosphere occurs as a series of nuclear collisions and electromagnetic interactions, with a loss of energy through absorption by the atmosphere (Desilets & Zreda, 2001). This absorption produces an approximately exponential reduction of cosmic ray intensity with increasing atmospheric depth between 200 g cm^{-2} (~12km) and 1033 g cm^{-2} (sea level) (Lifton *et al.*, 2005). A surface at higher altitude will therefore be exposed to a greater intensity of cosmic radiation than one at lower altitude with a greater depth of atmosphere above it.

2.2.2 Spatial Scaling Factors for Cosmogenic Nuclide Production Rates

In order to estimate cosmogenic nuclide production rates at any given site, a requirement of cosmogenic nuclide analysis, it is necessary to model variation in received cosmic radiation due to the geomagnetic field and atmospheric attenuation. Lal (1991) provided the first, and until recently widely used, scaling factors for terrestrial cosmogenic nuclide production that corrected for these influences. The experimental measurement of star producing radiations or neutron flux data collected at a variety of geomagnetic latitudes has been used to calculate latitude-altitude variation curves for the rate of nuclear disintegration (Lal & Peters, 1967). The Lal (1991) model is calibrated to production rates at presumed 'zero-erosion' surfaces of a known age (Nishiizumi *et al.*, 1989) and provides a set of equations for the calculation of ^{10}Be and ^{26}Al production rates for any given latitude and elevation. There is considerable uncertainty of between 10-20% associated with these production rates.

The Lal (1991) model relies on a number of approximations and simplifications in its characterisation of the cosmic radiation flux. There are a variety of proposed modifications and alternatives that seek to address some of the following: (i) a presumption of uniform thickness of the atmosphere; (ii) revision of production rates at surfaces and an improved calibration data-set; and (iii) the simplification of the geomagnetic field as non-varying dipole and models of particle trajectories, the subject of ongoing debate within the community. Subsequently, there have been various proposed modifications and alternatives that address these issues.

Stone (2000) provides a modification of the Lal (1991) model based on the same scaling model, but adapts it to replace an assumed uniform atmospheric thickness with a pressure dependent correction factor that can incorporate regional differences. The significance of this modification is region specific, with production rates in most regions adjusted by at most ± 3-4%, although in Antarctica where the difference is largest these may be up to 25-30% higher. Stone (2000) also recalculates ^{10}Be production rates as 5.1 ±0.3 atoms g^{-1} a^{-1} for ^{10}Be, reduces the relative importance of muonic production to 2.6%, and includes an independent slow (negative) muon component.

Underlying the Lal (1991) and Stone (2000) production model is an ordering of neutron measurements by geomagnetic latitude assuming a simple dipole field as an approximation of the Earth's magnetic field. Subsequent models have sought to provide more realistic representations of the geomagnetic field. Dunai (2000) orders neutron monitor data based on geomagnetic inclination and the horizontal component of geomagnetic intensity to allow for non-dipole effects. Desilets & Zreda (2003) and Desilets *et al.* (2006) take an alternative approach of directly modelling effective vertical cutoff rigidity through numerically simulating the trajectories of primary cosmic ray protons through a geomagnetic reference model. Lifton *et al.* (2005) fit a model of trajectory-derived cutoff rigidities to geomagnetic latitudes. All three of these models provide a means of modelling temporal and spatial variations in the geomagnetic field and, for Lifton *et al.* (2005) solar variations. All three are an advance on that of Lal (1991). However, there remains uncertainty in all models of

cosmogenic nuclide production, something the CRONUS-EU (Dunai *et al.*, 2005) and CRONUS-Earth (Schaefer *et al.*, 2005) projects seek to address.

The various production models can generate significantly different scaling factors depending on the location and altitude of sampling site. For this study, there are relatively modest differences, as Dartmoor is located at relatively high latitude (50.7°N) and doesn't deviate substantially from standard geomagnetic field models. Figure 2.1 plots scaled production rates for each scaling model for an elevation range (200-600 m) typical of Dartmoor (50.7°N). The models all vary similarly with changes in elevation. However, there is an offset in production rates depending on the model chosen. There is a <1% difference between the production rates calculated by Lal (1991) and Stone (2000), as would be expected given the shared basis of the models. There is a 5-10% difference between Lal (1991) and the more recent models of Desilets *et al.* (2006), Dunai (2000), and Lifton (2005); these all return lower scaled production rates. There is a <4% difference between these newer models.

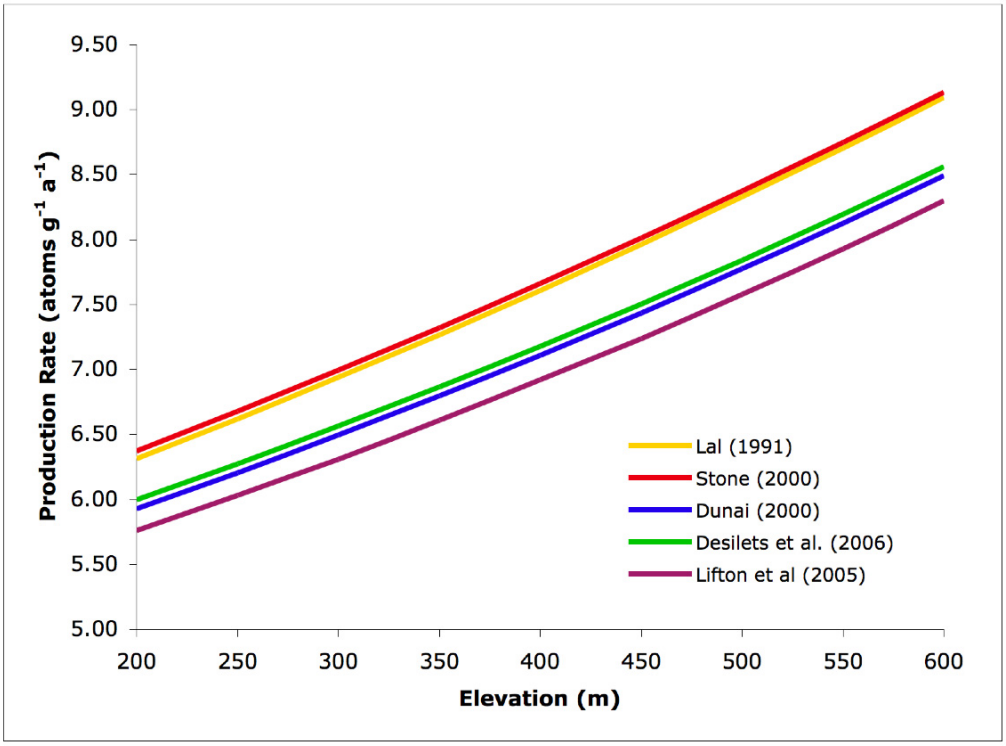

Figure 2.1 Cosmogenic nuclide ^{10}Be production rates scaled using various models for the elevation range 200-600 m of Dartmoor (50.7°N)

The selection of production scaling model can have a significant impact on the production rate of cosmogenic nuclides for a sampling site. This will in turn impact on the calculation of exposure ages or denudation rates for samples. In studies attempting to precisely date landscape features or compare rates across regions the variability and inaccuracies in production scaling models can be a significant source of uncertainty. However, as the main interest in this study is a comparison between samples, the selection of production scaling model is not of critical importance.

2.2.3 Geometric Shielding of a Surface

In standard models of cosmogenic nuclide production, the surface is assumed to be a horizontal plane extending in all directions, with incoming cosmic radiation received from all parts of the sky. However, at most field sites intervening topography and/or local surface geometry will result in a reduced radiation flux at the surface. This section first describes the geometric properties of incoming radiation, followed by details of specific corrections for topographic obstructions, sloping surfaces and shape effects.

Although radiation will be received from all unobstructed parts of the sky to which a surface is exposed, it is important to recognise that the intensity of this flux depends on the angle of inclination. This variation is due to the atmospheric depth through which radiation must pass, which is thickest near the horizon and thinnest vertically overhead. The angular distribution of this can be described as $F(\phi) = F_0 \cos^{2.3}\phi$ (Gosse & Phillips, 2001). Consequently, the vertical component is of greater significance than that from nearer the horizon. Gosse & Phillips (2001) illustrate this by calculating that with incoming radiation excluded from angles < 45°, the surface will still receive 80% of the total potential radiation flux. The implication of this is that corrections for shielding due to topographic exclusion will in most situation be relatively minor, becoming important only in very steep terrain.

2.2.3.1 Shielding by Topographic Obstruction

A surface can be shielded from incoming radiation by intervening topography that prevents radiation reaching it from some section of the sky. This obstruction can be either due to distant topographic features that rise above the horizon (e.g. mountains), the surrounding topography (e.g. local hills if site is in valley), or nearby local obstructions (e.g. a rock outcrop). The effect of this is to: (i) reduce the amount of total radiation received at the surface; and (ii) increase the effective attenuation length (Λ_{eff}) of incoming radiation, as a greater proportion is received from vertical inclinations (Dunne *et al.*, 1999).

The typical approach to deriving a correction factor for obstructions is to calculate the amount they do not exclude and multiply this by the total radiation that would be received at an unobstructed surface. There are a variety of calculations that work on similar principles, although differently derived (e.g. Dunne *et al.*, 1999; Gosse & Phillips, 2001; Balco *et al.*, 2008). For example, Dunne *et al.* (1999) derive a correction factor for a series of n rectangular obstructions (also provide a modified version for triangular obstructions) as a ratio of remaining flux to maximum potential flux as follows:

$$S_T = 1 - \frac{1}{360^\circ} \sum_{i=1}^{n} \Delta\theta_i \sin^{3.3} \phi_i \qquad [2.1]$$

In most circumstances, the effect of topographic obstructions will be small and it is only in very steep terrain or in close proximity to local obstructions that a significant modification of the radiation flux at a surface will be observed.

2.2.3.2 Shielding of a Sloping Surface

If the surface is on a slope the incoming radiation flux will be modified in several ways (Dunne *et al.*, 1999; Gosse & Phillips, 2001). Firstly, there will be a topographic obstruction of the skyline in the upslope direction. This will effect an azimuthal range of 180°, with a maximum inclination of exclusion in the upslope direction reducing

to zero at the axis of rotation. Secondly, as the majority of incoming radiation is received from more vertical inclinations, there will be: (i) an increase in the path-length of radiation in the near-surface due to the obliquity of angle (Figure 2.2a); and (ii) a foreshortening effect that reduces the radiation flux as it is spread over a larger area (Figure 2.2b). These two effects counteract each other, and in the calculations of Dunne *et al.*, (1999) the terms cancel. Finally, the effective attenuation length of radiation will be reduced in a sloping surface, which is also due to the increased obliquity of incoming radiation.

The calculation of the effects of a sloping surface on the received radiation flux is difficult due to the complex way in which shielding varies with azimuthal angle. Both Dunne *et al.* (1999) and Gosse & Phillips (2001) provide a means of solving this for slopes. However, some difficulty arises when topographic obstructions are also present as the models for calculating exclusions are mutually exclusive (Dunne *et al.*, 1999).

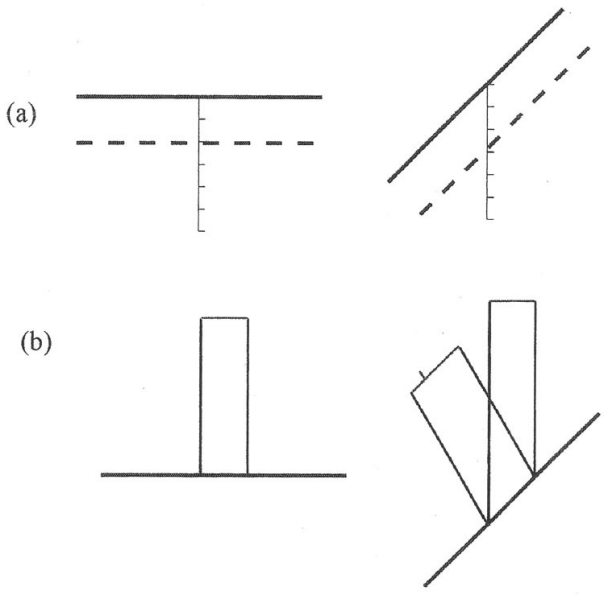

Figure 2.2 A comparison of the effects of surface slope (horizontal versus 45°) on (a) radiation path-length, which is increased in sloping surface due to obliquity of angle; and (b) the foreshortening effect on radiation distribution, which spreads radiation over greater surface area on sloping surface.

2.2.3.3 Shape Effects

In standard models of cosmogenic nuclide production the sampled surface is assumed to be part of a continuous plane. In many situations we are interested in sampling surfaces that deviate from a plane; in the case of Dartmoor both boulders and outcropping tors. The shape of these features becomes important as it changes the irradiation geometry of the surface with a range of slopes present. In addition, Masarik & Wieler (2003) highlight a potential loss of spallation inducing neutrons to the atmosphere following reactions in a protruding object. For such an object, incoming neutrons do not match loss, as would be the case in a planar-surface (Figure 2.3). This shape effect will depend on the size and geometry of the object sampled, but it is worth noting that the production rate on some boulders may be 10-12% lower than on a similarly exposed planar surface (Masarik & Wieler, 2003). However, easily applied calculations are not available. Consequently, samples should be taken away from edges where possible; and when this is not possible, the potential change in production rate should be recognised.

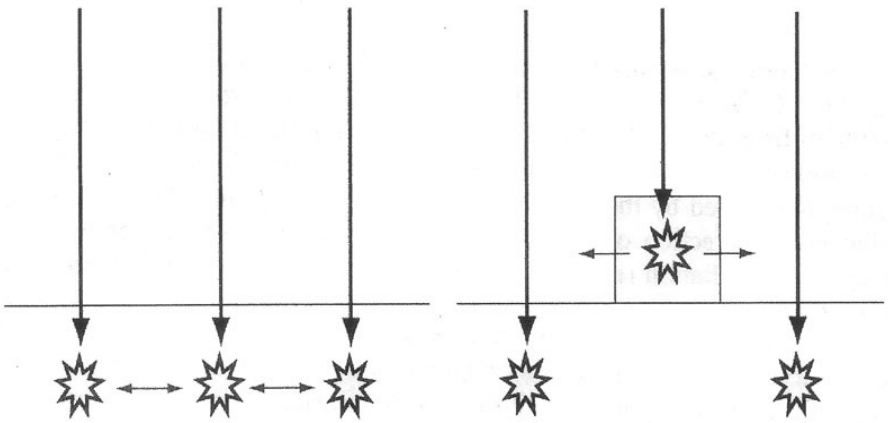

Figure 2.3 Shape effect of a target object extruded above a planar surface, with potential loss of spallation inducing neutrons to atmosphere.

2.3 *In Situ* Production of Cosmogenic Nuclides

Upon reaching the Earth's surface, the secondary particle flux of cosmic radiation interacts with the atomic nuclei of minerals producing a variety of cosmogenic nuclides. In this study, use is made of the concentration of cosmogenic nuclide ^{10}Be in quartz. The production of these radionuclides in quartz is principally through high-energy nucleon spallation in the near surface with a smaller contribution from muonic production, although the significance of the muogenic component increases with depth (Nishiizumi *et al.*, 1989). This section provides a brief outline of the mechanisms by which ^{10}Be is produced *in situ* within the Earth's surface.

2.3.1 Spallation

A spallation reaction occurs when a high-energy nucleon (predominately neutrons) collides with an *in situ* atomic nucleus. This collision causes the nuclear disintegration of the target atom resulting in the spalling of nucleons (individually or in clusters) as energy is dissipated and the nucleus re-stabilises as a lighter residual nucleus (Gosse & Phillips, 2001). In quartz (SiO_2) the cosmogenic nuclide ^{10}Be is produced by high-energy nucleon spallation principally through the reactions of ^{16}O (n, 4p3n) $\rightarrow$ ^{10}Be, with some additional ^{10}Be produced by spallation of the other oxygen and silicon isotopes (Nishiizumi *et al.*, 1989).

The production of ^{10}Be at the Earth's surface is dominated by high-energy neutron spallation. Stone (2000) estimates that spallation accounts for 97.4% of ^{10}Be production at high latitude, sea level reference locations. However, spallation inducing high energy neutrons are limited in their ability to penetrate the dense rock and soils of the lithosphere. These high energy (>10 MeV) secondary neutrons lose energy through successive reactions and, once down to the 1-5 MeV range, are no longer capable of causing spallation reactions (Gosse & Phillips, 2001). With values of between 150 and 170 g cm^{-2} commonly used for fast nucleon attenuation length in near surface rock (Gosse & Phillips, 2001), the decline in spallation reactions will decrease exponentially within the upper few metres of the Earth's surface; at Λ = 160 g cm^{-2} in granite (ρ = 2.6 g cm^{-3}) the production rate will decrease by a factor of e^{-1} at a depth of 65 cm (Gosse & Phillips, 2001).

2.3.2 Muonic Production

Also a product of the secondary particle cascade (from the decay of unstable $\pi^{\pm}$ and $K^{\pm}$ mesons), muons are of considerably lower mass than high energy nucleons that induce spallation reactions (Gosse & Phillips, 2001). The principal means of muonic production of cosmogenic nuclides is through the capture of stopping (or slow) negative muons by a charged nucleus, with the subsequent emission of a few particles and a reduced residual nucleus (Gosse & Phillips, 2001; Heisinger *et al.*, 2002b). Additional muonic production can result from fast muon interactions with target nuclei, although this is less common (Heisinger *et al.*, 2001a). In quartz the cosmogenic nuclide ^{10}Be is produced by slow negative muon capture by the reactions of ^{16}O (μ^-, 3p3n) $\rightarrow$ ^{10}Be (Nishiizumi *et al.*, 1989).

Although energetic muons constitute approximately half of the secondary cosmic ray flux reaching the lithosphere (Gosse & Phillips, 2001), they are only responsible for a few percent of cosmogenic nuclide production at the surface (Stone, 2000). However, muons have a lower mass than nucleons (~1/9 mass of neutron) and with an average attenuation length of approximately 1300 g cm^{-2} are able to penetrate to significant depth (Brown *et al.*, 1995b; Gosse & Phillips, 2001).

2.3.3 Overview – Cosmogenic Nuclide Production

In most geomorphological applications of cosmogenic nuclide concentrations, the vast majority of the nuclides measured will be the product of high-energy neutron spallation in the upper few metres of the Earth's surface. In these shallow depths production by spallation exceeds that of muons by a couple orders of magnitude. It is only at depths exceeding ~4 m, by which the flux of high-energy nucleons has been severely attenuated, that muonic production pathways begin to exceed spallation (Figure 2.4; Heisinger & Nolte, 2000). Consequently, the muogenic component of cosmogenic nuclide concentrations is only significant in geomorphological situations where there are high rates of denudation or when considering depth profiles and burial.

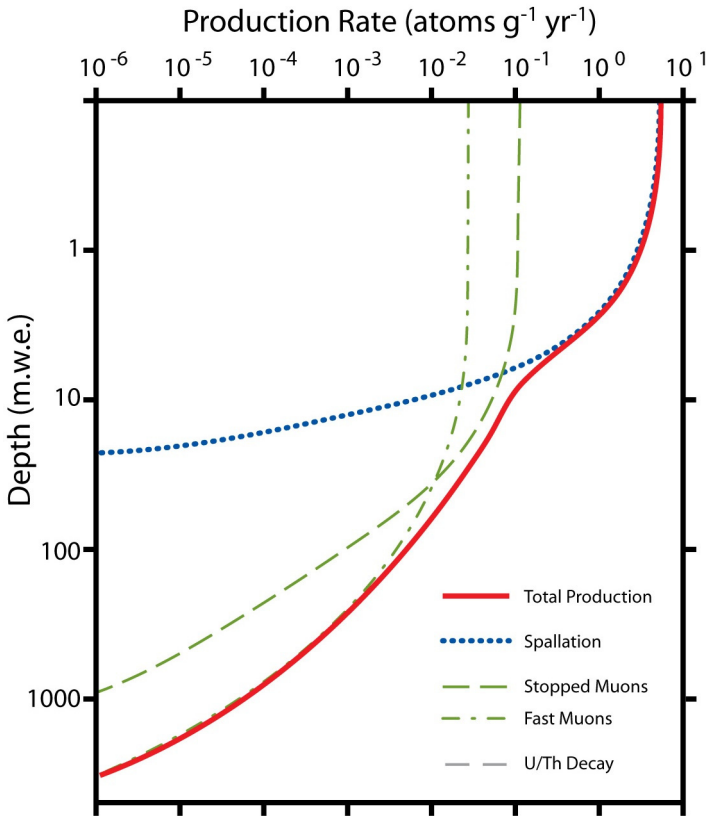

Figure 2.4 Production rate of ^{10}Be in SiO_2 with depth (mean water equivalent)

Source: (redrawn) Heisinger & Nolte (2000)

2.3.4 Correction for Sample Thickness

The rapid decline in production rate of cosmogenic nuclides with depth requires a correction to be made for sample thickness; particularly if samples are more than a few centimetres thick. This is achieved by integrating the production rate over the thickness of the sample (z); for spallation reactions this can be calculated as follows (Gosse & Phillips, 2001):

$$Q_S = \frac{\Lambda_{eff}}{z}\left(1 - \exp\left(-\frac{z}{\Lambda_{eff}}\right)\right) \qquad [2.2]$$

This approach assumes an exponential decay of spallation production with depth. Masarik & Reedy (1995) note that there is a region of surface-air interaction in the upper ~12 g cm^{-2} that may produce a relatively flat profile. Kubik & Reuther (2007) experimentally demonstrated that long attenuation lengths and non-decreasing (or 'flat') sections near the surface might be present. However, corrections remain unclear and this effect will only have a significant impact on a few studies.

2.4 Exposure Age and Erosion Rate Models

In order to make a geomorphological interpretation of a measured cosmogenic nuclide concentration, we require a model that can describe how those nuclides accumulate at the sampled site. Lal (1988; 1991) provides the basic model by which most researchers have been able to interpret cosmogenic nuclide data. This can be calculated as follows:

$$N(x,t) = \frac{P_0}{\lambda + \varepsilon\rho\Lambda^{-1}} e^{-x\rho\Lambda^{-1}} \left(1 - e^{-(\lambda+\varepsilon\rho\Lambda^{-1})t}\right) + N_{inh} e^{-\lambda t} \qquad [2.3]$$

In this model, the cosmogenic nuclide concentration, N, is determined for a given depth, x, by calculating production rate for the sampled surface, P_0, as well as constants for the nuclide decay half-life, λ, absorption in material by attenuation length, Λ, and rock or soil density, ρ. The variables of time, t, and denudation rate, ε, are of geomorphological interest; in solving for these, using a single cosmogenic nuclide, we are able to interpret concentrations as either an exposure 'event' or the incremental erosion of landforms (Cockburn & Summerfield, 2004).

This section provides the conceptual framework for the interpretation of cosmogenic nuclide concentrations as they are applied in this study. The exposure 'event' age model is explored first, with a consideration of its applicability to the outcropping tors of Dartmoor. However, as will be explained, this approach has limited applicability when applied to erosional landforms that are undergoing incremental change. The

remainder of the section explores the interpretation of cosmogenic nuclide concentrations as erosion rates. It begins by establishing the basic premise of an erosion rate model for cosmogenic nuclide concentrations, and is followed by discussion of erosion rate models that can be applied to different landscape elements relevant to this study.

2.4.1 Exposure Age Model

The interpretation of cosmogenic nuclide concentrations using an exposure age model has been applied to a range of geomorphological problems (see reviews by Cockburn & Summerfield, 2004; Bierman & Nichols, 2004). The application of exposure age dating requires a geomorphological 'event', defined by Cockburn & Summerfield (2004) as "an 'instantaneous' occurrence of sufficient magnitude to expose material that has previously been effectively shielded from cosmic radiation". The exposure of this 'event surface' to cosmic radiation leads to accumulation of cosmogenic nuclides over time; the abundance of which can then be used to determine its age.

To calculate an exposure age, Equation 2.3 can be rearranged to solve for the variable time, *t*, producing the following:

$$t = \frac{-1}{\lambda + \varepsilon\rho\Lambda^{-1}} \ln\left(1 - \frac{N\left(\lambda + \varepsilon\rho\Lambda^{-1}\right)}{P_0}\right) \qquad [2.4]$$

In this solution, the variable for erosion rate, ε, persists. To solve for time, *t*, we must know the erosion rate. In some cases, there may be an independent (and reliable) measurement of the post-exposure 'event' erosion rate available. More commonly, the erosion rate is unknown and, therefore, has to be estimated in order to solve for time. In some geomorphological settings it may be useful to assume a zero erosion rate for the post-exposure surface. This simplifies Equation 2.4 as follows:

$$t = \frac{-1}{\lambda} \ln\left(1 - \frac{N\lambda}{P_0}\right) \qquad [2.5]$$

In this study, the only landforms that could plausibly be interpreted as exposure 'event surfaces' are tors, and these only given a very specific set of geomorphological circumstances. To provide an exposure age for a tor the following criteria would have to be met: (i) the granite of the tor would have to have been effectively shielded from cosmic radiation by overlying material prior to the exposure event; (ii) the removal of this overlying material should be sufficiently rapid that minimal accumulation of cosmogenic nuclides occurs in the surface during its unearthing; (iii) there should be negligible erosion of the tor surface subsequent to its exposure.

2.4.2 Erosion Rate Model

The specific geomorphological circumstances required for a valid interpretation of an exposure age on an 'event surface' (section 2.4.1) are relatively unusual in the landscape (e.g. ice-marginal moraines, large landslides, or fault scarps). It is more typical for a landform to be the product of the progressive weathering and removal of material, usually by increments that are significantly smaller than characteristic attenuation lengths (~0.6 m in rock) of spallogenic cosmogenic nuclide production (Cockburn & Summerfield, 2004). In such a surface, the concentration of cosmogenic nuclides will reflect a dynamic balance between the ongoing production of nuclides and the rate at which they are lost through denudation (and for radionuclides by decay).

In some geomorphological settings, it may be reasonable to assume that the denudation of the surface is occurring in, or at least approximating, steady-state (continuous process of material removal at a uniform rate over time). Lal (1991) provides reworking of Equation 2.3, solving for the concentration of cosmogenic nuclides when exposed to continuous long-term irradiation, $t >> 1/(\lambda + \mu\varepsilon)$, and undergoing steady-state erosion, $\varepsilon(t)$ = constant = ε, as follows:

$$N(x,t) = e^{-x\rho\Lambda^{-1}}\left(\frac{P_0}{\lambda + \varepsilon\rho\Lambda^{-1}}\right) + N_{inh}e^{-\lambda t} \qquad [2.6]$$

This is further simplified when samples are taken from the surface, $x = 0$, and when there is no inheritance, N_{inh}, of cosmogenic nuclides from incomplete shielding at $t = 0$. The resulting equation, after sufficient time, $t >> 1/(\lambda + \varepsilon\rho\Lambda^{-1})$ is:

$$N_0 = \frac{P_0}{\lambda + \varepsilon\rho\Lambda^{-1}}$$

[2.7]

This can be rearranged to solve for the geomorphologically interesting variable of erosion rate, ε, as follows:

$$\varepsilon = \frac{\Lambda}{\rho}\left(\frac{P_0}{N} - \lambda\right)$$

[2.8]

A surface achieves secular equilibrium when continued nuclide production is matched by loss through denudation and radioactive decay, resulting in a constant ^{10}Be concentration over time. The length of time taken to reach secular equilibrium is determined by the denudation rate (Figure 2.5). For slowly denuding surfaces this can take more than 100 ka, and sometimes a few million years, while rapidly denuding surfaces can achieve secular equilibrium in 10-100 ka.

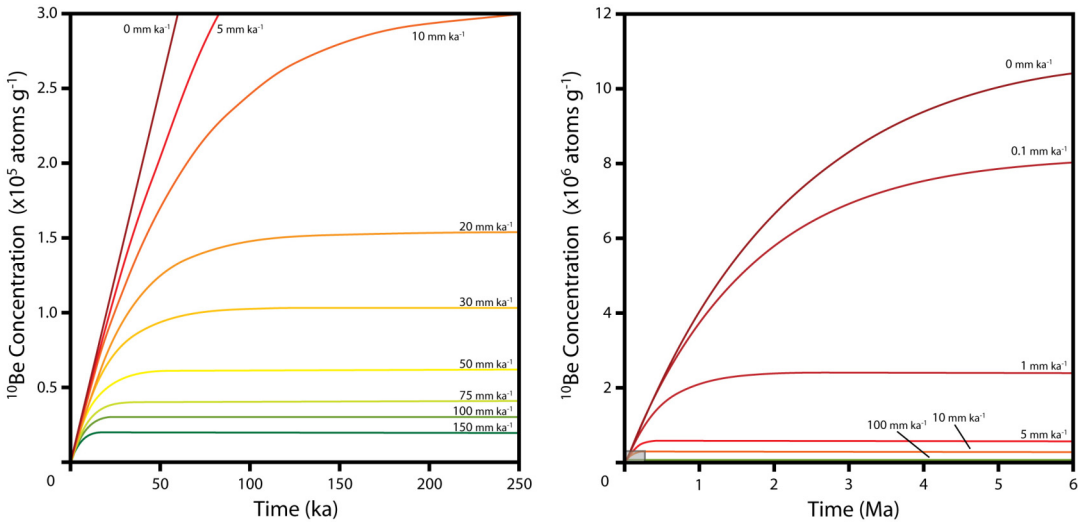

Figure 2.5 The increase in ^{10}Be concentration (initially zero in surface) with time in a denuding surface; secular equilibrium is reached when production is matched by denudation and radioactive decay resulting in constant ^{10}Be concentration.

2.4.2.1 Contribution from Muons

While the solution for erosion rate in Equation 2.7 is often applied, this only accounts for production of cosmogenic nuclides by high-energy neutron spallation. As previously discussed (Section 2.3), while spallation reactions dominate near the surface, the rapid attenuation of high-energy neutrons means that muonic production becomes proportionally more significant with increasing depth (Figure 2.4). In a slowly eroding surface, the target minerals will have spent a considerable amount of time resident in the upper few tens of centimetres accumulating cosmogenic nuclides by neutron spallation reactions, at a rate far in excess of muonic production. However, as denudation rates increase the residence time of target minerals in the near surface is reduced. Consequently, cosmogenic nuclides produced by muonic interactions at depth become increasingly significant in such cases and need to be taken into account.

There have been attempts at modelling cosmogenic nuclide production that include the muonic component, most notable are those of Granger & Smith (2000) (subsequently developed in Granger & Muzikar, 2001; Granger *et al.*, 2001) and Schaller *et al.* (2001). Here the focus is on the model developed for eroding landforms by Granger and co-workers. Unlike spallation reactions, the muonic production of cosmogenic nuclides is not characterised by a simple e-folding exponential. Utilising muonic production estimates of Stone (1998) and Heisinger (1998; cited in Granger & Smith, 2000), Granger & Smith (2000) derive a set of exponential terms that allow for the calculation of production rate that includes a muonic contribution as follows:

$$P_{^{10}Be,\mu}(z) = B_1 e^{-z\rho/L_1} + B_2 e^{-z\rho/L_2} + B_3 e^{-z\rho/L_3} \qquad [2.9]$$

where the first and second terms describe production by slow negative muon capture and the third term by fast muon interactions. In this derivation, SLHL production rates (atoms g^{-1} yr^{-1}) of ^{10}Be in quartz are $B_1 = 0.096$, $B_2 = 0.021$, and $B_3 = 0.026$. The attenuation lengths are given as $L_1 = 738.6$ g cm^{-2}, $L_2 = 2688$ g cm^{-2}, and $L_3 = 4360$ g cm^{-2}. This approximation is considered to be within a few percent for depths up to 20 m in rock.

With an approximation of muonic production rate mechanisms it is possible to model cosmogenic nuclide concentrations in an eroding surface to include these additional terms. For a surface where nuclide inheritance is negligible and erosion has been occurring for a sufficient period of time, $t >> 1/(\lambda + \mu\varepsilon)$, the concentration of cosmogenic nuclides in a surface can be calculated as follows (Granger & Muzikar, 2001):

$$N_0 = \frac{P_0}{\lambda + \varepsilon\rho\Lambda^{-1}} + \frac{B_1}{\lambda + \varepsilon\rho L_1^{-1}} + \frac{B_2}{\lambda + \varepsilon\rho L_2^{-1}} + \frac{B_3}{\lambda + \varepsilon\rho L_3^{-1}} \quad [2.10]$$

where the first term describes production by high-energy neutron spallation, as derived in Equation 2.7, and the remaining terms muonic production.

As previously stated, the relative contribution of muonic production to the cosmogenic nuclide concentration in minerals at a surface is dependent on the denudation rate. Using Equation 2.10, the relative contribution of spallation and muonic production for a range of denudation rates at SLHL are plotted in Figure 2.6. This demonstrates, as observed by Granger & Muzikar (2001), that for denudation rates < 1 mm ka^{-1} the contribution from muonic production is not significant, with near surface spallation production dominating and nuclides produced at greater depths by muonic interactions likely to have decayed before reaching the surface. For denudation rates between 1 and 10 mm ka^{-1} the relative contribution from muons increases rapidly from ~ 5 to 15%. When considering, and particularly when comparing, denudation rates in this range it is important to consider the muonic contribution. For erosion rates > 10 mm ka^{-1} there is a non-negligible contribution from muonic production that gradually increases to ~20%. A spallation-only derivation of denudation rate will underestimate the denudation rate for samples in this range. However, as this offset is relatively consistent for rates > 10 mm ka^{-1}, there may still be some validity when the more important aspect of the geomorphological interpretation is a comparison of sample denudation rates rather than their precise measurement.

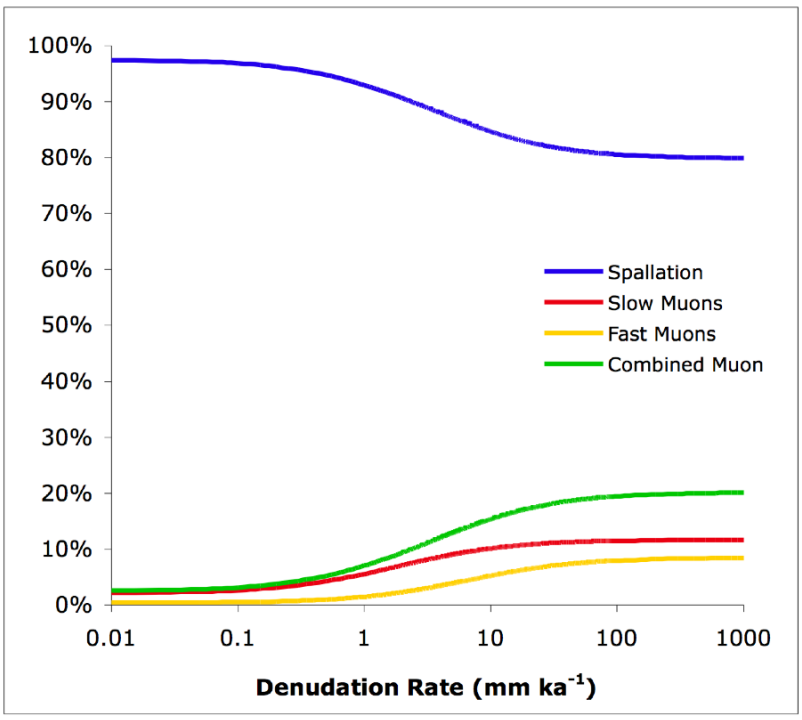

Figure 2.6 The percentage contribution of spallation and muon production for ^{10}Be at a range of denudation rates from 0.01 to 1000 mm ka^{-1}.

2.4.2.2 Averaging Time Scales

On an eroding landform material is continually being removed from the surface and replaced by underlying material. This means that over time material at depth is progressively moving towards the surface and as it does so it is exposed to increasingly intense cosmic radiation. Consequently, the cosmogenic nuclides in an eroding surface will have accumulated over the interval in which it was brought from depth to the surface. The concentration of cosmogenic nuclides in a sample taken from an eroding surface is determined by: (i) the denudation rate – which controls the rate at which a sample moves towards the surface and, hence, the residence time in near sub-surface in which it accumulates cosmogenic nuclides; and (ii) the production rate and absorption depth scale ($z^* = \Lambda / \rho$) - which represents the attenuation of cosmic radiation (and thereby production rate at depth) in the material of the landform.

Lal (1991) defines a concept of an 'apparent exposure age' for an eroding surface and calculates this as follows:

$$T_{eff} = \frac{N_0}{P_0} = \frac{1}{\lambda + \varepsilon\rho\Lambda^{-1}} \qquad [2.11]$$

This term for an 'apparent exposure age', T_{eff}, is a function of the surface denudation rate, ε, the absorption parameters attenuation length, Λ, and density, ρ. For most situations $\lambda << \varepsilon\rho\Lambda^{-1}$ (e.g. erosion rates > 0.1 mm ka^{-1}), so the decay constant is insignificant and useful information can be obtained about erosion of the surface. This has also been termed an 'averaging time scale' (e.g. von Blanckenburg, 2005), the term adopted here. The averaging time scale, as defined here, represents the amount of time required to remove one length of the absorption depth scale. In a typical granite rock (ρ = 2.6 g cm^{-3}) and with a spallation attenuation length ($\Lambda \approx$ 160 g cm^{-2}) this would be a depth of 61.5 cm. The averaging time scale is plotted against denudation rate in Figure 2.7. It is clearly evident that averaging time scale becomes significantly longer at lower denudation rates.

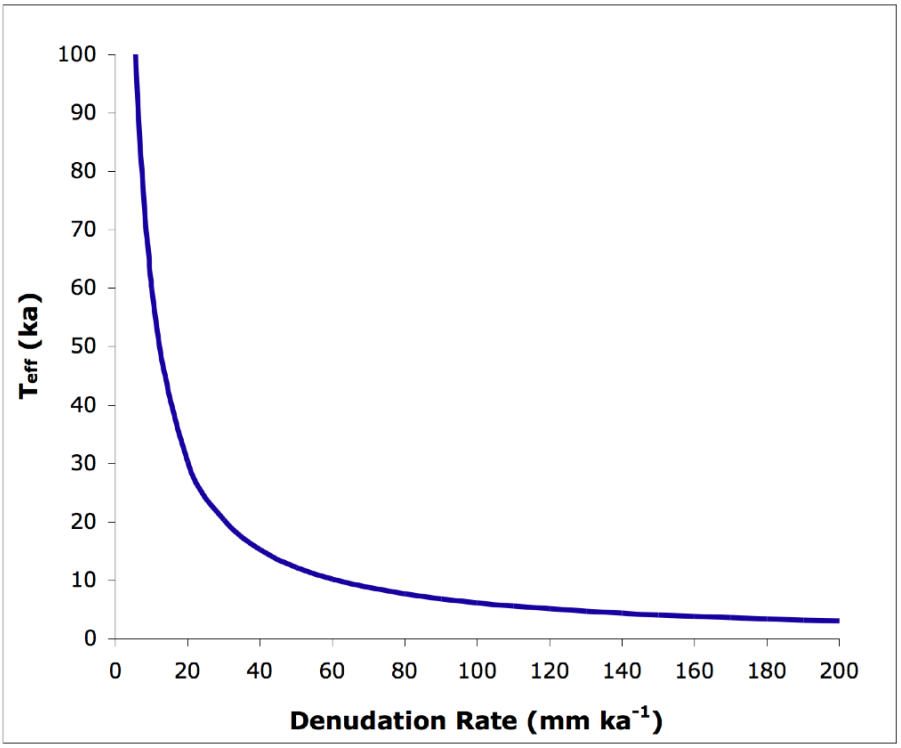

Figure 2.7 The 'apparent exposure age' or 'averaging time scale' for denudation rates of 0-200 mm ka^{-1}

The averaging time scale becomes a more significant concept when we consider landforms in which there has been a change in denudation rate. Bierman & Steig (1996) identify that the response time of cosmogenic nuclide concentration to a change in rate is directly related to the denudation rate. The removal of 2-3 m of material (3-5 absorption depth lengths) from the surface will almost entirely erase any preceding erosion rate signal. If < 2 m of material has been removed the cosmogenic nuclide concentration will reflect a composite signal of the different erosion rates; in many situations this might be useful as the cosmogenic nuclide concentrations will reflect a long-term average rather than shorter-term fluctuations in erosion rates.

In Dartmoor there is evidence for a significant change in the geomorphological processes operating following the transition from LGM periglacial environments to one of Holocene upland moorlands (Gerrard, 1993). The cosmogenic nuclide concentrations measured will reflect a composite signal if, as is almost certain, Holocene erosion has not been sufficient to remove > 2 m of material. To assess the impact of this change in erosion rate, a model is presented for the calculation of the impact of a step-change between two erosion rates at a given time in the past.

The concentration of cosmogenic nuclides in the sampled surface, N_S, can be calculated for a given time, t, since change and erosion rate before, ε_1, and after, ε_2, change. This can be calculated by:

$$N_S = \frac{P_0}{\lambda + \varepsilon_2 \rho \Lambda^{-1}} - \left[\left(e^{-x\rho\Lambda^{-1}} \frac{P_0}{\lambda + \varepsilon_2 \rho \Lambda^{-1}} \right) - \left(e^{-x\rho\Lambda^{-1}} \frac{P_0}{\lambda + \varepsilon_1 \rho \Lambda^{-1}} \right) \right] \quad [2.12]$$

where the first term calculates what the concentration at the surface would be based on the new erosion rate, ε_2. The second part works out concentrations for the surface when the step-change occurred, t, when the present surface was buried at a depth; which can be calculated as $x = x$. The difference between the actual concentration at the step change (the calculation using the old rate ε_1) and what would have been if the new rate had been in effect (the calculation using ε_2) is the offset that can be

subtracted from the first term. This can then be used to calculate an erosion rate for the surface using Equation 2.11 with the value $N = N_S$. This provides a potentially useful tool for the evaluation of changing erosion rates; however, it is usually the case that neither old or new erosion rates are known.

Figure 2.8 plots the erosion rate that would be measured by cosmogenic nuclides at a surface following a step-change in erosion rates of (a) 150 to 50 mm ka^{-1} and (b) 50 to 10 mm ka^{-1}. The time taken for the erosion signal from cosmogenic nuclides to respond and adjust to the new erosion regime is largely determined by the new erosion rate. If the new rate is slow there will be a considerable period of adjustment, with the earlier erosion signal persisting until up to 2-3 m of material has been removed. However, there will be a significant adjustment to erosion rate over shorter time scales with a composite erosion signal present in the surface sampled. In the examples in Figure 2.8, after 10 ka the change from 150 to 50 mm ka^{-1} will register an erosion rate of 71 mm ka^{-1}; while for the 50 to 10 mm ka^{-1} change the erosion rate will be 31 mm ka^{-1}.

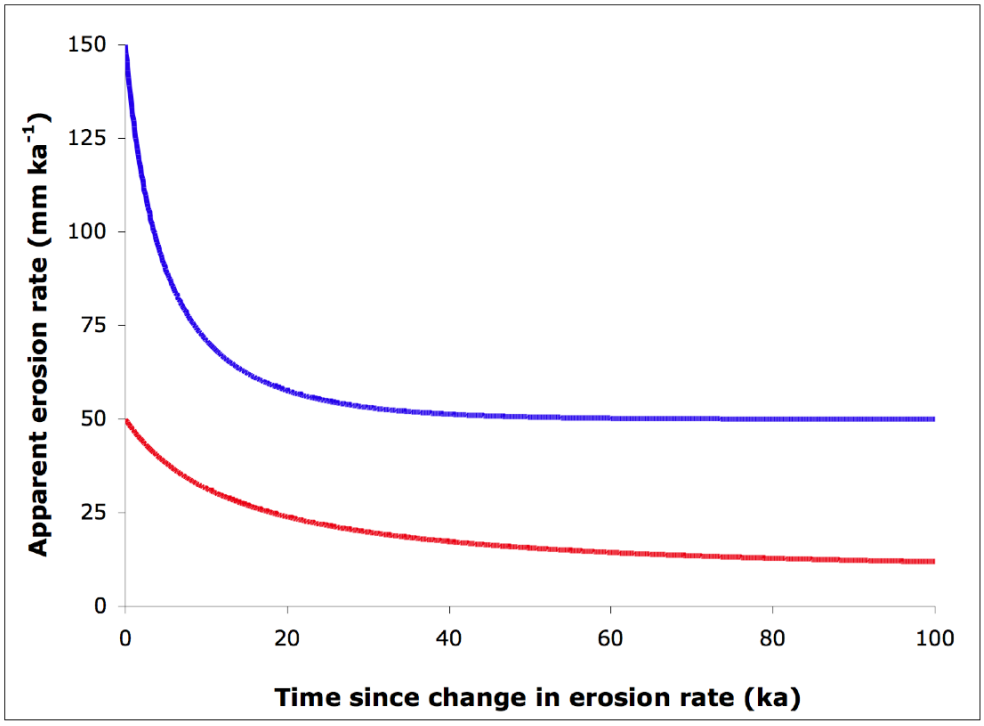

Figure 2.8 Apparent erosion rate from ^{10}Be concentration in surface following a change in dendudation rate of 150 to 50 mm ka^{-1} (blue) and 50 to 10 mm ka^{-1} (red).

2.4.2.3 Episodic Erosion

The erosion rate model assumes that surface erosion is constant (or steady-state) over time, $\varepsilon(t) = \bar{\varepsilon}$, which must be valid over the timescale of cosmogenic nuclide accumulation (i.e. averaging timescale), and that it has persisted long enough that $t >> t_{eff}$ (Figure 2.7). However, in many (or most) environments and lithologies the episodic removal of material from the surface will be of a thickness (L) of the same order of magnitude as the erosional depth scale ($L/\varepsilon \approx z^*/\varepsilon$), and the steady-state assumption is invalid (Small *et al.*, 1997). Small *et al.* (1997) demonstrate, by modelling episodic chipping of an eroding surface, that ^{10}Be erosion rates vary between greater and less than the true mean erosion rate (Figure 2.9). While the maximum erosion rates derived are further from the mean than minimum rate, the mean erosion rate is nearly identical to the actual mean.

The implication is that a sample taken from a surface undergoing episodic erosion may deviate substantially from the long-term average erosion rate. However, the mean of many measured erosion rates can provide an accurate estimate of the actual mean outcrop erosion rate.

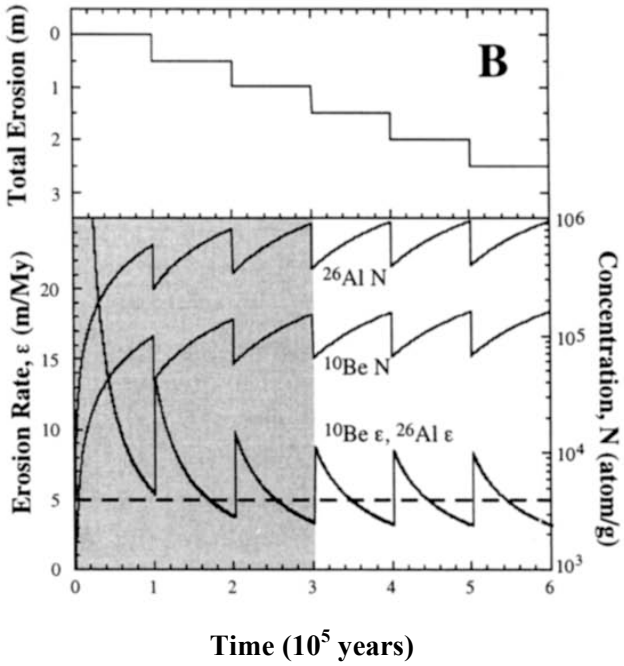

Figure 2.9 Simulation of ^{10}Be and ^{26}Al concentrations and derived denudation rates for a surface undergoing episodic removal of 0.15 m thickness followed by no erosion. (Source: Small *et al.*, 1997)

2.4.2.4 Mixed Soil/Regolith Profiles

In the preceding sections cosmogenic nuclide concentrations have been discussed in terms of an eroding bedrock surface. While this applies to features such as outcropping tors, most landscapes are mantled in a layer of regolith. In regolith, the emergence of a grain is disrupted by mixing processes like bioturbation, freeze-thaw, and soil creep (Brown *et al.*, 2003). However, Granger *et al.* (1996) show that in a well-mixed regolith the average cosmogenic nuclide concentration is the same as that derived for an eroding bedrock surface (i.e. Equation 2.6), where the regolith has thickness, x, the average concentration is:

$$N_{regolith} = N_{bedrock} + P_{regolith} t_{regolith}$$
$$= \left[e^{-x\rho\Lambda^{-1}} \frac{P_0}{\varepsilon\rho\Lambda^{-1}} \right] + \left[P_0 \left(1 - e^{-x\rho\Lambda^{-1}} \right) x\Lambda\rho^{-1} \right] \left[\frac{x}{\varepsilon} \right] = \frac{P_0}{\varepsilon\rho\Lambda^{-1}} \qquad [2.13]$$

where the average concentration in the regolith, $N_{regolith}$, is equal to the concentration inherited from the underlying bedrock, $N_{bedrock}$, and the depth-averaged production rate in the regolith, $P_{regolith}$, over the average residence time of the regolith, $t_{regolith}$.

The averaging of concentrations throughout the mixed-layer of regolith provides a useful buffer against short-term perturbations in erosion, with events like the anthropogenic acceleration of erosion, not registering an effect on the cosmogenic nuclide signal unless it removes material to the base of the mixed-layer.

2.4.3 Catchment-Averaged Denudation Rates

While the majority of research has sought to establish exposure ages and erosion rates for specific surfaces, there has been a sub-set of investigations that have attempted to use the cosmogenic nuclide concentrations in alluvial sediments to infer basin-wide denudation rates (see review Cockburn & Summerfield, 2004). Some of the early researchers, in laying out the basis for the application of in-situ cosmogenic nuclides in the earth sciences, recognised the potential use of alluvial sediment nuclide inventories for the estimation of parent rock erosion rates (e.g. Lal & Arnold, 1985). The basis for this interpretation is that a sample of sediment taken from a

stream channel will consist of many thousands of individual grains; and that in a well-mixed body of sediment these will be derived from areally diverse sources in the basin. The cosmogenic nuclide inventories of each of the grains will reflect the exposure history at its origin, and consequently, the inventory of the entire sample will provide an erosion rate integrated over the entire basin. The first applications of this approach were published in the mid-1990s in three seminal papers. Brown et al. (1995a) field-tested the approach in a small catchment in Puerto Rico, characterising major landform elements and recognising the influence of bioturbation, biomass, and local topography amongst other factors. They found that the long-term average denudation rate derived using cosmogenic nuclides (~43 mm ka^{-1}) was consistent with mass balance studies, thereby validating the technique. Similarly, Granger et al. (1996) compared the cosmogenic inventory derived denudation rate with that of well-dated alluvial fan deposit volumes, and found that these estimates agreed to within one standard error. Finally, Bierman & Steig (1996) assessed the theoretical basis and assumptions of the method and conclude that in many basins, where the key assumptions are at least approximated, this approach should provide an effective and reasonable estimate of spatially averaged rates of erosion. Subsequently, the approach has been applied to catchments in a wide range of environments (see reviews by Cockburn & Summerfield, 2004; Bierman & Nichols, 2004; von Blanckenburg, 2005).

The fundamental concept that underpins the approach is that the basin or fluvial system studied is in isotopic steady state. This requires the production of *in situ* cosmogenic isotopes over the land surface of the catchment (I_{IN}) to be equal to that removed from the system (I_{OUT}) through weathering and transport ($I_{TRAN} = I_{SOL} + I_{SED}$) or in the case of radioactive isotopes also through decay (I_{λ}). Given a landscape in isotopic steady state, it follows that it must be in erosional equilibrium with the flux of weathered material leaving the system invariant over time. This conceptual model (Bierman & Steig, 1996) can be characterised as:

$$I_{IN} = I_{OUT} = I_{\lambda} + I_{TRAN} = I_{\lambda} + I_{SOL} + I_{SED}$$

$$\text{therefore, } N_{IN} = N_{OUT} = \text{constant} \qquad [2.14]$$

The calculation of a denudation rate from cosmogenic nuclide concentration in alluvial sediment is based on the same principles as those for a incrementally eroding rock outcrop, Equation 2.8 (Lal, 1991). However, in a catchment with spatially non-uniform denudation, the relative importance of the radioactive decay correction will vary depending on denudation rate. Bierman & Steig (1996) note that for three sub-catchments (A_1-A_3) of differing denudation rates:

$$\frac{\overline{P}_0}{\lambda + \overline{\varepsilon}\rho\Lambda^{-1}} \neq \frac{P_{A_1}}{\lambda + \varepsilon_{A_1}\rho\Lambda^{-1}} + \frac{P_{A_2}}{\lambda + \varepsilon_{A_2}\rho\Lambda^{-1}} + \frac{P_{A_3}}{\lambda + \varepsilon_{A_3}\rho\Lambda^{-1}} \quad [2.15]$$

the averaged cosmogenic nuclide concentration is not equal to the sum of its isotope reservoirs, the consequence of variable decay. This is problematic for the application of radionuclides to catchment-averaged denudation rates; however, Bierman & Steig (1996) conclude that for long-lived radionuclides like ^{10}Be (λ = 1.51 Ma) the error introduced by spatial heterogeneity of denudation is low, particularly when denudation rates are high enough (more than several mm ka^{-1}) and sediment storage time is short (less than several 100 ka^{-1}). The decay correction can be neglected and the average concentration ($\overline{N}$) an be calculated as:

$$\overline{N} = \frac{\sum_i A_i P_{A_i}}{\sum_i A_i \varepsilon_{A_i} \rho\Lambda^{-1}} = \frac{\overline{P}_o}{\overline{\varepsilon}\rho\Lambda^{-1}} \quad [2.16]$$

where the sum of concentrations in all catchment areas (A_i) is equal to the average concentration ($\overline{N}$), which is a function of spatially averaged nuclide production rate ($\overline{P}_0$) and erosion rate ($\overline{\varepsilon}$).

The catchment-averaged denudation model is based on the same set of assumptions as the surface erosion model (i.e. Lal, 1991), with some additional considerations. Bierman & Steig (1996) identify these as follows: (i) the rate of denudation is constant,

but not necessarily uniform; (ii) the catchment is in isotopic steady state; (iii) sampled sediment is spatially and temporally representative of all sediment leaving the catchment, i.e. it is well-mixed; (iv) mass loss in the catchment is occurring primarily by incremental surface lowering; and (v) the mineral selected for isotopic analysis is uniformly distributed through the catchment, i.e. lithology and non-selective dissolution. Although these assumptions will invariably be violated in a natural setting, the accuracy of the method is usually sufficient for many applications, especially given the uncertainty inherent in other methods of estimating denudation (von Blanckenburg, 2005).

2.5 Cosmogenic Nuclide Sample Analysis and Calculations

This section details the preparation of sample targets, analysis at the SUERC AMS facility, calculation of sample nuclide concentrations, and finally the derivation of exposure ages and denudation rates. The results are presented in the relevant sections of Chapters 3, 4, and 5.

2.5.1 ^{10}Be Target Preparation

This section describes the procedures followed in the preparation of samples for analysis of ^{10}Be concentrations by AMS. All such work was conducted at the University of Edinburgh's Cosmogenic Nuclide Laboratory during the period 2004-2006. It is based on the laboratory protocols described by Binnie (2005), with some adaption for individual sample requirement. These protocols are largely an adaptation of protocols developed by Kohl & Nishiizumi (1992) and Bierman *et al.* (2002). Further details of sample preparation are given in Appendix I.

Physical preparation of samples is required to yield sediment grain-size appropriate for the quartz separation process. Rock samples were crushed and sieved to yield 250-710 μm size fraction, while regolith and alluvial sediment were only sieved to 250-710 μm to avoid over representation of larger grain sizes. The purification of quartz separates involved agitation in weak HCl, followed by acid digestion in ~1%

HF and ~1% HNO_3 (in 2004) or ~ 35% H_2SiF6 and ~1% HNO_3 (from 2005). Heavy liquid separation in sodium heteropolytungstate solution (LST) and magnetic separation then removed minerals of density greater than quartz. A sample of 40-60 g was then etched repeatedly in a solution of dilute ~2% HF and ~1% HNO_3 (at 7 g L^{-1}), with rinsing in 15 and later18 MΩ H_2O. The purified and etched quartz separates were then spiked with ~250 μg of beryllium carrier solution standard 1000 mg L^{-1}, and dissolved in concentrated ~48% analytical grade HF. Perchloric fuming was used to convert insoluble fluorides to perchlorates, and an anion exchange column to remove Fe from samples. By adjusting the solution to pH 3.8-4.0 titanium contaminants were precipitated. The Be fraction of solution was separated using cation exchange column chromatography. Finally, $Be(OH)_2$ gels were precipitated at pH 8-9, oxidised to BeO over a butane-propane flame (2004-2005) or high temperature furnace (2006), mixed with Nb and pressed into target cathodes for AMS analysis.

Table 2.1 Sample Submission to the SUERC AMS Facility

AMS Run	Run ID	Primary Standards	Samples Submitted	Blanks Submitted
Feb-05	22Feb05-Be-S1-2	b217-nist; b228-nist; b240-nist; b250-nist	HW1B; HW2B; HWBS1; BT2D	D-NOVBLA
Dec-05	20051215-Be-S1	b469-nist; b480-nist; b490-nist; b502-nist; b512-nist; b522-nist; b532-nist; b542-nist; b552-nist; b564-nist; b576-nist Secondary: kn51; kn52	MV01(250); MV01(710); ED01; TB01; KN02; UCB01; WD01; SM01; EO01; WB01; SAT01	JHH-B2*; JHH-B3
Jun-06	20060629-Be-S1	b798-nist; b800-nist; b810-nist; b820-nist; b830-nist; b840-nist; b850-nist; b860-nist; b870-nist; b880-nist; b890-nist; b900-nist; b910-nist; b917-nist;	BF1(1); BF1(2); BF2(1); BF2(2); BF3(1); BF3(2); BT2C	JHH-B5
Nov-06	20051026-Be-S1	b1161-nist; b1162-nist; b1176-nist; b1190-nist; b1230-nist; b1258-nist	HWPIT2; M2; M3; R2; R3; HW1G(2); HW1G(4); LT03; GLT2; GLT3; GLT4; GLT5; KT03; DT01; HWBS2; GLT1A; GLT1B; HWPIT4; HWPIT4; HW5D; HW5F; HW1A; R1; BF2(3); M1	JHH-B7; JHH-B6; JHH-B4; JHH-B8

Feb-05, Dec-06 & Jun-06 nominal ratio = 3.00 E-11
Nov-06 nominal ratio = 3.06 E-11

2.5.2 Accelerator Mass Spectrometry

The analysis of ^{10}Be samples was undertaken at the AMS laboratory of the Scottish Universities Environmental Research Centre (SUERC) in Scotland. This recently established facility measures isotope ratios using a National Electrostatic Corporation (NEC) 5MV Pelletron accelerator mass spectrometer (Freeman *et al.*, 2004; 2007). A total of 47 sample targets and 8 process blanks were submitted to the facility; these were analysed in four ^{10}Be AMS runs in 2005-2006 (Table 2.1).

The SUERC AMS is shown in Figure 2.10; details of its operation are given in Freeman *et al.* (2004; 2007), Maden *et al.* (2007), and Schnabel *et al.* (2007). The sample material in a target cathode is sputtered by a high intensity positive ion source (6 keV Cs^+ primary beam) to produce a beam of negatively charged secondary ions, $^{10}Be^{16}O^-$ and $^{9}Be^{16}O^-$. These are then passed through an electrostatic deflection unit and a low-energy magnetic analyser. This negatively charged ion beam is then accelerated towards the high voltage terminal of a 5MV Pelletron accelerator, where an argon gas stripper breaks up molecules and removes electrons from the incoming negative ions to produce $^{10}Be^{3+}$ and $^{9}Be^{3+}$. The now positively charged ions are accelerated away from the terminal and towards a magnetic analyser that deflects ions dependent on weight. The stable isotope $^{9}Be^{3+}$ is diverted into Faraday cups, which measure the electrical current to determine abundance. The rare $^{10}Be^{3+}$ is further analysed with an electrostatic deflector and passes through a gas absorber cell (to suppress interfering ^{10}B) before each atom is counted in a 5-segment gas ionisation detector, which further segregates ions based on their incoming trajectory and corresponding energy loss signal.

The SUERC AMS can accommodate up to 134 cathodes on a wheel for a ^{10}Be run; these will be a combination of submitted targets (sample and blanks) and SUERC-NIST standards. Each cathode is run a minimum of three times with additional measurements (up to six) until required precision in reached or the sample is exhausted. The facility returns a $^{10}Be/^{9}Be$ ratio of the target as well as a 1σ uncertainty of the measurement.

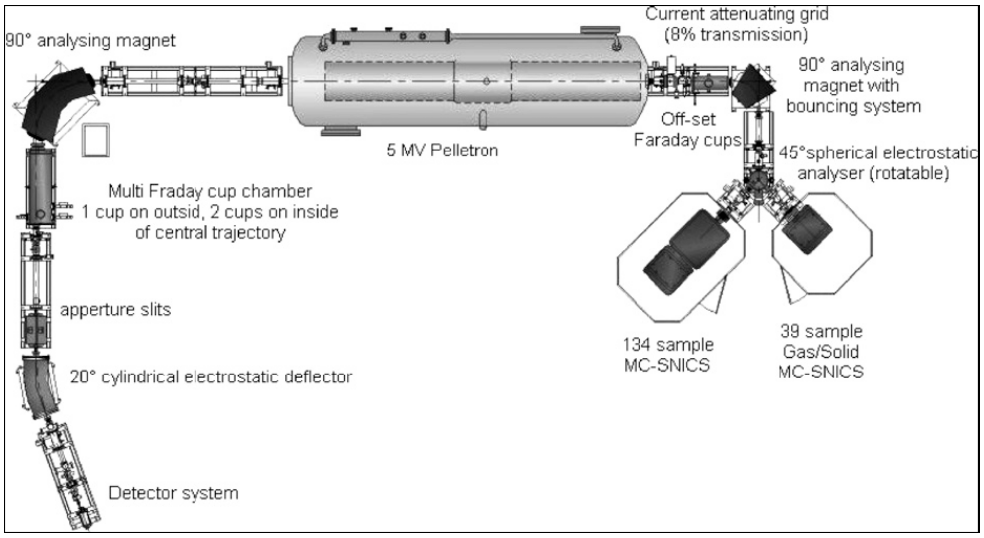

Figure 2.10 Schematic layout of the SUERC accelerator mass spectrometer

Source: Maden *et al.* (2007)

2.5.3 Calculation of ^{10}Be Concentration

The $^{10}Be/^{9}Be$ ratio measured by the AMS facility must be converted to a measure of the ^{10}Be concentration in the sample. From the $^{10}Be/^{9}Be$ ratio, the number of ^{10}Be atoms can be calculated given the mass of ^{9}Be carrier solution added during processing (m_c) and the constants of Avogrado's Number (N_A = 6.02214179 ± 0.00000030 x10^{23} $mole^{-1}$)[1] and the Atomic Weight of Beryllium (A_{Be} = 9.012182)[2]. The $^{10}Be/^{9}Be$ ratio returned for the sample contains not only ^{10}Be from the dissolved quartz, but also additional ^{10}Be that has contaminated the sample during post-dissolution processing. To account for this a processing a blank is also run with each batch of samples. The number of ^{10}Be atoms in the blank are subtracted from that measured in the sample. To achieve a concentration, the total number of ^{10}Be atoms is divided by the mass of quartz dissolved (m_{qtz}) to provide a measure of ^{10}Be atoms g^{-1} of quartz. The calculation of ^{10}Be concentration is as follows:

$$\frac{\left[{}^{10}Be/_{9}Be_{(sample)}\, m_{c(sample)}\left(\frac{N_A}{A_{Be}}\right)\right]-\left[{}^{10}Be/_{9}Be_{(blank)}\, m_{c(blank)}\left(\frac{N_A}{A_{Be}}\right)\right]}{m_{qtz}} \qquad [2.17]$$

[1] Avogrado's Number – *2006 CODATA recommended values* http://physics.nist.gov/cuu/constants.

[2] ^{10}Be atomic weight – Sansonetti & Martin, *Handbook of Basic Atomic Spectroscopic Data*, http://physics.nist.gov/PhysRefData/Handbook

It is also necessary to calculate the uncertainty associated with the concentration. The AMS facility returns a 1σ uncertainty for the measurement of the $^{10}Be/^{9}Be$ ratio for each sample and blank analysed, for most samples submitted as part of this research this value was 3-5%. In equation 2.17, an uncertainty will be associated with each term, although many of these will be insignificant given the AMS analytical error. The mass of carrier solution is attributed uncertainty of 2%, while measurements of quartz mass are considered accurate to ±0.005g, both conservative estimates. The uncertainty associated with the constants is insignificant in calculations. An estimated uncertainty of 3% for sample preparation was used in accordance with estimates of Gosse & Phillips (2001; p1545).

2.5.4 Exposure Age and Erosion Rate Calculations

The concentration of ^{10}Be in a sample is not, in itself, of geomorphological interest. To interpret either an erosion rate or exposure age, it is necessary to model the production rate of cosmogenic nuclides at the site. There are various approaches to calculating these rates (see Section 2.2). In the interest of presenting results that are easily reproduced, consistent, and have widely accessible documentation, the CRONUS-Earth Online Cosmogenic Nuclide Calculator (http://hess.ess.washington.edu/math) was used to calculate erosion rates and exposure ages for samples.

The online calculator is described in detail on the website (above) and by Balco *et al.* (2008). It is based on MATLAB scripts developed by Greg Balco and is made available for data submission to a centralised web server (the MATLAB scripts are also available to download). The data presented in this manuscript was submitted to the server in August 2007 when version 2.0 of the calculator was in operation (with the exception of muons component version 1.1).

2.5.4.1 Input to the Calculator

An advantage of using the CRONUS-Earth online calculator (or other standardised alternatives, e.g. Vermeesch (2007) MS Excel add-in CosmoCalc) is that some consistency can be established for the processing of input data. The data input is described here.

Latitude & Longitude:

Measured in the field using handheld GPS. The latitude and longitude are used for spatial scaling of production models. These correct production rates for the varying influence of the geomagnetic field on incoming radiation. For samples from rock outcrops, boulders, and regolith, the latitude and longitude measured at the sampling location is appropriate. For alluvial samples used to infer a catchment-averaged erosion rate it would be most accurate to calculate the effects of varying latitudes across the catchment. Dartmoor spans < 0.3° latitude, individual catchments even less. Consequently, there is no significant influence of latitude within Dartmoor and it is acceptable to use the sampling site coordinates as input data from alluvial samples.

Elevation: The elevation of the site is used to approximate the atmospheric depth through which cosmic radiation must be attenuated before reaching the Earth's surface. This scaling is included in the production rate models. Elevation was derived at most sampling sites from ordinance survey maps and calibrated pressure altimeter readings. At the High Willhays, the tors were surveyed using a total station and elevations tied to the local trig point. For rock outcrop, boulder, and regolith samples the elevation measured is appropriate for entry into the online calculator.

At present, the online calculator is only implemented for surface erosion rates and exposure ages. This is problematic for catchment-averaged erosion rates derived from alluvial sediments, as these consist of grains exposed to cosmic radiation at a range of elevations throughout the catchment. The relationship between elevation and production rate can be complicated and non-linear. The correct calculation of production rate for alluvial samples requires the implementation of a topographic model (e.g. Codilean, 2006) for the catchment (Balco *et al.*, 2008) (this is also the case for topographic shielding and latitudinal variations). The input of an average elevation for the catchment is a simplification and can lead to the incorrect calculation of production rates. Over the elevation range of Dartmoor there is an up to 30% difference in calculated production rates (Figure 2.1), and while the median elevation of the catchment may be a reasonable approximation for production rate,

an uneven distribution of elevation within the catchment could lead to inaccurate estimation.

For the results from alluvial sediments presented in this study, the average elevation of the catchment was derived as a median from digital elevation models (DEM). Although it would not be too difficult to derive production rates in a catchment using a GIS model and a scaling model, this would lead to inconsistency in applied production rate models as the CRONUS-Earth online calculator uses modified versions of scaling models. In the interest of internal consistency when comparing samples within the study area (e.g. tor vs. alluvial) the errors associated with inputting a average elevation were decided to be preferable to using differently derived and implemented production models.

Density: A density of 2.6 g cm^{-3} was used as an input value for all samples. This is a reasonable approximation for density of unweathered granitic bedrock. Although the density of regolith will be lower, it was not measured for Dartmoor. However, ^{10}Be derived denudation rates reflect lowering of the surface in steady state, so the regolith density is unnecessary.

Sample Thickness: The thickness of bedrock and boulder samples was measured and input into the online calculator, and a scaling factor derived (see section 2.3.4). For regolith and alluvial samples the thickness is presumed to be 0.

Shielding Correction: A shielding scaling factor was derived for three samples taken from vertical or sloping surfaces of tors. These were estimated from the numerical solutions of Dunne *et al.* (1999) for sloping surfaces (see Section 2.2.3.1). For all other samples there wasn't a significant shielding effect and a value of 1 was input.

^{10}Be Concentration: The derivation of the ^{10}Be concentration for a sample is described in Section 2.5.3. The concentration and 1σ uncertainty for each sample is input into the online calculator.

2.5.4.2 Calculations in the Program

The CRONUS-Earth online calculator provides modelling of production rates based on all the main currently available scaling models: Stone (2000); Dunai (2000); Lifton *et al.* (2005) and Desilets *et al.* (2006). However, there are some significant modifications and deviations in the way in which these models are implemented; these may have significant impacts on the calculated results.

To improve comparison of the various production rate scaling models, each has been re-normalised to the same calibration data set. The use of a single calibration set allows for comparison of results from the different models. It is important to note that one of the by-products of this re-normalisation of the models is that SLHL production rates are recalculated (Table 2.2).

Table 2.2 Reference production rate (atoms g^{-1} a^{-1}) inferred from the re-normalised calibration data set (Balco *et al.*, 2007)

Production Scaling Model	Reference (spallation) Production Rate (SLHL)
Stone (2000)	4.94 ± 0.45
Dunai (2000)	4.89 ± 0.60
Lifton *et al*. (2005)	5.37 ± 0.55
Desilets *et al*. (2006)	4.87 ± 0.60

To further aid in the comparison of results, the online calculator also applies a standardised model for variations in the geomagnetic field to all scaling schemes. This model is described in detail in Balco *et al.* (2008).

A muonic scaling based on the Heisinger (2002a; 2002b) production rates is applied by the calculator to all production models. The derived muonic production rates do not consider the effect of the geomagnetic field on muons; as such they are only modified by atmospheric depth and do not vary with time or latitude. This is a simplification that may lead to inaccuracies, although Balco *et al.* (2008) suggest that these are likely to be insignificant.

2.5.4.3 Output from the Calculator

The output of results from the web-based CRONUS-Earth online calculator is as a standardised form. This first reports results that are not dependent on the choice of production scaling model: (i) the muonic production rate which is derived by a single means; (ii) the thickness scaling factor and shielding factor which are derived from input variables; and (iii) the internal uncertainty of the sample which is derived solely form measurement errors in the nuclide concentration. It then reports either the exposure age or erosion rate of samples and the associated external uncertainty that includes an estimate of errors from the production models. The spallation production rate is also reported for the Stone (2000) scaling production model.

There are some limitations to this standardised form in the version of the online calculator used. The internal uncertainty is reported as an absolute value of m Ma^{-1}. The internal uncertainty being independent should be a value relative to all erosion rates or exposure ages, i.e. a percentage uncertainty. As reported, it is only the appropriate internal uncertainty for the Stone (2000) production scaling model. It is relatively straightforward to convert the reported value to a relative uncertainty and then apply this to the erosion rates calculated for each of the production models. In addition, spallation production rate is only reported for the Stone (2000) scaling model.

These and other variables of interest are calculated during the running of the MATLAB scripts on which the calculator is based. However, they are not reported in the simplified web-server based output forms. The original MATLAB programming is available on the website.

2.6 Conclusion

The development of geomorphological applications for measurements of *in situ* cosmogenic nuclide concentrations has lead to increasingly widespread use in the geosciences. This chapter has provided an overview of the systematics of cosmogenic nuclide production at the Earth's surface, the modelling of which is fundamental to

the approach. It also provides a background on the interpretative models for the calculation of surface exposure and denudation rates. This provides the basis for the application of measured ^{10}Be concentrations to the development of specific landforms (tors and blockslopes) and estimation of catchment-averaged denudation rates in Dartmoor. The final section details the processing and analysis of samples, as well as the calculation of exposure ages and denudation rates.

3: The Formation of Tors

3.1 Introduction

> "Everyone knows the tors of Dartmoor. They rise as conspicuous and often fantastic features from the long swelling skylines of the moor, and dominate its lonely spaces to an extent that seems out of proportion to their size. Approach one of them more closely and the shape that seemed large and sinister when silhouetted against the sunset sky is revealed as a bare rock mass, surmounted and surrounded by blocks and boulders; rarely will the whole thing be more than a score or so feet high. But if on closer examination the tor loses something of grandeur it loses nothing of its strangeness."
>
> (Linton, 1955; p470)

This was the description of the Dartmoor tors given by Linton (1955) in the opening of his seminal paper on tor formation, now widely considered a 'classic' paper in geomorphology (Gerrard, 1994; Campbell *et al.*, 1998). The 'strangeness' of the tors has attracted geomorphological interpretations of their formation for nearly two centuries. Early investigators identified the key concepts of differential subsurface weathering and periglacial processes to explain tors, as well as discounted notions of tors as relict sea stacks or formed by wind-driven sand (see review by Campbell *et al.*, 1998). However, it was the conceptualisation of two 'models' of tor formation in the 1950s that has formed the basis for most subsequent theories and discussions (Campbell *et al.*, 1998). Linton (1955) proposed a two-stage formation in which there is differential weathering in the subsurface followed by the stripping of incoherent growan leaving a tor outcrop. An alternative hypothesis was proposed by Palmer & Neilson (1962), who built upon earlier work in the Pennines (Palmer, 1956; Palmer & Radley, 1961), to suggest that tor development was a single-phase process occurring under periglacial conditions. Subsequent research has focussed primarily on the conditions under which subsurface weathering of granite occurred (Eden & Green, 1971; Doornkamp, 1974; Dearman & Bayes, 1978) and the classification of tors based on their jointing structure, geomorphology, and petrography (Gerrard, 1978; Ehlen, 1991; 1992). Despite continued interest in the Dartmoor tors, the mechanism of their formation has remained enigmatic. This has lead some to suggest that tors may be generated by different processes in the same landscape, and even that they may be a good example of equifinality (Gerrard, 1984; French, 1996).

The broader geomorphological significance of the Dartmoor tors largely arises from their importance in the development of the two-stage concept of landform development. In his discussion of the 'problem of tors' in Dartmoor, Linton (1955) "formalised and provided the essential scientific underpinning for two-stage ideas that were in circulation at the time" (Twidale, 2002; p49). These concepts of two-stage landform development feed back into other regions and environments (arid and tropical), and Twidale (2002) suggests "… the revival and present wide acceptance of the two-stage concept are due largely to Linton and Büdel" (p48). The Linton (1955) article on the 'problem of tors' has generated ongoing research over the last 40 years, and continues to be extensively cited (Gerrard, 1994).

In previous studies of tor development, there has been no means available to directly assess the age and erosion rates of tor landforms. Researchers have relied on observation of the physical properties of landforms and deposits, the interpretation of which has often been equivocal (e.g. roundness of blocks, or the conditions required for growan development). Yet this is of critical importance to understanding the development of these landforms and assessing the different 'models' of tor formation. In this study, ^{10}Be concentrations were measured in twenty samples from tor and bedrock surfaces and a further six samples from regolith. These were collected from six tor groups in north-western Dartmoor, although the majority of samples analysed were from the High Willhays and Great Links Tor groups. The results of these cosmogenic nuclide analyses are used as an indicator of the near surface history of exposure of the samples, and allow for the quantitative assessment of the timescale of landform development and an estimate of long-term surface erosion rates. This is the first time that such data has been available for the tors of Dartmoor and it is used to assess the feasibility of different 'models' of landform development.

3.2 Geomorphological Context

3.2.1 Dartmoor Tors

The tors of Dartmoor are diverse in form, with appearance ranging from precariously stacked piles of blocks to outcrops that seem little more than rubble. Palmer & Neilson (1962) make a distinction between massive and lamellar structures

in tors, with the former dominated by strong vertical joints and the latter by closely spaced pseudobedding of horizontal joints. The key factor that appears to distinguish the tors and determine their shape is the spacing of horizontal and vertical joints in the granite, although other factors such as mineralogy, grain-size and texture are probably an influence (Ehlen, 1992).

In a series of papers, Gerrard (1978) and Ehlen (1991; 1992; 1994) evaluated the importance of these various factors on the development of tors and their position within the landscape. These classified tors into three types based on their landscape position: summit, valley-side and spur. They were able to demonstrate semi-quantitatively variations in the tor attributes based on these spatial associations, and provided some rudimentary models of tor evolution based on landscape position (e.g. Ehlen, 1991). Ehlen (1992; 1994) provides a detailed examination of geomorphic, structural and petrographic variables for 48 tor groups across Dartmoor. In doing so, she observed a wide range in the joint spacing of tors, the results of which are summarised in Table 3.1.

The most distinctive and visually compelling of the Dartmoor tors, and perhaps as a consequence those that have received the most attention, possess a 'cyclopean masonry' in which blocks with 'rounded and pillowy forms' are stacked in an apparently precarious arrangement, likened by Linton (1955) to a 'great heap of piled woolsacks'. In some cases the widening of joints and rounding of blocks will even produce 'rocking-stones' or 'logan-stones' that can be moved by hand (Linton, 1955). While these tors may give the impression of a pile of individual blocks, the joints are typically only weathered to a shallow depth and the outcrop is one coherent mass (Palmer & Neilson, 1962). Tors with this delicate, stacked superstructure are fairly common in Dartmoor. Figure 3.1 shows the 'pinnacle' or 'steeple' form of the Great Staple Tor and the rounded edges and complex overhanging form of Vixen Tor, both in the Merrivale area of central Dartmoor.

(a)

(b)

Figure 3.1 Tors with 'cyclopean masonry'; a stacked superstructure and widely spaced joint sets at (a) Great Staple Tor and (b) Vixen Tor.

Table 3.1 Summary of structural characteristics of Dartmoor tors (from data in Ehlen, 1994)

	Mean Vertical Spacing (cm)		Mean Horizontal Spacing (cm)	
	Primary	Secondary	Primary	Secondary
Of 48 tor groups studied:				
Median	246	64	72	13
Minimum	75	18	25	5
Maximum	959	192	160	28

Although tors with a precariously stacked superstructure are amongst the most distinctive landforms, there is a far more diverse range of tor form in Dartmoor. Palmer & Neilson (1962) highlight the widespread occurrence of lamellar structures in tors, in which closely spaced horizontal jointing (or pseudobedding) and poorly developed vertical joints produce a tor with a more tabular or humped form. These include some of the largest tors in Dartmoor, such as Haytor (Figure 3.2) and the Great Links Tor (Section 3.5). There are also numerous smaller lamellar tors that feature strongly developed pseudobedding and take on rounded-tabular form (e.g. High Willhays tor HW1; Section 3.4) or a flat slab-like structure (e.g. Wind Tor, Figure 3.3).

There are also examples of tors in Dartmoor in which little structure has been developed or maintained. These tors have a 'ruined' appearance in which the intact bedrock is surrounded by blocks derived from the collapse and disruption of the outcrop. Examples of these include Sharpitor (Figure 3.4) and the metadolerite Cox Tor (Figure 3.5). As with other tors, the determining factor in the form of these tors appears to be joint spacing. It appears that closely spaced vertical joints are well-developed in these outcrops and favours the formation of blocks. There may not be a large difference between tors with delicate 'pinnacle' superstructures and those with a 'ruined' appearance. Both appear to be controlled by closely spaced vertical joints. Palmer & Neilson (1962) also suggest that landscape position and local slope may influence the form of the Sharpitor outcrop by enabling the transportation of blocks.

Figure 3.2 The massive lamellar Haytor, the largest tor outcrop in Dartmoor

Photo: David Mitchell – flickr/davidmitchell

Figure 3.3 Wind Tor with a flat slab-like structure and close horizontal jointing

Photo: Richard Knight – www.richkni.co.uk

Figure 3.4 Sharpitor with a closely spaced joint sets and a blocky 'ruined' appearance with collapse of structure.

Photo: Richard Knight – www.richkni.co.uk

Figure 3.5 The metadoleritic Cox Tor with blocky appearance and closely spaced joint sets, although few detached blocks.

Photo: Richard Knight – www.richkni.co.uk

3.2.2 Two-Stage Development

The two-stage development of tors was famously argued by Linton (1955) based on an interpretation of sites in Dartmoor. He suggested that deep-weathering of granite (during tropical climates in the Tertiary) had occurred in which there was 'profound rock rotting effected by groundwater and guided by joint systems' (p476) producing heavily decomposed granite (growan or grus) juxtaposed with residual masses of unaltered bedrock and isolated corestones. A tor is a surface expression of this residual mass of granite that is exposed following a 'phase of mechanical stripping of the incoherent products of chemical action' (Linton, 1955: p476), typically ascribed to periglacial conditions during the Pleistocene. As the efficacy of weathering is determined by joint spacing, variations in the structural characteristics of the granite bedrock will lead to differential weathering of the landscape. Accordingly, tors form in locations where joint spacing is the widest and weathering the less intensive. This 'model' of tor development is shown schematically in Figure 3.6.

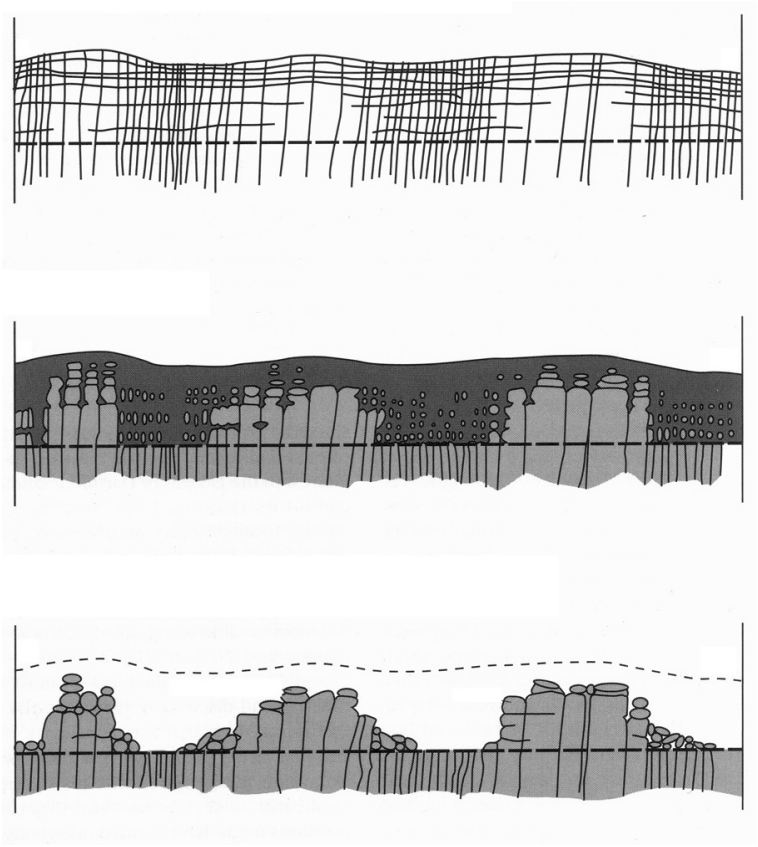

Figure 3.6 Two-stage 'model' of tor formation proposed by Linton (1955); through initial jointed bedrock, a phase of deep-weathering, and the stripping of unconsolidated material.

Source: Campbell *et al.* (1998); after Linton (1955)

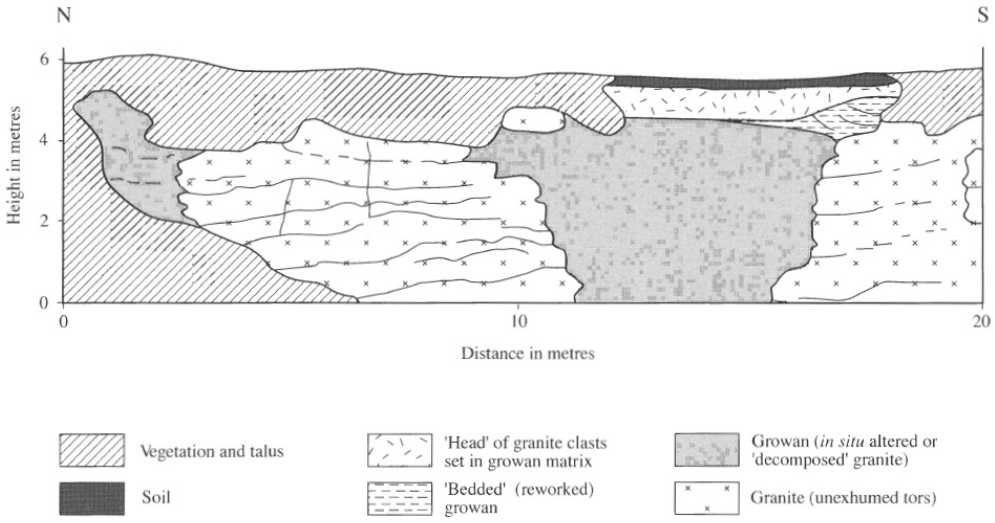

Source: Campbell *et al.* (1998)

Figure 3.7 The exposure at Two Bridges Quarry revealing a cross-section that juxtaposes unweathered granite with *in situ* decomposed growan

There is clear evidence for differential weathering/alteration of granite in the subsurface in Dartmoor. The most important site is the Two Bridges Quarry near Princetown in central Dartmoor. The quarry wall (some 20 m long and 6 m high) provides an excellent section that exposes areas of *in situ* decomposed granite juxtaposed between masses of unaltered bedrock granite (Campbell *et al.*, 1998; Figure 3.7). This section was key to Linton's (1955) proposal that differential subsurface weathering of granite forms tors. While subsequent research has challenged or modified some of the interpretations of this site (Palmer & Neilson, 1962; Brunsden, 1964; Green & Eden, 1971; Doornkamp, 1974; Dearman & Baynes, 1978), it is unquestionably evidence that subsurface alteration of the granite (by whatever mechanism) can lead to the generation of tor-like forms of residual bedrock.

In the present Dartmoor landscape, there is an uneven distribution of decomposed granite. There is no evidence of remnants of decomposed granite in proximity to the tors at Merrivale (e.g. Great Staple Tor, Vixen Tor etc) or other major tor outcrops in Dartmoor, and in most cases the depth of regolith on summits and interfluves is less than a few metres (Campbell *et al.*, 1998). Although this might be expected in circumstances where the tors are residual masses protruding from, as Linton (1955) termed it, the 'basal platform' of a weathering profile, it is surprising that localised weathering has not left pockets of decomposed granite. Gerrard (1984) observes that layers of head and weathered granite are generally less than 4 m thick. Eden & Green (1971) assessed the thickness of decomposed granite across the upland plateau surfaces (devoid of tors) and found depths of at most 2-3 m. They suggest that in a deeply and extensively weathered landscape, these surfaces should have been covered in a deep layer of decomposed rock enveloping unexposed tors. From these observations, Eden & Green (1971) conclude that the process of deep weathering of Dartmoor granite is localised in most cases in or adjacent to river valleys.

In some valleys, decomposed granite can reach considerable depths. The most comprehensive section of a deep weathering profile in Dartmoor was excavated during the construction the Burrator Reservoir in 1898 (Figure 3.8). The *in situ*

decomposed granite uncovered reached depths in excess of 30 m and was juxtaposed with sections of unaltered granite masses, pinnacles and corestones (Sandemand, 1901 *indirect cit.*; Palmer & Neilson, 1962; Green & Eden, 1971; Croot & Griffith, 2001). Palmer & Neilson (1962) also report findings from boreholes in the valleys of the Rivers Harter and Cowsic (very close to Two Bridges) in which decomposed granite was encountered at depths of up to 40 m, with alternating layers of weathered and unaltered granite encountered. The occurrence of deep weathering profiles in the granite is considered to be a widespread in Dartmoor, although mostly associated with river valleys (Croot & Griffith, 2001).

Linton (1955) associated the deep weathering of granite to the chemical action of groundwater, and probably during hot, humid conditions in the Tertiary. Palmer & Neilson (1962) and Exley & Stone (1964) challenged this view, instead suggesting that the alteration of granite was largely due to hydrothermal processes (i.e. pneumatolysis). In subsequent research (e.g. Brunsden, 1964; Eden & Green, 1971; Doornkamp, 1974), a combination of hydrothermal alteration, chemical and physical weathering has generally been suggested (Campbell *et al.*, 1998). This research has indicated that the decomposition of the granite is not as profound as initially suggested and did not necessarily occur under 'tropical' climate conditions. Although chemical weathering is still recognised as the most significant process in granite weathering, this action is considered more localised than originally suggested and focussed in valleys (Eden & Green, 1971).

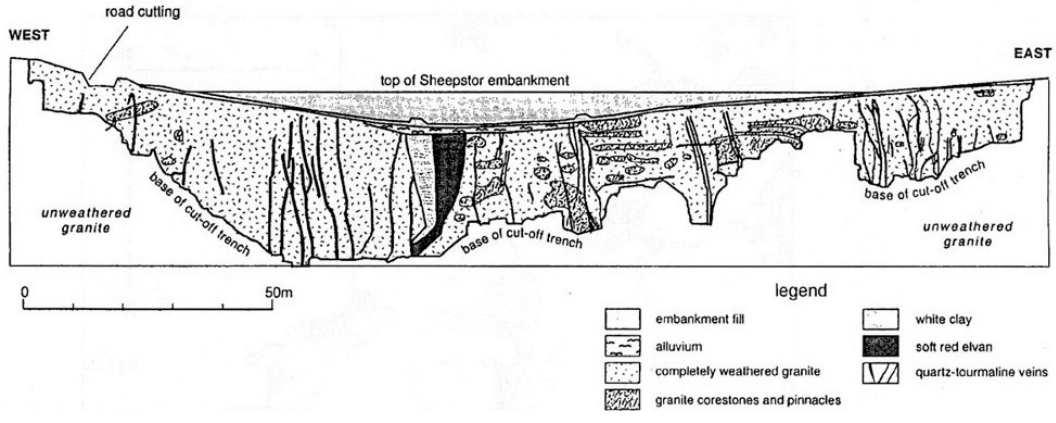

Figure 3.8 Burrator Reservoir – cross-section at Sheepstor embankment foundation showing deep-weathering of granite. NB: there is no vertical exaggeration so the scale is applicable to depth.

Source: Croot & Griffith (2001); after Sandeman (1901)

The relative contribution of different mechanisms of granite alteration is perhaps not as important as the nature and distribution of the decomposed granite. Where this exists in juxtaposition with residual masses of bedrock, it provides the basis for a two-stage development of tor landforms, irrespective of the alteration mechanism.

The second phase of the two-stage tor development 'model' involves the 'mechanical stripping of the incoherent products of chemical action' (Linton, 1955: p476). This phase was proposed by Linton (1955) to have occurred under periglacial conditions during the 'last glacial episode', where solifluction and 'melt water from ice… and snows' washed away finer material. Although understanding of timing and processes has been refined, the principle of effective periglacial processes removing regolith has been generally accepted. Te Punga (1957) recognised the impact of successive Pleistocene cold stages on Dartmoor, and southern England, as having severely denuded the landscape through 'vigorous down-wearing by mass wasting' mainly by solifluction (Campbell *et al.*, 1998). There has been a recognition of head deposits (solifluction) and a range of other periglacial landforms across Dartmoor (Waters, 1964; Green & Eden, 1973; Gerrard, 1989) which confirm the efficacy of periglacial processes.

If tors develop according to a two-stage 'model', their form and location should be largely determined by the initial phase of deep weathering. At sites like Two Bridges Quarry (Figure 3.7) there is convincing evidence that differential weathering in the subsurface can and does lead to the development of tors in Dartmoor. The question that must be asked is how ubiquitous is the two-stage development of tors? At the basis of the two-stage model is the idea that the residual mass of unaltered bedrock from which the tor is formed is a relict feature of an earlier weathering phase. The implication is that, once exposed, erosion is an entirely destructive process on tors and, consequently, that they are a transient feature in the landscape with no mechanism for renewal under contemporary conditions. On this basis, tors are only present for a period of time following their exhumation until their eventual destruction. It might be concluded that a 'true' two-stage tor occupies a

geomorphological niche, and is a transient feature associated with the base of weathering profiles.

If two-stage tors are considered a transient feature in the landscape, the rate at which they erode following exhumation becomes of critical importance. In situations in which there is minimal post-exhumation modification of the tor, these landforms may persist for considerable periods of time. However, it was recognised by even Linton (1955) that most upland tors have been 'considerably affected by exposure to the elements', and in some cases this has lead to their 'virtual destruction or collapse'. If tors are being eroded to the base of the weathering profile, then the time over which they are present is determined by the erosion rate. If the tors are being eroded rapidly they would be present for only a limited interval of time during the development of the landscape, and their widespread occurrence would not be expected.

An important aspect of the two-stage model is the idea that the form of the tor is determined in the subsurface. In situations where there is significant modification of the tor following exhumation, the degree to which the form of the tor is influenced by subsurface weathering should be considered. It may be the case that differential weathering in the subsurface is an influence on the location of a tor, but not its shape.

3.2.3 Single-Phase / Dynamic Model of Development

The two-stage 'model' of tor formation of Linton (1955) was immediately challenged in the discussion that followed its presentation (Woolridge *et al.*, 1955). The main alternative that subsequently developed was that of Palmer & Neilson (1962) who contended that tors were not relict features of deep weathering in the Tertiary, but 'upward projections of solid granite left behind when the surrounding bedrock was broken up by frost-action and removed by solifluction' (p337). This was based on the observation that 'decayed granite' was 'generally found in valley bottoms and is never found around the tors', and that tors are being actively eroded and, therefore, unlikely to have been preserved for an extensive period of time (suggesting that 'two-stage' hilltop tors would have been first exposed in the Early Pleistocene). Palmer &

Neilson (1962) provided a single-phase 'model' of tor development that involved the stripping of soil and regolith with the onset of periglaciation, followed by the break-up and removal of the granite through frost action and solifluction, resulting in tor outcrops (Figure 3.9).

The single-phase development of tors proposed by Palmer & Neilson (1962) still maintained the importance of the properties of the underlying granite, in particular, that tors were 'formed in resistant, well-jointed granites'. It assumes that tor formation is intimately linked to slope evolution, and that they reflect the remnants of frost-riven bedrock outcrops surrounded by low-angled surfaces across which frost-shattered debris is transported by solifluction and mass wasting processes (French, 1996). In subsequent work, relationships between joint structure, petrology, and landscape position were established (Gerrard, 1978; Ehlen, 1991; 1992) and the origin of decayed granites (as discussed in 3.2.2). However, the interpretation of tors and mechanisms of granite weathering remains contentious, and it is generally considered that tors may be both exposed and modified two-stage and single-phase periglacial landforms contemporaneously in different parts of Dartmoor (French, 1996; Campbell *et al.*, 1998).

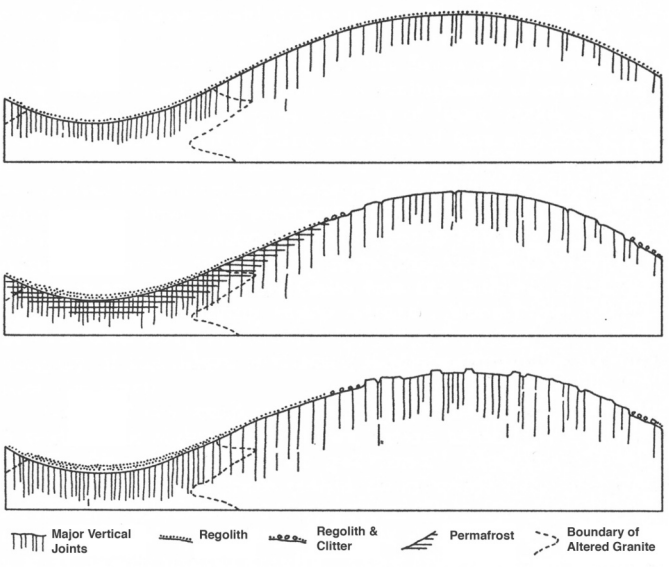

Figure 3.9 Single-phase model of tor development under periglacial processes of frost action and solifluction

Source: Palmer & Neilson (1962)

The formation of a tor is the result of an imbalance between weathering and erosion rates of these bare rock surfaces and the surrounding regolith. In recent years there has been a renewed interest in soil production functions, first outlined by Gilbert (1877) and elaborated by Carson & Kirkby (1972), to investigate regolith production rates using numerical modelling and cosmogenic nuclide concentrations (Heimsath *et al.*, 1997; 2000; Small *et al.*, 1997; Wilkinson *et al.*, 2005). This has also lead to specific consideration of tor emergence in steady state (Heimsath *et al.*, 2000), but also the potential feedback between sediment transportation and bedrock weathering in the initiation of tor emergence and the promotion of tor growth (Anderson, 2002; Strudley *et al.*, 2006a; 2006b). This is a useful concept in explaining potential mechanisms of single-phase development under a dynamic model of tor emergence from regolith mantled slopes.

The basis of a dynamic model of landscape development is the relationship between the breakdown of bedrock to unconsolidated regolith and the processes that move this loose material downslope. The balance between these is a fundamental concept in geomorphology, with slopes in either: (i) a *weathering-limited* state (or detachment-limited), in which the potential for transportation exceeds the rate at which bedrock is transformed into unconsolidated material, typical of exposed bedrock; or (ii) a *transport-limited* state, in which transportation downslope is insufficient to remove all material being generated by weathering processes, resulting in the development of a regolith/soil mantle on the slope (Carson & Kirkby, 1972).

Most slopes are mantled in some thickness of regolith indicating a prevalence of a transport-limited mode of hillslope development. These slopes are in a dynamic equilibrium between rates of bedrock weathering and transportation, with a balance between these due to a functional dependence of bedrock weathering rate on regolith thickness. This was recognised by Gilbert (1877) when he observed that "…the chief agents of rock decay, are both retarded by the excessive accumulation of disintegrated rock" (p.103). This reduction in the effectiveness of weathering processes with depth is fundamentally important. In transport-limited situations it

means that, through the development of a regolith layer, the rate of bedrock weathering is reduced to balance that at which material is removed from the slope.

This relationship between the rate of bedrock conversion to regolith and the thickness of the regolith layer can be defined as a soil production function (SPF)[1]. The concept of an SPF is useful as it provides a basis for understanding and modelling of slope development and landscape evolution. However, depending as it does on the complex interaction of weathering and slope processes as well as variability in location specific factors such as climate and lithology, the SPF remains difficult to define for many locations. There are two principle types of SPFs that have been developed; an exponential decline model and a 'humped' model.

The exponential decline model is a simplification of the SPF in which the weathering rate is at a maximum at the surface, where soil cover is absent or very thin, and declines exponentially with increasing depth of regolith (Figure 3.10). This approach has been utilised in modelling experiments in hillslope development by Ahnert (1967; cited in Humphreys & Wilkinson, 2007) and Dietrich *et al.* (1995). It has also been shown to be an appropriate model by Heimsath and co-workers, who used cosmogenic nuclides to constrain SPFs at sites in California (1999; 2000) and south-eastern Australia (2001a; 2001b).

The 'humped' model of an SPF is based on the notion that the maximum potential weathering occurs not at the surface, but under some shallow depth of regolith cover. This was integral to Gilbert's (1877) description of the relationship between rates of weathering and soil depth, where he recognised that soils act as a '… reservoir to catch rain… and store it up for the work of solution and frost, instead of letting it run off at once unused' (p.103). The concept of a humped SPF gained widespread recognition when described by Carson & Kirkby (1972; p.105), who schematically

[1] Humphreys & Wilkinson (2007) provide a recent review of the history of the soil production function; from it's inception in the descriptions of Gilbert (1877), through development and formalisation of the concept by Carson & Kirkby (1972), and finally quantitative testing of SPFs using cosmogenic nuclides in recent years by Heimsath *et al.* (1997; 2000), Anderson (2002) and Wilkinson *et al.* (2005).

represented a 'humped' relationship between the rate of bedrock weathering and soil depth (Figure 3.10). The essential feature of this 'humped' model is that weathering rates are not at a maximum at the surface, where there is a lower bare bedrock weathering rate. Instead weathering rates rapidly increase under regolith cover, reaching a maximum at a depth determined by the processes operating at the location. At depths greater than this maximum, the weathering rate is generally considered to decline exponentially in a similar way to the exponential decline model.

The shape of an SPF is determined by the properties of the bedrock (e.g. jointing, mineralogy) and the interaction of these with agents of weathering for the location. The more resistant the bedrock, the lower the potential weathering rate and the thinner the regolith, as shown by the dashed-lines in Figure 3.10(c). In general, the SPF maintains an equilibrium in the regolith between rates of weathering and erosion (Carson & Kirkby, 1972). It also acts to suppress irregularities in the bedrock-regolith interface, as at shallower depth these will be subject to increased weathering rates (Strudley *et al.*, 2006b).

The potential for tor emergence under an exponential decline SPF is limited by the weathering rate being at a maximum at the surface. If this is the case, then an exposed surface can only be present when the erosion rate exceeds the maximum weathering rate. While this would result in the exposure of bedrock, it would not allow for any regolith. The alternative 'humped' model of SPF provides a better mechanism for tor formation. Although irregularities are suppressed at depth, there is a zone of regolith thickness instability in the 'humped' SPF on the rising limb in the near surface (Figure 3.10). In these shallow depths any change in the regolith thickness will result in a positive/negative feedback (i.e. thinning → decreased weathering → thinning; and in reverse) (Carson & Kirkby, 1972; Strudley *et al.*, 2006b). This provides an effective mechanism for tor formation, especially in marginal regolith profiles where a small change in regolith thickness or the resistance of bedrock might push the SPF into instability.

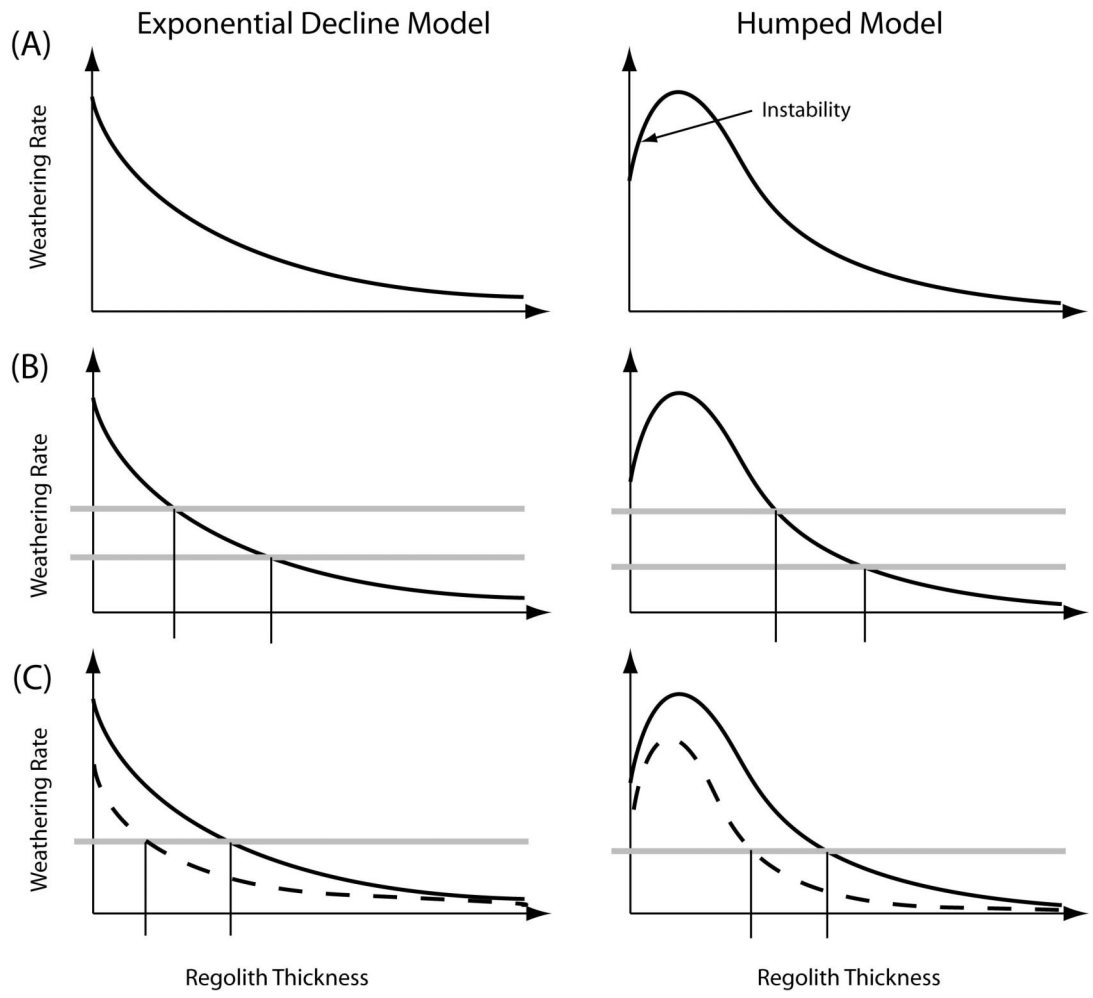

Figure 3.10 Soil production functions (SPF) in two main forms of the Exponential Decline Model and Humped Model. (a) is the basic form of each model; (b) shows how a change in regolith thickness can change weathering rate; and (c) how different shape of the function (determined by site-specific weathering processes) can produce significantly different regolith thicknesses for the same weathering rate.

The position in the landscape can also be considered in terms of SPF and the balance between the generation of regolith through weathering and removal by erosion. The mass balance on a slope is a balance between the input of regolith from upslope, that produced from underlying regolith, and that removed downslope. At the summit, or to a lesser extent on divergent slopes, the input from upslope will be reduced relative to potential for removal. This will result in thinner regolith, and while this may give rise to higher regolith production rates, it also increases the potential for incursions into instability, and thus favouring the emergence of tors.

The SPF proves a useful concept as a possible mechanism for single-phase tor emergence. In particular, an SPF approximating the 'humped' model allows for the instability of regolith thickness that might lead to the initiation of tors. It also favours outcrop in locations of either increased bedrock resistance to weathering (e.g. jointing) or topographic divergence (e.g. summit or spurs), which is compatible with observation of tor location in Dartmoor.

3.3 Research Strategy

3.3.1 Overview of Study Sites

The tors selected for cosmogenic nuclide analysis in this study are all located in the north-west of the Dartmoor granitic uplands. The summits in this area are amongst the highest elevations in the region, including the High Willhays at 621 m, which is the highest ground in southern England. This upland granitic plateau is dissected by deeply incised rivers with a basin relief of up to 400 m in catchments less than 30 km^2. The upland surfaces are covered in only a thin layer of regolith, which is less than 2-3 m thick on the nearby Okement Hill according to Green & Eden (1971). There is probably a greater depth of regolith in the valleys, although the depth is unknown in this area. Despite being on the fringe of the granitic uplands of Dartmoor, this region has comparatively limited evidence for anthropogenic impacts due in parts to its relative inaccessibility, marginal conditions for agriculture, and rugged topography. In terms of sampling bedrock outcrops this is desirable, as human manipulation and quarrying of granite blocks is frequently observed in other parts of Dartmoor (e.g. Merrivale).

In this study, only tors from a limited area of north-western Dartmoor were analysed using cosmogenic nuclides. This restriction was intended to focus the study given the limited number of analyses available, and to allow for assessment of variability of exposure of tor surfaces and the influence of landscape position. For the most part, the tors in this part of Dartmoor tend towards tabular form with lamellar structure controlled by strong closely spaced horizontal jointing or pseudobedding. This study does not cover a full range of tor outcrop types present in Dartmoor (section 3.2.1), this is an unavoidable limitation of the restricted number of analyses available for the spatially and structurally diverse range of tors that occur on Dartmoor.

The majority of analyses in this study are focussed on two principal summit tor groups at the High Willhays (621 m) and Great Links Tor (587 m). At the High Willhays the cosmogenic nuclide concentrations of three tor outcrops are contrasted with that of the regolith to provide an indication of differential rates of denudation. At the Great Links Tor group a series of outcrops are located down a slope and at different heights above regolith, which allows for the assessment of exhumation/erosion with local position. In addition, samples are taken from a further four tor groups around the West Okement Valley to extent the spatial range of tors studied and assess variations in landscape position. In total, the ^{10}Be concentration was measured in 20 samples from tor and bedrock surfaces, with a further 6 samples taken from regolith near the High Willhays tors.

3.3.2 Interpretation of ^{10}Be Concentration

The measured ^{10}Be concentration reflects the time that sampled material has been exposed to cosmic radiation in the near surface. This can be interpreted in a geomorphological context by applying models that describe nuclide accumulation at the sample site and can be used to calculate either exposure age or erosion rate for the surface, although not both (section 3.4). This section looks at the specific application of ^{10}Be to tor surfaces and regolith, and the derivation of geomorphologically useful variables of erosion rates and exposure age.

3.3.2.1 Exposure Age for Tor Surfaces

The surface exposure age model assumes a sample was collected from an 'event surface' that was effectively shielded from cosmic radiation prior to a rapid uncovering (section 3.4.1). It is necessary to consider the geomorphological scenarios of tor surface development in Dartmoor for which 'exposure ages' derived from ^{10}Be concentrations would be a valid interpretation.

The basis of the two-stage model of tor development (section 3.2.2) is that differential weathering produces the form of the tor in the subsurface, and that subsequent removal of surrounding incoherent growan reveals an intact tor outcrop. This exhumation of a tor could conceivably produce an 'event surface' that is compatible with the surface exposure age model. Even under a scenario of tor exhumation, the calculation of exposure ages will be complicated if there is significant sub-surface exposure to cosmic radiation or, more significantly, there is sub-aerial erosion of the tor surface following exhumation.

The surface exposure age model assumes that there is no exposure to cosmic radiation prior to the surface being uncovered.[2] This would require overlying material to be thick enough for cosmogenic nuclide concentrations to be negligible (at >3m depth in granite, more for regolith, the concentration approaches detection limits of measurements: Phillips *et al.*, 2006) and for the removal of this material to be an 'instantaneous event', at least in terms of cosmogenic nuclide production. In the case of tor exhumation, the 'exposure event' is the removal of overlying material to expose the tor surface. The amount of time this takes is dependent on the erosion rate, and during this uncovering the tor surface is exposed to an increasing intensity of cosmic radiation as it progresses towards the surface. During this interval of sub-surface exposure to cosmic radiation it will accumulate cosmogenic nuclides, such that when it reaches the surface it will have an inherited inventory of ^{10}Be that matches the concentration found in the eroding overlying material. The size of this inheritance is determined by the erosion rate, the faster the overlying material is

[2] It is possible to correct for ^{10}Be inheritance if this is independently known or can be estimated. The N_{inh} term in Eqn 3.4.1.

removed the less time the buried surface is exposed to cosmic radiation. Therefore, at high erosion rates the exhumation of a tor surface might approach an 'instantaneous event surface', and at lower erosion rates the inheritance will lead to a surfeit of ^{10}Be and an overestimation of the age of surface exposure. The importance of inherited ^{10}Be is relative to the length of post-exhumation exposure of the surface, the older a surface gets the proportionally less significant the contribution.

The surface of an emerged tor outcrop is exposed to the full intensity of cosmic radiation for the site location, and with no shielding by overburden ^{10}Be production rate will be at a maximum at this surface. If there is no erosion of the tor then cosmogenic nuclides will simply continue to accumulate in the surface over the interval of exposure. However, a tor outcrop will undoubtedly be exposed to subaerial weathering processes and erosion of the surface. In the case of an eroding surface, the material that is removed takes with it accumulated cosmogenic nuclides. The removal of rock from the surface also exposes 'fresh' material that had previously been partially shielded from cosmic radiation by overlying material. An eroding surface will result in a reduced abundance of cosmogenic nuclides, and consequently, if no correction is applied an underestimate of the 'true' surface exposure age.

The problems in dealing with both erosion of a surface and the age of its exposure arise from the fundamental model for the interpretation of cosmogenic nuclide data (Eqn 2.3), in which both variables of time and erosion rate are unknown. It is only possible to solve for one of these, so in order to make a geomorphological interpretation of ^{10}Be concentrations we need to know or assume a value for the other. The problem with calculating exposure ages is that it is unusual to independently know erosion rates. One approach is to assume that post-exposure erosion of the surface is negligible and calculate an exposure age based on a zero-erosion rate. This is a minimum exposure age for the surface, as any erosion would result in reduced cosmogenic nuclides and an underestimate. Alternatively, it is possible to apply a correction to exposure age calculations for given erosion rates. However, for the granite surfaces of the Dartmoor tors there is no reliable,

independent measure of erosion rates. The only previous measurement of erosion rates on Dartmoor, by Williams *et al.* (1986), was based on contemporary catchment rates that estimated a rate of 6.5 mm ka^{-1}, with 1.5 mm ka^{-1} the mechanical component (although the provenance of this is unclear). The applicability of these rates to long-term erosion of tors is highly questionable. Phillips *et al.* (2006) apply a correction of 1.6 mm ka^{-1} to cosmogenic nuclide exposure ages, based on independent measurements of granite erosion in the Cairngorms, Scotland. André (2002) reports a similar erosion rate of 1 mm ka^{-1} determined from numerous measurements in Lapland, Sweden. Although these may be comparable to subaerial weathering rates of granite in Dartmoor, they only represent rates for surfaces of coherent granite blocks.

The erosion of the tor landform, and therefore its surface, is not solely determined by the relatively low rate of subaerial weathering of exposed granite. It is widely observed on Dartmoor tors (section 3.2.1) that fracturing of the granite along joints leads to the episodic removal of blocks from the tor landform. This would potentially lead to significantly higher erosion rates for the surface of the tor landform than indicated by weathering rates of massive granite.

Although exposure ages can be calculated for a variety of erosion rates, as these rates increase in magnitude the relevance of these 'ages' must be questioned. The production of cosmogenic nuclides is inherently biased towards the surface (due to attenuation of cosmic radiation), if the surface is being eroded the nuclide signal for the 'exposure event' will transition quickly into one that informs only about the erosion rate of the landform. In applying corrections to exposure ages, there is a risk that input value for erosion rate becomes the most important factor in the calculation. This problem is compounded if the erosion rate used is poorly constrained or not known for the site.

It is important to recognise the limits to the 'exposure' dating of tor surfaces, and the specific geomorphological circumstances for which these are appropriate. The two-stage model of tor development does provide the possibility of 'true' surface exposure

dating for tor surfaces, although this is dependent on minimal post-exposure erosion of the tors. Even under the two-stage model of tor development, there is the possibility of significant modification of the tors by subaerial weathering and erosion processes, something that even Linton (1955) allowed. Despite these limitations, it is still useful to consider 'exposure ages' derived for tor surfaces. Some constraints can be placed on the time intervals over which the sampled surfaces developed. The zero-erosion exposure age sets the minimum amount of time that the sample has been exposed to cosmic radiation at or near the surface. A range of possible erosion rates can be used to make corrections to exposure age calculations, and while it may be useful to assess the impact of varying rates on ages, it must be recognised that the lack of independent controls on erosion for the Dartmoor tors limits this application.

3.3.2.2 Tor Surface Erosion Rates

The ^{10}Be concentration of a surface can be used to derive an erosion rate for a surface. This interpretation of cosmogenic nuclide data is based on the premise of steady-state erosion of the surface (both continuous and uniform through time), which results in an equilibrium between nuclide production and loss through erosion and decay (section 3.4.2). To achieve this state the erosion has to have removed a sufficient depth of material (>2-3 m of granite) to eradicate any preceding cosmogenic nuclide signature. In these circumstances, the erosion rate derived from the ^{10}Be concentration of a sample will accurately reflect the present (and ongoing) erosion rate of the surface.

If the depth of material removed under the present erosion rate is insufficient, the ^{10}Be signature will be a composite that reflects the varying rates over its residence time within a few metres of the surface. The rapid attenuation of cosmic radiation with depth means that cosmogenic nuclide production is concentrated near the surface and, consequently, there is an inherent bias towards more recent erosion. There is effectively a 'response time' for the adjustment of cosmogenic nuclides to a change in erosion rates (section 2.4), which is shorter with higher erosion rates.

As the surface of the tor first emerges from the surrounding regolith, there will be a change in denudation rate from that of the overlying material to the lower rate of the tor surface. At the time of emergence the ^{10}Be concentration of the surface will equal that of the overlying material and not that of the tor. This will be followed by an interval of transition, as concentrations adjust to the new equilibrium, until eventually enough material has been removed from the tor landform to preserve only its erosion rate signal. This adjustment is inherent in the emergence of granite from more rapidly eroding material, and consequently, a similar transition will occur regardless of the mode of tor formation (two-stage vs. dynamic). Although, under a two-stage development the tor takes its form in the sub-surface and this suggests that erosion is limited following emergence. It is probably typical of the cosmogenic nuclide signature in two-stage tors to be in a state of transition following emergence.

A requirement of the surface erosion model is that erosion is continuous and uniform over time. This is rarely likely to be the case. The weathering and erosion of a tor landform are almost certain to vary over time. If these are short-term fluctuations, they cause minor deviations in the cosmogenic nuclide signature. However, the composite nature of the signal is inherently averaged over time which limits the effect of minor deviations and provides a long-term average, which is often more useful. More significant changes to erosion rates, for example due to change from LGM to Holocene climate, will initiate a transition in cosmogenic nuclide concentrations similar to that described above for tor emergence.

The development of blocks along joint boundaries is common on Dartmoor tors (section 3.2.1). The episodic removal of these blocks from the tor surface is a violation of the surface exposure age model (see Section 2.4.2.3). A surface of a tor undergoing episodic erosion will vary between high ^{10}Be concentrations prior to removal to substantially reduced ^{10}Be concentrations on the newly exposed (and previously shielded) surface following block removal. Although the mean erosion rate of the tor surface over time (or substituting space; as did Small *et al.*, 1999) will be reflected in the cosmogenic nuclide concentrations, it is important to recognise that variation between samples is expected.

To determine an average erosion rate for these surfaces it is necessary to collect a number of samples representing the distribution of cosmogenic nuclide concentrations. In this study, sampling was probably biased towards surfaces exposed for longer periods of time as weathering of the granite and joints provided weakness that could be exploited with hammer and chisel.

3.3.2.3 Regolith Erosion Rates

The cosmogenic nuclide concentration in regolith is determined by: (i) ^{10}Be production within the regolith; (ii) ^{10}Be included from the weathering of underlying bedrock; (iii) loss through the dissolution of quartz; (iv) loss through radioactive decay; and (v) removal by denudation (Small *et al.*, 1999). The concentration of cosmogenic nuclides will be relatively uniform with depth in a well-mixed profile, as shown in Figure 3.11. For a steady-state erosion rate, the cosmogenic nuclide concentration of a well-mixed regolith is equivalent to that of an eroding bedrock (or unmixed) surface (Small *et al.*, 1999). Even a short-term disturbance to the regolith does not significantly alter the averaged ^{10}Be concentration in a well-mixed profile (Figure 3.11: truncated profile).

The ^{10}Be concentration measured in vertically mixed regolith has the potential to provide long-term estimates of denudation rates (and regolith production). The mixing of regolith also provides a buffer against short-term variations in erosion rates, unlike that of a tor surface (i.e. episodic erosion). However, assumptions that should be recognised (or corrected for) are: (i) the thickness of regolith (or mixed layer) is steady over the interval relevant to cosmogenic nuclide production; (ii) there is steady-state erosion; and (iii) there is no selective dissolution in the regolith (Small *et al.*, 1999).

The preferential dissolution of non-quartz minerals in the regolith can lead to quartz enrichment, with quartz grains spending a disproportionate length of time in the regolith exposed to cosmic radiation. Consequently, the denudation rate derived from the measurement of ^{10}Be in quartz grains will be an underestimate of the regolith denudation rate. If there is significant differential dissolution occurring in the

regolith the errors involved could be significant, however, in all but extreme weathering environments bias due to differential dissolution will be a small component of the overall uncertainty in cosmogenic nuclide erosion rates (Small *et al.*, 1999; Riebe *et al.*, 2001).

There is some evidence for preferential dissolution of non-quartz minerals in Dartmoor. In a chemical analysis, Williams *et al.* (1986) measured an increase in SiO_2 content from 72.2% in solid granite to 76.4% in decomposed granite. Although this is not solely a measurement of quartz, it does indicate that non-silica bearing minerals are being preferentially weathered. Similarily, they found that while the percentage of quartz remained constant at ~40% throughout the soil profile, there was a decline in feldspar from 40% to 15% and an increase in groundmass (material too fine for measurement) from 10% to 35%. This suggests that other minerals are being preferentially weathered in the regolith; however, as the percentage of quartz remains constant there does not appear to be significant enrichment of quartz.

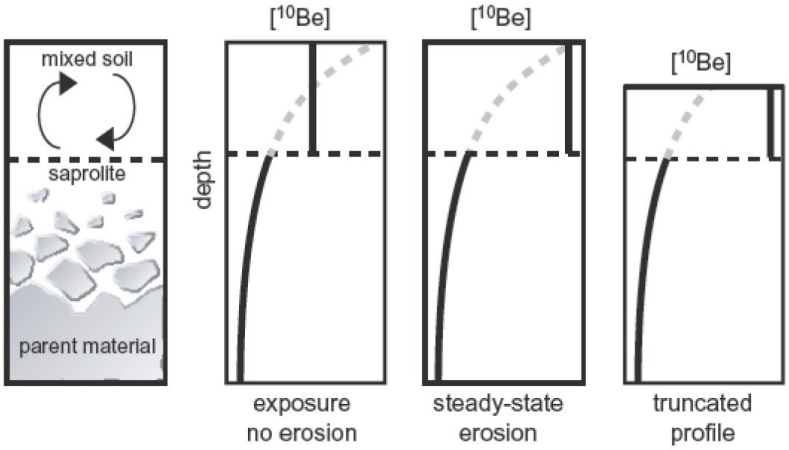

Figure 3.11 Cosmogenic nuclide concentration in vertically mixed regolith profiles; the ^{10}Be concentration in a well-mixed profile (black-line) and the equivalent in a non-mixed profile (grey-line)

Source: Granger & Riebe (2005)

3.4 High Willhays

The presence of tors in a landscape is the result of an imbalance of erosion rates between these emergent bedrock features and the surrounding regolith mantled slopes. To understand how the tor landform developed it is essential to know the rates at which weathering and erosion are occurring on both the tors and the surrounding regolith. The results are presented for each of these with: (i) the regolith being investigated through a number of excavated pits and observations, with ^{10}Be concentrations used to estimate long-term denudation rates and assess sediment mixing; and (ii) the tors at High Willhays being studied and ^{10}Be used to provide an indication of the long-term exposure of these landforms. The results from these studies, in combination, allow for an assessment of potential models of landform development.

3.4.1 Study Site

The High Willhays is located in the north-west of the Dartmoor granitic uplands, and with an elevation of 621 m is the highest point in southern England. The summit of High Willhays is joined to that of Yes Tor (619 m elevation) to the north by a shallow saddle over which elevations fall to no less than 590 m (Figure 3.12). These summits are bound to the southwest by the deeply incised West Okement River valley, to the east by the headwaters of the East Okement River, and to the north and west by the Red-a-Ven Brook and the Meldon Quarry (also the edge of the granite pluton). The summit of High Willhays is a low gradient surface approximately 700 m north-south and 250 m west-east (Figure 3.12), which gradually transitions into the surrounding hillslopes. The summit is mostly mantled in regolith, although there are a number of places in which bedrock granite is exposed including six outcropping tors with heights ranging from 1.5 to 5.4 m above the surrounding ground.

3.4.2 Regolith at High Willhays

The transformation of bedrock to unconsolidated regolith and the subsequent removal of this material is the fundamental geomorphological process in the development of slopes and the emergence of tors. This section presents the results of field observations and excavation profiles.

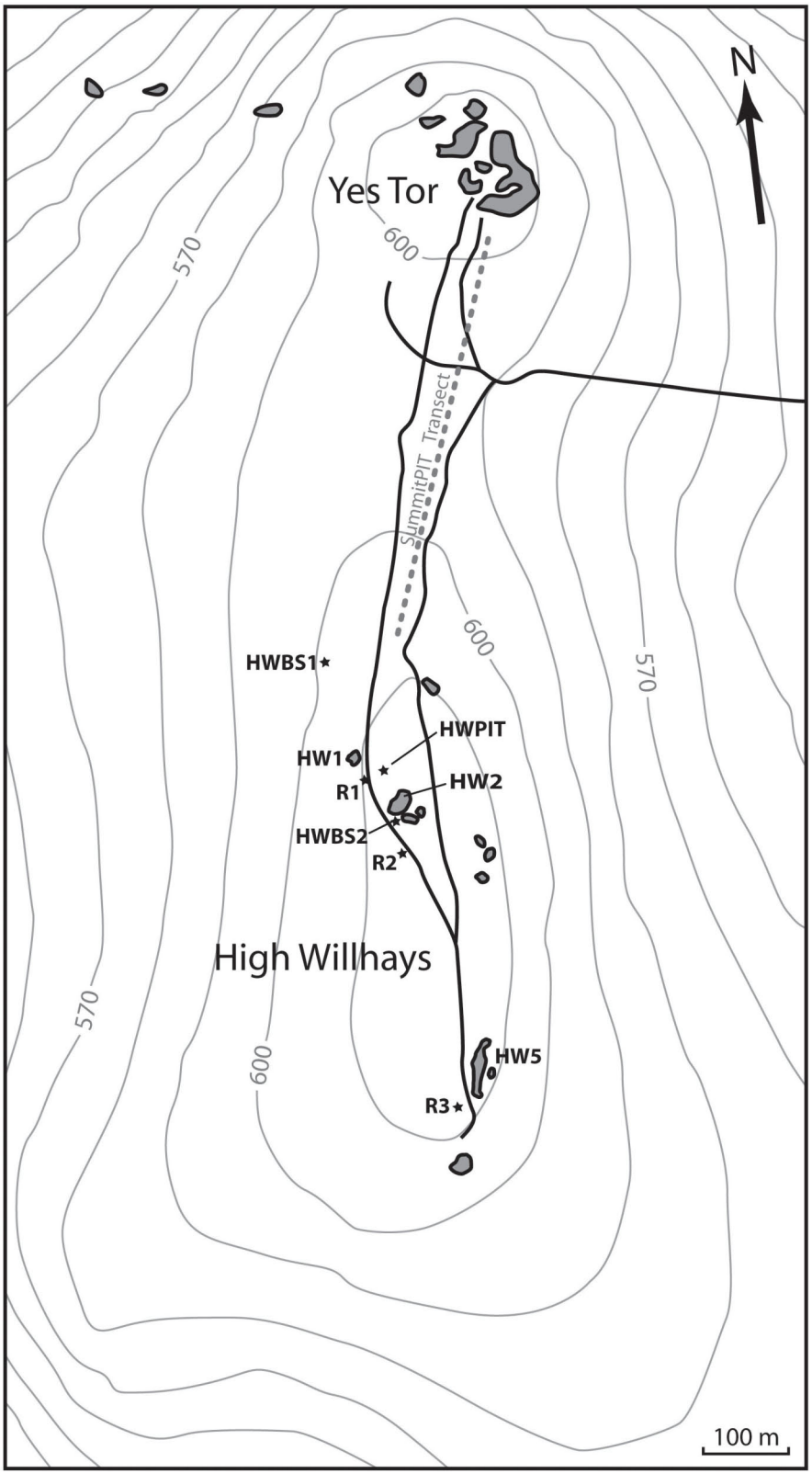

Figure 3.12 Map of the High Willhays and Yes Tor summit area in north-western Dartmoor' showing tor outcrops (dark grey), cosmogenic nuclide sampling sites (stars), summit transect (dashed line) and roads (black lines).

3.4.2.1 Observations of the Summit

The High Willhays summit surface, while visually dominated by tors, is predominately covered in a mantle of regolith. This low gradient surface (<2-5°) only transitions gradually into the surrounding hillslopes. The summit is covered in moorland vegetation typical of upland Dartmoor, which consists of a variety of heath, mire and acid grassland types (Kirkham *et al.*, 2005). This cover of vegetation is nearly continuous across the summit, only punctuated by the occasional boulder, exposed bedrock surface, or outcropping tor (Figure 3.13).

The granite bedrock that underlies the summit is largely impermeable with limited groundwater penetration. Despite this, there is no surface expression of a drainage network at, or in proximity to, the summit of High Willhays. Instead water is retained and transmitted through the regolith, with boggy ground and some pooling noticeable at the summit and especially in proximity to tors (in particular HW2).

3.4.2.2 Sub-surface Excavations

To understand regolith development it is necessary to observe the structure of the sub-surface. At the High Willhays summit a series of pits were excavated: (i) the HWPIT located midway between the tors HW1 and HW2 (Figure 3.13) was the largest excavation and the sampling site for cosmogenic nuclides analyses presented in Section 3.4.4; and (ii) the SummitPIT which consisted of a series of excavations at 100 m intervals between the summits of Yes Tor and the High Willhays (Figure 3.12). Further observation of the shallow subsurface was provided by the removal of 10-30 cm from the surface for the construction of military vehicle tracks across the summit.

3.4.2.3 Regolith Characteristics

The excavations across the summit area of High Willhays and Yes Tor provide a consistent impression of the subsurface and regolith development (Figure 3.14). The key observations are summarised as follows:

Regolith thickness – the maximum thickness of regolith from the pits excavated in this study was 100 cm at SummitPIT 1 (Figure 3.14a) and 57 cm at HWPIT (Figure

Figure 3.13 Aerial photography of the High Willhays summit area showing location of main tor outcrops and location of samples (red = tor; orange = exposed bedrock; yellow = regolith)

Image: GoogleEarth™

3.14b). The other pits were less than 50 cm deep with many less than 20 cm. The indication from this is that regolith forms only a thin veneer across the summit, probably not much more than a metre thick. Despite attempts to excavate the pits to the regolith-bedrock transition, there is uncertainty that the base has been reached due to the presence of large blocks across the summit. It was never clear whether the base of a pit was *in situ* bedrock or a large block underneath which lay further unconsolidated regolith. Although it is possible that the regolith is substantially thicker than the pits indicate, this seems unlikely given observations elsewhere in the upland surfaces of Dartmoor. Seismic surveys by Eden & Green (1971) suggested that the average depth to solid rock was 2 m on the uplands of Dartmoor, with a maximum of 3 m at Okement Hill (on the eastern edge of the West Okement River valley), which has a far broader surface than the High Willhays. In addition, the Merrivale Quarry in central Dartmoor provides a section in which unconsolidated regolith only forms a thin veneer of at most a few metres on the hillslope (Figure 3.15). Thicker regolith in the form of head deposits is observed in Dartmoor (Waters, 1964; Green & Eden, 1973; Gerrard, 1989), although this is usually downslope and in valleys. Likewise deep weathering of granite into *in situ* growan is mostly lacking on the upland surfaces of Dartmoor (Eden & Green, 1971), although in valleys it can reach significant depths (Figure 3.8). Gerrard (1989) suggests that, in general, head and weathered granite in Dartmoor is less than 4 m thick.

Development of organic-rich soil - the summit area of High Willhays is covered with a moorland type vegetation typical of upland Dartmoor. This has developed an organic-rich soil layer that is between 10-20 cm thick across the summit area. There is a distinct transition, occurring over a couple centimetres at the base of this layer and it is rare for roots to penetrate much beneath this layer. Evident in HWPIT and the cut road is that at the base of this layer there are a number of boulders (Figure 3.16a) that form a near continuous base to the soil layer. This organic-rich soil is likely to have developed with the establishment of moorland vegetation on the summit following the climatic amelioration at the onset of the Holocene.

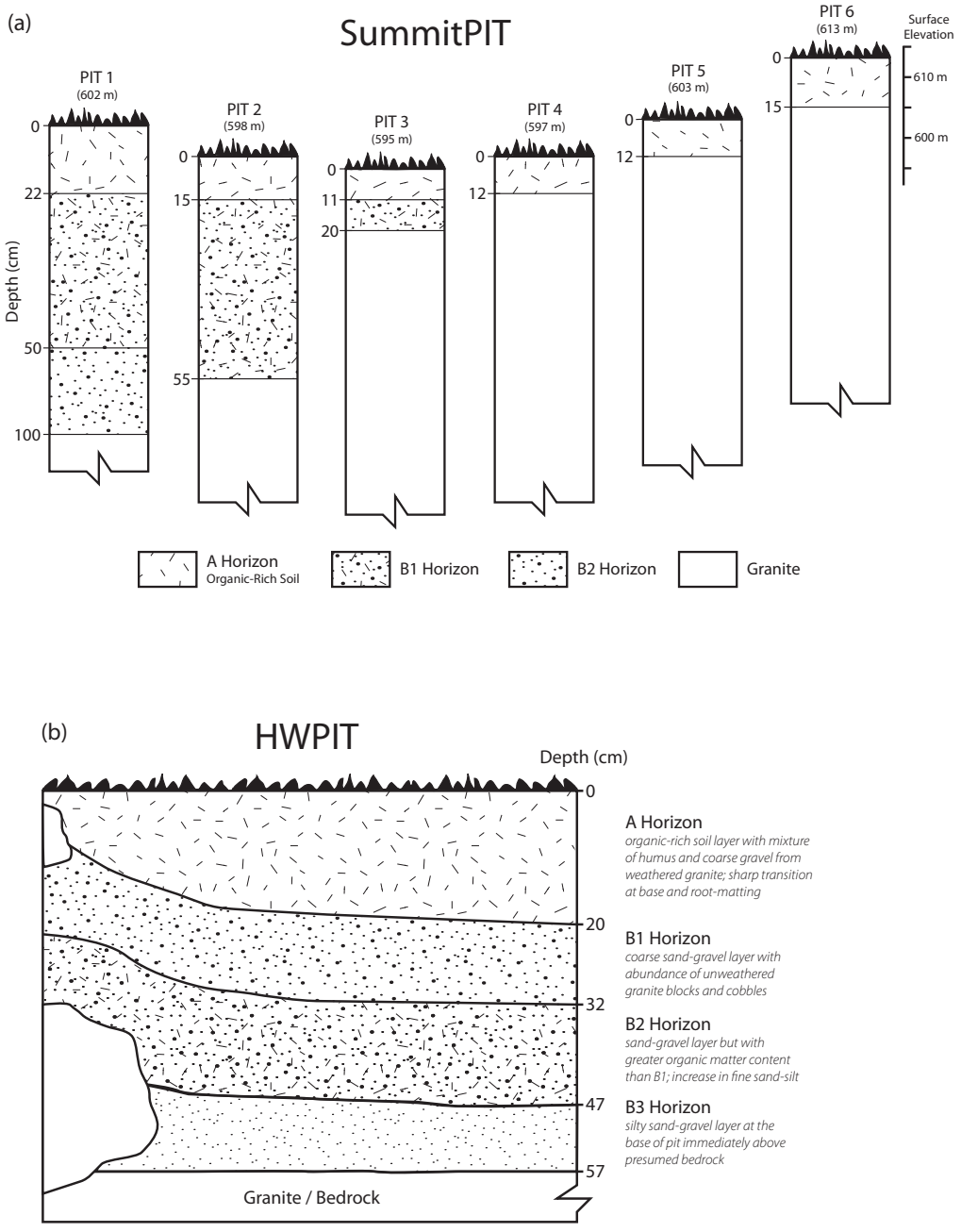

Figure 3.14 Regolith profiles for excavated pits in the High Willhays - Yes Tor summit area; with (a) series of pits in the comprising SummitPIT at 100 m intervals between the Yes Tor and High Willhays; and (b) the HWPIT at the summit of High Willhays between tors HW1 and HW2, cosmogenic nuclide analysis of samples from B1, B2, and B3 horizons.

(a)

(b)

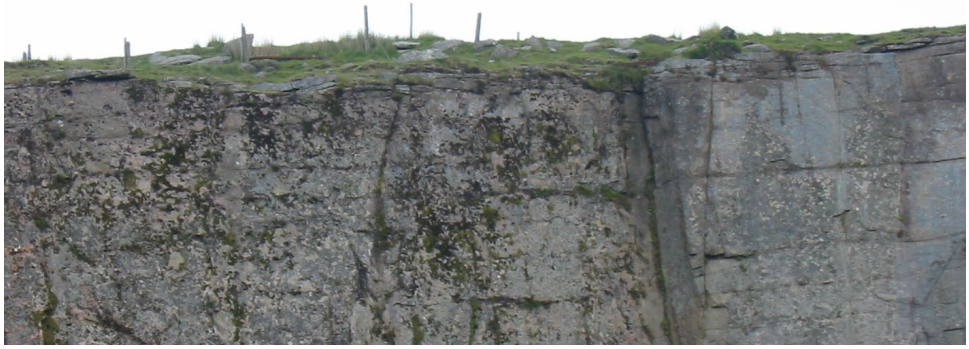

Figure 3.15 Merrivale Quarry excavation reveals the thin veneer of regolith indicating a shallow depth of weathering on hillslopes

Figure 3.16 The excavation of a pit in the regolith at the summit of High Willhays (HWPIT)

Regolith – the remainder of the regolith mostly consists of a coarse sand-gravel with little fine sand-silt sized grains present, although there was an increase in fine material with depth. This weathered regolith is quartz-rich, indicating a preferential weathering of other minerals in the granite, mostly feldspars and biotite. This sand-gravel matrix supports numerous cobble to boulder sized blocks of unweathered granite. The regolith layer appeared disrupted. The regolith does not resemble the *in situ* weathered growan developed as saprolite in other locations (e.g. Two Bridges), and lacks any obvious structural features. The appearance is of a well-mixed regolith layer heavily disrupted with processes competent at detaching bedrock from the base of the weathering profile.

3.4.3 Tors at High Willhays

Tors are an enigmatic landform that has given rise to multiple hypotheses on their development (see Section 3.2). This section provides details of the geomorphology of tors at High Willhays, in particular the three tors sampled for cosmogenic nuclide analysis.

3.4.3.1 High Willhays Tor Group

There are a number of granite outcrops that protrude from the regolith-mantled summit of High Willhays. The most prominent of these are the six tor outcrops that stand more than 1 m above the surrounding ground (Figure 3.13). These tors are spread over the long north-south axis of the summit and there is an ~450 m distance between the northernmost (HW1) and southernmost (HW6) tors. The tors range in height from about 1 m to 5.4 m. Three of these tors were selected for cosmogenic nuclide sampling, HW1, HW2, and HW5.

The High Willhays tors are lamellar type tors, with closely spaced secondary horizontal joint spacing of at most 5 cm that gives them a 'pancake-stack' appearance. In contrast, the vertical joint spacing is much wider (>1 m). These combine to give the tors a massive, rounded appearance with minimal development of delicate superstructure.

3.4.3.2 Tor HW1

The HW1 tor is on the north-western edge of the summit, and also one of the smallest tors (Figure 3.13; 3.17). It has an ellipsoidal plan form with an upper surface some 6.3 m wide by 8.7 m long. The surface dips at 15° on the long axis towards the west, an angle similar to that of the slope. The tor height above the regolith is highest on the north-eastern side at 1.75 m, this face of the tor is approximately vertical. The tor is more rounded on the downslope face.

The granite of the HW1 tor has well-developed pseudo-bedding with horizontal joints spaced at 2-5 cm (Figure 3.18). The joints dip at an angle of ~15° and are parallel to the hillslope. These joints are the main structural weakness in the granite and it appears that there is spallation of rock sheets 2-5 cm thick from the surface. In sampling for cosmogenic nuclides these horizontal joints were exploited as planes of weakness, and upon removal of the rock there was clear evidence of water seepage and weathering along the joint plane (dark staining of the rock). There are no vertical joints apparent in the HW1 tor, although the shape of the tor is probably determined by vertical joint patterns that run along its boundaries. The tor is separated from granite exposures on its southern side by a vertical joint.

3.4.3.3 Tor HW2

Located ~60 m south-east of HW1, the HW2 tor cluster is the most prominent on the High Willhays summit (Figure 3.17; 3.19). The main tor outcrop is roughly triangular with dimensions of 10.5 x 11.8 x 12.2 m. This is highest on the northern side where it reaches a maximum height of 5.4 m above the regolith at the base of the rock face (Figure 3.19a). There are three main surfaces to the tor. The surface in the north-eastern corner is the highest point although it is a relatively small surface of ~2 x 3 m; it is raised some ~20 cm above the main surface. The main (or middle) surface is larger and oval shaped with dimensions of ~5 x 7 m. There is a vertical joint a few centimetres wide that dissects this surface in an W-E direction. The remainder of the tor consists of a lower surface on the southern and western sides. This surface is little more than a metre above the vegetated regolith cover.

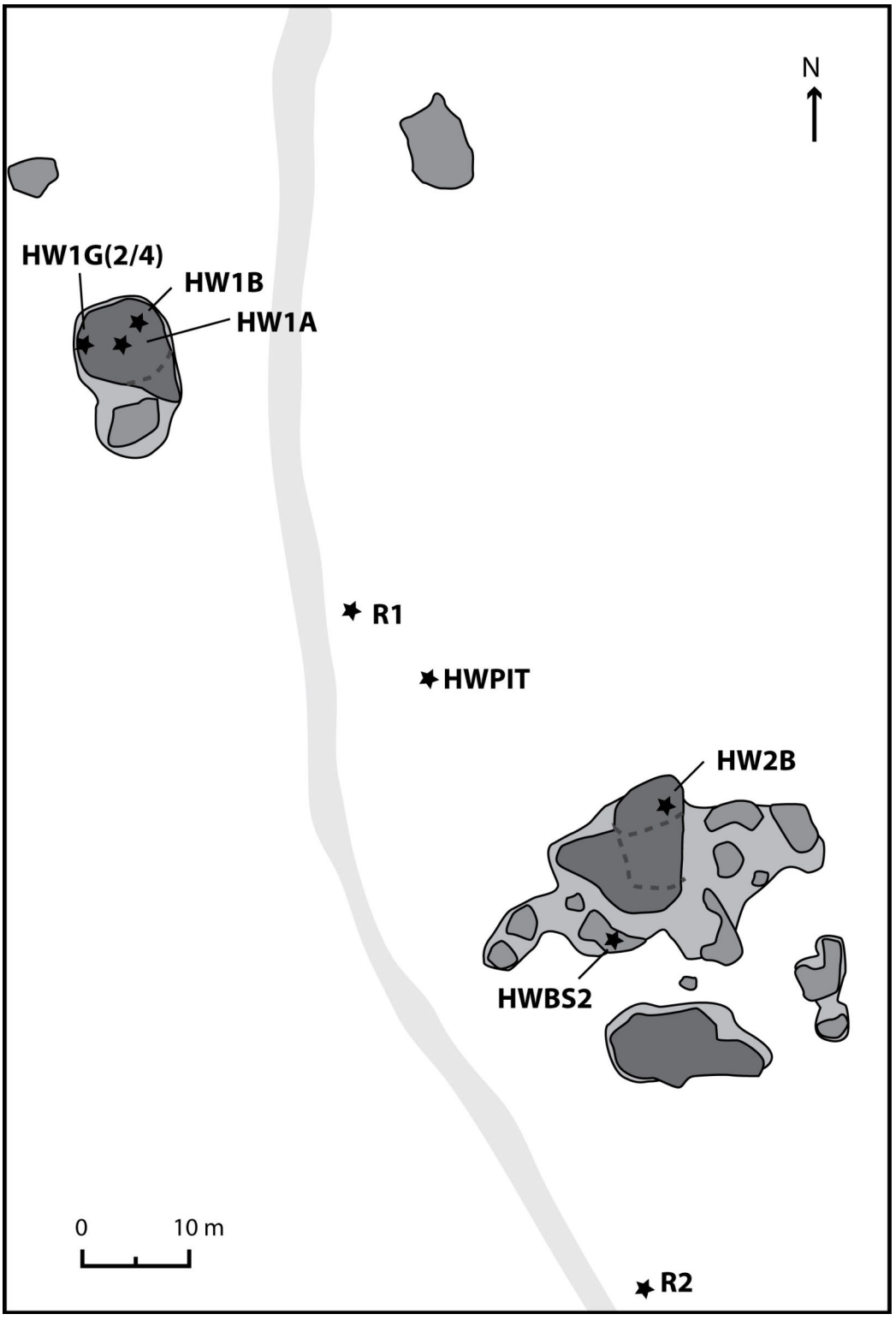

Figure 3.17 Schematic map of the High Willhays tor outcrops HW1 and HW2, showing sampling sites for outcrop and regolith samples; dark grey is main outcrop, medium grey is minor rock outcrop and light grey is vegetation covered basal platform.

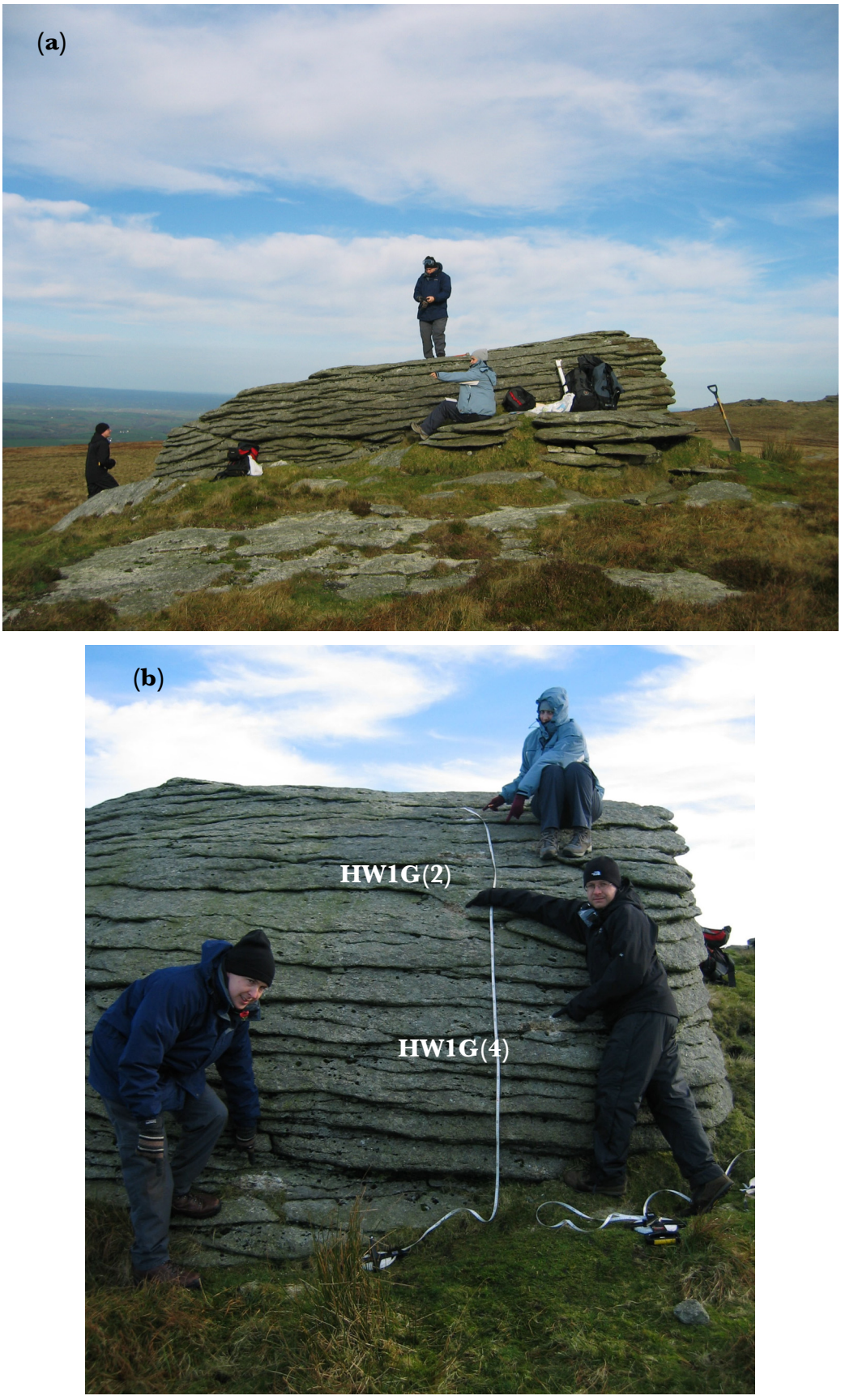

Figure 3.18 The tor outcrop HW1 in the High Willhays group (photo (b) shows the sampling profile)

Figure 3.19 The HW2 tor outcrop in the High Willhays summit group; from (a) north side and (b) south side with sampling of HW-BS2.

This main outcrop of the HW2 tor is not isolated; instead it lies on the northern edge of a larger area of raised ground that features a number of granite outcrops and exposed surfaces (Figure 3.17). This area is roughly circular with a diameter of ~30 m. Most of the other rock outcrops are <1 m high, although on the southern edge there is a smaller tor with a plan form approximately 4 x 12 m and 1.5 m high.

As with the other tors in the High Willhays group, HW2 features extensive horizontal jointing with spacing of 2-10 cm. These provide a structural weakness in the rock and probably lead to the spalling of rock in sheets. Vertical jointing of a few metres in scale is evident in the tor and appears to exert a strong influence on the plan form of the tor as well as the division of tor surfaces discussed above.

Although there are a number of rock outcrops and/or boulders surrounding the main tor at HW2, these do not appear to be derived from block erosion from the tor (as observed at other locations in Dartmoor, including the nearby Yes Tor). The lack of block erosion, even on the steep-sided tor of HW2, is likely due to the strong control of horizontal jointing on weathering.

3.4.3.4 Tor HW5

Towards the southern end of the High Willhays summit, and 250 m south of HW2, the HW5 tor cluster is the highest elevation in Dartmoor at 621 m. The HW5 tor formation (Figure 3.20) is an elongated area of raised ground only ~20 m wide but running ~60 m north-south; in line with the long-axis of the High Willhays summit. The main tor outcrop runs almost this entire length, 56 m, but is narrow with a width of at most 10 m. The surfaces of the tor range from at least 1 m to a maximum of 3.7 m above the surrounding summit regolith. The upper surfaces of the tor are broadly flat, only gently rising to the highest elevations in the middle section of the tor, although this is obscured by the construction of a cairn. In the north-eastern corner there is a smaller, semi-detached tor outcrop with dimensions of 6.5 x 3.5 m that reaches a maximum height of 1.6 m. The remainder of the HW5 area is mostly mantled in a vegetated regolith; although there is a shelf/step of exposed granite about 1 m high on the eastern edge of the area.

Unlike HW1 and most faces of HW2, the edges of HW5 are abutted by a rampart of vegetated regolith, and therefore only expose limited rock faces. The transition from the sides to the top surface is also more gradual (Figure 3.21a), with a layered retreat from the face. Also unusually, vegetation cover extends over the top of the tor surface, especially in the northern section of the tor (Figure 3.21b). This material may be saprolitic weathering products or remnants of regolith from the tor emergence.

As with the other tors, the rock outcrops at HW5 display strong horizontal jointing on a 2-5 cm scale. It is evident that material is removed from the upper surfaces through periodic spallation of sheets (Figure 3.22). There are some vertical joints evident, especially in the southern end of the tor, others might be obscured by vegetation cover. There is little evidence of block removal from the tor, although this would again be consistent with narrow horizontal joint spacing and erosion by thin-sheet spallation.

3.4.3.5 Summary

There is a scattering of granite outcrops across the summit area of the High Willhays. They range in size from small outcrops less than a metre in size, to the larger tors that reach up to 5.4 m in height (HW2) and almost 60 m in length (HW5). The tor outcrops are not isolated features; instead they are usually part of a larger complex of raised ground that is punctuated by exposed bedrock surfaces, boulders and smaller outcrops.

Closely spaced horizontal joints (mostly between 2-5 cm), which give the tors a 'pancake-stack' appearance, dominate the structure of these lamellar tors. There was clear evidence of weathering along these joints and sampling revealed deep staining of the subsurface rock along these fractures. It is considered likely that removal of rock from the tor occurs mostly through the spalling of thin sheets. Vertical joints are not as obvious a feature in the tors at the High Willhays, but they probably have a significant influence on the shape and lateral extent of the tor outcrops.

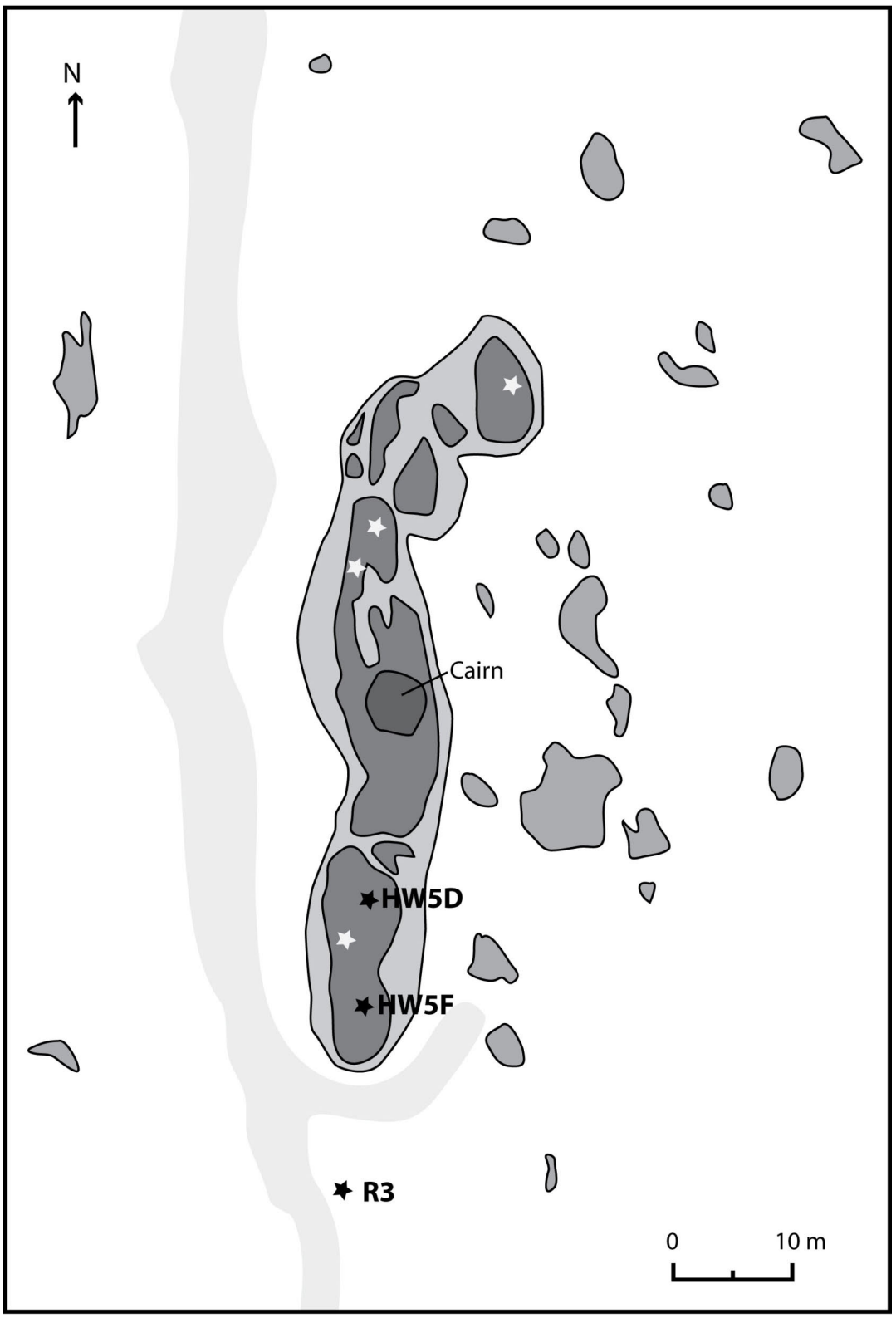

Figure 3.20 Schematic map of the HW5 tor outcrop in the High Willhays group; showing sampling sites for outcrop (white not analysed) and regolith samples; dark grey is main outcrop, medium grey is minor rock outcrop and light grey is vegetation covered basal platform

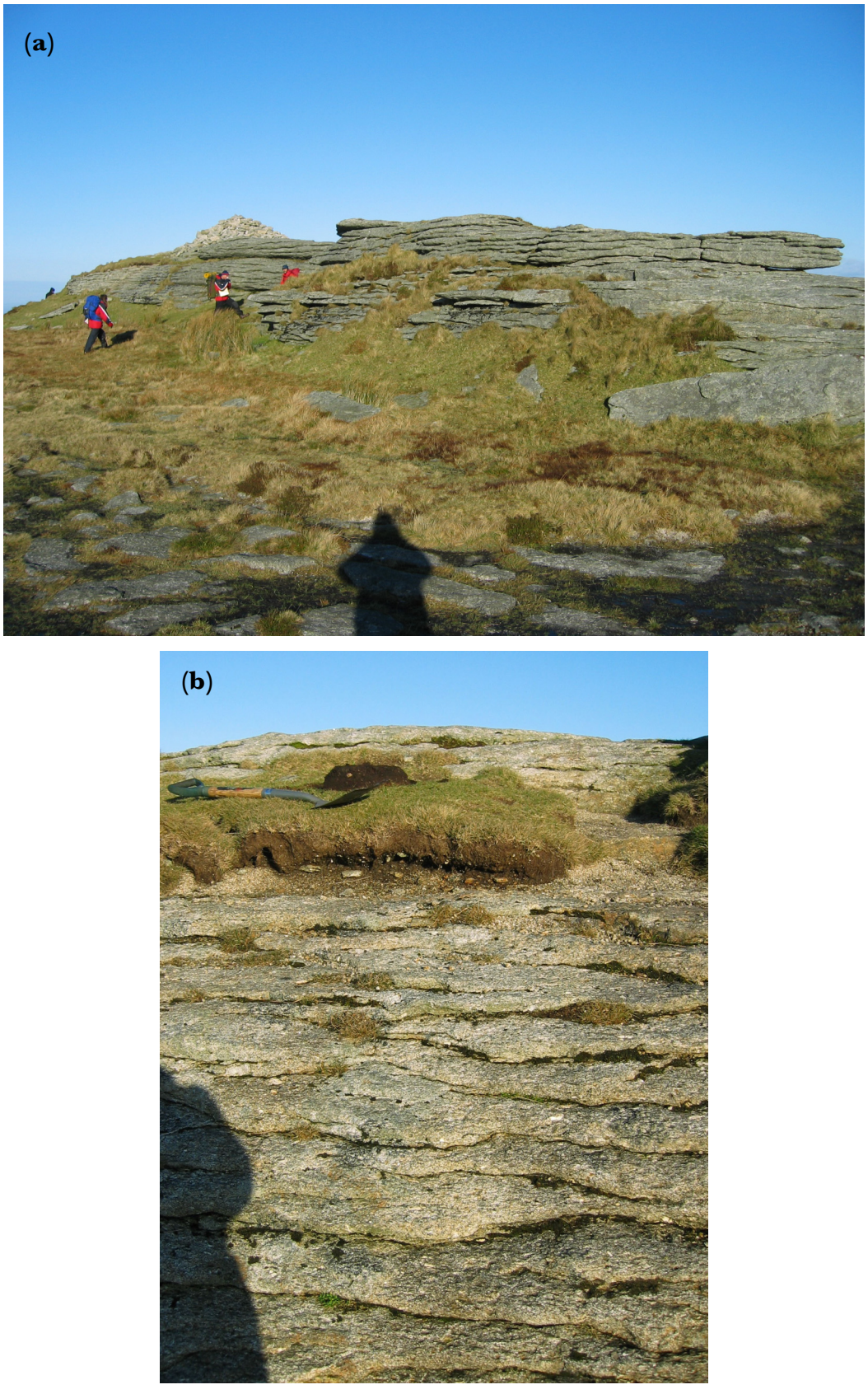

Figure 3.21 The HW5 tor outcrop in the High Willhays group showing (a) the tor in profile from the south, and (b) grus and vegetation on the tor upper surface

Figure 3.22 The HW5 tor outcrop in the High Willhays group, with sample sites HW5D (furthest bag) and HW5F (closest bag).

3.4.4 Cosmogenic Nuclide Results

The results of ^{10}Be measurements from the High Willhays are presented in Table 3.2. In total 15 samples were analysed from: (i) the upper surfaces of tors HW1/HW2/HW5 with 5 samples; (ii) in profile from the side of tor HW1 with 2 samples; (iii) exposed bedrock surfaces (not protruding above surrounding surface) with 2 samples; and (iv) from the regolith with 6 samples. The ^{10}Be concentrations measured ranged from the lowest in regolith at 1.13 ± 0.07 x10^5 atoms g^{-1} to that from the surface of tor HW1 at 3.50 ± 0.16 x10^5 atoms g^{-1}, a nearly three-fold difference in accumulated cosmogenic nuclides. Of the tor surfaces sampled, the ^{10}Be concentration ranged from 2.09-3.50 x10^5 atoms g^{-1}, although interestingly the variation in concentrations from the same tors (with samples only metres apart) was as great as the range across the tor group. The samples taken in profile from the side of HW1 returned concentrations of 1.95-2.04 x10^5 atoms g^{-1}, similar to those from tor upper surfaces despite self-shielding from incoming cosmic radiation by the tor. One of the bedrock surfaces returned a concentration similar to that of tors, at 2.26 ± 0.10 x10^5 atoms g^{-1}, while the other was considerably lower at 1.52 atoms g^{-1}, and more comparable to those measured in regolith samples which returned concentrations ranging from 1.18-1.79 x10^5 atoms g^{-1}.

Table 3.2: High Willhays - ^{10}Be results and derived surface exposure ages and erosion rates

Sample ID	Surface Type	Elevation	10Be Conc.	Exposure Age (ka)			Erosion Rate	Averaging
		(m)	(10^5 atoms g^{-1})	ε = 0 mm ka^{-1}	ε = 5 mm ka^{-1}	ε = 10 mm ka^{-1}	(mm ka^{-1})	Time Scale (ka)
HW1A	Tor Summit	610	2.09 ± 0.09	25.2 ± 1.1	28.1 ± 1.4	32.1 ± 1.9	32.0 ± 1.5	19.2
HW1B	Tor Summit	610	3.50 ± 0.16	42.0 ± 2.0	51.2 ± 2.9	69.2 ± 5.6	18.5 ± 0.9	33.3
HW1G(2)	Tor Profile	608	2.04 ± 0.08	27.5 ± 1.1	31.0 ± 1.4	36.0 ± 2.0	29.9 ± 1.3	20.5
HW1G(4)	Tor Profile	607	1.95 ± 0.08	29.5 ± 1.3	33.5 ± 1.7	39.4 ± 2.3	28.8 ± 1.3	21.4
HW2B	Tor Summit	617	2.20 ± 0.08	26.2 ± 1.0	29.4 ± 1.2	33.8 ± 1.6	30.6 ± 1.2	20.1
HW5D	Tor Summit	621	2.10 ± 0.07	24.9 ± 0.9	27.7 ± 1.1	31.5 ± 1.4	32.3 ± 1.2	19.0
HW5F	Tor Summit	621	3.13 ± 0.11	37.0 ± 1.3	43.8 ± 1.8	55.7 ± 3.0	21.1 ± 0.8	29.1
HWBS1	Bedrock Surface	600	2.26 ± 0.10	27.3 ± 1.3	30.8 ± 1.6	35.7 ± 2.2	29.4 ± 1.4	21.0
HWBS2	Bedrock Surface	614	1.52 ± 0.06	18.5 ± 0.7	20.0 ± 0.8	21.9 ± 1.0	44.4 ± 1.8	13.9
R1	Surface Regolith	608	1.56 ± 0.08	18.6 ± 0.9	20.1 ± 1.1	22.0 ± 1.3	43.9 ± 2.2	14.0
R2	Surface Regolith	614	1.30 ± 0.07	15.5 ± 0.8	16.5 ± 1.0	17.8 ± 1.1	53.1 ± 3.0	11.6
R3	Surface Regolith	618	1.13 ± 0.07	13.4 ± 0.8	14.2 ± 0.9	15.1 ± 1.0	61.7 ± 3.6	10.0
HWPIT2	Subsurface Regolith	608	1.26 ± 0.07	15.1 ± 0.8	16.1 ± 0.9	17.3 ± 1.1	54.6 ± 3.1	11.3
HWPIT3	Subsurface Regolith	608	1.18 ± 0.06	14.1 ± 0.7	14.9 ± 0.8	15.9 ± 0.9	58.8 ± 2.9	10.5
HWPIT4	Subsurface Regolith	608	1.79 ± 0.07	21.3 ± 0.8	23.3 ± 1.0	26.0 ± 1.2	38.1 ± 1.5	16.2

3.4.4.1 Regolith & Bedrock Surfaces

The concentration of cosmogenic nuclides in a well-mixed regolith profile can be used to derive a long-term denudation rate (section 3.3.2.3). At the High Willhays summit, six samples of regolith were analysed for their ^{10}Be concentration. Three of these were taken from a depth profile to assess regolith mixing, with the remaining from the surface to assess spatial variability of exposure.

The HWPIT was excavated to a depth of 60 cm at the summit of High Willhays (Figure 3.14). This vertical profile in the regolith was sampled at depth of 20-32 cm (HWPIT2), 32-47 cm (HWPIT3) and 47-57 cm (HWPIT4). These were analysed for ^{10}Be concentrations, with the resulting depth profile allowing an evaluation of mixing in the regolith. The concentration of ^{10}Be would be expected to decline exponentially with depth in an unmixed regolith profile, while in a well-mixed regolith it should be uniform. The samples from the uppermost two samples in the HWPIT are within 1σ of each other with ^{10}Be concentrations of 1.26 ± 0.07 and 1.18 ± 0.06 x10^5 atoms g^{-1}. Curiously, the deepest sample from the HWPIT, at depth of 47-57 cm, has the highest concentration of ^{10}Be at 1.79 ± 0.07 x10^5 atoms g^{-1}. This is an inversion of the expected decline or uniform distribution of ^{10}Be concentrations with depth. While there does appear to be vertical mixing of the regolith profile, the non-uniform distribution of ^{10}Be concentrations indicates that this is complex and incomplete.

An inverted profile might occur in regolith due to the emplacement of lower ^{10}Be concentration material over an older, more stable body of regolith that has been exposed to an extensive interval of cosmic radiation (e.g. head deposits in Dartmoor; Waters, 1964; Gerrard, 1989). While there are differences in regolith composition with depth in the profile (e.g. an increase in the silt/clay content; Figure 3.14), its location on a low gradient summit makes it difficult to conceive of a source for overriding sediment.

Another explanation might be that there is variability in the residence time of quartz grains in the near surface, and incomplete mixing is leading to differences in the measured ^{10}Be concentrations. In the regolith at the High Willhays summit, it is

possible that blocks have a longer residence, and higher ^{10}Be concentration, than the more readily mobilised grus. The breakdown of blocks in the subsurface would then contribute high ^{10}Be concentration quartz grains that, in an incompletely mixed regolith layer, would result in localised variations in samples. Unfortunately this remains speculative, as the ^{10}Be concentration of blocks was not measured in this study.

The samples of regolith from the surface were taken in the vicinity of the sampled tors across the High Willhays summit area (Figure 3.13). The measured ^{10}Be concentrations are shown in Table 3.2, and range from 1.13 to 1.56 x10^5 atoms g^{-1}. These are a similar to measurements in samples from the depth profile. The relative uniformity of ^{10}Be concentrations both across the surface and at depth supports an interpretation of vertical mixing of the regolith across the summit. In well-mixed regolith, the concentration of ^{10}Be can be used to derive the long-term denudation rate of the regolith, these calculations are presented in Table 3.2. The denudation rates of the regolith from the High Willhays summit range from 38.1 to 61.7 mm ka^{1}.

In addition to the sampling of regolith and tors, two exposed bedrock surfaces that do not protrude from the surrounding regolith were sampled. The HWBS2 sample was taken from an exposed surface of granite at the base of the HW2 tor outcrop (Figure 3.17; 3.19b). The ^{10}Be concentration in this sample was 1.52 ± 0.06 x10^5 atoms g^{-1}, which is significantly lower than those of nearby tor outcrop surfaces (HW2), but comparable to concentrations in nearby regolith (R2). As discussed in section 3.3.2, a bedrock surface on emerging from underneath regolith cover will have a ^{10}Be concentration equivalent to that of the regolith. It is probably the case that the HWBS2 surface has only recently emerged from regolith cover.

This is in contrast to the ^{10}Be concentration of 2.26 ± 0.10 x10^5 atoms g^{-1} measured in sample HWBS1. This was collected from a larger expanse of exposed bedrock granite (Figure 3.23), located to the northwest of the HW1 tor and on the edge of the High Willhays summit area (Figure 3.12). The ^{10}Be concentration of this surface is

Figure 3.23 Bedrock exposure on the edge of the High Willhays summit area, sampling site HWBS1

higher than those measured in regolith and comparable to those of the High Willhays tor surfaces. This suggests that the cosmogenic nuclides are reflecting a bedrock erosion rate (or transition to) for the surface, which has been exposed for sufficient time for these to adjust.

3.4.4.2 Tors

The ^{10}Be concentration was measured in 5 samples from the upper surfaces of 3 outcrops in the High Willhays tor group (Table 3.2), with values between 2.09 and 3.50 x10^5 atoms g^{-1}. Interestingly, there is as much variation in ^{10}Be concentrations in samples from the same tor outcrop as there is across the tor group. The two samples from the HW1 tor returned concentrations of 2.09 ± 0.09 and 3.50 ± 0.16 x10^5 atoms g^{-1} while the HW5 tor samples had concentrations of 2.10 ± 0.07 and 3.13 ± 0.11 x10^5 atoms g^{-1}.

An exposure age for a surface can be derived from ^{10}Be concentrations, although this is only valid under certain conditions (section 3.3.2.1). The calculated exposure ages ($\varepsilon = 0$) for the tor surfaces range from 25-40ka (Table 3.2), this represents a minimum length of time that the sample has been at (or near) the surface and subjected to cosmic radiation. However, there is a difference in calculated exposure ages ($\varepsilon = 0$) of 17 ka between samples from the HW1 tor and 11 ka at HW5, and correction for post-exposure erosion exacerbates these age differences (Table 3.2). This difference in exposure ages from samples that are part of the same tor surface (and only metres apart) suggests that a simple surface exposure model is not appropriate for these tors. This variation is either from a time delay in the uncovering of part of the surface, different long-term erosion rates of the surface, or most likely, episodic removal of blocks.

A further indication of post-emergence modification of tors is that there is no consistent difference in ^{10}Be concentrations on the tor surfaces, despite the sampled surfaces having varying heights above regolith of 1.75 m (HW1), 5.4 m (HW2) and 2.5 m (HW5). If tor surfaces were exposed following regolith stripping, it would be expected that higher surfaces would have accumulated a greater inventory of ^{10}Be. That there is no trend evident in the High Willhays tor surfaces indicates that there

has been sufficient erosion of the surface to obscure or remove any cosmogenic nuclide signal from the 'event surface' at the time of tor emergence. An 'exposure age' is probably an inaccurate geomorphological interpretation of the tor surface.

The ^{10}Be concentrations from tor surfaces can also be interpreted as erosion rates (section 3.3.2.2), which range from 18.5 to 32.3 mm ka^{-1} for samples from the High Willhays tors. The difference in ^{10}Be concentrations in samples from the same outcrop surface only a few metres apart is best explained by episodic erosion of blocks from the surface. There is well-developed horizontal jointing in the granite of the High Willhays tors, and it is along these weaknesses that block-sheets form. The erosion rate is determined by the thickness and frequency of block removal. While an individual sample could yield an erosion rate that is either greater (recent block removal) or less than (long surface exposure) the actual long-term average erosion rate, the mean value of multiple steady-state erosion rate measurements provides a good estimate of long-term surface erosion rates (Small *et al.*, 1997). The High Willhays tor surface samples yielded average erosion rate of 26.9 mm ka^{-1}.

It is difficult to assess how closely this average rate reflects the actual long-term average erosion rate of the tor surfaces. This is in part due to the limited number of cosmogenic nuclide analyses that could be allocated to measure ^{10}Be concentrations on the High Willhays tors. There may be sampling bias towards surfaces with greater exposure length (they are easier to sample as joints are more weathered and rock protrudes from the surface) that would result in an underestimation of the actual mean erosion rate. Although the ^{10}Be concentration in episodically eroding surfaces will not be in steady-state with the average erosion rate (it fluctuates around this), it is also possible that the signal has not fully adjusted to a change in the dynamics of the tor erosion. For example, the transition in erosion rates following initial emergence of the tor or the cessation of processes that facilitate block removal (i.e. frost action). If this does occur, there will be an interval of adjustment until a sufficient depth of material has been removed to eradicate the earlier signal, and this will depend on the recent erosion rate. For the surfaces at the High Willhays, the erosion rates measured are high enough that no 'emergence signal' is preserved. However, if the onset of

Holocene climate conditions has lead to a reduction in tor surface erosion rates, the signal is still adjusting (erosion of 5 mm ka^{-1} would remove 5cm over 10ka). In this case, a lower Holocene rate would mean that erosion under periglacial conditions is higher than the average. It is important to note that, while lower Holocene rates are suggested (e.g. Gerrard, 1994), there is no independent quantitative measure of these and no means of differentiating the two with this ^{10}Be dataset.

As well as sampling the top surfaces of tors at the High Willhays, two samples were analysed from a profile sampled at 70 cm intervals down the western face of the HW1 tor (Figure 3.18b), these being HW1G(2) and HW1G(4). In other studies, samples taken from tor profiles have been used to constrain tor emergence (e.g. Heimsath *et al.*, 2000; Phillips *et al.*, 2006). Although insufficient samples were analysed to fully explore the profile, those measured can still allow for some interpretation of the exposure and erosion of the lateral face of the tor. The measured ^{10}Be concentrations of 2.04 ± 0.08 and 1.95 ± 0.08 are within 1σ, and statistically indistinguishable. The similarity of these concentrations precludes a scenario under which the emergence of the tor by regolith lowering is gradual and followed by minimal post-exposure erosion. To explain these similar concentrations there are two possible scenarios: (i) the rate of regolith lowering is so rapid that there is little time for cosmogenic nuclides to accumulate between the uncovering of the upper and lower sample locations; (ii) there has been sufficient erosion of the surface following uncovering that the erosion rate signal dominates any signal from difference in timing of first exposure.

The sample HW1G(4) is ~0.7 m and HW1G(2) ~1.7 m above the present regolith surface. At the calculated average regolith denudation rate of 51.7 mm ka^{-1}, these sample locations would have emerged from regolith cover at 14 ka and 34 ka respectively. The 20 ka interval between the uncovering of the sample locations is enough time for the accumulation of a significant quantity of ^{10}Be, so unless the rate of regolith denudation during tor emergence was much higher than that calculated from measurements in this study, there has most likely been significant erosion of the tor surface since it emerged from the regolith.

As previously discussed, it is probably not appropriate to interpret ^{10}Be concentrations from tor surfaces as exposure ages. This is due to a lack of an appropriate exposure 'event surface' and the likely significant erosion of tor surfaces. However, it has been possible to calculate an average erosion rate for both tor surfaces (26.9 mm ka^{-1}) and the regolith (51.7 mm ka^{-1}) at the High Willhays. If it is assumed that these rates are applicable over the entire emergence of the tor landform, then the difference between them is a tor emergence rate, in this case 25 mm ka^{-1}. Using this rate, it is possible to calculate the time since a tor first emerged from regolith cover by dividing the tor height by the emergence rate. For the studied tors in the High Willhays group the time since emergence would be HW1 = 70 ka (1.75 m), HW5 = 100 ka (2.5 m), and HW2 = 216 ka (5.4 m). Over this interval a significant depth of material would have been removed from the tor surface, for example ~5.8 m from HW2 over the 216 ka (at surface erosion rate of 27 mm ka^{-1}).

These results are highly reliant on both the measured rates being an accurate reflection of the actual erosion rate and these being applicable to long intervals over which tor emergence has occurred. The latter is a question of whether the erosion rate derived from the cosmogenic nuclide signal reflects a Quaternary average. The tor surface erosion rates have averaging timescales of 20-30 ka (Table 3.2) which spans both Holocene and glacial climatic conditions. The averaging timescale calculated for the regolith erosion rates are shorter, and at 10-16 ka spans only the Lateglacial-Holocene. However, as the ^{10}Be concentration is averaged over the depth of mixing in a regolith profile, the averaging timescale concept is not fully applicable and the erosion rate signal in regolith will be integrated over a greater timespan than that of an unmixed or bedrock surface. Although the erosion rates derived from ^{10}Be concentrations are only averaged over part of a glacial cycle, they do integrate an erosion signal of the two extremes of Quaternary climate at a glacial maxima and full interglacial climate.

3.5 Great Links Tor

Tors emerge in a landscape when the surrounding ground surface is lowering at a more rapid rate than bare-rock surfaces. If the disparity in erosion rates is persistent, the interval over which the tor has been uncovered should be reflected in its height above the surrounding ground surface. The Great Links Tor group provides an opportunity to assess ^{10}Be concentrations in a series of outcrops that span a range of tor heights and slope positions. This allows for an assessment of whether the cosmogenic nuclide signature reflects surface erosion rates or preserves some exposure signal from tor emergence.

3.5.1 Study Site

The Great Links Tor is located in the north-west of Dartmoor, some 3.8 km south-west of the High Willhays. The summit is one of the highest in Dartmoor with an elevation of 586 m. To the west there is a long slope from the summit to the River Lyd (270 m over a 1 km distance), which also marks the boundary of the granitic uplands of Dartmoor. To the south it is bounded by the headwaters of the deeply incised and anthropogenically disrupted (tin mining) Doetor Brook. To the north and east the slopes are more gentle falling only ~60 m in elevation before rising into the broad Amicombe Hill which forms the southern side of the West Okement valley.

The summit of Great Links Tor has a raised basal platform in which the regolith appears very thin and there are numerous outcroppings of exposed granite and boulders. This covers an area with a diameter of 200-300 m. There are five major tor outcrops at Great Links Tor, which extend from the largest tor at the summit (GLT1) downslope in a easterly line over a distance of 200 m, with the furthest tor (GLT5) just off the main raised basal platform (Figure 3.24; Figure 3.25).

Ehlen (1994) included the Great Links Tor in her study of geomorphological, structural and petrographic properties of tors. The tors in this group had mean vertical joint spacing of 441.7 cm (primary) and 128.0 cm (secondary), and horizontal joint spacings of 53.1 cm (primary) and 9.4 cm (secondary). Although the secondary horizontal joints are slightly wider than those observed in tors at the High Willhays

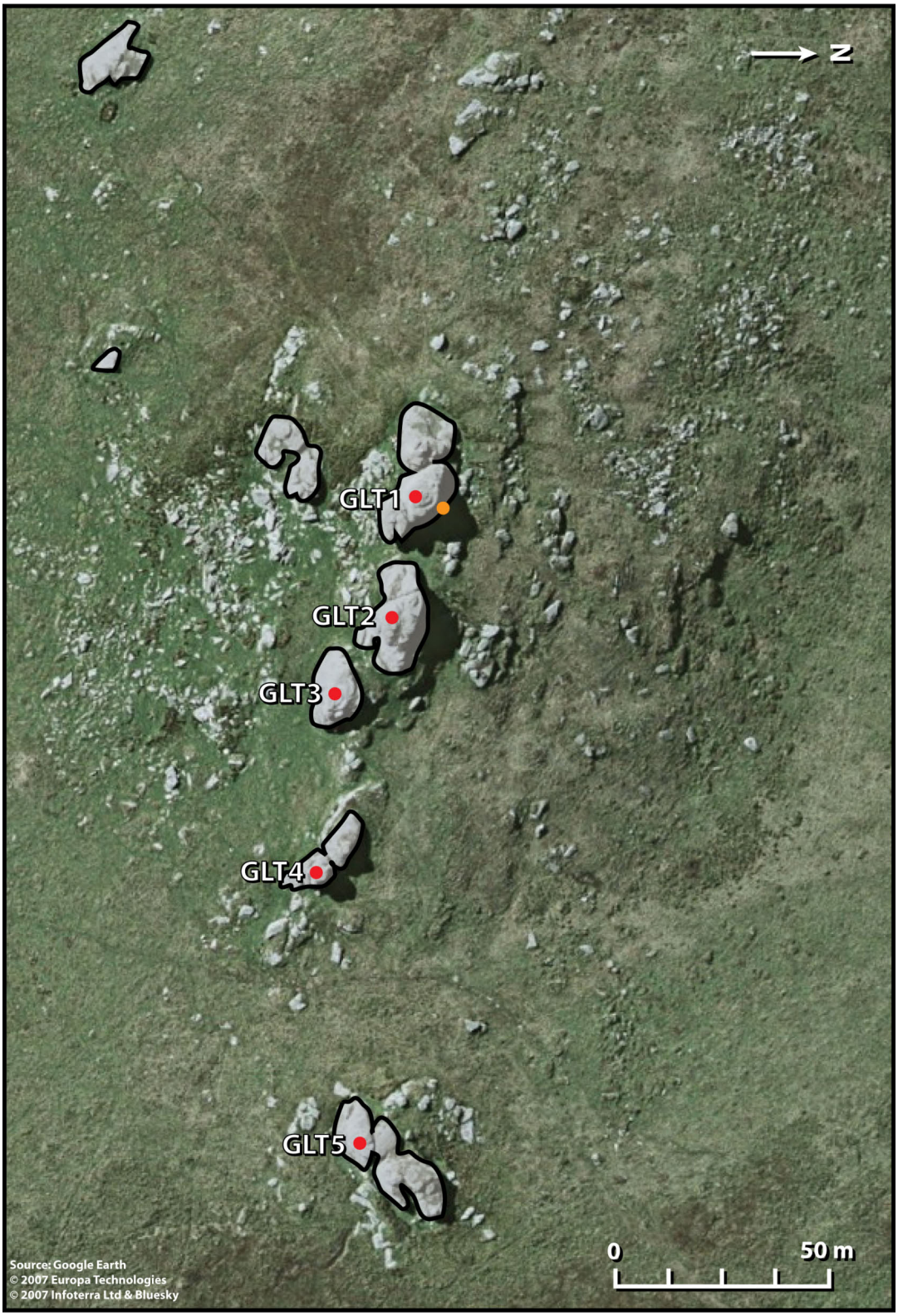

Figure 3.24 Aerial photograph of the Great Links Tor summit area showing the main outcrops of the tor group and sample locations (red = top surface; orange = side of tor).

Image: GoogleEarth™

(~2-5 cm), they are still below average for Dartmoor tors (Table 3.1). Weathering appears to be concentrated along these horizontal joints, when rock was removed during sampling the joints provided weaknesses and the freshly revealed rock was stained and moist. As with the tors at High Willhays, the horizontal joints lead to the formation of block-sheets of rock that match the joint spacing (Figure 3.26). The removal of these block-sheets by spallation is probably an effective process in the removal of rock from the tor surface.

3.5.1.1 Tor GLT1

Located at the summit of the Great Links Tor, GLT1 is the largest outcrop in the group

at 9 m high and covering an area with dimensions of approximately 30 x 15 m (Figure 3.27; 3.28). The upper surface of the outcrop has the appearance of a slab of rock ~50 cm thick (Figure 3.27), which is equivalent to the primary horizontal joint spacing summarised by Ehlen (1994). It has area dimensions of approximately 8 x 6 m and is broken into smaller joint-bound blocks with exposed rock surfaces showing small weathering pit development and protrusions of tourmaline (Figure 3.26a). Samples for cosmogenic nuclide analysis were taken from the upper surface (GLT1a; Figure 3.26a; 3.27) and from the northern face of the tor at an elevation of 1.9 m above the base of the outcrop (GT1b; Figure 3.29).

3.5.1.2 Tor GLT2

This tor is smaller than the nearby GLT1, although the GLT2 outcrop does reach a height of 8 m. It covers an area with dimensions of ~ 20 x 12 m with a smaller upper surface of 8 x 4 m. On the upper surface are two slabs of rock detached from the main outcrop (Figure 3.26b), these appear to be result of weathering on horizontal joints and the rest of this layer has been previously removed. These blocks are approximately 2.4 x 2.1 m with a thickness of ~ 50 cm, the GLT2 sample for cosmogenic nuclide analysis was collected from one of these blocks.

3.5.1.3 Tor GLT3

The GLT3 tor is effectively the downslope end of the same bedrock outcrop as GLT2 (Figure 3.24). Whereas GLT2 is on the summit of Great Link Tor, GLT3 is

Figure 3.25 The tor outcrops of the Great Links Tor group.

(a)

(b)

(c)

Figure 3.26 Great Links Tor surfaces (a) GLT1 (b) GLT2 and (c) GLT5. Block-sheets have developed with a thickness equivalent to the horizontal joint spacing.

Figure 3.27 The GLT1 tor outcrop of the Great Links Tor group from the eastern side (from top of GLT2), person is sampling location GLT1a.

Figure 3.28 The GLT1 outcrop of the Great Links Tor group from the south side

Figure 3.29 Sampling from the northern face of tor outcrop GLT1 in the Great Links Tor Group.

(a)

(b)

Figure 3.30 The tor outcrops (a) GLT4 and (b) GLT5 in the Great Links Tor group

on the slope and consequently it has a height above regolith of < 2 m upslope but 7.5 to 10.5 m downslope. The upper surface of this outcrop has an elevation ~6 m less than that of the adjoining GLT2. The total coverage of the outcrop has dimensions of 12 x 16 m with the upper surface an area of 10.6 x 5.7 m from which cosmogenic nuclide sample GLT3 was taken.

3.5.1.4 Tor GLT4

The GLT4 outcrop is a narrow tor covering an area with dimensions of 23 x 7 m. It has twin summits that both rise to narrow upper surfaces, the one furthest downslope was sampled for cosmogenic nuclide analysis, and has an upper surface of 4 x 3.5 m at a height above regolith of 8.4 m (Figure 3.30a). Vertical joint spacing probably controls the division between the upper surfaces.

3.5.1.5 Tor GLT5

The furthest from the summit of the outcrops in the Great Links Tor group, the GLT5 outcrop covers a large area with dimensions of 35 x 12 m (Figure 3.24). The exposed bedrock at GLT5 is divided into a number of smaller outcrops by vertical jointing. The surface sampled for cosmogenic nuclide analysis is on the southern side of the tor and measured some 14 x 8 m with a height above regolith on the downslope side of 7.8 m (Figure 3.30b; 3.26c).

3.5.2 Cosmogenic Nuclide Results

The results of ^{10}Be measurements from surfaces in the Great Links Tor group are presented in Table 3.3. A sample was analysed from top surface of each of the five main outcrops in the tor group (GLT1-5), with measured ^{10}Be concentrations ranging from 2.32 to 4.41 x10^5 atoms g^{-1}. In addition, sample (GLT1b) was taken from the vertical face of the largest summit tor in the group at a height of 1.9 m above the ground surface of this 9 m high tor, returning a concentration of 1.97 ± 0.08 x10^5 atoms g^{-1} in this self-shielded vertical surface.

Table 3.3 Great Links Tor ^{10}Be derived exposure age, erosion rates and averaging times

Sample ID	Elevation (m)	10Be Conc. (10^5 atoms g^{-1})	Exposure Age (ka)			Erosion Rate (mm ka^{-1})	Averaging Time Scale (ka)
			ε = 0 mm ka^{-1}	ε = 5 mm ka^{-1}	ε = 10 mm ka^{-1}		
GLT1a	587	3.15 ± 0.12	38.6 ± 1.4	46.1 ± 2.1	59.7 ± 3.6	20.3 ± 0.8	30.3
GLT1b	580	1.97 ± 0.08	48.0 ± 1.9	60.0 ± 3.0	86.0 ± 6.8	19.9 ± 0.8	30.9
GLT2	586	2.32 ± 0.09	28.5 ± 1.1	32.3 ± 1.4	37.9 ± 2.0	28.1 ± 1.1	21.9
GLT3	580	3.36 ± 0.12	41.5 ± 1.5	50.3 ± 2.3	67.5 ± 4.3	18.9 ± 0.7	32.6
GLT4	576	2.85 ± 0.11	35.4 ± 1.3	41.5 ± 1.9	51.7 ± 3.0	22.4 ± 0.9	27.5
GLT5	569	4.41 ± 0.14	55.1 ± 1.7	72.4 ± 3.0	126.7 ± 10.9	14.0 ± 0.5	44.1

As only a single sample was analysed from each surface, it is not possible to assess the variability of ^{10}Be concentrations on individual outcrop surfaces (as was done at High Willhays: section 3.4.4.2). Across the tor group the concentrations vary by as much as a two-fold difference (GLT2 vs GLT5). However, there does not appear to be any relationship between concentration and height of the tor above the ground surface. Although the GLT2 and GLT3 outcrops share the same base, the surface of GLT2 is more than 4 m higher. If the ^{10}Be concentrations were a tor emergence signal it would be expected that GLT2 would have a higher concentration of ^{10}Be. Instead, the measured concentration of 3.36 ± 0.12 x10^5 atoms g^{-1} is higher on the GLT3 surface than the 2.32 ± 0.09 x10^5 atoms g^{-1} from GLT2. Neither does there appear to be any relationship between position on the slope and ^{10}Be concentration, with the highest concentrations measured on the summit tor GLT1 at 3.15 ± 0.12 x10^5 atoms g^{-1} and the outcrop furthest downslope GLT5 at 4.41 ± 0.14 x10^5 atoms g^{-1}, despite the 18 m difference in surface elevation.

As there is no trend in ^{10}Be concentration that would indicate an emergence signal, and with no other exposure 'event surface', the surface exposure age model interpretation of the measurement is unlikely to be meaningful. The exposure ages ($\varepsilon = 0$) calculated for the tor surfaces ranged from 28.5 to 55.1 ka. These are the minimum amount of time that would be required to accumulate the measured ^{10}Be in the sample had it been continuously exposed at the surface (maximum) production rate.

The variation in the measured ^{10}Be concentrations indicates that the tor surfaces are undergoing episodic erosion. This interpretation agrees with the observation of block-sheets the thickness of horizontal jointing on tor surfaces (Figure 3.26). Using a steady-state erosion model, the measurements on tor surfaces at Great Links Tor yielded erosion rates between 14.0 and 28.1 mm ka^{-1}, with a tor group average erosion rate of 20.6 mm ka^{-1}. As discussed in the interpretation of High Willhays group tors, the erosion rate is subject to errors arising from the small sample size, potential sampling bias, and disequilibrium during periods of adjustment to changes in erosion.

The average erosion rate for the Great Links Tor group at 20.6 mm ka^{-1} is slightly lower than that measured on tor surfaces at the High Willhays at 26.9 mm ka^{-1}. The actual erosion rate on an episodically eroding surface will be determined by the thickness of the blocks removed and the frequency with which they are removed. The Great Links Tors have a wider horizontal joint spacing than the High Willhays tors, which results in thicker blocks. Although the depth of material removed from these blocks is greater, if they are removed less frequently it may be the case that actual erosion rate is lower. However, if the block removal is less frequent and of greater depth, then there will be an increase in the maximum (long time since block removal) and minimum (block recently removed from surface) concentrations. This would exacerbate the potential sampling bias in this study which quite possibly favoured surfaces of greater length of exposure, and would result in a calculated erosion rate lower than the actual long-term average rate.

The GLT1b sample was taken from the northern face of the large summit tor at Great Links Tor (Figure 3.29). The ^{10}Be concentration of 1.97 ± 0.08 x10^{5} atoms g^{-1} is lower in this sample than other measured from Great Links Tor surfaces, however, it was taken from a vertical face of the tor and therefore shielded from 50% of incoming cosmic radiation. A correction for this in the interpretative models results in an exposure age ($\varepsilon = 0$) of 48.0 ka and an erosion rate of 19.9 mm ka^{-1}. The erosion rate of the regolith surrounding Great Links Tor is not known, although it may be reasonable to assume it is similar to the average erosion rate measured at

High Willhays (~50 mm ka^{-1}). If this is the case, then the GLT1b sample elevation was uncovered at ~38 ka ago; a reasonable fit with the derived exposure age (also includes inheritance from subsurface). However, it is not possible to disentangle the influences of exposure and erosion for this single sample in a profile, thus limiting possible interpretation.

If the High Willhays regolith erosion rate of ~50 mm ka^{-1} is assumed to be applicable to the ground surface surrounding the Great Links Tor, the tor emergence rate can be calculated as the difference between this and the average erosion rate of 20.6 mm ka^{-1} for the tor group, resulting in an emergence rate of 30 mm ka^{-1}. For the 9 m high GLT1 tor this would suggest a time since emergence of ~300 ka, with some 6 m of material having been removed from the tor surface since it first emerged. The same caveats as discussed in similar interpretations at High Willhays (section 3.4.4.2) apply here: that rates are an accurate reflection of the actual tor surface erosion rate and that these are representative of erosion rates over the time span of tor emergence. The averaging timescales of the tor surfaces range from 22 to 44 ka, so the erosion rates are integrated over both Holocene and LGM climate conditions.

3.6 Other Tors in West Okement Valley

The tor groups at High Willhays and Great Links Tor are summit tors with elevations amongst the highest in Dartmoor, at 621 m and 587 m respectively. This section investigates four additional tor groups from the West Okement catchment in northwest Dartmoor (Figure 3.31). These are in the vicinity of the High Willhays tor group (Section 3.4), the Yes Tor blockslopes (Chapter 4) and catchment-averaged denudation in the West Okement River (Chapter 5). These tor groups include two valley-side tor groups (Black Tor and Dinger Tor), a summit/valley side tor on the Amicombe Ridge (Steng-a-Tor) and a lower elevation summit tor within the West Okement Valley (Lints Tor). The study of these tors increases the range of landscape positions of outcrops. The ^{10}Be concentration was measured in 5 samples from these tors, one each from Black Tor, Dinger Tor, Lints Tor, and two from Steng-a-Tor. The results of these analyses are presented in Table 3.4.

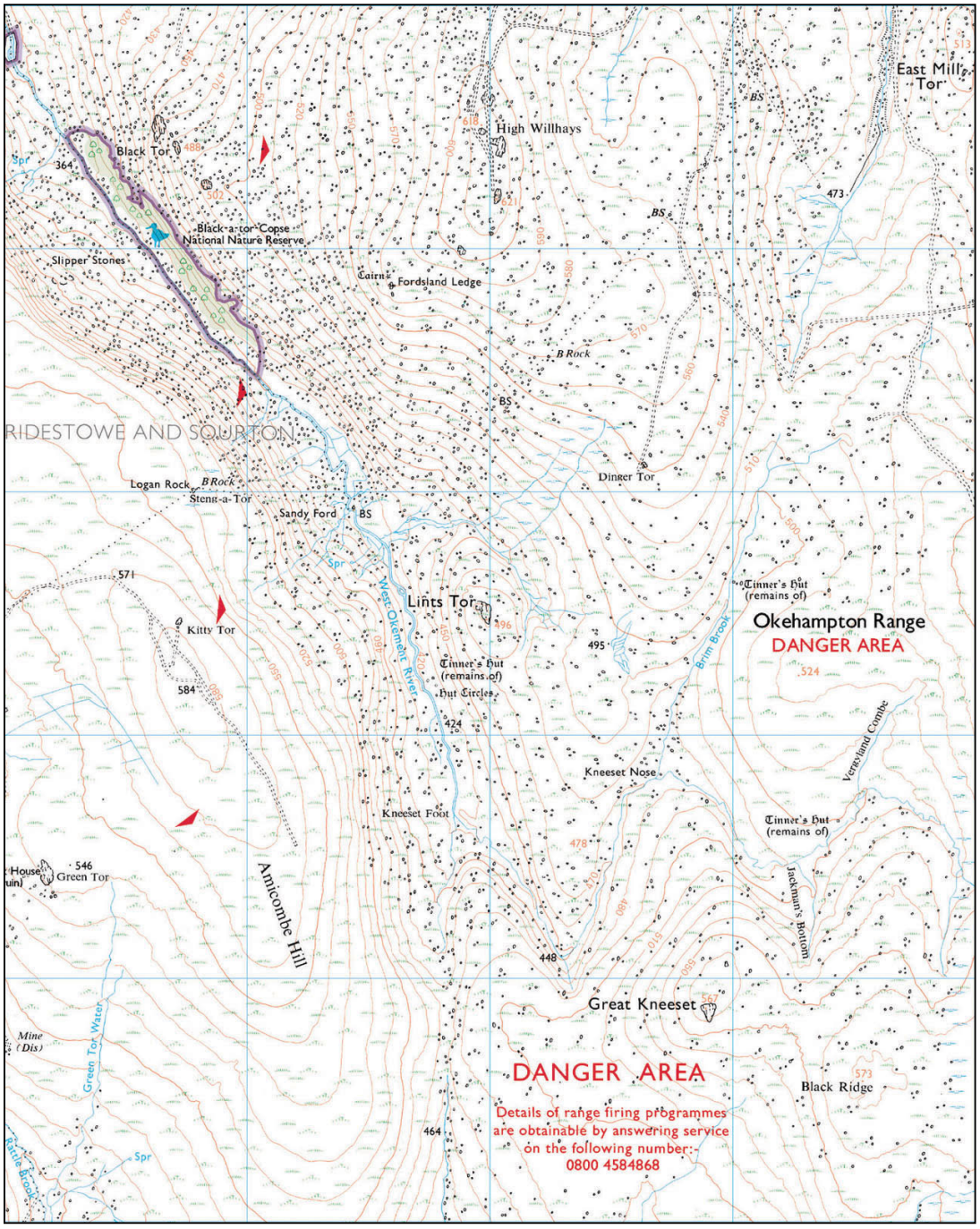

Figure 3.31 Location of tor sampling sites in the West Okement River valley catchment; Black Tor, Lints Tor, Steng-a-Tor, and Dinger Tor.

Map: Digimap/Ordinance Survey

Table 3.4 West Okement Valley Tors - ^{10}Be derived exposure age, erosion rates and averaging times

Sample ID	Elevation (m)	10Be Conc. (10^5 atoms g^{-1})	Exposure Age (ka) ε = 0 mm ka^{-1}	ε = 5 mm ka^{-1}	ε = 10 mm ka^{-1}	Erosion Rate (mm ka^{-1})	Averaging Time Scale (ka)
Black Tor							
BT2D	470	3.14 ± 0.12	42.7 ± 1.6	52.2 ± 2.4	71.2 ± 4.7	18.6 ± 0.7	33.0
Lints Tor							
LT03	496	2.21 ± 0.10	29.5 ± 1.3	33.6 ± 1.7	39.6 ± 2.4	27.7 ± 1.3	22.2
Dinger Tor							
DT01	550	1.43 ± 0.06	18.2 ± 0.8	19.7 ± 1.0	21.5 ± 1.1	45.6 ± 2.1	13.5
Steng-a-Tor							
SAT02	540	3.79 ± 0.17	48.5 ± 2.2	61.4 ± 3.5	91.8 ± 8.6	16.1 ± 0.8	38.3
SAT03	540	3.66 ± 0.13	46.8 ± 1.7	58.6 ± 2.7	85.0 ± 6.1	16.7 ± 0.6	36.8

3.6.1 Black Tor

The Black Tor group is located on the break in slope between the broad low gradient hillslope that descends from the summit of High Willhays (~7° slope from summit to Black Tor) and the steep valley sides of the deeply incised West Okement River (~25° slope from Black Tor to the river) (Figure 3.32). Black Tor consists of three main granite outcrops that are located along a 400 m length of the break in slope, which runs parallel to the West Okement River (the tors actually form a small topographic ridge, although the depression to the north-east is only a few metres). There is an ~110 m difference in elevation between Black Tor and the West Okement River, and the steep slope leading down from Black Tor is covered in large blocks. The tor outcrops at Black Tor are being undermined by slope retreat and collapse of the tors is observed on their downslope face.

Ehlen (1994) included the Black Tor group in her study of the structural, geomorphological and petrographic characteristics of tors. The Black Tor group is described geomorphologically as a valley side tor. The mean vertical joint spacing measured at the Black Tor group was 334 cm (primary) and 52 cm (secondary) while horizontal joint spaces were 118 cm (primary) and 14 cm (secondary). These are mostly a little wider than average for Dartmoor tors (Table 3.1), and the horizontal joint spacing (as observed in Figure 3.33) is more similar to that at Great Links Tor (Section 3.5) than the narrower horizontal joint spacing observed at the upslope High Willhays tors (Section 3.4). The rock of the Black Tor outcrops is being weathered into blocks with size determined by secondary joint spacing (Figure 3.33).

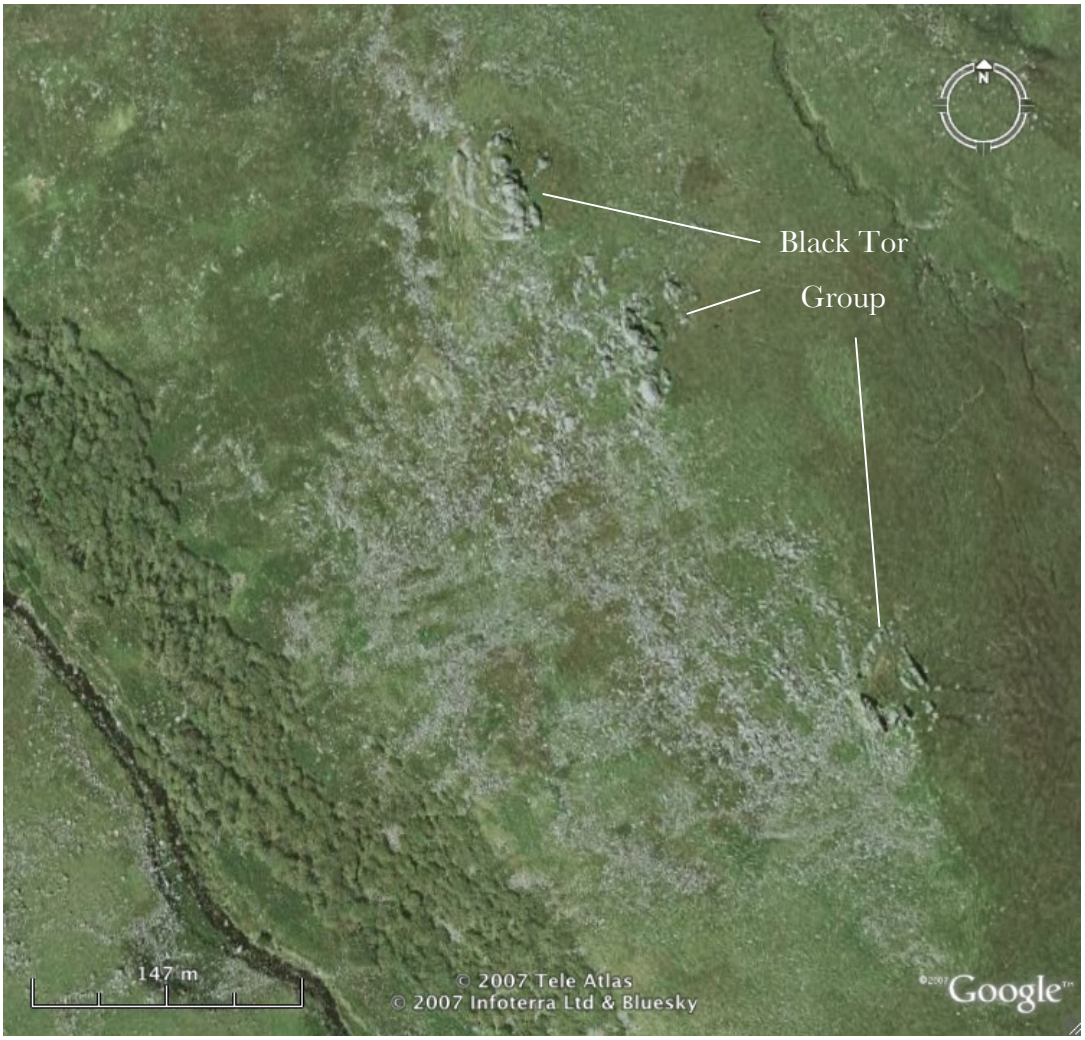

Figure 3.32 Aerial photography of the Black Tor group on the ridge and valley slope of the West Okement River including forested area of Black-a-Tor Copse.

Image: GoogleEarth™

(**a**)

(**b**)

Figure 3.33 The tor outcrops of the Black Tor group on a ridge above West Okement River valley.

Photos: Terry Hurt – flickr/terryjh

Figure 3.34 The sampled surface on tor outcrop BT2 in the Black Tor group; BT2D is the middle sample bag.

A sample from the middle outcrop of the Black Tor group (BT2) was analysed for ^{10}Be concentration. The entire BT2 complex stretches ~50 m along the ridge, and is up to 20 m across. It consists of a number of smaller rock outcrops. The sampled surface was at the southern end of the main cluster, with a surface area of 4.1 x 2.8 m and height upslope of 1-1.5 m and downslope of 7 m. As can be seen in Figure 3.34, the surface is split lengthwise by a vertical joint and vegetated. There are also shallow weathering pits developing where pools are visible. It was observed during sampling that the rock was much harder than that at the High Willhays upslope.

The ^{10}Be concentration of 3.14 ± 0.12 x10^5 atoms g^{-1} measured in the sample from BT2 (Table 3.4) is comparable to the upper end of those measured on High Willhays and Great Links Tor. As with surfaces in those tor groups, the Black Tor is probably better interpreted as an eroding surface, with a calculated erosion rate of 18.5 mm ka^{-1}. This should be treated with caution as a single sample from a surface undergoing episodic erosion could fall anywhere in the range of concentrations. The weathered appearance of the sampled surface suggests that this is probably on the older end of exposure lengths for this tor surface. Given the location of the tor on the cusp of a sharp break in slope and the evidence for wall collapse of the tors downslope, it might have been expected that the tor was eroding more rapidly that the summit tors. However, the erosion rate measured is a vertical erosion rate on an upper surface, and the rate of lateral retreat may be far greater.

3.6.2 Lints Tor

Lints Tor is a summit tor, although an unusual one as it does not cap one of the large upland summits, but a smaller hill within the West Okement valley (Figure 3.31; 3.35). This hill is created by the more than 90° change in direction of the West Okement River south of Lints Tor which forms the south-eastern and western boundary for the hill. It is also separated from the main hillslope to the north and east by a small tributary stream. The Lints Tor is isolated from the surrounding topography and the summit at 496 m is lower than the other summit tors nearby (High Willhays and Steng-a-Tor). The slope on the western side of the summit is the steepest at ~13° and with a 70 m difference in elevation to the West Okement River.

The tributary to the north and east is not as deeply incised as the main trunk river, limiting the slope. To the south-east the Lints Tor hillslope merges with that of the spur from the High Willhays.

The Lints Tor outcrop covers a relatively small area at 16 m long and 4 m wide, although is between 4.5 and 5 m high. It has vertical rock-faces on all sides and a blocky appearance with horizontal joint spacing of 15-50 cm and vertical jointing of 50-100 cm (Figure 3.36). There are a large number of blocks on the ground surrounding the tor. It appears that many of these were derived through the collapse of the tor, with many of these blocks having both rounded and sharp edges (Figure 3.36b), suggesting they were once part of an outcrop (weathering of exposed sides). The combination of vertical sides and large numbers of blocks suggests that lateral retreat of the rock face is occurring at Lints Tor.

The upper surface of Lints Tor has a highly weathered appearance (Figure 3.37). The edges of the blocks are well-rounded and the surface of the granite is uneven with a number of knobbly protrusions of tourmaline. Interestingly, there is grus developed within the joint spacings (Figure 3.37b), this unconsolidated material is either being developed *in situ* with the weathering of granite or could potentially be remnant of pre-tor emergence regolith cover. These joint spacing filled with grus allow for grasses to colonise the upper surface of the tor.

The sample LT2 from the Lints Tor upper surface (Figure 3.37a) was analysed for ^{10}Be concentration (Table 3.4), with a measured value of 2.21 ± 0.10 x10^5 atoms g^{-1}. This is comparable to ^{10}Be concentrations measured on tor surfaces at the High Willhays and Great Links Tor. As with those surfaces, an interpretation of the ^{10}Be concentration as an erosion rate is probably most appropriate. The erosion rate derived from the LT2 sample is 27.7 ± 1.3 mm ka^{-1}, although this single value should be used with caution as the surface is probably undergoing episodic erosion. This rate is close to the average erosion rate of sampled surfaces from the High Willhays tor group (26.9 mm ka^{-1}). This represents a vertical erosion rate for Lints Tor, and lateral retreat of the faces of this stack tor is likely more rapid.

Figure 3.35 Aerial photography of the vicinity of Lints Tor (centre of photo). The West Okement River flows south to north on the western side of the image. The Lints Tor is isolated within the valley by the drainage network.

Image: GoogleEarth™

(**a**)

(**b**)

Figure 3.36 The tor outcrop at Lints Tor with a blocky appearance and vertical faces.

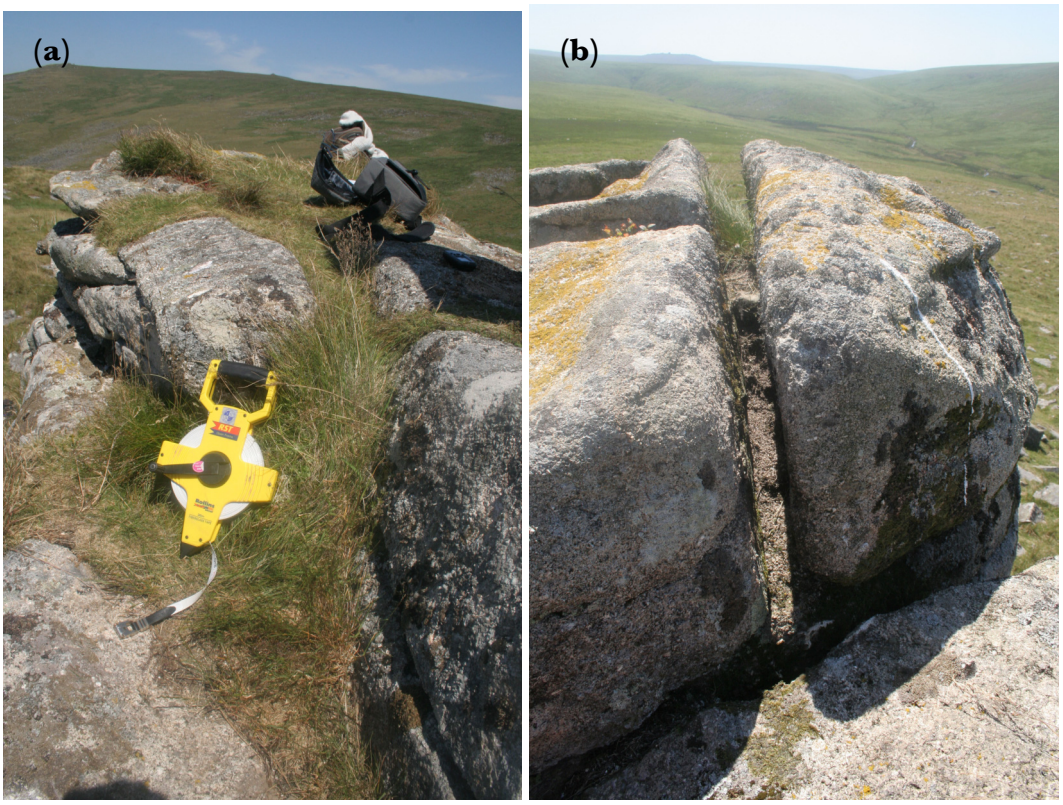

Figure 3.37 The top surface of Lints Tor which features vegetation development and a weathered surface with grus present in joints.

3.6.3 Dinger Tor

The Dinger Tor outcrops on the gentle hillslope (<4°) that descends from the High Willhays to Kneeset Nose on the West Okement River (Figure 3.31). This location would make it a spur or emergent tor under the categorisations of Gerrard (1978) and Ehlen (1992). Dinger Tor is a buttress tor (as defined by Linton, 1955) that has not fully emerged from the surrounding hillslope. On the downslope side there is an approximately 25 m long and 3.5 m high exposed rock face (Figure 3.38a). This face has an appearance typical of many tors in this study, with horizontal joint spacing of ~10 cm and vertical joints on the order of ~1-5 m. The surface on top of this rock face is also exposed granite with a width of ~5 m (Figure 3.39). Upslope the outcrop merges into the regolith mantled hillslope with no emergent vertical face of granite, the slope retreat also appears to be uncovering new granite bedrock (Figure 3.38b). Although the buttress outcrop is the main exposure of granite at Dinger Tor, as can be seen in Figure 3.39, this appears to be the southern extent of a larger mass of granite that forms a raised platform extending some 70 m to the north-east and 25 m wide. In the upslope northern part of this mass some bedrock is also exposed, although this height of these outcrops is < 1 m.

The outcrop of Dinger Tor could be interpreted as tor in the earlier stages of emergence from the surrounding ground surface. If development was to continue through the stripping of regolith and detached blocks it could uncover a greater mass of intact granite, and the formation of larger and more numerous tor outcrops. Alternatively, this outcrop might lack some structural, lithological or geomorphological property that would allow larger tors to form at this location.

The sample DT01 was taken from the surface of the Dinger Tor buttress outcrop. The analysis of ^{10}Be in this sample returned a concentration of $1.43 \pm 0.06 \times 10^5$ atoms g^{-1}, and a calculated erosion rate of 45.6 mm ka^{-1} (Table 3.4). This erosion rate is substantially higher than any other tor surface sampled in this research, and is more similar to sampled bedrock surface at the base of HW2 tor and regolith at the High Willhays. This is perhaps not surprising given the proximity of the sampled surface to regolith that is ramped behind the buttress. It is quite possible

(**a**)

(**b**)

Figure 3.38 The tor outcrop at Dinger Tor which is a buttress-type outcrop.

Figure 3.39 Aerial photography of the Dinger Tor outcrop. The exposed rock face of this buttress tor is located to the south, close to the military track. There are emerging bedrock outcrops in the north-east, although these are less than 1 m high.

that this surface was only recently uncovered and bearing the cosmogenic nuclide signature similar to regolith. Alternatively, it could simply be that the tor is eroding more rapidly than others studied, or a 'freshly' exposed surface where episodic erosion is occurring. Further interpretation is not possible without additional analyses of the tor surface and measurement of regolith erosion rates at the site.

3.6.4 Steng-a-Tor

Steng-a-Tor (elevation 540 m) is a small and isolated tor outcrop on the edge of the broad upland surface only a hundred metres before the transition to the steep valley sides of the deeply incised West Okement River (Figure 3.31). The hill on which it is located, consisting of Amicombe Hill, Woodcock Hill, and Corn Ridge, is a very low gradient (<5°) plateau that extends ~5 km parallel to the main trunk of the West Okement River. To the southeast this mass extends to include Great Links Tor (section 3.5), some 2 km from Steng-a-Tor.

There is a large outcrop measuring 13 m x 6.5 m and a smaller one of 4 m x 2 m to the side (Figure 3.40). There is obvious pseudobedding in the granite with narrow horizontal joint spacing of approximately 10 cm and vertical jointing of 2-5 m that controls the extent of the tor and separates the two outcrops. At the south-eastern end of the tor (left of Figure 3.40a) there is a 'logan-stone' which can be rocked by hand. The ground surrounding Steng-a-Tor is water-logged, as is much of the upland surface.

The concentration of ^{10}Be was measured in two samples from Steng-a-Tor, one from the centre of the main outcrop (SAT02) and another from the smaller detached outcrop (SAT03). The resulting concentrations of 3.79 ± 0.17 and 3.66 ± 0.13 x10^5 atoms g^{-1} respectively, are indistinguishable at 1σ internal uncertainty. Because these values are similar, it is not possible to dismiss the interpretation of an exposure 'event surface' for Steng-a-Tor. Also, the modelled ($\varepsilon = 0$) exposure ages of 48.5 and 46.8 ka are not implausible for an ~2 m high outcrop (if ground surface lowering is similar to High Willhays ~50 mm ka^{-1}). However, there is no particular reason to believe that this outcrop is behaving any differently from other similar tors studied. Therefore,

(**a**)

(**b**)

Figure 3.40 The tor outcrop at Steng-a-Tor on the Amicombe Hill.

erosion rate is probably the most appropriate interpretation of the ^{10}Be concentrations, with rates of 16.1 ± 0.8 and 16.7 ± 0.6 mm ka^{-1} amongst the lowest on any tor surface studied.

3.6.5 Summary

Although there are too few results at each site to be confident of the average denudation rates for each tor group, those measured are consistent with results from tor surfaces at High Willhays and Great Links Tor. This suggests that tor surface erosion rates are comparable across the study area in north-western Dartmoor, and that landscape position (i.e. non-summit sites on spurs and valley-sides) is not a clear influence on erosion rate. The exception is the result returned from the buttress-style outcrop at Dinger Tor, where a surface that may have only recently been uncovered returned a higher surface erosion rate.

3.7 Discussion

3.7.1 Erosion of Tor Surfaces

The erosion of tor surfaces is fundamental to understanding their origin, development, and persistence in the landscape. Prior to the development of the cosmogenic nuclide technique, the age constraints on tors were generally made on the basis of weathering features (e.g. weathering pits, block roundness, quartz vein relief etc) and tor height. However, these features are open to a variety of interpretations and have been used in different ways to support conflicting landform development models (e.g. Linton, 1955 vs. Palmer & Nielson, 1962). In this study, the analysis of ^{10}Be concentrations in tor surfaces provides a quantitative measure of surface exposure and allows for the calculation of long-term erosion rates of the tor landforms.

The erosion of crystalline granite bedrock outcrops occurs in two primary ways: (i) through granular disintegration at the bedrock surface; and (ii) by the detachment from the surface of blocks that develop along joints. On most tors the gradual process of granular disintegration of the surface will be interspersed with the periodic

removal of blocks. In most situations, episodic block removal will determine the overall erosion rate of the tor landform (granular disintegration is only important if it has eroded more than a block thickness between block removal events). The cosmogenic nuclide erosion signal will reflect this with an exposed surface accumulating nuclides (at the production rate of an eroding surface where ε = granular disintegration) until the removal of a block, at which time a 'fresh' surface is uncovered and accumulation begins again (although if block thickness is less than 2-3 m this surface will have an inheritance of nuclides accumulated at depth).

3.7.1.1 Granular Disintegration

An exposed granite surface is subjected to constant subaerial weathering resulting in the grain-by-grain removal of material from the surfaces. In crystalline granitic rock, this is likely to be a conjunction of mechanical breakdown (e.g. frost action) and chemical weathering, which act along fractures and grain boundaries of minerals (Small *et al.*, 1999). This generates weathering features on surfaces, including weathering pits, raised resistant-mineral relief (e.g. quartz veins or tourmaline), the widening of joints and rounding of edges, and the formation of grus. All of these are evident on tor surfaces in Dartmoor (Figure 3.41), although they are not as well developed on the tors included in this study (i.e. in north-west Dartmoor). This is probably due to smaller than average horizontal joint spacing in these tors, which limits the development of weathering features and is likely to increase the frequency of block spallation. Prior to development of the cosmogenic nuclide approach, geomorphologists relied heavily on relative age criteria such as the development of weathering features on tor surfaces (Hall & Phillips, 2006a). It is important to recognise that this weathering provides an indication of block surface exposure age and erosion, but does not necessarily reflect on the tor landform erosion rate, although it may provide some indication of the frequency of block removal. The following provides a brief summary of the development of weathering features on Dartmoor tors.

Weathering Pits – are a common weathering feature of many granite surfaces. They develop on near-horizontal surfaces where slight depressions allow water to collect and be retained at the surface, thereby enhancing weathering. As the pits grow they

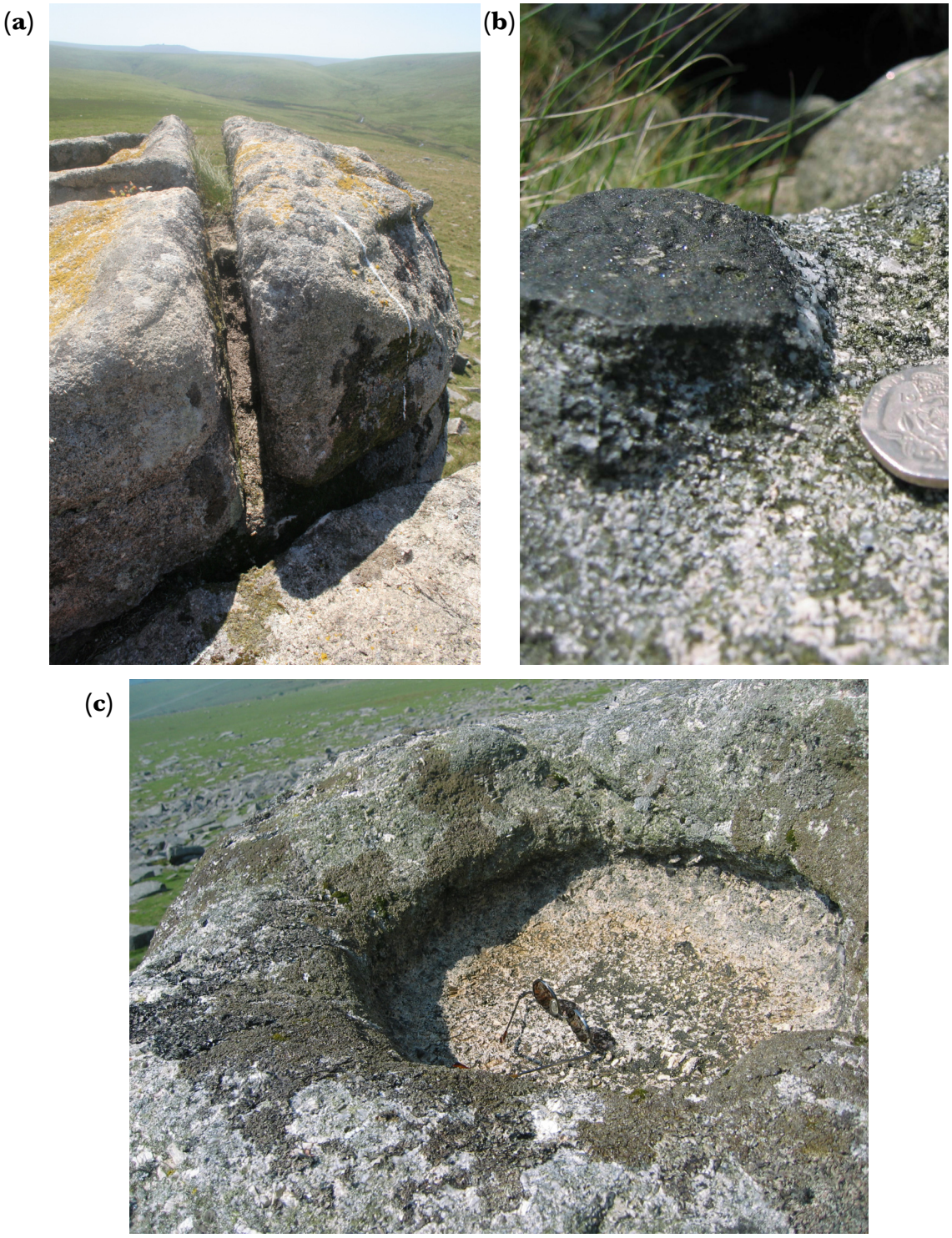

Figure 3.41 Surface weathering features on granite surfaces in Dartmoor; (a) Lints Tor with widening of joints and granular disaggregation producing grus; (b) raised relief of a tourmaline mineral assemblage near Yes Tor; and (c) weathering pit developed on top surface of Great Staple Tor outcrop.

can reach considerable size, until they eventually coalesce with neighbours or reach joint boundaries and drain (Hall & Phillips, 2006a). There are few weathering pits developed on the tors included in this study, most likely due to the narrow spacing of horizontal jointing in these tors. Elsewhere in Dartmoor, there has been a considerable size of weathering pit development (Figure 3.41c), with some reported to reach diameters of up to 2.4 m (Ormerod, 1858). Weathering pits were observed to occur in outcrops with wider joint spacing than those studied.

Raised Mineral Relief – is developed by the differential weathering of crystalline granite. Some minerals (e.g. quartz and tourmaline) are more resistant to weathering processes and, consequently, a difference in micro-relief develops as the surrounding granite erodes more rapidly. This is a feature of most exposed surfaces in Dartmoor, with quartz vein relief and other protruding minerals commonly observed (Figure 3.41b). In other regions the relief of features like quartz veins has been used as a relative dating technique for surfaces (e.g. Cairngorms, Scotland: Phillips *et al.* 2006). In Dartmoor there is no clear formative event for surfaces apart from block removal, and therefore, no age control for such an approach. Consequently, the observation of raised mineral relief is limited to a qualitative indicator of surface exposure.

Joint Widening and Edge Roundness – are more contentious weathering features, as they have been ascribed to both weathering in the sub-surface (e.g. Linton, 1955) and to surface weathering (e.g. Palmer & Nielson, 1962). The orthogonal jointing of granite produces sharp-edged blocks, and where weathering occurs it preferentially weathers edges and leads to an increased roundness. This has been observed to occur in the subsurface with rounding of corestones and unaltered granite masses (e.g. Linton, 1955). However, it has also been demonstrated that significant edge rounding can occur on exposed blocks (e.g. post-glacial block rounding in the Cairngorms, Scotland; Kirkbride, 2005) and the roundness of Dartmoor tors ascribed to surficial weathering (e.g. Palmer & Nielson, 1962). On the studied tors there was clear evidence of both joint widening and edge rounding of tor outcrops, a good example being from the upper surface of Lints Tor (Figure 3.41a). There has been much discussion of the relevance of roundness of granite boulders, but this has proved futile

given the difficulty in defining a division between angularity and weathering process (Gerrard, 1994).

Granular Disaggregation (Grus) – the collection of gravel and sand sized particles in tor joints and crevices suggests the granular disaggregation of the granite. Examples of this were observed on Lints Tor (Figure 3.41a) and on the High Willhays tor HW5, but also, to a lesser extent, on many of the other tor surfaces sampled. It is possible that these are deposits of weathered granite left behind following the emergence of tor. However, the high erosion rates observed on the studied tors suggests that preservation of this incoherent grus is unlikely, hence it is probably also be produced *in situ* following the initial emergence of the tor landform.

The erosion rate of crystalline rock by granular disintegration is suggested by André (2002) to be similar irrespective of climate conditions, and reports rates in Sweden of 0.2 mm ka^{-1} (homogenous crystalline rocks) to 1 mm ka^{-1} (biotite-rich crystalline rocks), although rates are up to ten times greater in weathering pits and joints. Similar erosion rates have been reported in granite of the Cairngorms, Scotland, by Phillips *et al.* (2006) at average of 1.6 mm ka^{-1} (but up to 5.3 mm ka^{-1}), and Everest *et al.* (2006) at 0.5 mm ka^{-1}. These studies were on surfaces scoured by glacial ice, and measured the quartz vein relief that has developed post-glaciation. There is no such 'event' from which a comparable mineral relief could be measured on Dartmoor rock surfaces.

The cosmogenic nuclide concentration in tor surfaces in Dartmoor determines erosion rates of 14-32 mm ka^{-1}. Given the low rates of granular disintegration reported elsewhere for crystalline bedrock, it seems that the rates measured on Dartmoor are too high to be recording an incremental erosion of surfaces. Instead this cosmogenic nuclide signal must be related to either surface erosion by episodic block removal or an interval since another exposure event. An assessment of weathering feature development on a tor surface provides insight into the frequency of surface renewal/exposure, although it does not directly measure the erosion of most tor landforms in which episodic erosion is occurring.

3.7.1.2 Episodic Block Removal

The physical disintegration of jointed granitic rock can occur by the sheeting, unloading, and spalling of rock, and is enhanced by frost action (Fookes *et al.*, 1971). The initial stages of granite weathering are accompanied by an increase in the intensity of fracturing as well as the discolouration and alteration of minerals along joint discontinuities (Fookes *et al.*, 1971; Ehlen, 2002). The weathering of tor outcrops included in this study would fall under the 'slightly weathered' classification of Ehlen (2002) or Fookes *et al.* (1971), in which discolouration and alteration of joint fractures is primarily limited to the discontinuities and does not extend into the rock to any substantial depth. This is most intense along joint surfaces near the surface, where discolouration was often observed following removal of samples (Figure 3.42a). There is also differential weathering at joints on the vertical faces of tor outcrops, with the joints widening and penetrating into the tor undermining overlying granite (Figure 3.42b), although these joints are usually only weathered to a small depth from the surface (Palmer & Neilson, 1962).

Block detachment along joint surfaces is a common feature of tor outcrops in Dartmoor, with the dimensions of blocks determined by the horizontal and vertical joint spacing. It is often possible to trace the bedrock surface of the tor to a joint in an adjacent upstanding part of the same outcrop, suggesting that surfaces form along joint planes. The tor groups studied have a horizontal joint spacing that is less than the Dartmoor average (Table 1; Ehlen, 1994), with resulting slab or sheet form of blocks. At the Great Links Tor group there is evidence for block detachment on both the primary horizontal joint spacing at 53 cm (Figure 3.26b; 3.27) and secondary spacing at 9.4 cm (Figure 3.26a,c). At the High Willhays tor group the horizontal joint spacing is less than 5 cm, leading to the exfoliation of thin sheets of rock from the surface (Figure 3.22).

It is difficult to directly relate blocks on the ground surface around tors to removal from the tor surface, with the exception in this study of Lints Tor. This is probably due to the development of peat that covers the block-strewn ground surrounding most tors. The comparatively small blocks that are generated by most of the studied

(**a**)

(**b**)

Figure 3.42 Joint weathering on tors – (a) discolouration of the joint surface following the removal of sample HWBS1 at the High Willhays; (b) joint widening and penetration on the vertical face of Great Links Tor, sampled surface GLT1b.

Figure 3.43 Great Staple Tor is a 'wool-sack' style outcrop and there appears to be many blocks detached from the outcrop and displaced onto surrounding ground surface.

Figure 3.44 An outcrop of bedrock near the Yes Tor summit surrounded by a blockslope deposits, it is difficult (or impossible) to distinguish between blocks detached from tor outcrops and those derived from the regolith.

tors (due to closely spaced joints) are also less likely to penetrate the peat cover and be observed at the surface. At more blocky tors (e.g. Lints Tor, Figure 3.37; Great Staple Tor, Figure 3.44), the similarity between outcrop block development and those on the surrounding ground surface is obvious, with evidence for outcrop collapse and displacement of blocks. However, it can be difficult (or impossible) to distinguish between blocks detached from outcrops and those derived from the disruption of bedrock under regolith (Figure 3.45), especially if joint sets are similar in the outcrop and sub-regolith bedrock.

The geomorphological evidence for block removal from tor surfaces in Dartmoor is supported by the interpretation of measured cosmogenic nuclide concentrations. These were observed to vary significantly between samples, even when collected from surfaces only metres apart on the same outcrops at High Willhays. The most plausible explanation for the variability in ^{10}Be concentrations is that episodic block removal has occurred on the tor surfaces resulting in samples with different exposure histories.

3.7.1.3 Cosmogenic Nuclide Erosion Rates

The erosion rates derived from ^{10}Be concentrations in tor surfaces ranged from 14 to 32 mm ka^{-1}, with an average of 22.5 mm ka^{-1} (excluding Dinger Tor at 45.6 mm ka^{-1}). The average erosion rate of the High Willhays tor group, at 26.9 mm ka^{-1}, is higher than the 20.3 mm ka^{-1} average measured on the other tor surfaces. It may be that there are higher erosion rates on the High Willhays granite outcrops (with closely spaced horizontal joints). Alternatively, this difference may be an artefact of a lower frequency of block removal (and sampling bias towards 'older' surfaces) on the other tors, or simply the result of variability within a limited sample size.

Cosmogenic nuclides have been used in a range of environments to measure erosion rates or exposure ages for granite bedrock surfaces (Table 3.5). In this study, the measurement of ^{10}Be indicated surface erosion rates of 14 to 46 mm ka^{-1} (or alternatively an equivalent minimum surface exposure age ($\varepsilon = 0$) of between 18 and 55 ka). These erosion rates are higher than most other locations, although this is not

unexpected as many are in locations of presumed slow denudation rates (e.g. central Australia and Namibia). Those with the most similar geomorphological settings are tor outcrops in formerly glaciated Scotland (Phillips *et al.* 2006) and northern Sweden (Fabel *et al.* 2002), and perhaps those on the mountain summit plateaus of the western USA (Small *et al.* 1997).

Table 3.5 Cosmogenic nuclide derived exposure ages and erosion rates for granite bedrock surfaces.

Source	Location	Surface Type	Erosion Rates (mm ka^{-1})	Exposure Ages (ka)
Small *et al.* (1997)	Western USA mountain range summits	Tors	2 - 19	35 - 236
Heimsath *et al.* (2000)	New South Wales, Australia	Tor	9.1 - 9.6	65 - 68
Wakasa *et al.* (2006)	South Korea	Dome	~56[a]	
Phillips *et al.* (2006)	Cairngorms, Scotland	Tors	2.8 - 39	15 - 200[b]
Fabel *et al.* (2002)	Northern Sweden	Tors		34 - 61[b]
Hancock & Kirwan (2007)	Appalachians, USA	Tors/Outcrops	2.2 - 9.5	61 - 242
Granger *et al.* (2001)	Western USA mountain ranges	Bedrock	6 - 18	
Briner *et al.* (2003; 2006)	Arctic Canada	Tors		22 - 170[b]
Quigley *et al.* (2006)	Flinders Range, Australia	Bedrock	4 - 14	42 - 144
Bierman & Turner (1995)	South-central Australia	Inselberg	0.6 - 4.9	114 - 628
Bierman & Caffee (2002)	Central Australia	Inselberg	0.3 - 5.7	105 - 1310
Heimsath *et al.* (2001)	New South Wales, Australia	Tors	3.6 - 28	22 - 162
Bierman & Caffee (2001)	Central Namib Desert, Namibia	Inselbergs	1.1 - 7.5	80 - 508
Cockburn *et al.* (1999)	Central Namib Desert, Namibia	Bornhardts	2.9 - 6.2	

[a]sheet exfoliation model was applied to derive an average erosion rate

[b]sample nuclide concetrations are interpreted as ice-free length of surface exposure

Phillips *et al.* (2006) measured ^{10}Be concentrations in samples from tors in the Cairngorms, Scotland. Although only moderately higher in elevation (650-1320 m) than the tors of Dartmoor (<621 m), the Cairngorm tors are located in a region of ice sheet growth during glacial stages of the Quaternary, resulting in long intervals of burial under ice and glacial modification of many tors. To address issues of the possible preservation of pre-Quaternary landscapes, the ^{10}Be data was primarily interpreted as minimum surface exposure, with ages ranging from 15 to 200 ka. However, the ^{10}Be signature for most tor surfaces is actually quite similar to those measured in Dartmoor. In particular, erosion rates calculated for 'glacially modified tors with slightly weathered surfaces' are between 14 and 39 mm ka^{-1}, whilst many of those with 'advanced weathering features' are between 7 and 30 mm ka^{-1}. They also reported some tors with maximum surface erosion rates as low as 2.8 mm ka^{-1}, much lower than any surface measured in this study on Dartmoor. In northern Sweden, Fabel *et al.* (2002) also measured ^{10}Be concentrations in tors on 'relict surfaces' and derived minimum surface exposure ages of 34 to 61 ka, which given long intervals of burial under ice suggest the tors landforms have been present for up to 845^{+461}_{-418} ka.

The development of tors in a landscape periodically covered by an ice sheet introduces specific considerations of the glacial modification (or preservation) of tors and shielding of the surface from cosmic rays by overlying ice. Both Fabel *et al.* (2002) and Phillips *et al.* (2006) were interested in demonstrating the potential for tor landform preservation under ice sheets, and consequently, interpreted their cosmogenic nuclide data primarily in terms of minimum surface exposure ages. This is useful in terms of their research question; however, without a defined initial exposure 'event surface' (at least in cases where tors are preserved under ice) a surface erosion rate may also be an appropriate geomorphological interpretation of the cosmogenic nuclide data.

Small *et al.* (1997) also studied tors developed under periglacial conditions on mountain summit ranges in the western USA. Like Dartmoor, these surfaces are thought to have remained ice-free during Quaternary glaciations, leaving the tors to develop over extensive intervals of intense periglacial conditions. These sites are at elevations of 3300-3750 m, considerably higher than those found on Dartmoor (<621 m). The cosmogenic nuclide data was interpreted as episodic erosion rates for the tor surfaces, with an average of 7.6 mm ka^{-1} and ranging from 2 to 19 mm ka^{-1}.

These are lower erosion rates than those measured for Dartmoor tor surfaces in this study. Small *et al.* (1997) suggest that frost action is limited at their study sites by a lack of available water. The importance of moisture for the effective operation of periglacial processes is highlighted by Hall *et al.* (2002), who suggest that in wetter cold regions frost action and wetting drying processes may be a particularly effective combination. Dartmoor is located close to the Atlantic Ocean and, even during the most intense cold intervals of the glaciations, southwest Britain is considered to have remained comparatively wet (Palmer & Neilson, 1962). The combination of long intervals of intense periglacial conditions (the highest parts of Dartmoor falling only marginally below ELA estimated for the LGM; Campbell *et al.*, 1998) with available moisture, provides a possible explanation for the higher erosion rates derived for Dartmoor tor surfaces than those in other regions.

The cosmogenic nuclide signature of an eroding bedrock surface is integrated over the interval of its emergence (i.e. in the near-surface where it is exposed to cosmic radiation). This is dependent on the erosion rate, and for Dartmoor samples the calculated averaging timescale for tor surfaces ranges from 14-45 ka. This indicates that the measured erosion rates reflect both interglacial and glacial climate conditions. It is often suggested that Holocene erosion is minimal in Dartmoor (e.g. Gerrard, 1993). If this is the case, then LGM erosion rates would have to be significantly higher to produce the cosmogenic nuclide signal measured. It may be that during intervals of intense cold the processes of block removal from outcrop surfaces are more effective, whilst during warmer periods there is effective weathering of joints. However, it is not possible to demonstrate such a relationship with the present data.

3.7.2 Emergence of Tor Landforms

The ^{10}Be measured in granite bedrock surfaces in Dartmoor has shown them to be eroding at relatively high rates of 14 to 45 mm ka^{-1}. These rates are incompatible with a simple two-stage model of tor development in which the form of the outcrop is determined in the subsurface by differential deep weathering. If this had occurred it would be expected that ^{10}Be were either: (i) related to the tor height as higher surfaces were exposed earlier; or (ii) if regolith stripping was very rapid then consistent across the tor surfaces. Instead, concentrations were found to vary considerably across (and upon) tor surfaces, indicating significant modification of the studied tors following exposure.

The cosmogenic nuclide signature in a surface can only reflect erosion over the interval that the last few metres were removed, and even this is biased towards the most recent. Consequently, beyond establishing an erosion rate for the surface, it is difficult (or impossible) to distinguish between possible origins of the landform (single-phase versus post-exposure modified two-stage tors) based on tor surface ^{10}Be measurements. However, if the erosion rates determined for tor surfaces (22.5 mm ka^{-1}) and regolith (51.7 mm ka^{-1}) are an approximation of long-term Quaternary averages, then some constraints can be placed upon scenarios of tor emergence.

A tor emergence rate of 25 mm ka^{-1} was estimated for the tors at the High Willhays, and from this it was estimated that the present tor elevations would have taken up to 220 ka to develop. An even longer 300 ka can be estimated for the larger outcrops in the Great Links Tor group. Over this timespan, many metres of rock would have been eroded from the surface of the tors. This is problematic for the two-stage hypothesis of tor development, as the removal of metres of material will mean little of the tors subsurface form is preserved, and consequently, relegating deep weathering to an influence on the location of tor outcrops. In addition, given that tors are a transient feature in the landscape under a two-stage model, at the erosion rates measured, the initial subsurface granite mass would have to be substantially larger than the present outcrop.

The single-phase concept of landform development is compatible with the relatively high erosion rates measured on the bedrock surfaces and surrounding regolith mantled ground. These rates are high enough for the studied tors to form entirely during the Quaternary, without the need for extensive preconditioning in the subsurface. Although it is not possible to differentiate between Holocene and periglacial processes, the ^{10}Be data indicates that periglacial conditions were effective in eroding tor surfaces at a rate substantially higher than typical rates of granular disintegration of granite (1.0-1.6 mm ka^{-1}: André, 2002; Phillips *et al.*, 2006).

Heimsath *et al.* (2000; 2001b) tested hypotheses of tor emergence in: (i) steady-state where there is long-term disequilibrium in tor and regolith erosion rates (an increase in ^{10}Be with height above surface); and (ii) an episodic model in which an interval of 'stripping' rapidly exposed the tor (no up-profile variation). Although only a limited number of tor profile samples were analysed in this Dartmoor research, there was no apparent up-profile variation. This is supported by the lack of relationship between ^{10}Be concentrations and tor height above the ground surface. While this could be interpreted as evidence for a 'stripping' event, the high erosion rates calculated for the surfaces and their variability suggest that for many tor surfaces the cosmogenic nuclide signal has adjusted to erosion and the 'emergence' component of the signal may have been removed by post-emergence erosion of the surface.

If the difference in calculated erosion rates for tor surfaces and the surrounding ground surface is applicable in the long-term, then it might be expected that this disequilibrium would lead to a continued increase in outcrop height (e.g. at 25 mm ka^{-1} for the High Willhays). However, the maximum height of a tor landform will be determined by the lateral erosion rate and the width at the base of the outcrop. For example, using rates from the High Willhays (tor surface erosion ~27 mm ka^{-1}; tor emergence rate ~25 mm ka^{-1}) and an outcrop base width of 10 m, lateral erosion will have eroded from both sides (i.e. 5 m) in 185 ka, over which tor height could have reached 4.6 m. At a tor that has reached this 'maximum' tor height, the erosion rate of the upper surface will be increased by the addition of the lateral component. This would also be evident in the cosmogenic nuclide signal from such a surface.

The observation of tor landforms on Dartmoor suggests that lateral erosion rates are likely to be highly variable, and determined by the spacing of vertical joints. For example, there appears to have been significant block removal from the vertical faces of the Lints Tor outcrop (section 3.6.2), while the lack of surrounding block-debris and rounded form of the tors suggests a more gradual process of lateral erosion on the High Willhays group outcrops. In this study, the rate of lateral erosion is not well constrained due to a limited number of analyses available. Those that were measured indicate that surface erosion rates may be similar to those on tor surfaces (20-30 mm ka^{-1}), although it may be problematic differentiating between an erosion and an emergence (exposure) signal in these samples (see sections 3.4.4.2 and 3.5.3).

The SPF is a useful concept in developing an understanding of tor emergence and landscape development. In studies by Heimsath *et al.* (1999; 2000; 2001a; 2001b; 2002; 2005) and Wilkinson *et al.* (2005), the relationship between regolith thickness and denudation rate has been explored with cosmogenic nuclide analysis. The potential to use SPFs as an explanation for tor formation is also discussed by Anderson (2002) and Strudley *et al.* (2006a; 2006b). However, in this study it was not possible to reliably determine the base of the regolith profile at excavated sites on the Yes Tor – High Willhays summit area (section 3.4.2). In these circumstances, it is not

possible to directly assess the relationship between regolith thickness and regolith production rates, and consequently, the SPF is not determined by this study.

Although it is not possible to directly assess the SPF for tor emergence at Dartmoor, it can still be a useful concept in exploring how and why outcrops develop. The basis of the SPF concept is the balance between weathering and transportation on a slope (Carson & Kirkby, 1972; see section 3.2.3). In Dartmoor, Gerrard (1988) argued that tors form in locations of imbalance between the production and removal of weathered material; and that this was likely to occur where processes of removal are most efficient (e.g. steep valley-side slopes, breaks of slope, and summit divides). This is similar to the basis of SPF concept, although it lacks detail and recognition of potential feedback relationships between regolith depth and weathering rate. This results in a simplified interpretation where he supposes that: (i) where ground surface is stable, regolith may deepen; (ii) where there is instability it may be removed; and (iii) that there may be locations in steady state balance of generation and removal. Although this is not an unreasonable interpretation, it lacks the explanatory depth of SPF concept for tor location.

In terms of Dartmoor tor emergence, weathering (or resistance to it) is widely considered to relate to the joint structure of the underlying granite (Gerrard, 1988), and it features in both the models of Linton (1955) and Palmer & Nielson (1962). In the context of an SPF, the increase in resistance to weathering would lead to a shallower function, which in the case of a 'humped' model would increase the chance of the profile entering the instability thickness. Therefore, tors would be more likely to emerge in locations with more resistant bedrock, a sensible conclusion. In this respect, the SPF could also be applied to the 'emergence event' of an outcrop under the two-stage hypothesis, with the less resistant (saprolite) grus producing a 'deeper' SPF and therefore more likely to remain regolith mantled.

The topographic location is also essential in understanding tor formation in terms of the SPF concept. At locations of topographic divergence or break in slope, the potential for transportation is increased relative to input from upslope transport. This

will lead to an increase in regolith generation at this location, but also increases the likelihood of the profile becoming unstable. Areas of topographic divergence are also less likely to receive and retain a supply of water in the subsurface, which would result in a lower potential for weathering. It is therefore likely that an outcrop would emerge in locations of topographic divergence or break in slope, something that is observed in the location of tors included in this study, as well as elsewhere in Dartmoor (e.g. Gerrard, 1988; Ehlen, 1992)

3.7.3 Implications for Landscape Development

A variety of mechanisms have been proposed to explain the development of tors, and it is conceivable that tors formed by different processes are present in the Dartmoor landscape (Gerrard, 1994; French, 1996). It is suggested by Gerrard (1994) that while most valley-side tors probably owe their origins to periglacial processes, some of the large summit tors have a composite origin of both chemical weathering and frost-action. The measured cosmogenic nuclide erosion rates, while not excluding a role of chemical weathering, indicate that Quaternary processes are effective enough to have generated even the largest tors in Dartmoor.

In Linton's (1955) model for the origin of tors, it was envisaged that a layer of deep weathering was present across Dartmoor, and that tors exist where this has been stripped to the base level by periglacial processes. Eden & Green (1971) investigated granite weathering across Dartmoor and found that weathering was localised to river valleys and the margins of the granite. They observed that tors also tend to occur on interfluves and summits near to the main river valleys and concluded that this was due to localised deep weathering. However, this apparent concentration of tors in the proximity of valleys could also be explained by the increase in slope in these locations, with an increase in potential downslope transport. This would fit well with an SPF concept of tor emergence, with an increase in transportation more likely to lead to instability in the regolith profile and the emergence of an outcrop. This would also explain the lack of tor outcrops on central plateau summit areas in Dartmoor, where the transportation of regolith is limited.

Although sites like Two Bridges Quarry provide strong evidence for the potential formation of tors in the subsurface, the widespread applicability of this as a mechanism of tor formation in the Dartmoor landscape is questionable. In this research, the cosmogenic nuclide derived erosion rates of 14-46 mm ka^{-1} for granite bedrock surfaces indicates that two-stage tors would have a limited lifespan following emergence. Given these rates of erosion, the tors observed in Dartmoor today must have been unearthed only during the last glaciation. This implies that the base of the deep-weathering profile has been reached across a fairly large area during the last glaciation and not in preceding glacial cycles of the Quaternary, requiring a very thick and widespread layer of weathered material that persisted through a number of glacial cycles.

The dynamic model of tor development (single-phase) provides a far more robust explanation for the mechanisms and location of tor formation. The ^{10}Be derived erosion rates of 14-46 mm ka^{-1} for granite bedrock surfaces are compatible with landforms generated during the Quaternary, as is the timescales estimated by 'tor emergence rates' of 200-300 ka for some of the larger outcrops in the tor groups at High Willhays and Great Links Tor. The concept of an SPF can be used to explain the location of tor emergence in terms of an imbalance between weathering and transport processes. This suggests that tors are most likely to occur in locations of topographic divergence or break in slope, and also locations of increased bedrock resistance (i.e. widely spaced joints). It may be that in some locations deep-weathering has provided the initial conditions for the emergence of an outcrop, but even where this does occur the form of the tor is most likely to be quickly shaped by post-emergence processes.

3.8 Conclusion

This study has demonstrated that the tors of northwest Dartmoor are eroding primarily by the episodic removal of blocks, with the measured tor surface erosion rates of 14-45 mm ka^{-1}. The size of these blocks and the frequency of their removal is likely controlled by the spacing of joints in the granite, although this has not been

fully tested in this study due to limited analyses available. The interpretation of the cosmogenic nuclide data indicates that tors have been substantially modified following their initial emergence, which is considered to have occurred within the Quaternary. A dynamic single-phase model of tor development is favoured for the studied tors in the north-west of Dartmoor, and this is considered to be widely, although not universally, applicable to tor formation throughout Dartmoor. The concept of a SPF in regolith profiles is considered a useful approach in explaining the mechanisms and location of tor formation.

4: The Development of Blockslopes

4.1 Introduction

The granite uplands of Dartmoor are widely understood to have remained beyond the southern extent of glaciations during the Pleistocene cold stages. Instead of being subject to glacial modification (or ice-sheet cover) like most areas that possess periglacial landforms (including the rest of upland Britain), the ice-free landscape of southwest Britain was exposed to intense periglacial activity over long intervals during the glacial cold stages. Consequently, it is a particularly suitable location for the assessment of long-term periglacial development. There has been an increased emphasis on the role of periglacial conditions and processes in the formation of the Dartmoor landscape since the 1950s (see Campbell *et al.*, 1998), with a periglacial origin of many landforms recognised. However, the efficacy of periglacial processes in modifying the landscape, and the timescale over which these landforms develop has not been convincingly established, mostly due to a lack of available age control. The concentration of ^{10}Be in a sample reflects the length of its near-surface exposure to cosmic radiation, and can be used to constrain the timescale that blocks are part of the surface layer of a blockslope landform. In addition, variation in the distribution of ^{10}Be concentrations across a blockslope can provide an indication of long-term processes in the landform and the source of blocks. In this study, cosmogenic nuclides are used to investigate the development of a blockslope on the western side of Yes Tor in northwest Dartmoor. This provides the first quantitative measure of long-term periglacial landform development in Dartmoor, and is one of only a few sites worldwide in which periglacial deposits have been analysed using cosmogenic nuclides (e.g. Barrows *et al.* 2004).

4.2 Geomorphological Context

4.2.1 Blockslope Terminology

The nomenclature used to describe boulder-covered ground is varied, with specific (and often contradictory) meaning assigned by researchers to a range of landforms that are both geomorphologically and geographically diverse. Here the terminology

used by White (1976; 1981) is applied to the landforms observed in Dartmoor. A blockslope describes an openwork structure of boulders covering an extensive area on a slope of >10°, extending parallel to the contour and with no obvious rock source (e.g. cliff) upslope. A more specific form of blockslope is that which occurs on a surface of <10° (or even <5°) gradient, which are termed blockfields. This is a significant slope threshold, as above ~5-10° gravity becomes the dominant influence in the operation of the landform (van Steijn *et al.*, 2002). White (1981) also describes blockslopes (and blockfields) as comprising material usually only a few metres thick, with blocks sub-angular to sub-round and most likely derived from underlying bedrock. The blocks at the surface are jammed together and interlocked, with the long axes often aligned parallel, or normal, to the slope direction.

4.2.2 Dartmoor Blockslopes

Boulder-strewn slopes are common in Dartmoor and are often locally referred to as 'clitter' (a Cornish term; Tilley *et al.*, 2000). The landforms that they create have typically been ascribed to periglacial processes and, frequently, the downslope transport of blocks away from tor-capped summits (e.g. Waters, 1964; Green & Eden, 1974; Gerrard, 1988). In places they also form a variety of patterns such as stone stripes, garlands, and runs in the vicinity of Great Staple Tor (Gerrard, 1988; Figure 4.1a). However, in most locations, including the study site at Yes Tor, the boulders blanket a broad expanse of the slope with blocks closely packed together, imbricated and orientated so that they protrude from the slope (Figure 4.1b and 4.1c). Gerrard (1988) suggested that block distribution is related to joint sets in underlying granite, and that where this produces a relative abundance of blocks it produces features like 'blockfields', 'boulder garlands' and 'stone runs', whereas 'stone stripes' form when fewer blocks are available. He also suggests that the close association of tors with 'boulder runs and garlands' suggests that much of the 'clitter' has not moved very far. It is difficult to assess the full extent of blockslope development in Dartmoor due to the Holocene development of moorland peat and vegetation. It is probable that this coverage obscures a far greater extent of blockslopes than is presently visible in the landscape, perhaps evidenced by the ubiquitous protruding boulders on the vegetated slopes of Dartmoor.

(a)

(b)

(c)

Figure 4.1 Blockslope landforms on Dartmoor at (a) Great Staple Tor that features well-developed patterned ground and stone-stripes; (b) on the west side of Great Mis Tor; and (c) on the east side of Yes Tor leading away from the tor outcrops at the summit.

4.2.3 Development of Blockslopes

The association between blockslopes and periglacial processes, in particular frost action, has been made since the earliest days of periglacial research (i.e. Lozinski, 1909; cited in Boelhouwers, 2004). The angularity and vertical orientation of elongated blocks was interpreted as evidence for effective frost-shattering during freeze-thaw cycles and frost sorting in the active layer. This view became so pervasive during the twentieth century, that blockslopes and blockfields often became a diagnostic landform for identifying (past or present) activity of periglacial processes (van Steijn *et al.*, 2002; Boelhouwers, 2004). This led to some widespread assumptions about frost weathering, and a belief that: (i) because coarse blocky material is widespread in cold regions, it follows that weathering in cold regions must be dominated by frost action (minimal chemical weathering); and (ii) since blocky material is widespread in formerly glaciated landscapes, frost weathering must be an effective mechanism to have generated a large volume of material since glaciation. The general validity of these interpretations has been challenged in recent years (see summary in van Steijn *et al.*, 2002; Boelhouwers, 2004). There is now a more widespread recognition that blocky material can be generated in a range of climate conditions, and is not necessarily diagnostic of periglaciation (Boelhouwers, 2004). Furthermore, in locations where cold conditions are prevalent, a number of studies have demonstrated that frost action is not necessarily the dominant weathering process, and that often chemical weathering can be more important (e.g. in Kärkevagge, Sweden: Rapp, 1960; Thorn *et al.*, 2002). The second assumption, that frost weathering is highly effective, has been challenged by an increasingly widespread recognition of landforms that are present for multiple glacial cycles (e.g. Fabel *et al.*, 2002; André, 2003). Although these are in part preserved by burial under cold-based ice, they are not considered to be significantly modified in non-glacial intervals, and in some cases are considered to even be remnants of Tertiary weathering profiles (Boelhouwers, 2004).

This re-evaluation of the genetic link of blockslopes with frost action has lead to a more nuanced view of processes operating in cold regions. The traditional view of periglacial geomorphology overestimated the importance of temperature, whereas

weathering is mostly limited by the supply of moisture (Hall *et al.*, 2002). It is now recognised that chemical weathering is an effective mechanism under many, if not most, periglacial environments, and consequently, is a significant contributor to the overall process of weathering (Hall *et al.*, 2002). Indeed, a variety of azonal processes (not cold specific) such as thermal creep, rapid mass movement and slope wash may well operate under some periglacial conditions (van Steijn *et al.*, 2002).

As the simple process-form relationship between frost action and blockslopes has been increasingly questioned, it is important to recognise how angular blocky slopes might develop in a cold environment like periglacial Dartmoor. Processes of bedrock heave, freeze-thaw creep, stone tilting and upfreezing can be an effective mechanism in disruption of bedrock and movement of large blocks (French, 1996). However, they tend to be a mechanism for the widening and extending of joint spaces (following water penetration), rather than a means of initiating new fractures in intact bedrock (Boelhouwers, 2004). Those processes previously attributed to the breakup of bedrock, such as frost shattering, are now recognised to be much less effective than previously thought (Hall *et al.*, 2002).

It follows that the most important factor in the development of a coarse angular blocky slope is the underlying lithology. Blockslopes are invariably associated with high strength, low porosity rocks with planes of structural weakness (Boelhouwers, 2004). These fractures in the bedrock act as a pathway for the penetration of water which enables both chemical and mechanical weathering and results in the widening and extending of joint spaces (Hall *et al.*, 2002; Boelhouwers, 2004). Away from the joints weathering is limited, and consequently, large cohesive blocks are produced that have a close association with the joint density of the bedrock. Annual freeze-thaw action, which commonly penetrates to depths of 1-2 m, is an effective agent for the detachment of metre-scale blocks and is likely to occur in many periglacial zones (Hall *et al.*, 2002).

The fundamental role of joint weathering in the supply of blocks has raised questions about the primacy of periglacial processes in the development of blockslopes. In some

locations, it has been suggested that blocks developed by deep-weathering of joints as far back as the Tertiary; and that periglacial processes are limited to a secondary role of block detachment and transportation (Caine, 1968; Rea *et al.*, 1996; Whalley *et al.*, 2004). This may well be the case in some regions, particularly where cold-based ice sheets have limited weathering and erosion for large spans of the Pleistocene. However, there is perhaps an overemphasis on the need for Tertiary (warm) conditions to allow joint widening and matrix development (i.e. in Boelhouwers, 2004); particularly when recent research has highlighted the potentially active role of chemical weathering even under cold conditions (Hall *et al.*, 2002). If the ongoing rate of weathering is sufficient to enable processes of physical erosion and block detachment from the bedrock, then the development of a blockslope becomes a balance between weathering preparation of the bedrock and the rate of mechanical disruption. The question over whether blockslopes result from active periglacial processes or are a relict of Tertiary weathering surfaces mirrors that for the Dartmoor landscape in general.

4.3 Research Design

The concentration of ^{10}Be was measured in samples from a blockslope on the western side of Yes Tor, northwest Dartmoor. The concentration of cosmogenic nuclides results from the length of exposure of the sampled rock to cosmic radiation in the near surface. In the case of a blockslope landform, these concentrations cannot be interpreted as a simple exposure age as there is no clear 'event' for block emergence and they are likely to have a complex history of exposure once part of the active surface layer. However, an interpretation of not only exposure age, but the distribution of ^{10}Be concentrations across the blockslope allows for a useful insight into long-term landform development.

4.3.1 Study Objectives

An important issue in the understanding of the Dartmoor landscape is the efficiency of periglacial processes in landform development. Essentially, were features such as blockslopes actively developed under periglacial conditions, or are they largely reworked relict of preceding Tertiary weathering? The measurement of ^{10}Be concentrations in samples from different parts of a blockslope seeks to address two

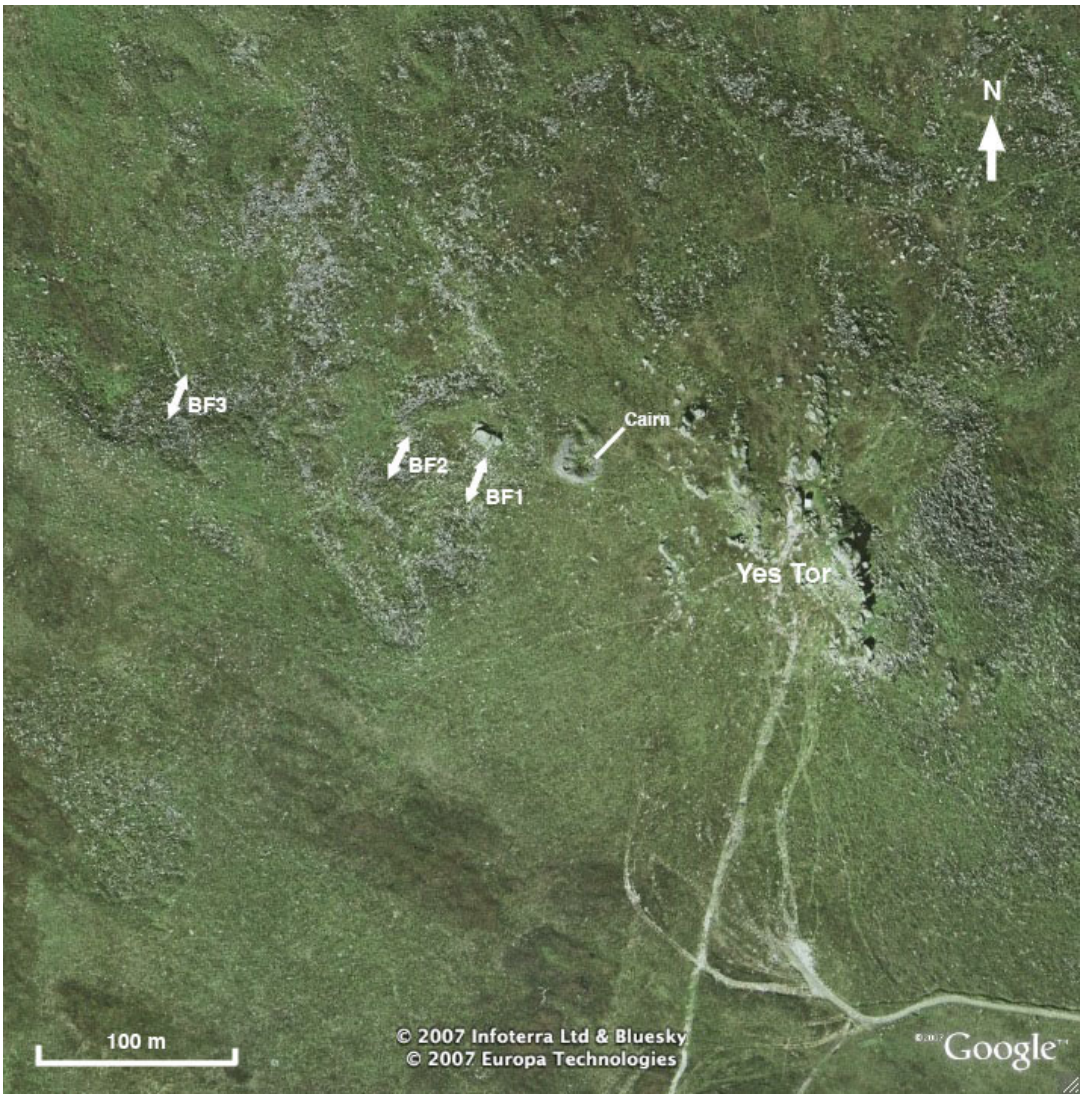

Figure 4.2 Aerial photography of the Yes Tor summit area and the surrounding block covered slopes. The location of sample transects on the western slope are marked.

Image: GoogleEarth™

Figure 4.3 Blockslope on the western side of Yes Tor at sampled transects (a) BF1 and (b) BF2.

key aspects of their development: (i) the length of time that blocks have been part of the active surface layer; and (ii) whether the distribution of concentrations measured across the blockslope provides any indication of block origin and/or transportation. This study does not seek to provide precise dating of the blockslope at Yes Tor; this would not be possible given the dynamic nature of blockslope development and lack of a clear formative event. Instead, the cosmogenic nuclide data is used to broadly constrain the timescale over which the present surface developed and provide useful insight into the long-term development of a blockslope landform.

4.3.2 Study Site - Yes Tor Blockslope

For this study, a blockslope on the western side of Yes Tor in northwest Dartmoor was selected. An important consideration in choosing this site was its close proximity to the intensively sampled tors at High Willhays (Chapter 4) and catchment of the West Okement River (Chapter 6). It is also an area where anthropogenic modification of blocks is most likely minimal[1]; this is not always the case in a region where humans have utilised boulders since Neolithic times, with modification not always easy to distinguish even in apparently 'natural' blockslopes (Tilley *et al.* 2000).

There are a number of rock outcrops scattered across the summit of Yes Tor. These have a rugged blocky appearance and the tors often grade into blocky slope deposits (in contrast to the nearby High Willhays tors). The slopes surrounding the summit range in gradient from 5-20º, and increase with distance from the summit. These slopes are covered in metre-scale blocks that constitute the blockslope landforms. In this study, samples were collected at three locations over a 160 m distance downslope on the western side of Yes Tor (Figure 4.2 and 4.3). The average gradient of the slope over this distance was 14º. This blockslope mostly consists of slab to elongated metre-scale blocks with a thickness of 5-10 cm. These are closely packed, often imbricated, and protrude from the slope with a typically downslope orientation. The blocks are set in a matrix of finer material with soil and vegetation developed around the base.

---

[1] There is a 'cairn' upslope of the sampling site that is evident on Ordinance Survey maps and aerial photography (Figure 4.2). However, it is probably an isolated feature and there was no obvious disruption of the sampled blockslope.

4.3.3 Sample Collection

This study is interested in the development of the Yes Tor blockslope as a landform, rather than individual blocks. There is potential for blocks to have significantly different exposure histories within the blockslope (and therefore concentrations of ^{10}Be). This is problematic when sampling for cosmogenic nuclide analysis, as there is a limited number of analyses available. To provide a measure of average block exposure at each transect, ten samples were collected at 2 m intervals across the slope. While sampling a large number of blocks and combining these into a single amalgamated sample would provide a reasonable average ^{10}Be concentration for the transect, it would provide no indication of variability amongst the blocks. To provide both an average concentration and some indication of variability, two samples consisting of equal proportions of crushed rock from three blocks (randomly selected) were analysed for each transect (a third sample was processed from BF2 transect due to a greater variability evident after the first two samples were analysed). This provides some balance between averaging ^{10}Be concentrations and still allows for an assessment of variation between blocks within the landform.

4.4 Results

4.4.1 Measured ^{10}Be Concentrations

The results of the measurement of ^{10}Be in samples from the Yes Tor blockslope are presented in Table 4.1. In total seven samples were analysed (each an amalgamation of material from three boulders), with measured ^{10}Be concentrations of 1.87 to 3.54 x10^5 atoms g^{-1}, an up to two-fold difference. The samples from the BF1 transect are similar with concentrations within 1σ of each other. There is more variation in the concentrations measured at the BF2 transect 45 m further downslope. The BF2(3) sample returned a concentration similar to those measured in the BF1 transect, while the BF2(2) was slightly higher at 2.18±0.22 x10^5 atoms g^{-1} (although the large measurement error of this sample means it is still within 1σ). The other sample from the transect, BF2(1) has a significantly higher ^{10}Be concentration at 2.61±0.14 x10^5 atoms g^{-1} than all other samples analysed from BF1 and BF2 transects, with the exception of BF2(2) which it is within 2σ. The samples from BF2 demonstrate that there is some variability in exposure between the different boulders; outliers have the

potential to heavily skew results in such a small sample of the population. The third transect, BF3, located 160 m downslope from BF1 has ^{10}Be concentrations almost twice some of those measured in the upper transects. The results from the two samples were remarkably similar, returning a concentration of 3.54±0.14 and 3.54±0.15 x10^5 atoms g^{-1}, with the difference between measurements only 250 atoms g^{-1}.

Table 4.1 ^{10}Be concentration and calculated exposure ages and erosion rates for the Yes Tor blockslope

Sample ID	^{10}Be Conc.	Equivalent Surface Exposure Age (ka)				Maximum Erosion
	(10^5 atoms g^{-1})	ε = 0 mm ka^{-1}	ε = 1.5 mm ka^{-1}	ε = 5 mm ka^{-1}	ε = 10 mm ka^{-1}	Rate (mm ka-1)
BF1(1)	2.02 ± 0.16	25.3 ± 2.0	26.1 ± 2.1	28.2 ± 2.4	32.2 ± 3.2	32.1 ± 2.6
BF1(2)	1.87 ± 0.16	23.5 ± 2.0	24.1 ± 2.1	25.9 ± 2.5	29.3 ± 3.2	34.8 ± 3.1
BF2(1)	2.61 ± 0.14	33.0 ± 1.7	34.3 ± 1.9	38.2 ± 2.3	46.4 ± 3.5	24.3 ± 1.3
BF2(2)	2.18 ± 0.22	27.6 ± 2.8	28.5 ± 3.0	31.1 ± 3.6	36.1 ± 4.9	29.4 ± 3.1
BF2(3)	1.87 ± 0.07	23.6 ± 0.9	24.3 ± 1.0	26.1 ± 1.2	29.5 ± 1.5	34.6 ± 1.4
BF3(1)	3.54 ± 0.14	45.7 ± 1.8	48.4 ± 2.0	57.0 ± 2.8	81.2 ± 6.0	17.1 ± 0.7
BF3(2)	3.54 ± 0.15	45.7 ± 2.0	48.4 ± 2.2	56.9 ± 3.1	81.1 ± 6.8	17.2 ± 0.8

4.4.2 Block Exposure to Cosmic Radiation

From the measured ^{10}Be concentration it is possible to derive an 'exposure age', which is equivalent to the length of time a sample would need to spend continuously exposed at the surface to accumulate the measured concentration of cosmogenic nuclides. However, for most blockslope samples the exposure history is not likely to be this simple, and a more complicated interpretation of the ^{10}Be concentration is required. This section evaluates the potential implications of a complex exposure history and provides the basis for interpreting the data measured in samples from the Yes Tor blockslope.

4.4.2.1 Exposure Age Model

Exposure ages are derived from ^{10}Be concentrations using the CRONUS-Earth online calculator and are based on the assumption of a simple exposure model in which a sample is taken from an 'event surface' (section 2.4.1). The application of this

model to samples from the Yes Tor blockslope almost certainly violates some of its fundamental assumptions, and this must be recognised in interpretations. The CRONUS-Earth online calculator model provides modelling using a variety of different production scaling models and integrates a scheme for corrections for muonic production and geomagnetic variations. This calculator was used in the interest of providing results that are well documented and easily reproducible (Balco *et al.*, 2008). The results of exposure age calculations presented in Table 4.1 used the Dunai (2000) production scaling model as implemented in the CRONUS-Earth online calculator. Equivalent surface exposure ages are calculated for a theoretical 'post-exposure' zero erosion rate, as well as three potential erosion rates. The 1.5 mm ka^{-1} rate is similar to measured average rates of granite erosion rates in other regions of northern Europe, while the 5 and 10 mm ka^{-1} would represent the higher end of such erosion rates (André, 2002; Phillips *et al.* 2006). These are used to assess the potential impact of erosion on exposure age estimates; care should be taken if they are to be used as a correction as there is no independent measurement of granite erosion rates for Dartmoor.

Finally, the ^{10}Be concentration can be used to calculate a steady state 'erosion rate' for the surface. This represents the maximum erosion rate that could have occurred for the block to have sufficient exposure to accumulate its inventory of cosmogenic nuclides.

4.4.2.2 Block Origin – Nuclide Inheritance

The surface exposure age model assumes that samples are collected from an 'event surface' that was rapidly uncovered, having been effectively shielded from cosmic radiation prior to reaching the surface. This scenario is not likely in a blockslope, where blocks will have a more complex history of exposure to cosmic radiation. Blocks accumulate cosmogenic nuclides during their residence in the near surface as either they are brought to the surface or overburden is removed. If this residence time is long, a block will arrive at the surface with an inventory of cosmogenic nuclides and any calculation of surface exposure will be an overestimate of its actual

time at the surface. The production of cosmogenic nuclides is biased towards the surface (broadly an exponential decline with depth) so the longer a sample is exposed at the surface the less significant the inheritance of cosmogenic nuclides. This study is more interested in the timescales involved in the development of the blockslope landform, rather than the surface exposure age of individual blocks. Consequently, the inheritance of cosmogenic nuclides will not change the interpretation significantly. This is especially the case if the emergence of the block was part of continuing development of the blockslope, in which case the exposure age measured in the block will be an underestimate of the age of the landform.

Even if blocks are assumed to have reasonably similar exposure to cosmic radiation during emergence (and thereby reach the surface with similar inheritance), it is necessary to consider the source of blocks as this has implications for the distribution of ^{10}Be concentrations across the blockslope. The Yes Tor blockslope is autochthonous, with blocks derived locally from the weathering of the underlying granite bedrock. However, within the context of the blockslope landform there are two possible sources of blocks: (i) they originate on the upper slope (perhaps in the vicinity of the summit tors) and are transported downslope; or (ii) they emerge from beneath the blockslope through processes like upfreezing and frost heave or are uncovered through the removal of overburden. The source of blocks will have a significant impact on the distribution of cosmogenic nuclide concentrations across the blockslope. If blocks are primarily sourced from upslope, they will be exposed to cosmic radiation as they are transported downslope as part of the surface layer, and consequently, an increase in ^{10}Be concentrations downslope would be expected. Alternatively, if blocks emerge locally and there is minimal downslope transport then ^{10}Be concentrations would be expected to be similar across the blockslope. A mixture of blocks from both sources would lead to variability in concentrations as transported blocks with long exposures are mixed with 'fresh' blocks emerging from beneath the blockslope.

4.4.2.3 Exposure in the Surface Layer

The surface exposure age model assumes that once uncovered the surface remains continuously exposed to cosmic radiation, which is a reasonable assumption if the surface is fixed in location. However, the position and orientation of blocks within a blockslope is likely to change over time. It is quite possible that at some time in the past the sampled surface was shielded from incoming radiation by either other blocks or itself (another part of the block). Any shielding of the sample will lower the production rate within the rock, leading to a reduced ^{10}Be concentration and an underestimation of the amount of time the block has spent as part of the surface layer. It is difficult to estimate how significant shielding within the surface layer might be to the estimation of exposure ages. Many of the blocks in the Yes Tor blockslope are imbricated and it is possible that this maintains the position of the upper-edge of the block and minimises the potential for shielding. While not attempted in this study, it might be possible to either measure the amount of shielding (measure different parts of a block or from different heights in the surface layer) or integrate exposure over the surface thickness. For example, if the block was integrated over a depth of 25 cm a self-shielding factor would be 0.82, while over a metre this would be 0.49 (using the same calculations as for sample thickness (Section 2.3.4). However, for the purposes of this study it is adequate to simply recognise that shielding may lead to an underestimate of the time a block has spent in the surface layer.

4.4.2.4 Block Geometry

The sampled blocks on the Yes Tor blockslope are metre-scale blocks with an elongated slab shape, with thickness typically less than 10 cm. The sample was taken from the uppermost surface of each block. It is highly likely that the production rate in these blocks is influenced by the shape effects described in Section 2.2.4.3, with the loss of secondary cosmic radiation to the atmosphere. The reduced rate of cosmogenic nuclide production will lead to an underestimate of block residence time in the surface layer. However, this effect is likely to be relatively minor compared to the other factors influencing exposure age calculations.

4.4.2.5 Block Erosion

The calculated surface exposure age represents the minimum amount of time that a block would have to spend at the surface to accumulate the measured concentration of ^{10}Be. Erosion of this surface will result in the loss of cosmogenic nuclides in the quartz grains removed. It is possible to correct for this loss in surface exposure age calculations if the erosion rate of the surface is known. However, there is no reliable independent estimate of granite erosion rate for Dartmoor. Instead, as discussed in section 4.4.2.1, corrections for three possible erosion rates are presented in Table 4.1. The 1.5 mm ka^{-1} rate is similar to that measured in northern Europe by André (2002) and Phillips *et al.* (2006), and also similar to that for 'mechanical denudation' in Dartmoor suggested by Williams *et al.* (1986). The higher rates of 5 and 10 mm ka^{-1} are used to assess the potential impact of higher erosion rates on exposure age estimates. As can be seen in Table 4.1, erosion can have a significant effect on the estimation of surface exposure ages, and this is most pronounced with those exposed the longest (e.g. BF3 samples exposure ages nearly double with an erosion rate of 10 mm ka^{-1}).

As there is no independent estimate of granite erosion rates, the selection of a correction rate for the Yes Tor blockfield is fairly arbitrary. Many of the blocks have noticeable tourmaline extrusions up to a couple centimetres from the block surface, suggesting a granular disintegration of the granite surface. Phillips *et al.* (2006) were able to use quartz vein relief to measure post-glacial erosion of granite surfaces at 1.6 mm ka^{-1}. However, it is not possible to undertake a similar approach in Dartmoor as there is no clearly definable starting surface. It would be expected that the blocks would be amongst the most resistant parts of the landscape; with little structural weakness (e.g. jointing) and erosion largely limited to granular disintegration. André (2002) suggests that this is fairly constant across most climate conditions in crystalline rocks, so an average erosion rate of <1.5 mm ka^{-1} is probably reasonable for the blocks of the Yes Tor blockslope.

The measured ^{10}Be concentrations can also be interpreted as maximum erosion rates (Table 4.1). These represent the maximum steady-state erosion rate that would allow the surface to accumulate enough cosmogenic nuclides to produce the measured concentration.

4.4.2.6 Summary

The surface exposure ages derived from ^{10}Be concentrations on blockslopes are likely to underestimate the actual residence time of a block in the surface layer. With the exception of nuclide inheritance, all of the variations in exposure history discussed in this section would lead to the underestimation of exposure age. There is insufficient information available to apply corrections to most of these factors; however, in recognising their potential impact and the various effects it is possible to better constrain not only the timescale, but also the processes of blockslope development.

4.4.3 Yes Tor Blockslope Exposure Ages

The trends in the calculated exposure ages (Table 4.1) are essentially the same as the ^{10}Be concentrations from which they were derived (see section 4.4.1). The $\varepsilon = 0$ mm ka^{-1} exposure ages are shown in Figure 4.4. The samples from BF1 have an average exposure age of 24.4 ka. Those from the BF2 transect (45 m downslope) have a slightly higher average age of 28.1 ka, although these are more varied with ages ranging from 23.7 to 33.0 ka with those at the lower end equivalent to samples analysed from BF1. The third BF3 transect located 160 m downslope (from BF1) have significantly longer exposure ages with both samples returning an exposure age of 45.7 ka. The $\varepsilon = 0$ mm ka^{-1} exposure age is considered a minimum length of exposure for the blocks. The correction of exposure ages with estimated erosion rates (Table 1) increases the exposure ages for blocks, especially for those exposed the longest. The calculated age for samples from the BF3 increase from 45 ka at $\varepsilon = 0$ mm ka^{-1}, to 57 ka at $\varepsilon = 5$ mm ka^{-1}, and up to 81 ka for $\varepsilon = 10$ mm ka^{-1}. Increases in exposure age are less severe for the shorter length of exposure in the BF1 and BF2 transects.

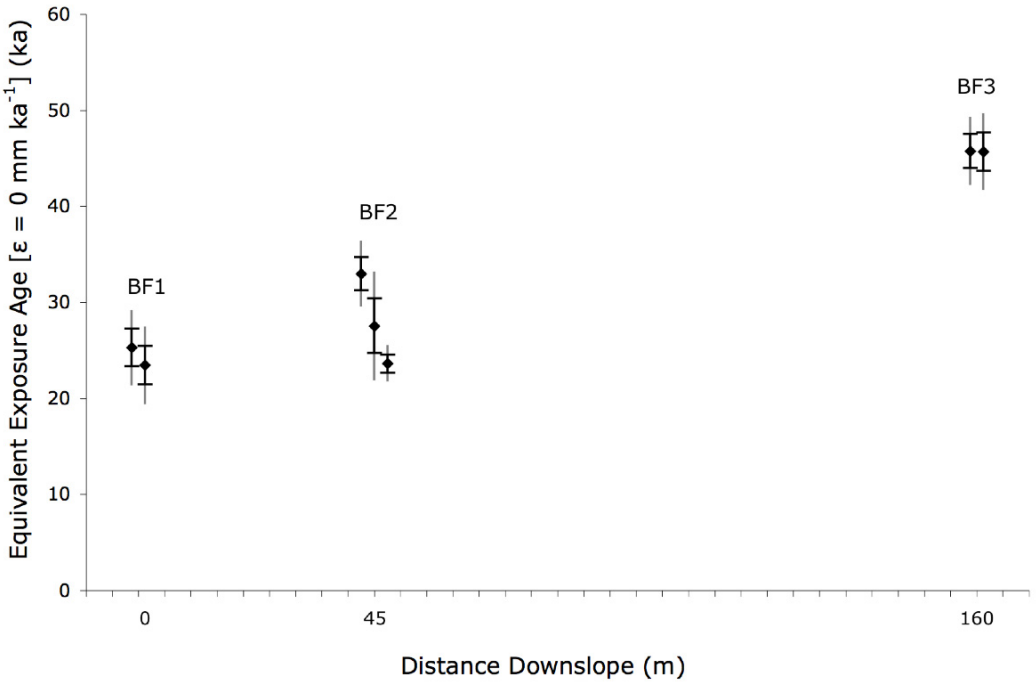

Figure 4.4 The ^{10}Be derived exposure ages (ε =0) of blockslope samples with distance downslope; error bars are 1σ (black) and 2σ (grey) internal uncertainty. (note: The distance downslope of samples are displaced to aid viewing, distances are 0, 45 and 160 m).

4.5 Discussion

The analysis of ^{10}Be concentrations on the Yes Tor blockslope provides a quantitative means of assessing the morphogenesis of these landforms and some constraint on the timescales over which they developed. The results from the three transects indicate that the blocks have been exposed as part of the blockslope surface layer since the last glaciation. In addition, the downslope increase in ^{10}Be concentration provides an indication of long-term downslope transport rates. This section provides a discussion of the findings from this study of the Yes Tor blockslope and considers the implications for periglacial processes in Dartmoor.

4.5.1 Timescale of Blockslope Development

Many landforms in Dartmoor have been associated with periglacial processes, including head deposits and inverted profiles (solifluction deposits), clitter and scree slopes (blockslopes), patterned ground, cryoplanation surfaces, and tors (Waters, 1964; Green & Eden, 1973; Gerrard, 1988; 1989). What has remained unclear is the timescale over which these landforms develop, and whether they formed during the last glacial cycle or are the product of periglacial activity during multiple cold stages of the Pleistocene (Gerrard, 1988). The ^{10}Be concentrations measured on the Yes Tor blockslope provide an indication of the time span over which the present surface developed.

The surface exposure age (ε = 0 mm ka^{-1}) represents the minimum length of time that the sampled rock has been exposed to cosmic radiation to accumulate the measured ^{10}Be concentration. It assumes that the sample has been at the surface (maximum production rate for site) and that there has been no loss of nuclides due to erosion. For the Yes Tor blockslope, exposure ages indicate that blocks have been part of the surface layer for at least 23 ka at transects BF1 and BF2 and for a minimum of 45 ka on the lower slope transect BF3. These results show that the blockslope was an active landform from prior to the LGM and, for BF3 at least, well into the Middle Devensian or Stage 3 interstadial.

These calculated exposure ages are probably an underestimate (section 4.4.2) of the amount of time that a block has actually resided in the active surface layer of the blockslope. Although it might be possible to correct for some influences like erosion and self-shielding, it is difficult given the lack of independent knowledge of erosion rates or landform development. Instead, a set of potential values can be used to assess the range of exposure that could result for the blockslope.

In the results presented in Table 4.1, erosion rates of 1.5, 5, and 10 mm ka^{-1} were used to calculate modified exposure ages. At the higher erosion rate of 10 mm ka^{-1} the exposure age is increased significantly, especially for the older BF3 transect blocks for which there is an increase from 45 to 81 ka of surface exposure. However, over an 81 ka time span an erosion rate of 10 mm ka^{-1} would remove 80 cm of material from the surface. Given the metre-scale size of the typical blocks on the slope (and observed around Yes Tor) very little of the block would remain. The blocks in the BF3 transect are not observed to be much different from those elsewhere in the vicinity[2]. Given the long exposure of these blocks indicated by the ^{10}Be concentrations, an erosion rate of 10 mm ka^{-1} is likely to be too high. Following this logic, even the lower rate of 5 mm ka^{-1} is problematic (30 cm over 60 ka), as it is likely that the erosion of block surfaces is occurring at a rate similar to those measured in other regions at 0.5 to 1.6 mm ka^{-1} (Phillips *et al.*, 2006; André, 2002). If erosion rates are no more than 5 mm ka^{-1}, then exposure age for the blocks is at most ~55 ka for the BF3 transect and somewhere between 25-38 ka for those upslope at BF1 and BF2.

There are other factors that can also increase the exposure ages calculated for the blocks, although these are more difficult to assess. There is potential for self-shielding within the blockslope surface layer (section 4.4.2.3) if the sampled surface (the highest point was sampled) spent part of its exposure history away from the top of the surface

[2] It might be possible to carefully measure changes in block shape and size across the blockslope (perhaps measuring features such as roundness i.e. Kirkbride, 2006) to assess erosional modification, although without knowledge of the original dimensions of the block (at the base of regolith) this might be difficult.

layer. It is very difficult to place constraints on an unknown block history, at least without further sampling of the blockslope. The lack of variability in the transects, in particular BF3 (the longest exposed) suggests that blocks at least have a similar average exposure history. As observed in section 4.4.2.3 the blocks on the Yes Tor blockslope are imbricated and this may keep the uppermost edge in position. However, if the blocks were being rotated within the surface layer, it might be possible to integrate production over its depth. If the entire surface layer was well-mixed over 50 cm (as a density; see section 4.2.4.3) then the production rate would be scaled by 0.68, this would increase the residence time of, for example, BF3 from ~45 ka to 65 ka. This study cannot do more than speculate on the possibility of shielding within the surface layer. While it may be possible that such shielding would increase block residence time by up to 50%, it is probably less significant.

In summary, it is clear from the ^{10}Be concentrations measured in samples from the Yes Tor blockslope that the blocks have been exposed as part of the surface layer for at least the last 25-35 ka for the upper slope (BF1 & BF2) and for at least 45 ka on the lower slope (BF3). This demonstrates that the blockslope was active over the LGM and into the Mid-Devensian (Stage 3). The determination of the upper limit on the residence time of the blocks in the surface layer is more complicated, but it is reasoned that it is probably, at most, 30-40 ka on the upper slope and 50-70 ka on the lower; most likely less. It is very likely that the blocks of the Yes Tor blockslope only became exposed to cosmic radiation during the Devensian glaciation.

4.5.2 Downslope Block Transportation

The average gradient over the study section of the Yes Tor blockslope is 14º, so gravity-driven downslope movement would be expected. Although mass wasting can occur under any environmental conditions, it is probably especially effective in the active layer of frozen ground where periglacial processes like frost creep are in operation (French, 1996). These processes are also capable of moving metre-scale blocks through frost heave and upfreezing, which is able to tilt and raise elongated blocks (Hall *et al.*, 2002; van Steijn *et al.*, 2002). Downslope transportation of material is widely recognised in Dartmoor blockslopes, with 'boulder runs and garlands'

leading directly from the base of tors, although it is suggested that 'much of the clitter has not moved very far' (Gerrard, 1988). There are also widespread head deposits or inverted profiles (solifluction layers) (Waters, 1964; Green & Eden, 1973; Gerrard, 1989).

The ^{10}Be concentration increases with distance downslope (Table 4.1). While the increase from BF1 to BF2 is slightly obscured by variability in measurements, the increase from these upslope transects to BF3 is an almost doubling of ^{10}Be concentrations. As described in section 4.4.2.2, a downslope increase would be expected if blocks were being transported as a surface layer. Interestingly, there is virtually no variation in the two samples measured at the BF3 transect, with each consisting of rock from three individual blocks. Although the sample size is not large enough to be conclusive, this indicates that the blocks have a similar history of exposure to cosmic radiation. If we accept that there is downslope transportation of blocks, this would indicate that 'fresh' blocks are not being added to the surface layer from underneath the downslope part of the blockslope.

It is difficult to envisage a feasible alternative to downslope transportation of blocks as an explanation of the differences in ^{10}Be concentrations on the Yes Tor blockslope. If the blocks are not accumulating cosmogenic nuclides during downslope transport, then the higher concentrations measured on the lower BF3 transect would have to be explained by an uncovering of the lower slope prior to the upper slope. The difficulty with this scenario is that material from the upper slope would still have to be transported downslope. Perhaps if the finer material was transmitted through an openwork boulder framework of the lower blockslope it might not cover the blocks, although this is not a simple geomorphological scenario. Downslope transportation of blocks in the surface layer of the blockslope landform is a far simpler geomorphological interpretation.

If we accept that the distribution of ^{10}Be concentrations is evidence for downslope transportation of blocks, the next question is whether we can estimate the rate of movement? If the blocks now at BF3 were once upslope at BF1, and we assume that

at this time they had a similar concentration to those now at BF1, the difference in calculated exposure ages will reflect the amount of time taken for the blocks to move downslope. It is debatable whether this is a valid assumption, as it requires a continuity of process over a lengthy period of time. This approach would be improved if more transects were analysed on the slope, but this would require further cosmogenic nuclide analyses to be available.

The assumptions made on the exposure ages for blocks are much the same as discussed in the preceding discussion in section 4.2.1. Assuming continuous exposure of the surface without shielding or erosion, the minimum amount of time taken for the blocks to move from BF1 to BF3 would be 20 ka (difference between 25 and 45 ka ages). If the blocks have been transported the 160 m distance downslope, this would equate to a transportation rate of 8 m ka^{-1} (or 0.8 cm a^{-1}). This should be considered a maximum transportation rate.

If the sampled surface on the block is eroding or has been shielded within the surface layer of the blockslope, then the exposure ages will be an underestimate of their actual residence time in the blockslope. In these circumstances, the longer a sample is exposed the greater the magnitude of the underestimation. When there is erosion or self-shielding the difference in age will increase and, consequently, the rate of transportation will be slowed. For example, using the ε = 5 mm ka^{-1} corrections in Table 1, the difference in age between BF1 and BF3 is 30 ka (difference between 25 and 55 ka) so the transportation rate would be slowed to 5 m ka^{-1} (or 0.5 cm a^{-1}).

Another complication is the potential for some blocks to emerge from beneath the blockslope. These 'fresh' blocks would have a lower ^{10}Be concentration than those being transported in the surface layer from upslope. If these are present in the sample they will lower the average concentration measured for the transect, and those that have travelled from upslope would have a higher ^{10}Be concentration than the average value for the transect. If the average values are used this would lead to an overestimate of the transportation rate. There is no evidence of variations in

concentrations at the BF3 transect that would indicate a mixture of block sources, although the dataset is of course limited in size.

If the assumptions outlined above are accepted, it would appear that blocks are being transported over the 160 m distance between BF1 and BF3 at a maximum average rate of 0.8 cm a^{-1}. It is worth noting that the blocks are likely to be the least mobile element of the hillslope regolith and finer material is potentially transported more rapidly. The 0.8 cm a^{-1} derived here is comparable to the lower-end of typical rates reported by Matsuoka (2001), who provides a useful summary of solifluction rates from around the world. The cosmogenic nuclide derived rates are unusual as they provide a long-term perspective, although a greater number of samples would have to be gathered to confirm some of the assumptions.

4.5.3 Implications for Landscape Evolution

While periglacial landforms are widely recognised in the Dartmoor landscape (Waters, 1964; Green & Eden, 1973; Gerrard, 1988, 1989), the timescales over which they develop has remained unknown. As discussed in section 4.5.1, there is uncertainty as to whether these landforms developed during Pleistocene cold stages or are the reworking of relict Tertiary weathering surfaces. The analysis of cosmogenic nuclide concentrations in the blocks of the Yes Tor blockslope has demonstrated that these have been part of the active surface layer since the Mid-Devensian. This section focuses on the implications for the blockslope landform; there will be further discussion of more widespread implications for Dartmoor landscape evolution in Chapter 6.

An essential element of the development of blockslopes is the fracturing of bedrock and the weathering of joint spaces that allows for the detachment of metre-scale blocks (see section 4.2.3). Some researchers have suggested that this weathering often occurs during the Tertiary and periglaciation is mostly responsible for reworking these relict weathering surfaces (Boelhouwers, 2004). Similar claims have been made for the Dartmoor landscape, with the Linton (1955) two-phase theory based on the premise of Tertiary deep-weathering.

This study shows that the blocks at the present blockslope surface have been part of the surface layer for the past 25-75 ka. Prior to this they must have been effectively shielded from cosmic radiation by overlying material (a few metres thick). If this amount of material was being removed from the summit of Yes Tor during the last glacial cycle, then it would be expected that similar processes were operating throughout the Pleistocene and a considerable depth of material removed.

The regolith is not observed to be very thick around the summit of Yes Tor and High Willhays (Chapter 3), or in other summit areas of Dartmoor (Eden & Green, 1971). The deep-weathering hypothesis would suggest that the blockslope at Yes Tor is a blocky lag deposit following the stripping of more mobile regolith, and what we currently observe at the summit is effectively the base of an older weathering profile. This is problematic given the exposure ages measured on the Yes Tor blockslope, which suggest an extended interval of block production and downslope transport.

It is appropriate to consider whether warm climate deep-weathering is necessary for the development of the blockslope landform. This study shows that the blockslope has been an actively developing landform during the last glaciation, with blocks uncovered and transported downslope. It would be simpler to explain the development of a blockslope if periglacial conditions are considered competent in weathering bedrock at the base of the regolith and actively widening and extending the joints. The prerequisite for block development is a fracturing of the bedrock, this is observed at other locations in Dartmoor (Figure 3.15) and is likely on the Yes Tor blockslope given the typical slab shape of blocks. These horizontal fractures probably develop due to stress release following the removal of overburden. Assuming that fractures are present, the other requirement is weathering processes that can exploit these joints to prepare the blocks for detachment. It is now considered likely that a range of weathering processes, including chemical weathering, occur under cold climate conditions and that these are largely moisture-dependent (Hall *et al.*, 2002).

The analysis of cosmogenic nuclide concentrations in samples from the Yes Tor blockslope, and the nearby High Willhays summit (Chapter 3) suggest that landforms

have developed primarily over the last glacial cycle. Although it may be possible to construct a scenario that fits the data to the Tertiary deep weathering model, it requires many unsubstantiated assumptions. It is far simpler to ascribe blockslope landform development to ongoing weathering at the base of the regolith and block detachment over the cold-stages of the Pleistocene.

4.5.4 Limitations of Study

The analysis of cosmogenic nuclides provides an indication of near surface exposure of a block. In this study the results only directly reflect the more recent phase of the blockslope development during the last glacial cycle. It is also possible to conceive of multiple origins for the blockslopes, and there may be an equifinality for the landform that cannot be solved using cosmogenic nuclide methods.

As is often the case with cosmogenic nuclide studies, a limited number of analyses were available for this study. Further samples would increase the confidence in interpretations, in particular, since variability of concentrations and their distribution is of fundamental importance. It would be interesting to sample more transects, over a greater downslope distance, with more samples analysed at each. The use of multiple cosmogenic isotopes could also elucidate information about block burial. In particular, *in situ* ^{14}C with its shorter half-life could provide constraints on short-term erosion and burial.

Dartmoor has generally been considered to have remained beyond the limits of glaciation during the Pleistocene (Campbell *et al.*, 1998). However, there is some suggestion that there may have been ice on Dartmoor (Harrison, 2001). If these were limited to rock glaciers or small valley glaciers then it is unlikely that, given its location, the Yes Tor blockslope was affected. If a small ice cap formed in Dartmoor during the Pleistocene this would have a far more substantial impact on the interpretation of results. If the blocks were buried under ice (shielded from cosmic radiation) for any length of time, this would increase the exposure age interpreted for the sample (e.g. Fabel *et al.*, 2002; Phillips *et al.*, 2006). At present there is no unequivocal evidence for the presence any form of glaciation in Dartmoor, let alone a cold-based ice cap.

4.6 Conclusions

This study of ^{10}Be concentrations on a blockslope has demonstrated that they can be useful in interpreting the geomorphological development of even a dynamic landform. It has been shown that blocks have been exposed for minimum of 25 ka on the upper slope and 45 ka on the lower section of the slope. A variety of potential scenarios for block exposure have been considered, and while these suggest that the exposure ages are an underestimate of block residence time in the blockslope, that this time probably does not extend beyond the Mid-Devensian. This study demonstrates that the Yes Tor blockslope is an active landform over the last glacial cycle, and in doing so suggests that periglacial processes are most likely sufficient in the development of the landforms, at least on the upland summit areas of Dartmoor. Although interpretation of cosmogenic nuclide data is complex, they provide long-term constraints on blockslope development not previously available. This study demonstrates the application of cosmogenic nuclides to complex landforms, and suggests great potential for future investigation.

5: Spatially-Averaged Denudation in the Dartmoor Landscape

5.1 Introduction

The landscape of Dartmoor has been the subject of extensive geomorphological investigation over the last century, with a number of researchers constructing denudation chronologies (e.g. Waters, 1960; Brunsden, 1963), proposing models of landscape evolution (in particular, for tor emergence and granite weathering) (e.g. Linton, 1955; Palmer & Neilson, 1962; Eden & Green, 1971; Dearman & Baynes, 1978; Gerrard, 1974), and evaluating the impact of periglacial processes on the landscape (Te Punga, 1957; Waters, 1964; Green & Eden, 1973; Gerrard, 1988). This has resulted in an understanding of the landscape in general terms that includes the formation of plateau surfaces (often considered peneplains) the recognition of a number of erosional surfaces, and the development of the drainage network. During the Quaternary, the Dartmoor uplands were subjected to intervals of intense periglacial conditions, which substantially modified the landscape and led to the formation of many of its most distinctive landforms (e.g. tors and clitter) and widespread solifluction (or 'head') slope deposits (Waters, 1964; Green & Eden, 1973; Gerrard, 1989). Since the 1950s it has been generally recognised that denudation of the landscape intensified under periglacial conditions, and some form of 'regolith stripping' of slopes, and in particular summits, is fundamental to all proposed models of landscape evolution (see review in Campbell *et al.* 1998). However, there have been no reliable methods available to provide age constraint on landform development, with interpretations ranging from a single glacial cycle to the entire span of the Quaternary (Gerrard, 1989). The Holocene has seen a stabilisation of the landscape following the cessation of periglacial conditions, with the development of soil and peat cover; but there has also been anthropogenic modification to the landscape over the last 4000 years (Gerrard, 1993). Consequently, the Dartmoor landscape is a palimpsest of landforms, with the Holocene modification of a (still well preserved) periglacial terrain, which in turn is imposed on a regional scale valley and drainage network that has been developing since the Tertiary. Although the relative importance of the various phases of weathering and denudation in the landscape has

received attention (see Campbell *et al.*, 1998), there has been no quantitative assessment of long-term denudation rates in the Dartmoor landscape.

The accumulation of cosmogenic nuclides within the upper few metres of the Earth surface provides a means of evaluating long-term denudation rates (see Chapter 2). By measuring the concentration of ^{10}Be in a sample of alluvial sediment it is possible to interpret for the upstream catchment a spatially averaged denudation rate that is also integrated over timescales of 10^3-10^6 years; an approach that has now been successfully applied in a diverse range of environments (see reviews by Cockburn & Summerfield, 2004; Bierman & Nichols, 2004; von Blanckenburg, 2005). In this study, the ^{10}Be concentration is measured in thirteen samples of alluvial sediment from across Dartmoor providing estimates of spatially averaged denudation rates for catchments ranging in size from 3 to 77 km^2. These samples are averaged over a timescale that spans the Holocene and extends into the cold stage of the Devensian and, therefore, provide an indication of the magnitude of denudation during these intervals of intense periglacial conditions. They also offer a useful long-term denudation rate with which to assess anthropogenic impact on the landscape.

5.2 The Dartmoor Landscape

The uplands of Dartmoor are the largest extent of exposed granitic pluton associated with the Cornubian batholith, which extends underneath southwest England to the Isles of Scilly (Exley & Stone, 1964). The topography of Dartmoor is essentially an upland plateau surface of elevation 400-600 m that has been dissected by a network of rivers (Figure 5.1). The highest ground is centred in northern Dartmoor where an upland mass forms a broad low gradient (<5°; Figure 5.2) plateau surface with elevations mostly above 500 m. It is from this central northern mass that most rivers on Dartmoor rise, and as these extend towards the periphery they incise deeply to form steep-sided valleys with relative relief of up to 200 m (Gerrard, 1993). It is on the ridges and interfluves in the proximity of these river valleys that most of the tors of Dartmoor outcrop, while the central area of the upland plateau surface is generally featureless and flat or gently sloping (Eden & Green, 1971; Gerrard, 1993).

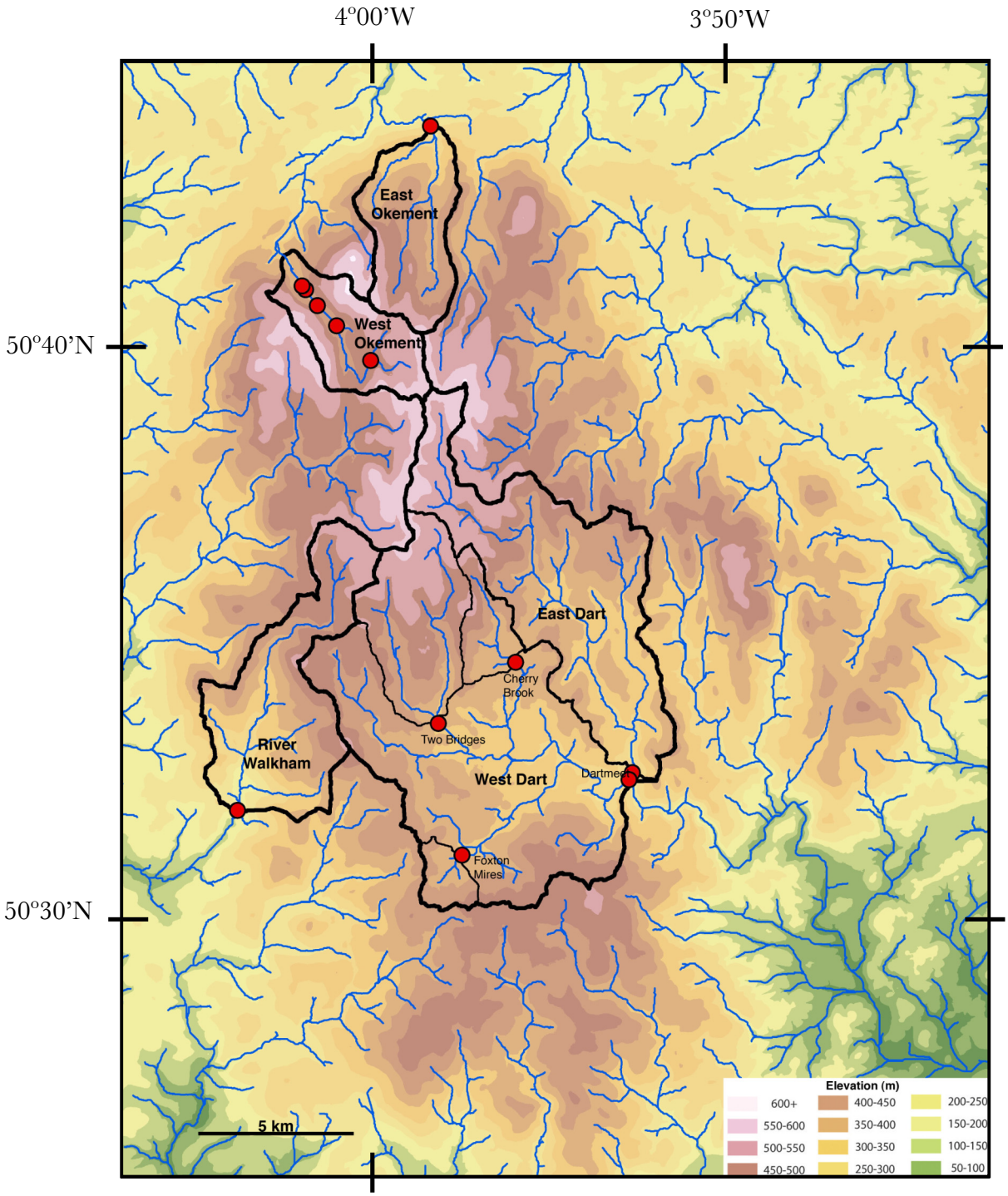

Figure 5.1 Dartmoor elevation map with major topographic drainage lines and demarcated upstream catchment boundaries for each alluvial sediment sampling site.

Data: 10m DEM from Digimap/Ordinance Survey

Processing: ArcGIS 9.2 and ArcHydro Tools

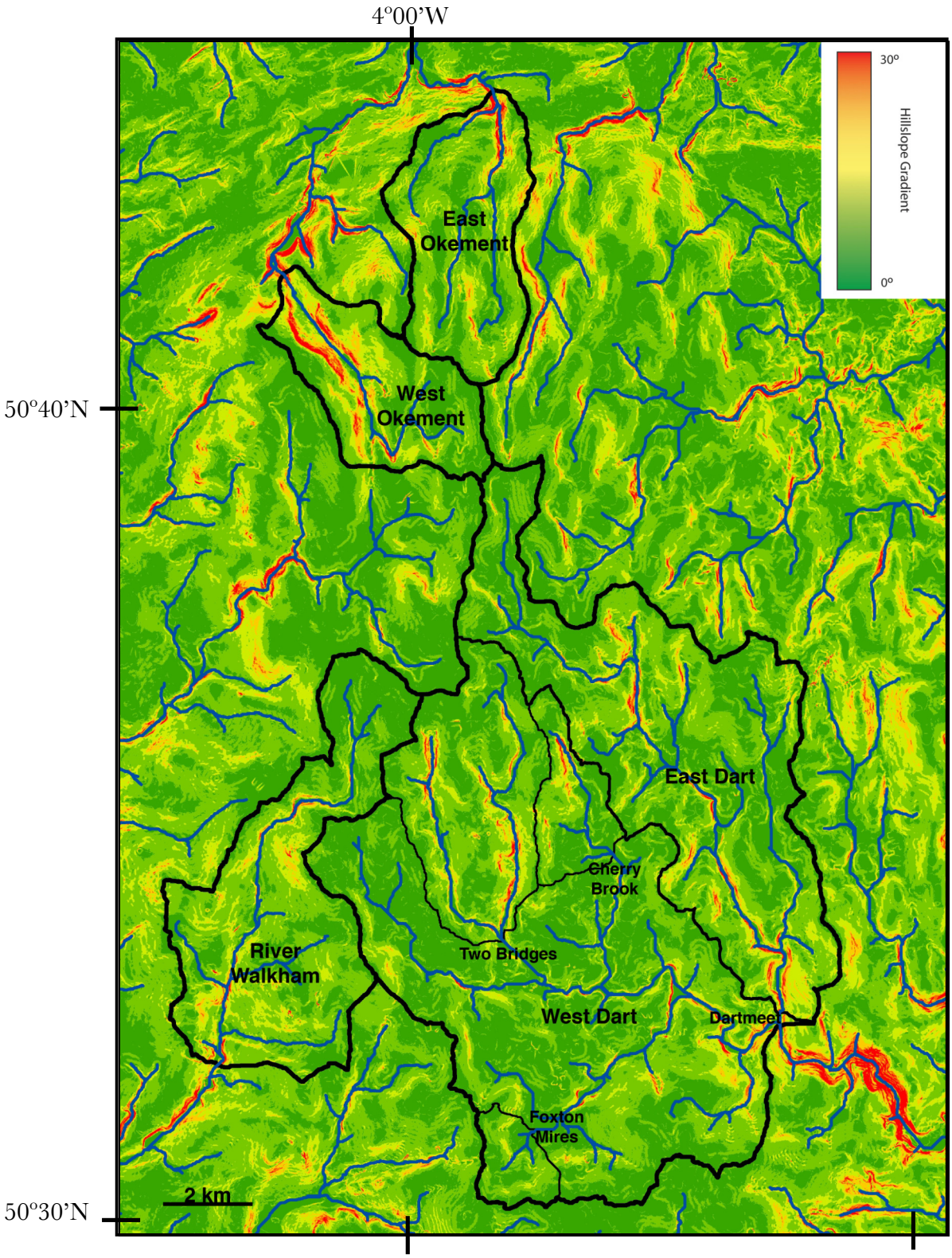

Figure 5.2 Hillslope gradient for northern Dartmoor with demarcated alluvial sediment sample catchment boundaries

Data: 10m DEM from Digimap/Ordinance Survey

Processing: ArcGIS 9.2 and ArcHydro Tools

Dartmoor is divided in two by the eastward flowing West Dart River, with a further upland mass centred in the south with elevations mostly between 400-500 m (Figure 5.1). The topography of the southern upland moorland is more subdued than that in the north, with a broad upland plateau surface of <5° mostly drained by southward flowing rivers that are not as deeply incised as their northern counterparts.

The drainage network extends radially from the upland masses in the north and south, with the centrally draining and eastward flowing River Dart catchment covering about one third of Dartmoor (Figure 5.1). The development of this drainage network has been linked to models of landscape evolution, with work by Waters (1957) and Brunsden (1964) suggesting that basin form is linked to denudation surfaces and that the present rivers in the region are incapable of forming the basins. More recently there has been an emphasis on the primary role of jointing in drainage network development, with weathering focussed on joints and these being further developed by unloading stress release following removal of overburden (Gerrard, 1974; in Campbell *et al.*, 1998). The influence of jointing is evident in the generally rectilinear pattern of valleys and interfluves (Gregory, 1969) and the right angle changes in stream course that are often observed in Dartmoor (Gerrard, 1993).

On upland Dartmoor the course of rivers is typically straight with sinuosity developing only once they leave the granite bedrock. Deep incision of the rivers means that channels are usually confined with little floodplain development. Instead the rivers appear to be mostly directly mobilising colluvial material to supply the alluvial load. The bedload of Dartmoor rivers is coarse, with sediment predominantly in the range of coarse sand-gravel to large boulders (Figure 5.3). This is similar in composition to slope material of solifluction 'head deposits', which consist of 40-60% gravel (>2 mm) and at most 10-20% fine sand to silt-clay; boulders are also found throughout slope profiles (Gerrard, 1989). The proportion of sand and finer material in the bedload is likely to be further reduced by preferential transport downstream. The rivers of Dartmoor do not appear to be competent to frequently entrain the larger size fraction of the bed.

Figure 5.3 The typical bedload of rivers on Dartmoor, with predominately coarse-gravel to boulder-sized grains; photos taken at Postbridge of the East Dart River

The slope deposits of Dartmoor have been well described by researchers interested in their formation, which has implications for models of landscape evolution under periglacial conditions (Waters, 1964; Brunsden, 1968; Green & Eden, 1973; Gerrard, 1989). Most hillslopes in Dartmoor are mantled with a solifluction (head) deposit of periglacial origin, which come in a 'fine' and 'coarse' variety and are of variable thickness and complex origin. These are often underlain by a variable depth of growan (grus), which is an *in situ* altered granite usually attributed to chemical weathering, although hydrothermal alteration and frost action may have been involved (Gerrard, 1989). The onset of Holocene climate conditions has seen the development of soils and peat cover on most slopes in upland Dartmoor, with heath-moorland vegetation (Gerrard, 1993; Kirkham *et al.* 2005).

In contrast to the relatively impermeable granite bedrock of Dartmoor, the coarse sand-gravel of the regolith is highly permeable and is capable of retaining water and transmitting it as interflow downslope. This throughflow of water is the dominant flow pathway on slopes in Dartmoor, with resurgence of water and overland flow occurring only when the soil becomes saturated (Williams *et al.* 1984). Even where water is resurgent it does not often lead to stream formation, and consequently, there is poor development of a low-order tributary stream network in the uplands of Dartmoor. As a result there are few pathways for sediment transportation into the alluvial system and in many situations colluival sediment is delivered directly to trunk channels.

There was a significant change in the environment of Dartmoor with the transition from Devensian cold stage to the Holocene. Compared to present, the LGM mean annual air temperatures were depressed as much as 25°C, while July mean air temperatures were as much as 10°C lower than present; this led to discontinuous permafrost across southwest England, although these extreme conditions were moderated by snow cover and maritime influences (Williams, 1975; Watson, 1977; Gerrard, 1988). Periglacial processes substantially modified the Dartmoor landscape during cold stages of the Quaternary, with widespread periglacial landforms of blockslopes, hummocky ground, frost wedges, and altiplanation terraces recognised

across the uplands (e.g. Te Punga, 1957; Waters, 1964; Gerrard, 1988). The transition to Holocene climate conditions has seen landscape stabilisation with the development of soil and peat covers (Gerrard, 1993), the chronology of which is summarised in Table 5.1.

From the late Holocene, humans have significantly modified the landscape and environment of Dartmoor. There was large-scale enclosure of fields and forest clearance beginning in the second millennia BC, in particular at lower elevations (Figure 5.4; Johnston, 2005). The intensity of enclosure and agricultural improvement has increased over the last 1000 years (Gerrard, 1993), although present landuse is principally livestock grazing (Kirkham *et al.*, 2005). There have also been significant localised effects from tin mining since prehistoric times, with the intensity of this activity increasing from the medieval period, during which hydraulic mining by stream diversion was common (Thorndycraft *et al.* 2004), and through the early industrial mining of the 18th and 19th centuries. For the most part tin mining reworked relatively shallow surface deposits only a few metres deep, although in some locations there are very significant impacts evident on a catchment-scale (Figure 5.5).

Table 5.1 Chronology of Holocene landscape change on Dartmoor (after Gerrard, 1993)

Time Interval (year BP)[a]	Geomorphological Activity
10250-9450	some solifluction, gullying, soil erosion
9450-8450	landscape stabilisation, soil and vegetation development
8450-7450	extensive soil development (brown earths?)
7450-4450	soil and vegetation changes, start of peat development
4450-3500	peat accumulation on high ground, forest clearance, some erosion
3500-2450	quite extensive erosion, soil modification
2450-1000	gradual landscape stabilisation, podzol development
1000-present	localised effects due to tinning, enclosure and improvement, a generally stable phase

[a] age model not stated in source, likely ^{14}C yr BP

Figure 5.4 Coaxial field systems of land enclosure that began in the 2nd millennium BC are the onset of significant anthropogenic modification of the Dartmoor landscape; this was focussed at lower elevations.

Source: Johnston (2005).

Figure 5.5 Aerial photography of the upper Doetor Brook in northwest Dartmoor (Great Links Tor in upper left), in which mining has had a significant impact on the catchment through the action of stream diversion and headwall retreat. This catchment is not included in this study but demonstrates the potentially severe impacts of tin mining activities.

Image: GoogleEarth™

5.3 Research Strategy

The measurement of ^{10}Be concentrations in alluvial sediment taken from rivers across Dartmoor allows for the calculation of landscape denudation rates that are integrated spatially and temporally. This research aims to assess the ^{10}Be derived denudation rates in terms of: (i) comparison with present-day estimates of denudation; (ii) the relative intensity of denudation in the Holocene versus the Devensian cold stage; (iii) placing constraints upon the efficacy of periglacial weathering, with implications for models of landscape evolution; and (iv) provide a wider geomorphological context for results obtained from tors and blockslopes covered in the preceding chapters.

5.3.1 Sampling Strategy

To meet the research objectives, the selection of sampling sites should cover a diverse range of catchments from across the Dartmoor landscape. Ideally, these would be representative of the diverse topography of Dartmoor, and include areas of the central upland plateaus, the peripheral uplands, deeply incised valleys and interfluves, and the larger river basins. There is also a need to analyse multiple samples from within an alluvial system to assess consistency and validate the denudation rates derived. Unfortunately, only thirteen ^{10}Be analyses were available for samples of alluvial sediment. Consequently, the choice of sampling sites had to balance the need to cover diverse and representative aspects of the landscape with the need to test consistency and variability of results. The analyses can be divided as follows:

(1) River Dart – with samples analysed from its two main components the East and West Dart, as well as three sub-catchments. This aims to assess any variability across catchment size and landscape elements.
(2) West Okement River – with six samples analysed from sites over the length of this single upland catchment, testing consistency and variability within a catchment.
(3) River Walkham and East Okement River – with a single sample from each, these extend the area covered in the research.

The morphological characteristics of the upstream catchment at each sampling site are shown in Table 5.2. The catchments range in size from the 3.1 km^2 Foxton Mires (SM01) to the 77 km^2 West Dart River (WD01). They span an elevation range of 200 to 620 m, with mean catchment elevation between 390 and 530 m. Most of the catchments have their headwaters in the north central upland of Dartmoor and have maximum elevations of between 550 and 620 m. The relief ratio is greater in the smaller upland catchments (25 to 48) than the larger East Dart and West Dart River catchments (18 to 20). At least 10% of most catchments have hillslope gradients greater than 10º, with the steepest terrain in the valley of the West Okement River (Figure 5.2).Each catchment is discussed in detail in the relevant section of results.

Table 5.2 Morphological characteristics of the study catchments

Sample ID	Site Coordinates		Catchment	Elevation (m)			Long. Flow Path	Total Basin Relief	Relief Ratio	Hillslope Gradient (º)		
	Latitude	Longitude	Area (km^2)	Min	Mean	Max	(km)	(m)		Median	P_{90}	P_{95}
River Dart Catchment			**120**	**227**	**408**	**602**	**19.2**	**375**	**19.6**	**4.2**	**11.2**	**15.1**
ED01	50.544	-3.876	42.5	229	411	602	18.8	373	19.8	5.4	11.7	15.3
WD01	50.542	-3.877	77.2	228	407	563	18.6	335	18.0	4.7	10.6	14.1
UCB01	50.577	-3.930	5.4	357	425	534	5.0	177	35.1	4.7	11.1	15.5
TB01	50.559	-3.966	17.4	338	473	563	9.1	225	24.8	5.6	12.4	16.5
SM01	50.519	-3.955	3.1	349	406	471	2.5	122	47.9	4.7	9.1	10.6
River Walkham Catchment												
WB01	50.530	-4.057	27.6	148	389	551	13.2	403	30.5	5.9	12.4	16.7
East Okement Catchment												
EO01	50.733	-3.976	15.8	205	419	595	8.3	390	47.1	6.1	13.2	17.3
West Okement Catchment			**13.2**	**293**	**502**	**620**	**9.4**	**327**	**34.8**	**6.6**	**17.5**	**22.3**
M0 (250 & 710)	50.685	-4.030	11.3	369	509	620	8.1	251	30.9	6.6	17.1	21.3
M1	50.685	-4.034	11.1	378	511	620	7.9	242	30.5	6.5	16.8	21.3
M2	50.679	-4.027	10.1	397	512	620	7.2	223	30.8	6	15.4	19.7
M3	50.673	-4.019	8.6	407	515	620	6.3	213	33.8	5.7	13.5	17.7
M5	50.663	-4.002	4.2	470	529	574	3.2	104	32.6	4.4	8.7	11.2

Note: Sample site co-ordinates were measured using GPS in the field. The upstream catchment area of each sampling site was determined from Ordinance Survey 10 m DEM data from Digimap, this was processed in ArcGIS 9.2 using ArcHydro Tools (see Appendix). The longest flow path is the longest upslope (based on DEM cells) pathway possible in catchment. Relief ratio is equal to total basin relief over longest flow path.

5.3.2 Sample Collection

The processing of alluvial sediment samples for cosmogenic nuclide analysis requires sand-sized grains for effective chemical preparation. In this study, the grain size used was 250-710 μm with the exception of the M0(710) sample with a grain size of 710-1000 μm. This requires the collection of sand-sized material from rivers in Dartmoor, which can be difficult to locate given the coarse gravel and boulder sized material that comprises most of the bed and is observed to form an armoured layer in many of the study sites. Deposits of sand-gravel sized material are usually found in small bars or lag deposits in the channel. These deposits are larger and more frequent for the larger catchments and further downstream (e.g. East Dart and West Dart Rivers at Dartmeet and the River Walkham and East Okement Rivers) than in the smaller upland catchments and those with confined channel (e.g. West Okement River, Foxton Mires). The lack of material of an appropriate size for sample processing is potentially problematic as it may: (i) increase the likelihood of collecting samples that are not representative of all sediment leaving the basin; (ii) limit the chance of the sediment being well-mixed when only small volumes are available; and (iii) of the sediment supply being overwhelmed by an injection of sediment from a localised source (e.g. bank collapse or slope mass movement).

5.3.3 Interpretation of ^{10}Be concentration

The calculation of denudation rates from ^{10}Be concentration in alluvial sediment is discussed in Section 2.4.3. It is based on the river system being the main conduit by which the products of erosion are transported out of a basin. It may therefore be reasonable to assume that a sample of alluvial sediment is representative of eroded material from across the basin. A sample of alluvial sediment consists of many thousands of grains each preserving a cosmogenic nuclide signal that reflects their individual exposure history from source. It follows that the ^{10}Be concentration measured in a sample is an integration of these exposures, and therefore an average for the entire catchment. This approach has been successfully applied to a diverse range of environments and time-scales (see reviews by Cockburn & Summerfield, 2004; Bierman & Nichols, 2004; von Blanckenburg, 2005).

The exposure of alluvial sediment to cosmic radiation is more complicated than that of an outcrop. Each grain will have a cosmogenic nuclide signature that reflects its pathway from bedrock, through weathering and transfer downslope in regolith, and finally residence as it is transported and stored in the alluvial system. The ^{10}Be concentration in a surface undergoing steady-state erosion reflects the long-term denudation rate, whether that surface is a bedrock outcrop or regolith. In the case of well-mixed regolith, the ^{10}Be concentration will be constant throughout, regardless of thickness, and still reflect the denudation rate (Granger *et al.*, 1996; Figure 3.11). The regolith on a slope is a combination of material derived by weathering at the bedrock-regolith interface and that transported from upslope. The ^{10}Be concentration in regolith on a slope will be an average concentration for the entire upslope section (Small *et al.*, 1999). Upon entering the alluvial system, sediment becomes mixed with that mobilised from throughout the drainage network and in a well-mixed sediment body will represent an average ^{10}Be concentration for the entire catchment upslope of the sampling site. While it is resident in the river system during transport and storage, alluvial sediment will continue to accumulate cosmogenic nuclides. However, this should be a relatively small contribution in catchments were the residence time is much shorter than the erosional timescale (Granger *et al.*, 1996).

The assumptions upon which this approach relies fall into three main categories (Brown *et al.*, 1995a; Bierman & Steig, 1996; Granger *et al.*, 1996): (i) there is temporal uniformity of erosion rates throughout the basin - this precludes occurrences of episodic erosion events (e.g. mass wasting) and changes to erosion rates that are non-uniformly applied; (ii) the sampled sediment is well-mixed and therefore spatially and temporally representative of all sediments leaving the basin; and (iii) that there is minimal long-term storage of alluvial sediment during transport through the basin. These assumptions are inevitably violated to some degree in a natural environment. However, the accuracy of the method is usually sufficient for many applications and relatively robust when compared to other methods of estimating denudation rates (von Blanckenburg, 2005).

The interpretation of ^{10}Be concentrations in terms of denudation rates requires an interpretative model. In this research, denudation rates were derived using the CRONUS-Earth online calculator (Balco *et al.*, 2008). This implementation allows for the calculation of denudation rates using a variety of different production rate scaling models (i.e. Stone, 2000; Dunai, 2000; Desilets *et al.*, 2006 and Lifton *et al.*, 2005), and integrates a scheme for muonic production and geomagnetic variations. By using this calculator the results benefit from being easily reproduced and supported by widely available documentation (Balco *et al.*, 2008). However, a limitation of using the current version (v2.0) of the CRONUS-Earth online calculator is that erosion rate calculations are only implemented for surfaces. This is problematic as the relationship between production rate and elevation is non-linear (as well as latitude and topographic shielding) and a correct implementation for catchments requires the use of a topographic model. While this may be significant in many locations, the relatively small size (<80 km^2) and limited total relief (<400 m) of the catchments in this study reduce the potential error from this source (see section 2.2.2). An average elevation for each catchment was derived from a DEM and latitude was fixed at the sampling site.

The denudation rates presented in this section are derived using an implementation of the Dunai (2000) production rate scaling model (input variables and results from other scaling models are shown in the appendices). This is given as a denudation rate in mm ka^{-1} (with density of 2.6 g cm^{-3}), which provides a rate of landscape lowering assuming that regolith depth is maintained. Results are also presented in terms of mass loss in t km^{-2} a^{-1} of material removed, although this isn't a denudation rate it is equivalent without a density conversion to volume. The internal uncertainty of measurements is reported to 1σ, which accounts for measurement and analysis errors only. The external uncertainty is appropriate when comparing results to other methods or regions (Balco *et al.*, 2008).

The results of ^{10}Be analysis of alluvial sediment samples are presented in Table 5.3, 5.4, and 5.5, along with calculated denudation rates and averaging times. The ^{10}Be concentration in samples ranged from 0.70 to 2.81 $x10^5$ atoms g^{-1}, although most

samples were between 1.5 and 2.8 x10^5 atoms g^{-1}. The most variation in sample results is in the West Okement River in which M2, M3, and, to a lesser extent, M5 have significantly lower ^{10}Be concentrations than those measured in other samples. The internal uncertainty of most samples is 4-8%; however, sample M0(250) has a very high uncertainty of 18.4% due the sample target being exhausted before sufficient counting statistics were obtained during AMS measurement.

The averaging time scale is a useful concept for assessing the response time of a landscape to changes in denudation (see section 2.4.2.2). It is defined as the length of time required to remove one length of the absorption depth scale, which in this study is calculated as 61.5 cm for the granite bedrock (when Λ =160 g cm^{-2} and ρ = 2.6 g cm^{-3}). Most of the averaging time scales estimated from ^{10}Be concentrations (Table 5.3; 5.4; 5.5) fall between 15 and 30 ka, although in those West Okement River catchment samples with high denudation rates these are much shorter at 6-12 ka.

5.4 River Dart and Sub-Catchments

The catchment of the River Dart is the largest in Dartmoor, covering approximately 1/3 of its area (Figure 5.1). In this study, the catchment is investigated upstream of Dartmeet, where there is a confluence of the West Dart River and East Dart River to form the River Dart. The total area of this catchment is 120 km^2 with a total basin relief of 375 m and relief ratio of 19.6 (Table 5.2). The northern half of the catchment extends across into the northern uplands, with elevations up to 602 m, and includes six long tributary rivers flowing southward until they reach the main eastward flowing channel of the River Dart. The southern extent of the catchment includes the northern edge of the southern upland mass, with elevation up to ~500 m, although most of these uplands drain southwards and do not contribute to the River Dart. The central and eastern parts of the catchment is the main basin of the River Dart and its tributaries, elevations in this area range between 225-300 m although rivers can still be deeply incised with steep valley slopes (Figure 5.1; 5.2).

5.4.1 Study Catchments

The ^{10}Be concentration was measured in five samples of alluvial sediment, with one each from the West Dart River and East Dart River a short distance upstream of Dartmeet, and the remainder from smaller tributary catchments to the West Dart River (Figure 5.1).

5.4.1.1 East Dart River (ED01)

A sample was taken a few hundred metres upstream of the Dartmeet confluence on the East Dart River (ED01). The East Dart River is the smaller of the rivers at the Dartmeet confluence, with an upstream catchment area of 42.5 km^2. The catchment is relatively long and narrow, with a longest flow path of 18.8 km, which is greater than the larger West Dart River catchment (Table 5.2). Most of the catchment drains into the main trunk channel of the East Dart River, with few tributaries apart from an unnamed stream (on Ordinance Survey 1:25k maps) in the east of the catchment (Figure 5.1). The maximum elevation in the catchment is 602 m, which is the highest ground in the entire catchment of the River Dart. The East Dart River rises close to this elevation, towards the centre of the northern upland mass, and flows in a south-westerly direction through the periphery of the northern uplands of Dartmoor. The river is deeply incised over most of its course, but in particular in the lower reaches near Dartmeet were slope is 20-30^o (Figure 5.2). However, steep slopes are largely confined to areas near the river channel and most of the catchment consists of low gradient (<10^o) upland plateau and interfluve surfaces.

5.4.1.2 West Dart River (WD01)

A sample was taken from the West Dart River upstream of the Dartmeet confluence (WD01). The West Dart River is the larger of the rivers at Dartmeet, with an upstream catchment area of 77.2 km^2. The eastward flowing channel of the West Dart River and the tributary Blackbrook River effectively divides the catchment. In the northern part of the catchment four main rivers drain from the edge of the northern upland mass, flowing in a mostly southerly direction until they turn eastward forming the main eastward flowing channel in the catchment. There are fewer tributaries from southern part of the catchment. The most significant is the River Swincombe, which drains the northern edge of the southern upland mass of

Dartmoor. Although the catchment area of the West Dart River is almost twice the size of that for the East Dart River, it has a slightly shorter longest flow path of 18.6 km (Table 5.2) due to the main rivers all having similar length. There is a total basin relief of 335 m in the West Dart River catchment, ranging from an elevation of 228 m at Dartmeet, to the highest elevation of 563 m in the north of the catchment. There are significant areas of upland in the north, northwest, and south of the basin in which elevations are over 400 m, while the central and eastern basin have lower elevations of 200-400 m. The catchment has a relief ratio of 18.0, which is similar to the East Dart River catchment (19.8), but less than that of other catchments in this study (Table 5.2). Most of the catchment consists of low gradient surfaces less than 5°; this includes both upland plateau and interfluve surfaces and those in the lower elevation central and eastern parts of the basin (Figure 5.2). Into the upland surfaces, the rivers are deeply incised with local relief in excess of 100 m and slopes of 20-30° found throughout the catchment, with this most pronounced upstream of Two Bridges and in the proximity of Dartmeet (Figure 5.2). The lower elevation areas of the catchment have a history of anthropogenic modification that extends back to the Neolithic, including extensive field enclosure and agricultural use. There is also localised impact of tin mining in many parts of the catchment, although this is most significant in the southern area around the Foxton Mires.

5.4.1.3 Two Bridges (TB01)

At Two Bridges there is a confluence of the River Cowsic and the upper West Dart River, both of which rise in the northern uplands and flow southwards in parallel (Figure 5.6). A sample was taken from a sand bar a few metres upstream of the main bridge at Two Bridges (TB01). This catchment is a sub-catchment of the West Dart River and has a total area of 17.4 km^2. The longest flow path is 9.1 km and extends up the West Dart River to the northern boundary of the catchment. There is a total basin relief of 225 m, with elevation ranging from 338 m at the Two Bridges sampling site to the highest elevation of 563 m in the north of the catchment. The relief ratio of 24.8 is lower than most other catchments in this study (Figure 5.2); this reflects the relatively long length of the river and low channel gradient following channel incision in the upper reaches. The northern part of the catchment extends into the southern edge of the low gradient (<5°) plateau surface of the northern

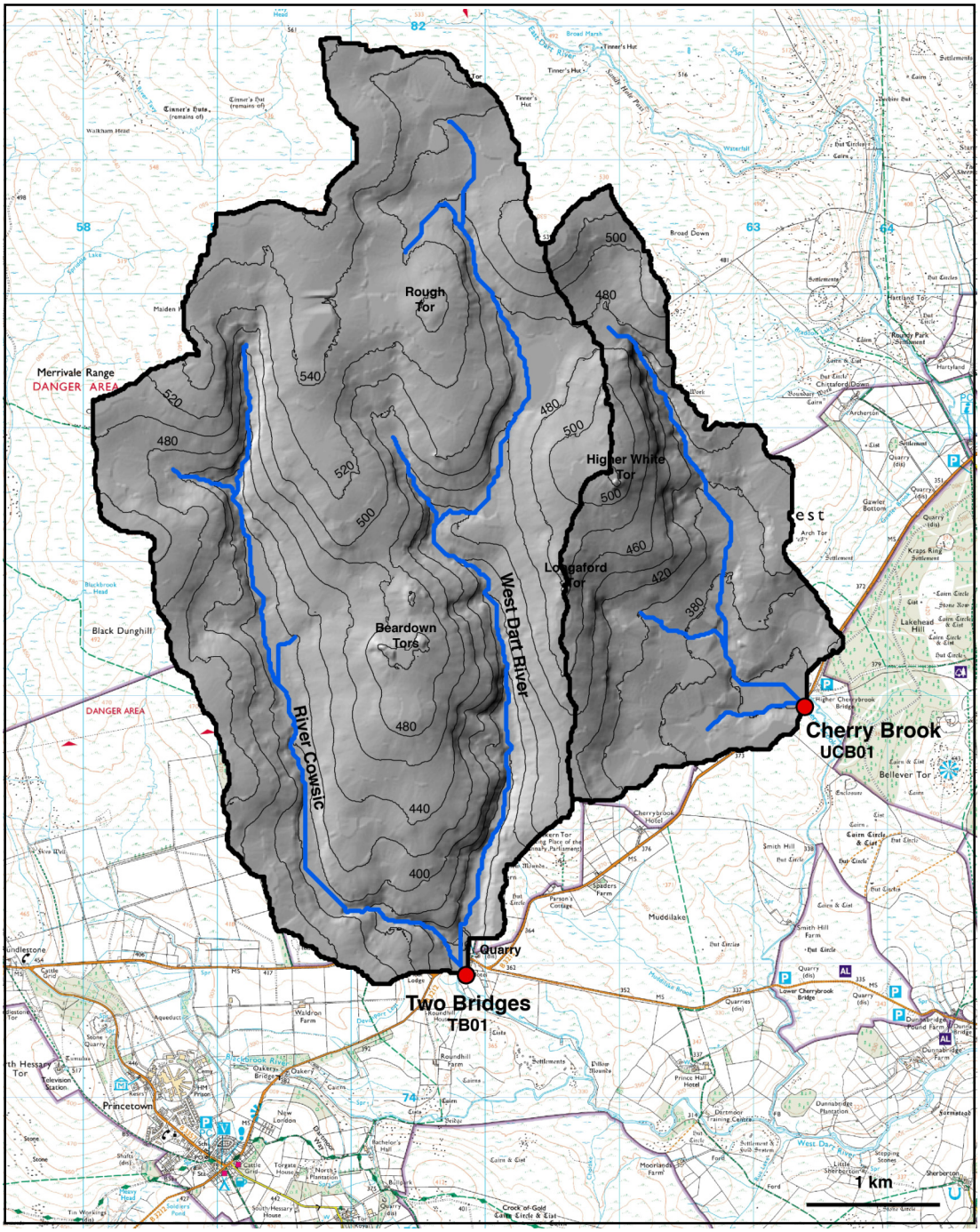

Figure 5.6 Catchment upstream of the alluvial sediment sampling sites at Two Bridges (TB01) and Upper Cherry Brook (UCB01); 20 m contours are overlaid on the digital terrain model.

Data: 10m DEM from Digimap/Ordinance Survey

Processing: ArcGIS 9.2 and ArcHydro Tools

Map image: Digimap/Ordinance Survey

Dartmoor uplands. Both rivers rise on this upland plateau surface, and rapidly incise a valley that for most of their lengths has local relief in excess of 100 m and steep valley slopes, with 5% of catchment having slopes in excess of 16.5° (Table 5.2) with these mostly localised near the river channels. Between the rivers are tor-capped interfluves with low-gradient (<10°) surfaces that maintain elevations in excess of 400 m (Figure 5.1; 5.6).

5.4.1.4 Upper Cherry Brook (UCB01)

The Cherry Brook is a tributary to the West Dart River that rises on the edge of the northern uplands and flows southward (Figure 5.6). A sample of alluvial sediment was collected at the Higher Cherrybrook Bridge (UCB01), upstream of which is approximately one third of the total Cherry Brook catchment area. This upper Cherry Brook catchment is flanked on the west by the West Dart River (Two Bridges) catchment and on the east by tributaries to the East Dart River. The catchment upstream of the Higher Cherrybrook Bridge is relatively small at 5.4 km^2. It is also a relatively narrow catchment, with the Cherry Brook the main river channel and only minor tributaries flowing from the interfluve and joining in its lower reaches. There is a total basin relief of 177 m, ranging from 357 m at Higher Cherrybrook Bridge to 534 m at Higher White Tor. The highest ground in the catchment is in the west and north, where there is an interfluve between the West Dart River and Cherry Brook capped by the Longaford and White Tors. The transition from the high ground occurs over a narrow zone with slopes of 10-30°. The Cherry Brook rises in an upland area, but rapidly incises and for most of its course in this catchment flows over a relatively low gradient surface (<5°) which has elevation of 360-400 m (Figure 5.6).

5.4.1.5 Foxton Mires (SM01)

The stream flowing through the Foxton Mires is a small tributary in the headwaters of the River Swincombe, which drains the northern side of the southern uplands in Dartmoor (Figure 5.1; 5.7). A sample of alluvial sediment was taken from the stream in the Foxton Mires (SM01), upstream of this site there is a small catchment with a total area of 3.1 km^2, the smallest included in this study, and total basin relief of 122 m. There is only a limited drainage network in the catchment with a few streams

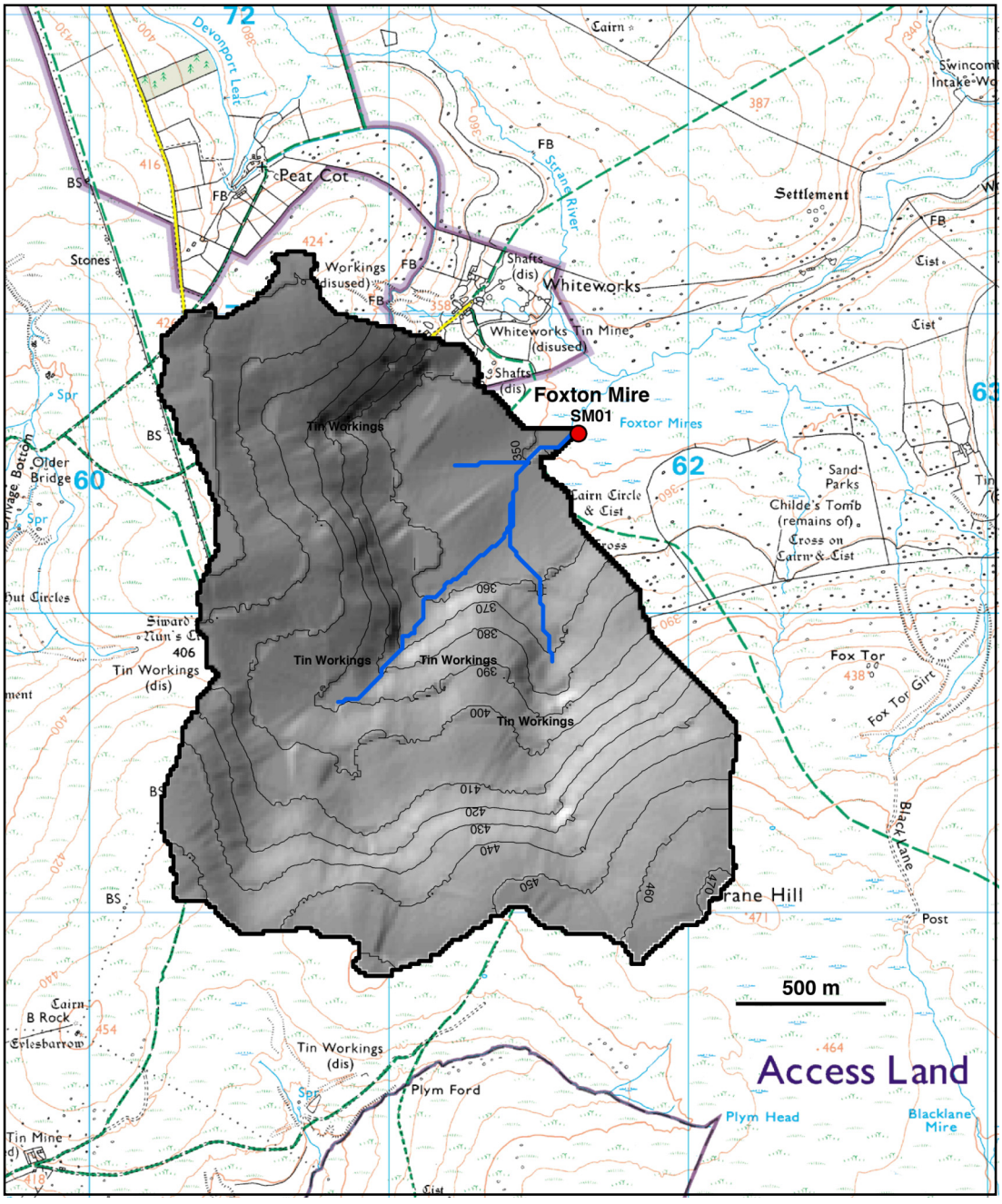

Figure 5.7 The catchment upstream of alluvial sediment sampling site at Foxton Mire (SM01); 10 m contour lines are overlaid on the digital terrain model

Data: 10m DEM from Digimap/Ordinance Survey

Processing: ArcGIS 9.2 and ArcHydro Tools

Map image: Digimap/Ordinance Survey

feeding into the channel through the Foxton Mires. This is due to the limited size of the catchment, with a longest flow path of only 2.5 km, and the water-logged expanse of the mire. The sampling site was from the main stream channel through the mires, a flat expanse of ground with elevation of 350-360 m. The transition from this surface to the higher ground in the catchment occurs over a relatively short distance, with a 30 m gain in elevation and slopes of 10-20°. It is also in this transition zone that tin workings are most prolific, with hydraulic mining by stream diversion leading to gully incision. Above elevations of about 390 m, the catchment is part of the low gradient plateau surface of the southern uplands of Dartmoor. This is typically covered by layer of peat observed to be >2 m thick in sections. The highest point in the catchment is at Crane Hill with an elevation of 471 m.

5.4.2 Cosmogenic Nuclide Results

The results of ^{10}Be concentration measurements on samples of alluvial sediment from sub-catchments of the River Dart are presented in Table 5.3. The ^{10}Be concentrations measured range from 1.62±0.07 to 2.81±0.12 x10^5 atoms g^{-1}, with the denudation rates derived from these concentrations between 21.2±0.9 and 36.6±1.7 mm ka^{-1}.

Table 5.3 ^{10}Be derived denudation rates and averaging time for River Dart sub-catchments

Sample ID	10Be Conc.	Denudation Rate		External	Averaging
	(10^5 atoms g^{-1})	(mm ka^{-1})	(t km^{-2} a^{-1})	Uncertainty	Time (ka)
ED01	1.88 ± 0.10	31.0 ± 1.7	80.5 ± 4.3	10.79%	19.9
WD01	2.14 ± 0.08	26.9 ± 1.1	70.1 ± 2.8	10.24%	22.8
UCB01	1.62 ± 0.07	36.6 ± 1.7	95.0 ± 4.4	10.34%	16.8
TB01	2.81 ± 0.12	21.2 ± 0.9	55.0 ± 2.4	10.68%	29.1
SM01	1.92 ± 0.10	30.2 ± 1.7	78.5 ± 4.3	10.86%	20.4

The East Dart River (ED01) and West Dart River (WD01) were each sampled a short distance upstream of their confluence at Dartmeet. The upstream catchments at each site represent the two main contributing catchments to the River Dart, with area of 42.5 and 77.2 km^2 respectively. The denudation rate derived for ED01 at

31.0±1.7 mm ka^{-1} is slightly higher than that for the WD01 at 26.9±1.1 mm ka^{-1}, although these are within 2 σ of internal uncertainty and effectively indistinguishable. These results suggest that denudation rates are similar across large areas of Dartmoor, despite the greater heterogeneity of the West Dart River catchment, which includes a larger central basin area and extends into the southern uplands.

Located on the periphery of the northern uplands, the Two Bridges (TB01) and Upper Cherry Brook (UCB01) are sub-catchments of the West Dart River. The denudation rate derived for Two Bridges (TB01) at 21.2±0.9 mm ka^{-1} is the lowest in the sub-catchments of the River Dart, despite deep incision of the river and it having the steepest slopes (P_{90} = 12.4°: Table 5.2). Conversely, the adjacent Upper Cherry Brook (UCB01) sample returned the highest denudation rate of 36.6±1.7 mm ka^{-1} measured for River Dart sub-catchments. The results from these upland catchments suggest that denudation rates are not significantly different from those of the larger downstream catchments of the West Dart and East Dart Rivers.

The sample taken from the Foxton Mires (SM01) on the periphery of the southern uplands returned a denudation rate of 30.2±1.7 mm ka^{-1}. This rate is similar to those obtained for other sub-catchments of the River Dart, which suggests that denudation rates in the topographically more subdued southern uplands are not significantly different from those in the northern uplands. There is also no obvious effect from tin mining in the catchment or its comparatively small river and catchment area.

The results for the five sub-catchments of the River Dart indicate that denudation is relatively consistent across the landscape, returning denudation rates of between 21-37 mm ka^{-1}. Many of the samples cannot be distinguished to 2σ internal uncertainty (which accounts for only analytical and laboratory error), and given the likelihood of a much greater uncertainty being associated with geomorphological variability and violations of model assumptions (not defined with limited dataset), no meaningful interpretation is made of differences between the derived denudation rates.

5.4.3 Summary

The analysis of five alluvial samples from tributaries to the River Dart suggests that the landscape denudation rate is ~20-40 mm ka^{-1}, with an average from the samples of 29 mm ka^{-1}. The results are consistent for catchments that cover both the northern and southern uplands, and range in size from 3 to 77 km^2.

5.5 River Walkham and East Okement River

The River Walkham and the East Okement River both rise in northern uplands and flow outward, south and north respectively (Figure 5.1). A single sample of alluvial sediment was analysed from each of these rivers and, while caution should be taken interpreting limited data, the results extend the spatial coverage of this research.

5.5.1 Study Catchments

5.5.1.1 River Walkham (WB01)

A sample of alluvial sediment was taken from a sand bar on the River Walkham at Ward Bridge (WB01), just prior to the river leaving the granite bedrock of Dartmoor (Figure 5.8). The catchment upstream of Ward Bridge has an area of 27.6 km^2, with elevation ranging from 148 m at Ward Bridge to 551 m in the far north of the catchment, a total basin relief of 403 m (Table 5.2). The longest flow path in the catchment is 13.2 km, following the River Walkham into the headwaters on the edge of the northern uplands of Dartmoor. The River Walkham flows in a southerly direction off the upland plateau, becoming deeply incised as it approaches Great Mis Tor. There are no significant tributaries in the upper reaches of the catchment, which is <2 km in width over most of its northern extent. From Great Mis Tor southward, the River Walkham dissects an area of central upland linking the main northern and southern upland masses in Dartmoor. Here the elevation on the western side of the catchment ranges between 350-450 m and on the eastern side between 400-540 m, where it shares a watershed boundary with the West Dart River catchment. The summits in the central catchment feature significant tors including Great Staple Tor (455 m), Cox Tor (442 m), Great Mis Tor (538 m) and Vixen Tor (317 m). There is significant valley relief of up to 200 m throughout the central and

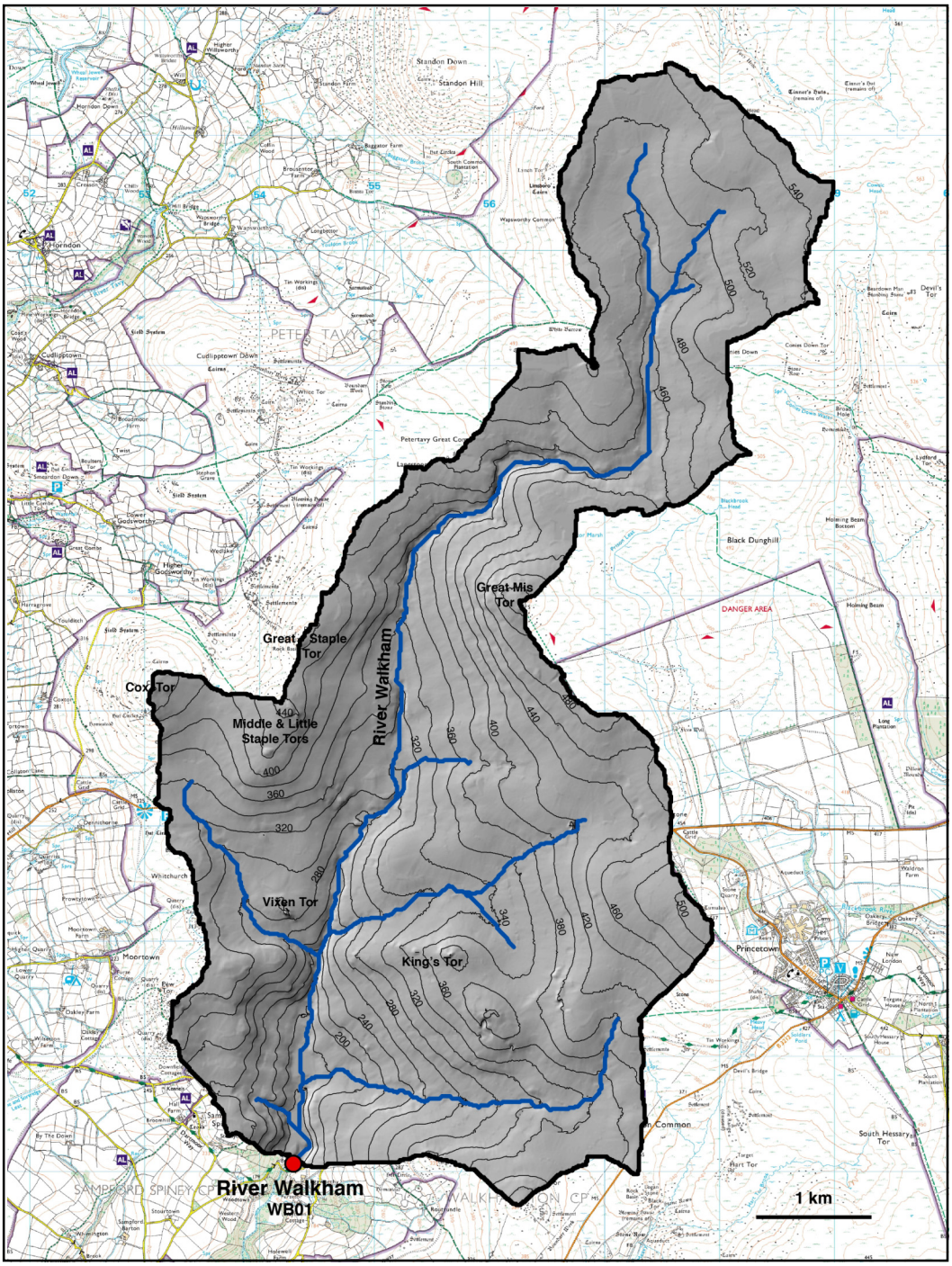

Figure 5.8 The catchment upstream of alluvial sediment sampling site at Ward Bridge on the River Walkham (WB01); 20 m contours are overlaid on the digital terrain model.

Data: 10m DEM from Digimap/Ordinance Survey

Processing: ArcGIS 9.2 and ArcHydro Tools

Map image: Digimap/Ordinance Survey

lower catchment. This occurs over long, relatively gradual slopes (5-15°) that extend from the summits to the river channel. This differs from most other study sites (and those typical of Dartmoor in general, that feature steep valley slopes in proximity to a deeply incised river channel, and a low gradient summit-plateau surface. In the lower catchment there are three significant tributaries to the River Walkham, which increases width of the catchment to up to 5 km. There is human modification of the landscape in the River Walkham catchment that includes field enclosure (although less than lower sections of the River Dart) and comparatively heavy grazing, stone-quarrying, and stream diversion. There is a small area of metadolerite bedrock in the vicinity of Cox Tor, however, due to its limited extent and likely insignificant contribution of quartz (fine grain-size and low quartz content in dolerite) it is reasonable to disregard this variation in lithology when interpreting a catchment average denudation rate from ^{10}Be concentration.

5.5.1.2 East Okement River (EO01)

A sample of alluvial sediment (EO01) was taken from the East Okement River 350 m upstream of the A30 Bridge. Although there is an upstream catchment area of 15.8 km^2, about 1/3 of the catchment is not on granite bedrock (Figure 5.9). The contact between granite and country rock in Dartmoor is sharp (Exley & Stone, 1964), and the lithology in the north of the East Okement catchment is of mudstone and siltstone (BGS Map Sheet). The grain-size of quartz in these rocks is too fine for cosmogenic nuclide sample preparation (250-710 μm analysed for EO01), and it is therefore reasonable to exclude this non-granite section of the catchment when interpreting ^{10}Be derived denudation rates. There is a total basin relief of 390 m in the catchment upstream of the sample site, although the East Okement River crosses the granite contact at 300 m (95 m above the sample site) and this would reduce the effective basin relief to 295 m. The highest elevation is 595 m on the slope of High Willhays in the west of the catchment, although an elevation closer to 570 m is probably more realistic (Figure 5.9 – see watershed anomaly). The catchment rises toward the High Willhays and Yes Tor summits in the west and abuts the West Okement River catchment on the south. There are two main channels in the catchment, the main East Okement River and the smaller Black-a-Ven Brook. These flow northwards, in parallel, until the Black-a-Ven Brook diverts eastward to join the

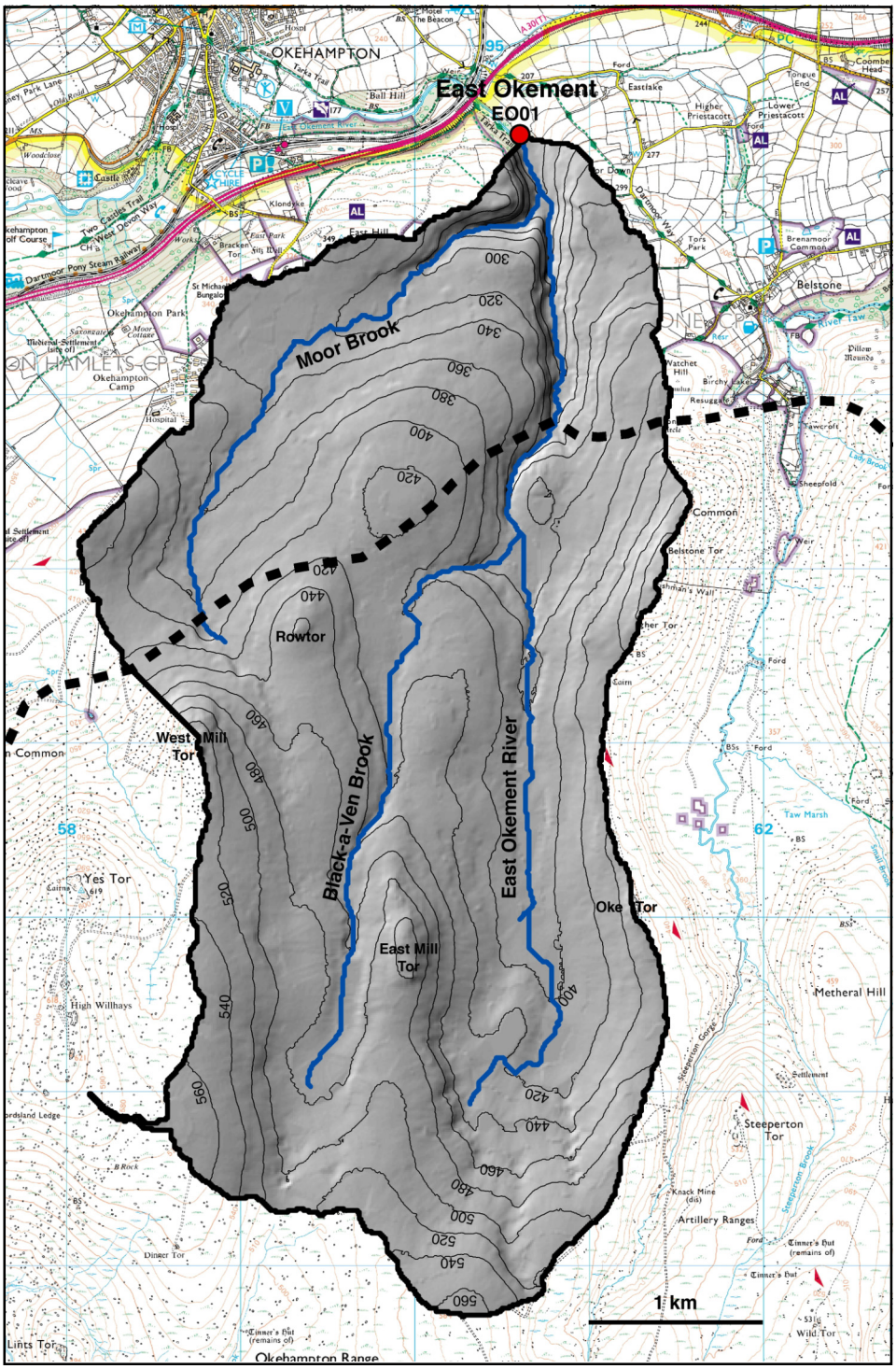

Figure 5.9 The upstream catchment of alluvial sediment sampling site at East Okement River (EO01); 20 m contours are overlaid on the digital terrain model. The dashed line is the boundary of the granite.

Data: 10m DEM from Digimap/Ordinance Survey

Data: Granite Boundary British Geological Survey MapSheet

Processing: ArcGIS 9.2 and ArcHydro Tools

main channel just prior to it leaving the granite bedrock. The Moor Brook drains mostly from country rock and includes only a small area of granite in its headwaters. The catchment is on the northern edge of the northern uplands of Dartmoor, with most of the granite bedrock catchment at elevation in excess of 400 m. Neither the East Okement River or Black-a-Ven Brook is deeply incised into this upland surface, with deep river incision (with slopes >20°) only occurring as the river leaves the granite. Hillslope gradients in the granite-bedrock catchment are mostly <10°, although there are slopes on 10-20° on the eastern face of East Mill Tor (Figure 5.2).

5.5.2 Cosmogenic Nuclide Results

Both the River Walkham (27.6 km^2) and East Okement River (15.8 km^2) are mid-sized catchments that drain from the main northern uplands mass of Dartmoor. The ^{10}Be concentrations measured for these catchments are similar at 2.71±0.16 x10^5 atoms g^{-1} for the River Walkham sample and 2.19±0.10 x10^5 atoms g^{-1} for the East Okement River (Table 5.4). The denduation rates derived for these catchments of 20.6±1.3 mm ka^{-1} (WB01) and 26.5±1.3 mm ka^{-1} (EO01) suggest similar denudation in these catchments. They are also comparable with the results from sub-catchments of the River Dart (Table 5.3), suggesting a consistency of denudation rates across the Dartmoor landscape.

Table 5.4 ^{10}Be derived denudation rates for River Walkham and East Okement River

Sample ID	10Be Conc.	Denudation Rate		External	Averaging
	(10^5 atoms g^{-1})	(mm ka^{-1})	(t km^{-2} a^{-1})	Uncertainty	Time (ka)
River Walkham Catchment					
WB01	2.71 ± 0.16	20.6 ± 1.3	53.6 ± 3.3	11.40%	29.8
East Okement Catchment					
EO01	2.19 ± 0.10	26.5 ± 1.3	69.0 ± 3.4	10.66%	23.2

5.6 West Okement River

Located in the northwest of Dartmoor, the West Okement River was selected for the most intensive sampling of alluvial sediments for ^{10}Be analysis in this study. In total six samples were analysed from five locations along the course of the river. These are intended to evaluate variability of results within an individual drainage system, and to compliment nearby investigations of tors (Chapter 4) and blockslopes (Chapter 5).

5.6.1 West Okement River Catchment

The West Okement River now flows into the Meldon Reservoir (Figure 5.10), with its natural course terminating at a weir (elevation 293 m). Above the weir there is a total upstream catchment area of 13.2 km^2, making the West Okement catchment small to medium sized in terms of this study (Table 5.2). Despite its limited size, the catchment includes the highest elevation in Dartmoor at High Willhays (621 m) and a large and deeply incised valley that dissects the northwest uplands. There is a total basin relief of 327 m between the weir and High Willhays summit. The longest flow path calculated for the catchment is 9.4 km and a relatively high relief ratio of 34.8 reflects deep incision of the valley.

The headwaters of the West Okement River are in an area of upland plateau in the southeast of the catchment, where the river and its tributary the Brim Brook rise at elevations of 560 m and 520 m respectively. These both flow over a low gradient surface until they confluence at Kneeset Nose, elevation 470 m. Between Kneeset Nose and Kneeset Foot there is a >90° diversion of the flow direction, from south-westerly to north-westerly (Figure 5.11). This unusual flow path is likely to reflect underlying structural controls in the granite bedrock, a common feature of Dartmoor rivers (Gregory, 1969; Gerrard, 1993). From Kneeset Foot the river continues to flow northwest some 4.5 km through the main section of the West Okement Valley until it reaches the weir above Meldon Reservoir. The West Okement River has a coarse bedload, with much of the bed consisting of cobbles and boulders and only isolated deposits of sand-gravel sized material. It appears the river is directly mobilising slope material, and lacks the capacity to transport the larger sized material of the valley fill.

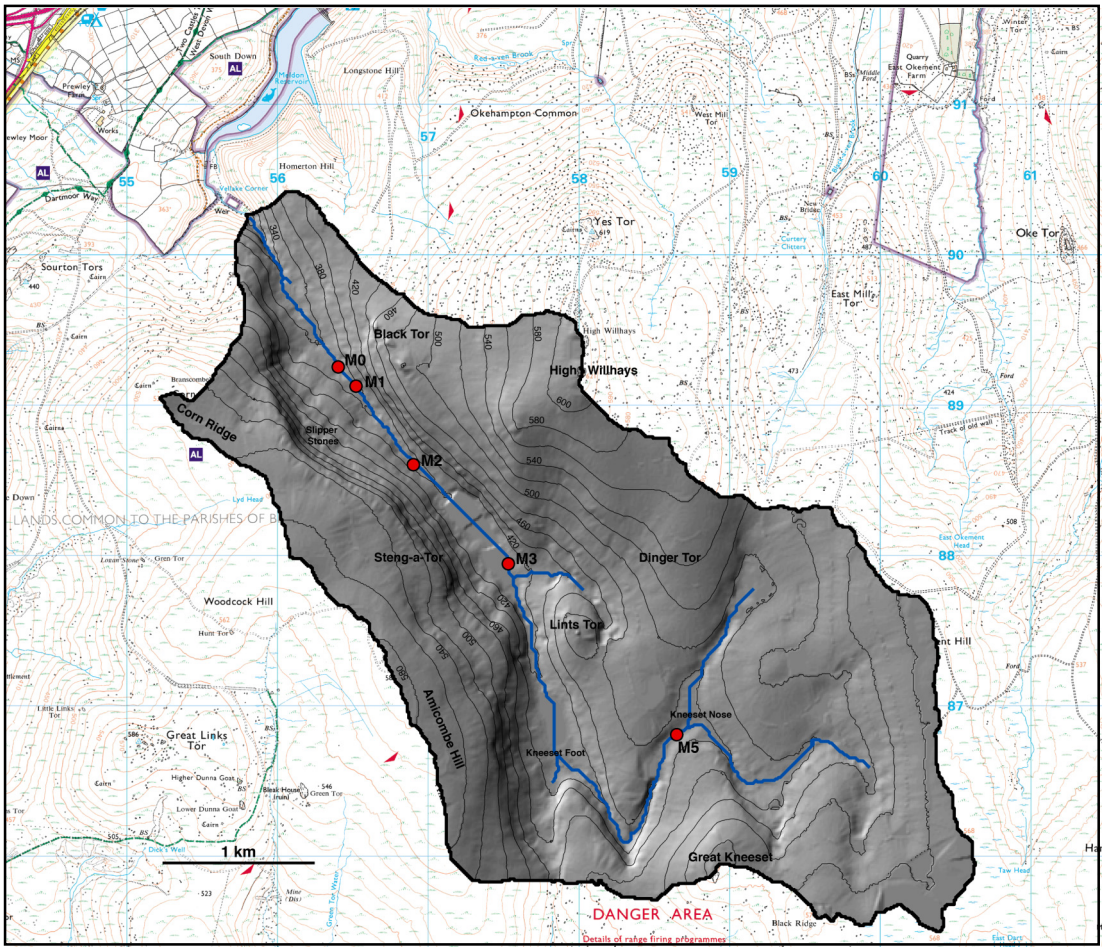

Figure 5.10 The catchment of the West Okement River showing the five alluvial sediment sampling sites along the length of the river; 20 m contours are overlaid on the digital terrain model.

Data: 10m DEM from Digimap/Ordinance Survey

Processing: ArcGIS 9.2 and ArcHydro Tools

Map image: Digimap/Ordinance Survey

Figure 5.11 Aerial photography of the West Okement River between Kneeset Nose and Kneeset Foot were it makes a >90° change in flow direction.

Image: GoogleEarth™

The main valley of the West Okement River is deeply incised into the uplands of north-western Dartmoor (Figure 5.12; 5.13). Local valley relief (from the river to break in slope) is up to 180 m and the slopes exceed 20º along most of the valley length (Figure 5.2; 5.9). On the north-east side of the valley the slopes are steep leading up to a break in slope at elevation of between 450-500m. The slopes are also boulder-strewn, especially in the proximity of the Black Tor outcrops (see section 3.6.1) where wall collapse and slope retreat is apparent (Figure 5.14). On the south-west side of the valley there is a sharp transition from low gradient surface to steep valley slopes, and in places there are probably large mass movements (e.g. Slipper Stones), with exposed bedrock headwalls (Figure 5.14). There is a large amount of blocky material on the slopes and valley floor, probably transported by mass wasting of slopes under intense periglacial conditions.

The West Okement River is incised between the mass of the High Willhays – Yes Tor summits on the north-east, the Amicombe Hill – Corn Ridge plateau on the south-west, and the Great Kneeset to the south-east (Figure 5.10). The High Willhays summit is the highest in Dartmoor at 621 m, and the slopes extending from this summit are mostly gradual (<10º) and continue for up to 1 km before there is a break in slope and transition to the West Okement Valley. The Amicombe Hill – Corn Ridge is a broad plateau surface at elevation between 500-580 m and slopes mostly <5º. It extends some 5 km SE-NW parallel to the West Okement River, and unlike the sharp transition into West Okement valley it slopes more gently to the south-west were it is linked to the mass of the Great Links Tor. The Great Kneeset in the southwest links into the main upland plateau of the central upland mass in northern Dartmoor.

Anthropogenic disruption of the West Okement River catchment (above the weir) is relatively low for the Dartmoor region. There is some minor tin working in the upper reaches of the river (upstream of Kneeset Nose). There has been minimal alteration of the landscape for agricultural purposes, with no significant enclosure and only low-density livestock grazing.

Figure 5.12 West Okement River valley from the southern side near Steng-a-Tor looking north towards Black Tor and the High Willhays

Figure 5.13 West Okement River valley looking west along the main valley from Lints Tor.

Figure 5.14 Aerial photography of the West Okement River in the main channel near Black-a-Tor copse, showing location of sampling sites M0, M1, and M2.

Image: GoogleEarth™

5.6.2 Cosmogenic Nuclide Results

The results of ^{10}Be concentration measurements on alluvial sediment from the West Okement River are presented in Table 5.5, and range from 0.70±0.06 to 1.83±0.11 x10^5 atoms g^{-1}. The denudation rates derived from these concentrations range between 34.3±2.2 and 93.5±7.7 mm ka^{-1}, which are generally higher and more variable than those measured in other basins in this study (Table 5.3; 5.4).

Table 5.5 ^{10}Be derived denudation rates and averaging time for the West Okement River

Sample ID	10Be Conc.	Denudation Rate		External	Averaging
	(10^5 atoms g^{-1})	(mm ka^{-1})	(t km^{-2} a^{-1})	Uncertainty	Time (ka)
M0 (250)	1.60 ± 0.29	39.4 ± 7.7	102.4 ± 20.0	21.67%	15.6
M0 (710)	1.83 ± 0.11	34.3 ± 2.2	89.0 ± 5.7	11.39%	18.0
M1	1.55 ± 0.09	41.0 ± 2.6	106.5 ± 6.6	11.21%	15.0
M2	0.70 ± 0.06	93.5 ± 7.7	243.0 ± 20.1	12.18%	6.6
M3	0.93 ± 0.06	70.0 ± 5.0	182.1 ± 13.0	11.52%	8.8
M5	1.25 ± 0.08	51.7 ± 3.2	134.5 ± 8.4	11.12%	11.9

5.6.2.1 M0/M1

The M0 and M1 sampling sites are located in a section of the river adjacent to the Black-a-Tor Copse in the lower reaches of the West Okement River at 1.3 and 1.5 km upstream of the weir (Figure 5.10; 5.14). The river channel in this reach is confined by steep hillslopes, in particular on the north-east side up to Black Tor, and there are a large number of boulders in the river bed (Figure 5.15; 5.16a). There is approximately 200 m between the sites and the samples were collected 20 months apart.

Two different grain size fractions were analysed from the M0 sample, 250-710 and 710-1000 μm (this is the only sample of >710 μm grain-size analysed). This provides a limited test of grain size dependence of ^{10}Be concentrations, which has been shown to occur in some bodies of alluvial sediment (e.g. Brown *et al.*, 1995a; 1998; Matmon *et al.*, 2003). The ^{10}Be concentrations measured of 1.60±0.29 (250-710 μm) and 1.83±0.11 (710-1000 μm) x10^5 atoms g^{-1} are within 1σ internal uncertainty, suggesting no grain-size dependence. Unfortunately the M0(250) sample target was exhausted during AMS analysis before sufficient counting statistics could be

Figure 5.15 West Okement River at sample site M0

obtained, resulting in substantial error associated with the measurement, with an internal uncertainty of 19.5%.

A ^{10}Be concentration of 1.55±0.09 x10^5 atoms g^{-1} was measured in the sample M1, a similar concentration to those of the M0 samples. This indicates a consistency of ^{10}Be concentrations in the sediment through this reach of the West Okement River. As the samples were taken 20 months apart, a comparison of the results provides an assessment (albeit limited) of potential for temporal variation in alluvial sediment ^{10}Be concentrations. A difference in concentration might indicate variable mixing of sediment or a sediment pulse from episodic mobilisation from specific source areas. There is no indication of this occurring over this reach of the West Okement River.

The denudation rates derived for the samples of 39.4±7.7, 34.3±2.2, and 41.0±2.6 mm ka^{-1} are comparable to those measured in the River Dart (Table 5.3) and the River Walkham and East Okement River (Table 5.4), although at the top end of rates measured.

5.6.2.2 M2/M3

The samples M2 and M3 were taken in the mid-section of the main West Okement River valley, at distances 2.2 and 3.1 km upstream of the weir (Figure 5.10). The river channel is still confined by slopes at site M2 and there is a high proportion of boulders and cobbles in the river bed (Figure 5.16b). At the M3 sampling site the channel is wider and surrounding ground, while still appearing to be slope deposits, is relatively flat. There are also few boulders in the river bed which is composed mostly of cobble sized material (Figure 5.17).

The ^{10}Be concentrations measured was 0.70±0.06 x10^5 atoms g^{-1} for M2 and 0.93±0.06 x10^5 atoms g^{-1} for M3 (Table 5.5). These are substantially lower ^{10}Be concentrations than those measured downstream at sites M0 and M1. As there are no significant tributaries to the West Okement River in the ~2 km distance between sites M3 and M0, the variation in ^{10}Be concentration suggests that there is incomplete mixing of sediment and/or localised mobilisation of sediment. This is

Figure 5.16 West Okement River at sample sites (a) M1 and (b) M2

Figure 5.17 West Okement River at sample site M3

problematic for the determination of catchment-averaged denudation rates as it violates several key assumptions.

The denudation rate determined for samples of 93.5±7.7 (M2) and 70.0±5.0 (M3) mm ka^{-1} are twice those measured downstream at sites M0 and M1, and also much higher than those calculated for any other sample in this study (Table 5.3; 5.4).

5.6.2.3 M5

The M5 sample was collected from the West Okement River at Kneeset Nose a short distance downstream from its confluence with Brim Brook (Figure 5.10). The M5 site is 6.2 km upstream of the weir and at an elevation of 470 m is in the headwaters of the catchment. The catchment for the site is small at only 4.2 km^2, although it still has a total basin relief of 104 m the slopes are more gentle (median 4.4°) than the rest of the West Okement River basin (Table 5.2). The river is only a few metres wide at Kneeset Nose and flows through an area of relatively flat, water-logged ground.

The ^{10}Be concentration measured in sample M5 was 1.25±0.08 x10^5 atoms g^{-1} (Table 5.5). While this concentration is higher than those measured in samples M2 and M3, it is still lower than those furthest downstream at M0 and M1. Accordingly, the calculated denudation rate of 51.7±3.2 mm ka^{-1} is in between those measured downstream in the West Okement River, and higher than those measured elsewhere in Dartmoor (Table 5.3; 5.4).

5.6.3 Summary

The denudation rates calculated from samples of alluvial sediment from the West Okement River ranged between 34 and 94 mm ka^{-1}, and are plotted with distance upstream in Figure 5.18. The denudation rates determined for samples M2 and M3 are significantly higher that those downstream at M0 and M1. There are no significant tributaries to the West Okement River between these sampling sites, so the change in ^{10}Be concentration cannot be explained by mixing of sediments from different streams (e.g. Bierman & Steig, 1996; Binnie *et al.*, 2006). It is possible that the addition of material from the slopes along this ~ 2 km reach of the river has been in proportion to long-term erosion rates and has lowered the denudation rate by

adding high ^{10}Be concentration sediment. However, this part of the valley has the steepest slopes in the entire basin and it does not seem likely that it would have a substantially lower denudation rate signal. Therefore, it appears that insufficient mixing of alluvial sediment is leading to variability in measured ^{10}Be concentrations.

The West Okement River has a narrow channel for much of its length and is often confined by valley slopes with little floodplain development. The sediment load of the river appears to be direct mobilisation of colluvial material. There is limited storage of sand-sized sediment within the alluvial system with most of the river bed comprised of gravel, cobbles and boulders. Where sand is found, it is mostly in small bar and lag deposits and often near the banks of the river where there is potential for a direct localised input of sediment. The scarcity of sand-sized material in the bedload reduces the effectiveness of mixing and increases the likelihood that episodic delivery of material (e.g. bank collapse or mass movement) will overwhelm the sample and bias the results. Insufficient mixing of sediment is a violation of a key assumption in applying cosmogenic nuclides to derive catchment-averaged denudation rates (Bierman & Steig, 1996). It has been demonstrated that mixing may be problematic in small drainage basins subject to episodic sediment delivery (Binnie *et al.*, 2006), and it is likely that the West Okement River is subject to these issues and exacerbated by relatively low sand-sized sediment volume.

Although there are some concerns over the 'catchment-averaged' nature of the denudation rates, they still reflect some averaging of the cosmogenic nuclide signal through hillslope and fluvial transportation. With denudation rates of ~35-95 mm ka^{-1} the results from alluvial sediment is similar to those derived from regolith at the summit of nearby High Willhays (40-65 mm ka^{-1}) and on the buttress outcrop at Dinger Tor (48 mm ka^{-1}) which is located in the headwaters of the basin (Chapter 4). The denudation rates derived from the M0 and M1 samples (34-41 mm ka^{-1}) are comparable to those measured in alluvial sediments from other Dartmoor catchments (20-37 mm ka^{-1}), although amongst the highest. The denudation rates at M2, M3, and M5 (52-94 mm ka^{-1}) are significantly higher than any other denudation rate measured.

Figure 5.20 Preservation of periglacial landforms in the Cox Tor – Great Staple Tor area; note the earth hummocks in the foreground and the patterned stone stripes on the slopes of Great Staple Tor across the valley.

Photo: W.M. Phillips

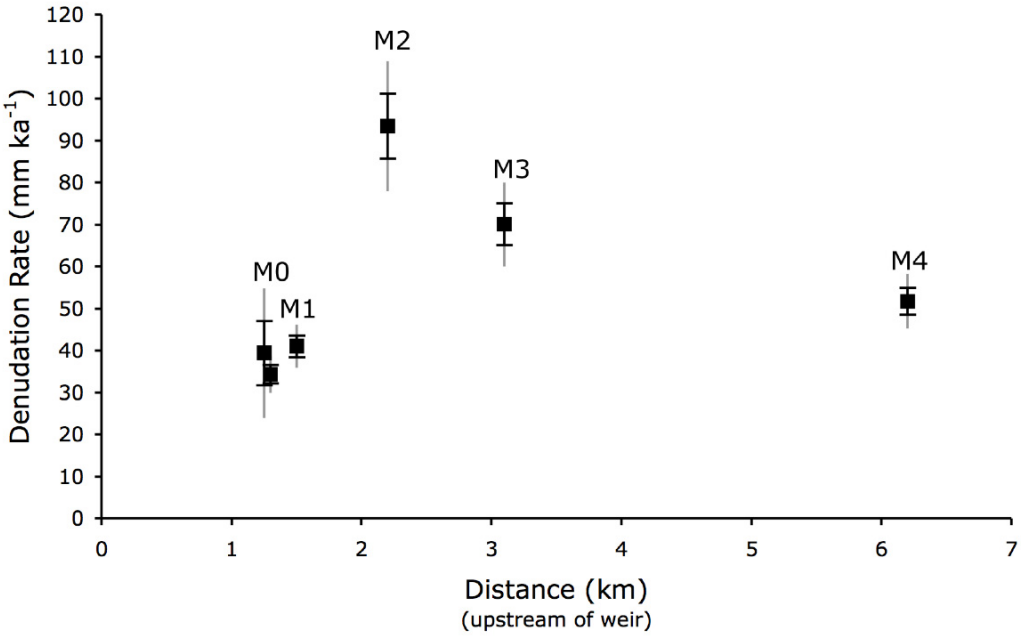

Figure 5.18 The ^{10}Be derived denudation rates determined from alluvial sediment sampled over the length of the West Okement River.

5.7 Discussion

The measurement of ^{10}Be concentration in alluvial sediments collected across Dartmoor provides a quantitative measure of denudation rates in the landscape. However, a meaningful geomorphological interpretation of this data requires careful consideration of the timescale of nuclide accumulation and the validity of assumptions inherent in the approach. Following this assessment, it is possible to consider the implications these denudation rates have for the variability of denudation across the landscape and over time, as well as comparing them to similar studies in other parts of the world.

5.7.1 Validity of Catchment-Averaged Denudation Rates

The derivation of catchment-averaged denudation rates from ^{10}Be concentrations in alluvial sediments is based upon a set of assumptions (see Section 2.4.3). In any natural setting, the complexities of a sedimentary system will inevitably lead to a violation of at least some of these assumptions. This section is an evaluation of the studied catchments in Dartmoor, and the implications for interpreting landscape denudation rates. It addresses each of the assumptions listed by Bierman & Steig (1996).

(1) The denudation rate is constant, but not necessarily uniform; and (2) the catchment is in isotopic steady state

If the denudation rate of a catchment is to be accurately reflected in the cosmogenic nuclide signature of alluvial sediment, it must be constant for long enough to allow the isotopic reservoir of the catchment to reach equilibrium. To effectively erase any prior denudation rate signal some 2-3 m of material should be removed from across the land surface (Bierman & Steig, 1996). Therefore, the time required for the isotopic reservoir to adjust will be determined by the denudation rate, at relatively high denudation rates this may take only a few thousand years (i.e. more than 50 or 100 mm ka^{-1}), while at lower rates this can take 100 ka or longer. Although variability in past denudation rates is difficult to determine (after all, this is a key reason for using the cosmogenic nuclide approach), in most landscapes it is unlikely that they will remain constant for a sufficient length of time. This means that the assumption of

constant denudation rate is violated, and the catchment will not be in an isotopic steady state. The isotopic signal will not reflect the present denudation rate, nor will it represent any specific past denudation regime. Instead, it will be a function of varying denudation over the time span the last 2-3 m of material was removed from the surface of the catchment (this will vary across the landscape if denudation is not spatially uniform). In many situations, this long-term averaging of the denudation rate signal is actually desirable (e.g. recent anthropogenic disturbance), although careful consideration of the results is required.

In Dartmoor, most samples of alluvial sediment returned denudation rates of 20-40 mm ka^{-1}, with an averaging time scale 15-30 ka (this is equivalent to removal of ~65 cm of material from the surface). An exception is the low ^{10}Be concentration in samples from the West Okement River with averaging time scales of 5-6 ka; however, the interpretation of what landscape elements these represent is complicated (see below). In general, the indication is that the denudation rate signal is a function of not only the Holocene, but a time span that extends into the Devensian cold stage. This is not unexpected in the context of the Dartmoor landscape, as many of its most distinctive landforms are attributed a periglacial origin (e.g. clitter, solifluction deposits, hummocky ground). It follows that if these landforms developed under periglacial conditions, the material of which they are comprised has been exposed to cosmic radiation since at least this time. The widespread preservation of periglacial landforms also confirms that Holocene denudation has not been sufficient to remove the more than 2-3 m required to eradicate the preceding denudation signal.

In summary, while the assumptions of constant denudation rates and an isotopic steady state for catchments in Dartmoor are almost certainly violated, the cosmogenic nuclide signal provides a denudation rate averaged over the Holocene and Devensian intervals. It is not possible to differentiate the relative contribution of time intervals from ^{10}Be data alone. Nor is it possible to determine the exact time span over which the cosmogenic nuclide inventory accumulated.

(3) Sampled sediment is spatially and temporally representative of all sediment leaving the catchment

It is assumed that alluvial sediment sampled is representative of all sediment leaving the catchment, with any given part of the basin contributing material in proportion to its long-term denudation rate. The mixing of sediment occurs throughout transport in colluvial and alluvial systems (see section 5.3.4); however, to be representative, material must be transferred into the alluvial system from throughout the catchment. When alluvial sediment is not well-mixed, the ^{10}Be concentration will be biased towards the source area of the sediment. If denudation is spatially non-uniform in the catchment, this may result in the calculation of an inaccurate catchment-averaged denudation rate. The magnitude of this error will depend on the heterogeneity of denudation within the catchment, and the degree to which the mixing of sediment is out of proportion with long-term supply.

There are potential problems with inadequately mixed sediment throughout Dartmoor. This is mostly due to the lack of sand-sized grains within the alluvial system, which is dominated by at least gravel-sized material and much of the bed is comprised of boulders. The percentage of sand-sized or finer material in slope deposits on Dartmoor is already relatively low (<10-20% in head deposits according to Gerrard, 1989); however, it appears that in upland rivers this is reduced even further by preferential transport downstream. The low volume of sand-sized sediment within the alluvial system increases the chance of an influx of material from a localised source (e.g. bank collapse) biasing the sample. The results from the West Okement River indicate that incomplete mixing of the sediment is problematic in this relatively small upland river system. The concentration of cosmogenic nuclides fluctuates along the length of the river, without additions from any significant tributaries (which might contribute a different concentration) or obvious geomorphological explanation (the concentrations increase through the steepest section of the valley). In this case, it is likely that sampled sediment is not well-mixed and material from localised sources within the valley are biasing the sample. Although these results cast doubt on the validity of 'catchment-averaging' in this river, they are still representative of some element of the landscape, albeit an

undetermined one (perhaps some part of the hillslope, which may be averaged over the entire upslope section).

This demonstration of inadequate sediment mixing in a small to mid-sized Dartmoor catchment (13.2 km^2) casts some doubt on the reliability of other results, especially as these were determined by analysis of a single sample. However, in many of the other river systems sampled there was a greater abundance of sand-sized material within the channel, increasing the likelihood of mixing. This is especially true of the much larger West Dart River (77.2 km^2) and East Dart River (42.5 km^2) channels, but also of mid-sized catchments like the River Walkham (27.6 km^2) and the West Dart River at Two Bridges (17.4 km^2), where samples were taken from reasonably large sand bars in the channel. The results from most samples of alluvial sediment across Dartmoor indicated catchment-averaged denudation rates of between 20 and 35 mm ka^{-1}. This relative consistency of results across Dartmoor suggests that sediment concentraions are representative of a wider landscape denudation rate. It would be desirable to analyse more than one sample from each study reach to assess variability in ^{10}Be concentrations; however, this was unfortunately not within the resources of this study.

In summary, there is evidence for an inadequate mixing of sediment leading to a violation of the representative sediment assumptions for at least some Dartmoor rivers. The results obtained from larger rivers are likely to be more reliable due to a greater volume of sediment in the alluvial system. However, this mixing of sediment homogenises the denudation rate signal across a large part of the landscape, and many of the interesting geomorphological questions may lie in elucidating differences (or similarities) within the landscape (e.g. upland plateau vs. Dart valley). Although it is difficult to assess, there is some consistency in the results for large parts of the Dartmoor landscape.

(4) Mass loss in the catchment is occurring primarily by incremental surface lowering

This assumption prohibits episodic erosion within the catchment as it delivers sediment to the alluvial system out of proportion to the long-term erosion rate in the

source area. In larger catchments there is potential for such episodic erosion to average out; however, in smaller catchments episodic erosion can result in either an over- or under-representation of an area in the alluvial sediment. In Dartmoor, the most weathering occurs beneath a mantle of regolith and denudational processes are probably incremental. During periglacial conditions this is dominated by solifluction and the effective mass wasting of slopes, while in the Holocene more gradual processes are prevalent (e.g. soil creep). Although there may be incidence of episodic events like landslides in Dartmoor (e.g. Slipper Stones in the West Okement valley), these do not appear to be a dominant process in the Dartmoor landscape. Perhaps more problematic is the erosion and delivery of sediment to the alluvial system caused by human modification of the landscape. In particular, tin mining has lead to the localised injection of sediment into river systems (i.e. hydraulic mining by stream diversion was a common technique). In many locations tin mining only reworked shallow depths of material (a few metres), and if the regolith was well-mixed to depth then ^{10}Be concentrations would still be an average for the local slope (although this would be over-represented in the alluvial sediment). However, if erosion penetrated beneath the mixed regolith layer, then this would introduce previously unexposed sediment and lead to an over-estimation of long-term denudation rates.

In summary, most denudation in Dartmoor is probably consistent with the requirement for incremental processes. However, there is potential for episodic erosion to occur through events like landslides, or more recent anthropogenic disturbance, and the importance of these is difficult to assess.

(5) Quartz is uniformly distributed through the catchment

The uniform distribution of quartz is required so that no area is over- or under-represented in the quartz content of alluvial sediment. The study catchments are almost entirely located on the granite bedrock of Dartmoor. This is a coarse-grained megacrystic biotite granite, with a uniform quartz content of ~34% (Exley and Stone, 1982). In those catchments that include areas with lithologies other than granite, the grain-size of quartz is these rocks is too fine to be included in sample

preparation and these areas can be excluded (East Okement – siltstone; River Walkham – metadolerite).

The preferential dissolution of non-quartz mineral can lead to a problematic quartz enrichment, in which the residence of quartz in the sedimentary system is longer than that of average material. As discussed in section 3.3.2.3, Williams *et al.* (1986) provided some evidence for the preferential weathering of non-quartz minerals in the regolith of Dartmoor; however, the overall percentage of quartz in the regolith remained constant (no enrichment). There is limited data available to fully assess potential dissolution effects.

Finally, there is a notable enrichment of quartz within the bedload of rivers. This is probably due to preferential transport of smaller grain-sizes (quartz tends to be larger) within the alluvial system. However, as storage time in the alluvial system is expected to be minimal, this enrichment of quartz is inconsequential.

5.7.2 Interpreting Denudation of the Dartmoor Landscape

The ^{10}Be concentrations measured in alluvial sediments provide a spatially and temporally averaged denudation rate signal. While the interpretation of these results is complicated by variability in the landscape, the results provide long-term measures of the rate of denudational processes in the Dartmoor landscape not available by any other method.

5.7.2.1 Variability of Denudation Rates

The sampling sites at which alluvial sediment was collected are dispersed across Dartmoor, with the intention that the catchments represent a range of spatial scales and topography. Before comparing the denudation rates derived from ^{10}Be concentrations, it is important to consider the degree of uncertainty in the results. The internal uncertainty is reported for each sample of alluvial sediment (Table 5.3; 5.4; 5.5); however, this only accounts for analytical and laboratory errors associated with target preparation and AMS measurement. The larger external uncertainties of 10-12% is an estimation that also includes error associated with production scaling

models, and is relevant when comparing results to cosmogenic nuclide data from other regions. However, there is also error arising from the violation of assumptions in the denudation rate model (Section 5.7.1), for which there is no calculated value of uncertainty. In the results from this study, this uncertainty is likely to arise from two main violations:

(1) There is an indication that alluvial sediments may not be well-mixed in at least some rivers. This is demonstrated by the results from the West Okement River, in which denudation rates (34-94 mm ka^{-1}) vary by more than the differences between all other sampled catchments (21-37 mm ka^{-1}). Although the consistency of results from the other catchments suggests that they may be better mixed, it is not possible to evaluate this as only one sample was analysed at each site.

(2) In Dartmoor, there have probably been significant changes in denudation rate over time. The timescale over which a cosmogenic nuclide signal is averaged is determined by the denudation rate. This means that, when comparing different measured denudation rates, the length of time over which they have been averaged will also differ (i.e. a lower denudation rate will be averaged over a greater length of time). This is problematic, as samples will have been exposed to a different set of conditions (e.g. length of periglacial conditions) depending on denudation rate. It also complicates the comparison of catchments based on morphological characteristics.

In summary, there is insufficient data available in this study to fully assess the uncertainty associated with denudation rate measurements. In the worst case, it may be that variability within sediment bodies is greater than differences between catchments. In general, caution should be taken when comparing results where uncertainty is undefined.

5.7.2.2 Comparison of Catchment Denudation Rates

The ^{10}Be derived denudation rates are plotted against various catchment characteristics in Figure 5.19. The most variation in denudation rates is observed in the results from the West Okement River (red), although this is probably due to inadequate mixing of alluvial sediments. If these are excluded, there is still no clear

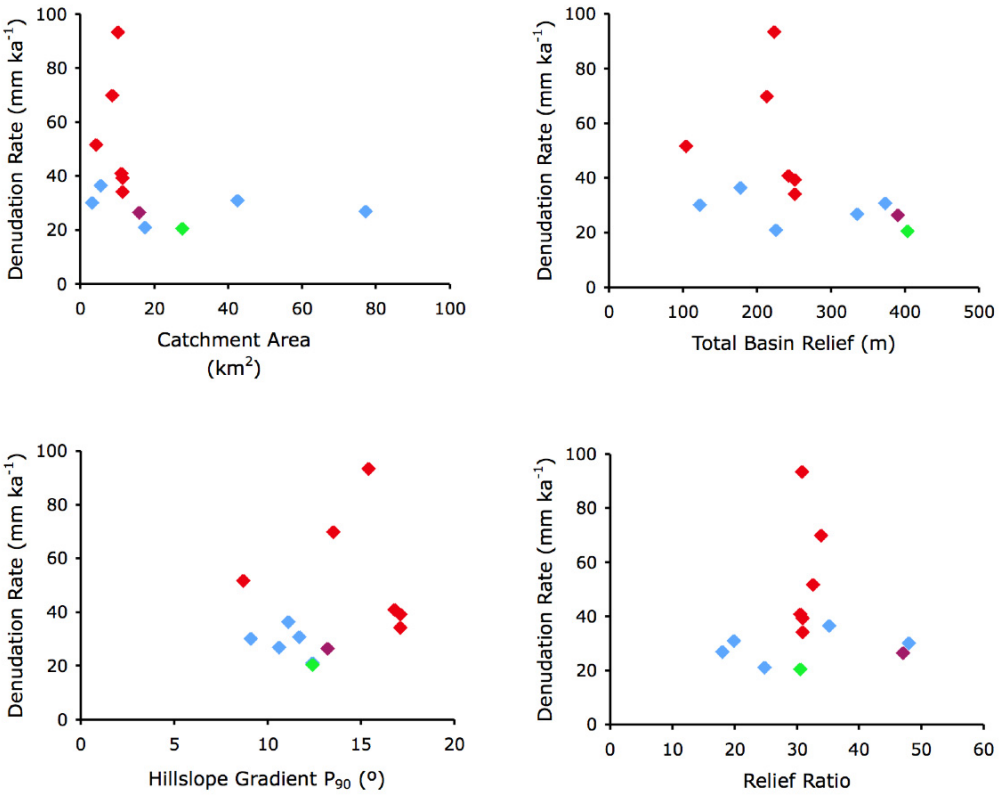

Figure 5.19 ^{10}Be derived denudation rates for Dartmoor rivers plotted against catchment characteristics of area, total basin relief, hillslope gradient and relief ratio. The rivers are the River Dart (blue), West Okement (red), East Okement (purple), and River Walkham (green).

influence of catchment area, total basin relief, hillslope gradient, or relief ratio on catchment-averaged denudation rates. This suggests a consistency of denudation across the landscape, with average rates between 20 and 40 mm ka^{-1}. Although it would be interesting to further investigate smaller sub-catchments with specific geomorphological characteristics, as the West Okement River valley samples demonstrate, there is potential for insufficient sediment mixing to influence results in small upland catchments.

The majority of alluvial sediment samples indicate a spatially averaged denudation rate of 20-40 mm ka^{-1}. Interestingly, these are slightly lower than measured regolith denudation rates of 38-62 mm ka^{-1}, but comparable to the erosion rates of 14-45 mm ka^{-1} measured on tor surfaces (Chapter 3). This suggests that denudation is evenly distributed across the landscape, and confirms the idea that tors are not relict landforms out of equilibrium with the wider landscape.

5.7.2.3 Changes In Denudation Rate Over Time

The varying intensity of denudation with climatic conditions has been recognised in most models of landscape evolution in Dartmoor since the 1950s (see review of Campbell *et al.*, 1998). However, there have been few attempts to quantify rates of landscape denudation, largely due to a lack of applicable methods. Williams *et al.* (1986) determined a chemical weathering rate of 5.0 mm ka^{-1} and estimated total denudation at 6.5 mm ka^{-1} for the Narrator basin in western Dartmoor. They considered this rate to be a "a close approximation to the geologically normal denudation rate for Dartmoor" (p571); however, this is a contemporary measure of denudation and the extrapolation of this 1-year dataset is problematic. If this denudation rate is considered representative of the Holocene, this would suggest 6.5 cm of denudation over the last 10 ka, a fairly minimal modification of the land surface. This is consistent with the widespread preservation of periglacial landforms throughout the landscape; for example the earth hummocks and stone stripes evident in Figure 5.20 and described by Gerrard (1988), and the blockslopes discussed in Chapter 4. Gerrard (1993) suggests a general stabilisation of the landscape during the Holocene, with the development of widespread soils and peat covers (Table 5.1). However, there are still significant changes in the landscape during this interval, and

this might be problematic for the extrapolation of contemporary solute load data (i.e. 6.5 mm ka^{-1} of Williams *et al.*, 1986).

This research aims to assess the relative intensity of denudation under Holocene and periglacial conditions. The measurement of ^{10}Be in alluvial sediment allows for the calculation of spatially averaged denudation rates (both chemical and mechanical) averaged over a time span that extends over the entire Holocene and into the Devensian cold stages (Section 5.7.1). These rates are mostly between 20-40 mm ka^{-1} (although up to 94 mm ka^{-1}), and are higher than those considered typical of the Holocene; for example the 6.5 mm ka^{-1} measured by Williams *et al.* (1986). This suggests that the component of the ^{10}Be denudation signal produced during periglacial conditions was under higher denudation rates. It is not possible to calculate precisely what periglacial denudation rates are from the measured ^{10}Be concentrations, as the variation in denudation over their averaging time is unconstrained. However, given the likelihood that Holocene denudation rates are lower than those derived from ^{10}Be concentrations, it is reasonable to expect they underestimate periglacial denudation rates (i.e. the period of adjustment to Holocene rates has seen an increase in ^{10}Be, thereby lowering the denudation rate).

5.7.2.4 The Denudation of Dartmoor in a Global Context

Since the methods inception in the mid-1990s, cosmogenic nuclides have been used to measure denudation rates in an increasingly diverse range of landscapes and climate regimes. Figure 5.21 plots the results from Dartmoor alongside those obtained in other catchment studies on granite lithologies; with precipitation ranging from 30 to 5000 mm a^{-1} and a temperature range of -0.4 to 25°C (von Blanckenburg *et al.*, 2004; von Blanckenburg, 2005). The Dartmoor rates are consistent in both magnitude and variability with those studies in Europe (e.g. Loire in Schaller *et al.*, 2001; 2002) and most sites in North America. Interestingly, the long-term denudation rates determined by cosmogenic nuclides show no apparent correlation with either precipitation or temperature (von Blanckenburg, 2005). Those that do deviate significantly in Figure 5.20 are at the extremes of climate (i.e. in arid Namibia and tropical Sri Lanka) or hillslope gradient (i.e. San Bernadino Mountains in which average catchment gradients were up to 38°; Binnie *et al.*, 2007).

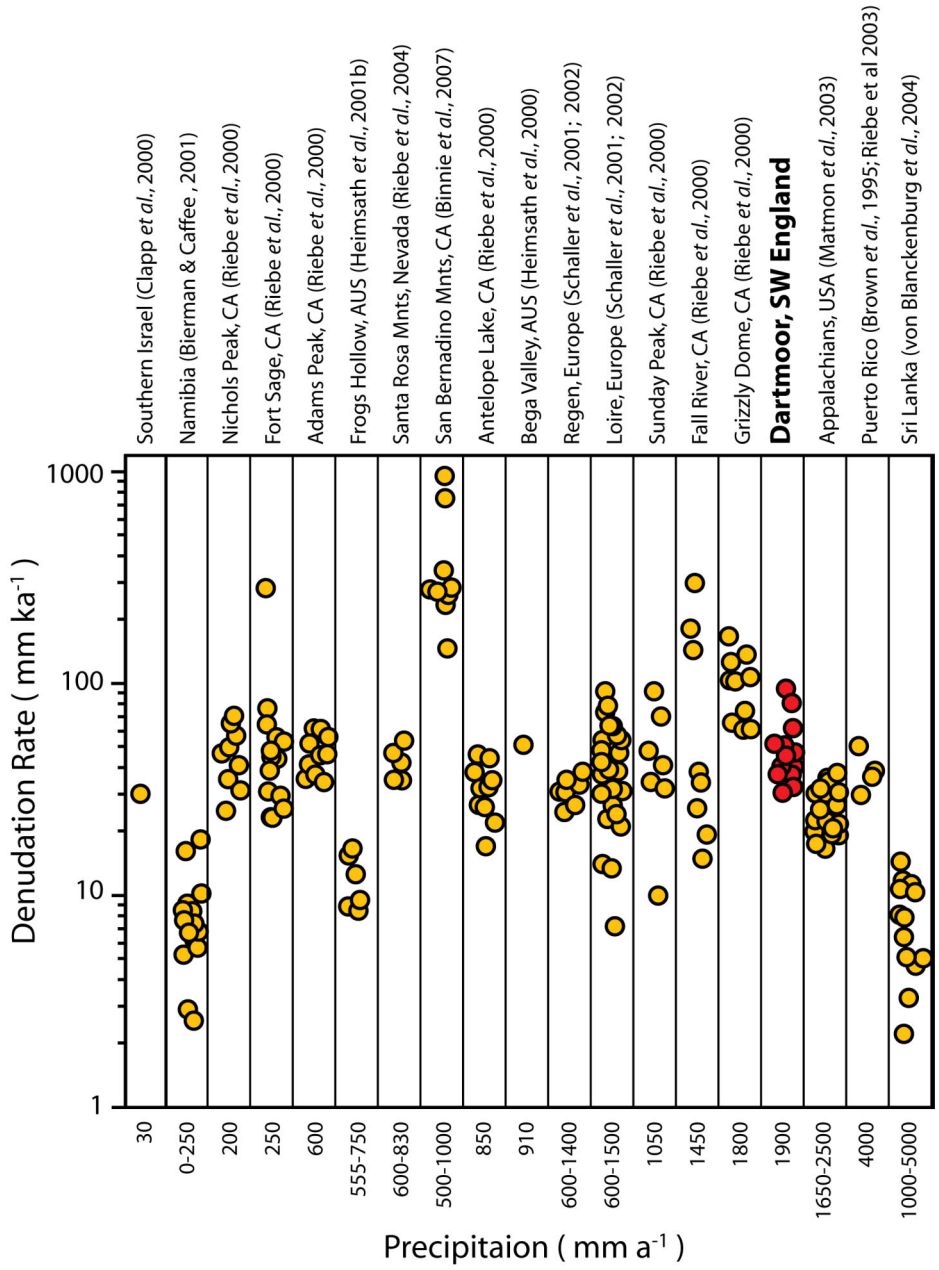

Figure 5.21 Cosmogenic nuclide derived denudation rates in catchments with crystalline bedrock. Adapted from von Blanckenburg *et al*. (2004) with additional data from San Bernardino Mountains (Binnie *et al*. 2007) and the present study in Dartmoor (red).

5.8 Conclusion

This study of ^{10}Be concentrations in alluvial sediments has determined spatially averaged denudation rates for much of the Dartmoor landscape at 20-40 mm ka^{-1}, although a few samples returned rates of up to 94 mm ka^{-1}.There was no evidence for variations related to difference in catchment size (from 3.1 to 77.2 km^2) and varying topography. These ^{10}Be derived denudation rates are averaged over an interval of time that spans the Holocene and extends into the Devensian cold stages. As such, they are the first quantitative measurement of long-term denudation of the Dartmoor landscape. They indicate that long-term rates are significantly higher than contemporary denudation rates, probably due to increased denudation of the landscape under intense periglacial conditions. Although this study has highlighted some of the limitations of the approach, it also demonstrates the potential of cosmogenic nuclides to provide some estimation of denudation rates, even in complex environments.

6: Implications for Landscape Evolution in Dartmoor

6.1 Introduction

As the only upland region of Britain to remain beyond the limit of Quaternary glaciation, Dartmoor has proved an ideal landscape for assessing long-term landform evolution since the late Tertiary. The significance of periglacial processes in modifying the landscape is one of the few agreed aspects of research over the last 50 years, although assessments of its intensity vary widely. Far less agreement has been reached regarding the origins of *in situ* decomposed granite (or growan), and there are widely divergent 'classic' models of landscape evolution, which are far too simple to explain tor and slope morphology (Campbell *et al.*, 1998). The lack of age constraint on the development of landforms has been a critical limitation to evaluating various models of landscape evolution.

In this study, cosmogenic nuclides have provided constraints on the development of tor and blockslope landforms; as well as a spatially-averaged estimate of denudation rates in the landscape. Although these results only directly measure mass removal of the last few metres from the surface, by doing so they provide a first indication of the intensity of periglacial denudation of the landscape and the timescale over which classic periglacial landforms developed. Detailed discussion is provided in each of the relevant chapters; here the implications are considered for aspects of the landscape not directly investigated.

6.2 The Weathering of Granite

The process by which *in situ* altered granite (or growan) is formed is one of the most contentious issues in Dartmoor research. There are three potential processes cited that might lead to the development of *in situ* altered granite: (i) chemical weathering; (ii) hydrothermal alteration; and (iii) physical weathering by frost action. Despite a large body of research trying to decipher the relative importance of these processes, there remains little agreement on the principal means by which alteration of the granite occurs. Campbell *et al.* (1998) conclude that the altered granite of Dartmoor probably reflects all three processes, sometimes in combination, over a protracted

timescale. Whatever the relative importance of each process, the nature and distribution of altered granite has been fundamental to interpretations of landform development; and are considered to have strongly influenced the formation of key landforms during the Quaternary (Gerrard, 1983).

As discussed in Chapter 3, the widespread presence of a weathered granite layer was fundamental to Linton's (1955) model of two-stage tor formation. Subsequent research has scaled back the distribution of deeply weathered (altered) material to a presence mostly near valleys, although it is still assigned a key role in tor formation (e.g. Green & Eden, 1971; Doornkamp, 1974). Gerrard (1982; 1988) developed composite models for the main features in the landscape (Figure 3.12), and recognised that pre-existing subaerial weathering profiles were unnecessary for the formation of tors in at least some locations (e.g. valley-side), although considered it still important for large summit tors.

The measurement of cosmogenic nuclides in this study has shown that the denudation rate of summit areas has been relatively high over a time span of the Devensian-Holocene. Even tor surfaces, likely the most resistant part of the landscape, have been shown to erode at 14-45 mm ka^{-1}; while measurements of regolith denudation at the summit of High Willhays varies between 43-62 mm ka^{-1} (Chapter 3). The interpretation of this data suggests that a two-stage development of these landforms is unlikely, and that there is active weathering of bedrock and generation of regolith at the summit over the Devensian-Holocene interval. Interestingly, the spatially-averaged rates of denudation (through sediment mixing in slopes and rivers) derived from alluvial sediments suggest a similar denudation rate of 20-40 mm ka^{-1}. As these cosmogenic nuclide derived rates are averaged over a time span that includes both interglacial (Holocene) and glacial maximum (Devensian) climate conditions, it might be reasoned that they are an approximation of those throughout the Quaternary. Hence, denudation rates across the landscape of 15-60 m Ma^{-1}, and substantial post-Tertiary modification of the landscape.

To sustain denudation rates of this magnitude across the landscape, there must be ongoing mechanisms for the weathering of granite. There is little evidence of remnant deep weathering profiles in the vicinity of tors (Palmer & Neilson, 1962), yet grussified material is observed near or on these eroding landforms (Section 3.7.1) and within the regolith (Section 3.4.2). This indicates that weathering of granite has continued throughout the Quaternary, at least during interglacial and interstadial intervals. Williams *et al.* (1986) measured present-day chemical denudation at 5 mm ka^{-1}, demonstrating that chemical weathering was an active and ongoing process in the landscape. It is also now recognised that chemical weathering can be an effective mechanism under many, if not most, periglacial environments, and consequently, is a significant contributor to the overall process of weathering (Hall *et al.*, 2002).

This suggests a reappraisal of the role that deep weathering (alteration) of granite has in influencing landscape development. In some locations it is undoubtedly important in the generation of specific landforms (e.g. Two Bridges Quarry; Figure 3.7); although this is unlikely to be a widespread mode of formation (see Section 3.7.3). The alteration of granite can also occur to great depths (e.g. Burrator Reservoir, Figure 3.9), and the presence of this relatively incoherent material will obviously influence the morphology of the landscape. It seems likely that, although active processes in the Quaternary are largely responsible for individual landforms and meso-scale landscape features, the large-scale 'dome and basin' topography of Dartmoor is related to the distribution of deeply altered granite, present since the Tertiary (or earlier) (Campbell *et al.*, 1998). The joint structures in the granite are probably crucial in focussing weathering, and guiding the development of drainage networks and basin topography (Waters, 1964; Gerrard, 1974).

6.3 Periglacial Hillslope and Landform Development

The typical geomorpholgical features of the Dartmoor landscape are shown in Figure 6.1; and feature: (i) summit with thin regolith cover and tor outcrops; (ii) upper hillslopes with at most a few metres of regolith cover and often covered in 'clitter' (blocks); (iii) lower slopes that are zones of accumulation of slope material featuring

well-developed 'head' deposits (solifluction); and (iv) valley floor depositional zone which may be underlain by a considerable depth of altered granite.

The stripping of regolith from summit areas and transportation and deposition of this material downslope by periglacial processes is a key feature of most landscape evolution models for Dartmoor. In particular, there was widespread recognition of a stripping of Tertiary weathering profiles during the periglacial episodes of the Pleistocene (e.g. Linton, 1955; Te Punga, 1957; Palmer & Neilson, 1962; Waters, 1964). Waters (1964) even attempted to relate the fine-grained lower 'head' deposit to these first periglacial episodes, although this was later shown to be an over-simplification of a complex slope deposit sequence (Green & Eden, 1973; Gerrard, 1989). Although there is little doubt that periglacial processes have removed a significant mass from summit and upper slope areas, little is known about the age of the slope deposits found across Dartmoor (Campbell *et al.*, 1998). It is likely that they have been developed over multiple periglacial episodes, with each reworking earlier landforms that inter-periglacial processes are not able to remove. It is unclear whether the landforms observed today are mostly Devensian in origin, or whether they formed over much longer timescales.

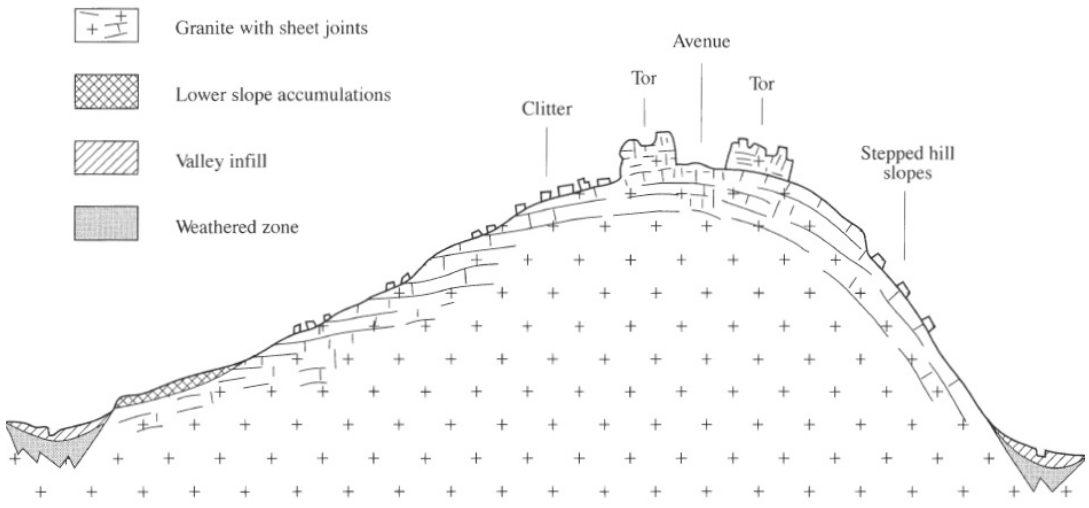

Figure 6.1 Schematic composite representing the main geomorphological features of Dartmoor

Source: Campbell *et al.* (1998); after Gerrard (1983)

In this study, the interpretation of cosmogenic nuclide samples from a blockslope indicated that blocks have only been exposed to cosmic radiation in the near-surface since the mid-Devensian (minimum exposure age of 25 to 45 ka), and, perhaps, a downslope transport rate of 8 m ka^{-1} (Chapter 4). As the blockslope was in close proximity to Yes Tor, the results support the notion that the association between tors and 'clitter' (amongst other periglacial features) is evidence of the features forming in a comparatively late stage of the Pleistocene (Waters, 1964; Gerrard, 1988). It is important to recognise that the Yes Tor blockslope is located on the upper hillslope, and therefore, not necessarily representative of periglacial landforms across the landscape. However, when these results are taken in conjunction Devensian-Holocene averaged denudation rates of 15-60 mm ka^{-1} on both summit and the wider landscape (see Section 6.2), it suggests that many of the periglacial landforms observed in Dartmoor were formed during the Devensian cold stage. So while the impact of periglaciation on the landscape may be cumulative over many glacial-interglacial climate cycles, most of the landforms were probably formed in the last Devensian (with the exception of some tors).

The intensity of denudation under periglacial conditions is of critical importance to models of landscape evolution. The results from cosmogenic nuclide analysis suggest that denudation processes have been active in the summit areas and the wider landscape; as discussed in the preceding Section 6.2, a Devensian-Holocene average of 15-60 mm ka^{-1} (or m Ma^{-1}) is indicated, and this may reflect rates over the Quaternary. The denudation rates measured on tor surfaces indicate that Linton's (1955) model of the stripping of relatively incoherent 'growan' to leave behind the base of the weathering profile (including tors) is not feasible (see discussion in Chapter 3). Similarly, Waters (1964) suggestion that periglacial mass wasting was only responsible for minor modification of the landscape (i.e. 'exposed summit tors, moulded slopes, and plastered valley floors with rubble-drift) underestimates the efficacy of periglacial processes. Instead, the cosmogenic nuclide analyses indicate that there has been significant long-term denudation of the summit areas, subsequent to the removal of any pre-Quaternary weathering profiles. It is then a question of the relative denudation rates at summits compared to the rest of the landscape. It may be

that the exposed summits are the focus of intensive mass wasting, with the eroded material deposited downslope and a reduction in topography (i.e. as implied by Te Punga, 1957; Palmer & Neilson, 1962). Alternatively, interfluve and plateau surfaces may have been affected by periglacial processes, but to a lesser extent than more sensitive valley-side slopes (Gerrard, 1991). Interestingly, spatially-averaged denudation rates were found to be comparable to those measured from summit area tor surfaces. However, while this may indicate a somewhat even denuding of the landscape, the dataset is not sufficient (sampling biased towards summits) to fully evaluate long-term hillslope evolution.

6.4 Evaluating Potential Glaciation of Dartmoor

It has been the generally accepted view that the uplands of Dartmoor were beyond the limits of Quaternary glaciation, with no definitive geomorphological evidence for glacial landforms on Dartmoor (Gerrard, 1988; Campbell *et al.*, 1998). However, there continues to be suggestions that glaciers and perhaps even a small ice cap were present on nearby Exmoor and Dartmoor (Harrison *et al.*, 2001; Harrison, 2001). The uplands of Dartmoor are marginal for the formation of ice, with an estimated snow line 30 m above the highest summits (Gerrard, 1988); however, these estimates are based on 1950s data and it is quite possible that these will be re-evaluated in the near future as new models become available. Although the geomorphological evidence for ice on Dartmoor remains equivocal, the prospect of glaciation should not be simply dismissed.

Investigating the potential for glaciation on Dartmoor with cosmogenic nuclides is an enticing prospect; however, this research was not specifically designed to address this issue. The use of $^{26}Al/^{10}Be$ ratios to assess burial by ice is an interesting approach (e.g. Bierman *et al.*, 1999; Fabel *et al.*, 2002); however, given the relatively low ^{10}Be exposure ages (or high erosion rate) and the unlikely scenario of more than occasional burial by ice in this ice-marginal location, it is probably not a useful technique in Dartmoor. This leaves an attempt to date supposed glacial features; but given the equivocal nature of these landforms and the variability of exposure as demonstrated by this study, this seems unlikely to be successful. It would also be

difficult to discern glacial from periglacial origin based on age of formation, since these would be coeval.

Although the application of cosmogenic nuclides to discerning glaciation on Dartmoor may be problematic, given the prospect of glaciers in the area it is necessary to briefly evaluate their potential effect on this study. The burial of any landform studied (or part of a catchment) under ice would shield it from incoming cosmic radiation, leading to an underestimation of surface age (or overestimation of erosion rate). So what is the likelihood of glaciation in the study sites?

There is potential for small cirque or rock glaciers to form in the uplands; however, most tors studied are not in a landscape position to be affected by these, with the possible exception of Dinger Tor (3.6.3). The appearance of rock glacier deposits and blockslopes can be similar (Harrison *et al.*, 2001), so this is a possible origin for some blocky landforms, although it is unlikely to be the case for the studied blockslope (Chapter 4). The formation of a small ice cap on Dartmoor is most likely to occur on the central upland plateau. Although High Willhays – Yes Tor summits are the highest elevations in Dartmoor, they are on the fringe of the upland region and are separated from the main plateau surface by the East and West Okement River valleys. The other tors sampled are also away from this central plateau.

An effect from glaciation is more likely to be recorded in the alluvial sediment samples, as they aggregate material from large sections of Dartmoor. In the event of a small ice cap, the headwaters of many of the catchments are in the northern uplands, although the West Okement and East Dart Rivers are the most likely to be effected (Figure 5.1). Smaller glaciers would also influence sediment yielded from the catchments, interestingly rock (or debris covered) glaciers might generate bimodal sediment exposure (buried and surface).

6.5 Conclusion

The constraints on landscape denudation provided by cosmogenic nuclides provide a useful insight into the evolution of the Dartmoor landscape. Previously, there was little available age constraint with which to decipher phases of periglacial denudation, and this left room for widely divergent interpretations of landforms and the landscape. Although this study only provides a limited dataset from a few sites and landforms, these have significant implications for models of landscape evolution. The relatively high denudation rates measured indicate that periglacial processes are effective at modifying the landscape, and that most small to meso-scale landforms of Dartmoor were formed in the later stages of the Pleistocene.

7: Conclusion

In this study, cosmogenic nuclide analysis has been used to investigate landforms in the granitic upland landscape of Dartmoor, southwest England. This region has long been the subject of geomorphological investigation, with a significant debate arising over appropriate models of long-term landform evolution (i.e. two-stage vs. single-phase tor formation). However, given the previous lack of quantitative techniques capable of constraining denudation and specific process rates, there remains much uncertainty in the interpretation of the regions classic landforms. By measuring ^{10}Be concentrations, this study has provided quantitative estimates of denudation for key landforms and averaged over the landscape. The results provide insight in two key areas: (i) the evolution of hill summits, including the development of tors and blockslopes; and (ii) the catchment-averaged denudation rates obtained from alluvial sediments.

Evolution of Summits:

The geomorphology of hill summit areas is key to understanding the evolution of the Dartmoor landscape. Many of these summits feature distinctive tor outcrops, and understanding how these form has significant implications for the entire landscape (i.e. the efficacy of periglacial weathering during the Quaternary). In this study, ^{10}Be concentrations were measured in samples taken from the surface of tors, regolith-mantled slopes, and a blockslope. These results allowed for the interpretation of denudation rates at the summits, and constraints on the transfer of block material by slope processes away from the summit. On the basis of these results, it has been possible to assess models of tor formation.

Erosion of Tors

The ^{10}Be concentrations measured in eighteen samples from tor surfaces provides a quantitative estimate of tor surface erosion rates. Although there is evidence for granular disintegration of tor surfaces (i.e. weathering pits and grussification), it is apparent that the dominant mechanism by which material is removed from tor surfaces is by the episodic spalling of blocks (with horizontal joint spacing and

inclination the primary control). These observations are supported by the cosmogenic nuclide data, which indicate tor surface erosion rates of 14-32 mm ka^{-1} (excluding Dinger Tor at 45 mm ka^{-1}). These rates are much higher than those reported elsewhere for erosion of crystalline bedrock surfaces (see section 3.7.1.1), and the variability in measured ^{10}Be concentrations also indicates episodic removal of material from tor surfaces.

The tors included in this study have relatively closely spaced horizontal joints, which would favour the more frequent spallation of material from the surface (although in thinner sheets). This generates a smaller range of ^{10}Be concentrations than would occur in tors with wider joint spacing and less frequent block removal (i.e. stacked superstructure tors), even if long-term average erosion rates for the landform are equivalent (a representative sampling strategy would be essential to the study of these tors).

The tor surface erosion rates of 14-32 mm ka^{-1} are higher than most derived using cosmogenic nuclides on granite surfaces elsewhere (section 3.7.1.3), although they are comparable to some of those reported by Phillips *et al.* (2006) for the Cairngorms, Scotland. An explanation for higher surface erosion rates may be that Dartmoor was exposed to intense periglacial conditions while remaining a comparatively wet climate. The tors included in this study are also unlikely to have ever been subjected to ice burial during Quaternary cold stages.

Regolith & Blockslopes

The summits are mantled in regolith that consists of unconsolidated material derived from weathering of granite, intact granite blocks detached from the underlying bedrock or nearby tor outcrops, and organic matter. The denudation of a regolith-mantled surface results from the generation of unconsolidated material at the weathering front and subsequent removal of material through downslope transportation. The measurement of ^{10}Be concentrations in samples of regolith provide an approximation of the surface denudation rate. In this study, regolith at the High Willhays summit had denudation rates of 38-62 mm ka^{-1}, higher rates than

those derived for tor outcrop surfaces. The results showed that there is vertical mixing of regolith profiles, although this is complex and incomplete (i.e. variability of concentrations). It is considered likely that weathering and mechanical disruption of granite has continued throughout the Quaternary, and may actually be enhanced by periglacial conditions.

The transportation of material downslope is key component of summit development, with slope processes likely to be effective under periglacial conditions (e.g. solifluction). In this study, ^{10}Be concentrations were used to interpret the development of a blockslope landform, a common feature on Dartmoor slopes, and closely associated with tor formation and the efficacy of periglacial processes. The results indicated that blocks near the Yes Tor summit had been exposed for a minimum of 25 ka (upslope) and 45 ka (downslope), with a likely near-surface exposure not exceeding the mid-Devensian. The results also indicated that blocks were being transported from a source area upslope, with an approximation of downslope transportation rate at 8 m ka^{-1}. This demonstrates the efficacy of processes transferring blocks away from the summit, probably during periglacial conditions.

Formation of Tors

The interpretation of cosmogenic nuclide data from tor surfaces, regolith, and blockslopes provides useful constraints on models of tor development. The ^{10}Be concentrations measured on tor surfaces varied significantly, even between samples from the same outcrop surface. There was also no evidence of a relationship between ^{10}Be concentration and tor height (above the surrounding surface). This indicates that cosmogenic nuclide data from the tor surfaces should be interpreted as an erosion signal (as opposed to an exposure age). There has been sufficient material removed from tor surfaces since emergence that the cosmogenic nuclide data do not preserve a surface exposure age signal for the landform.

The presence of a tor reflects an imbalance in erosion rate between the outcrop and the surrounding surface. This is shown in the cosmogenic nuclide data, with tor surface erosion rates of 18-32 mm ka^{-1} lower than those derived for regolith at 38-62

mm ka^{-1}. If it is assumed that these erosion rates are consistent with long-term erosion rates, an estimated tor emergence rate of 25 mm ka^{-1} can be calculated for tors at High Willhays, indicating that the tor landforms may have taken up to 220 ka to develop to their present height. At the Great Links Tor group, the emergence time for the largest tors may exceed 300 ka. These results indicate that the larger tors have developed over considerable time intervals. However, given the relatively high surface erosion rates measured, many metres of rock would have been removed from the landform since emergence.

The results of this study have significant implications for models of tor formation. The simple two-stage model presented by Linton (1955), in which the form of the tor is developed in the subsurface and subsequently exposed by the stripping of weathered material, is not compatible with the results of this study. The measured erosion rates and estimated tor emergence intervals indicate that there has been considerable post-emergence modification of tor outcrops. Consequently, the present form of the tors is not determined by sub-surface form (if there was any), but produced by subsequent weathering. For the studied tors, this limits the role of two-stage weathering to a possible influence on outcrop location, although even this not a requirement for tor formation.

A dynamic single-phase model of tor development provides a more robust explanation for tor formation, and is compatible with the results of ^{10}Be analysis in this study. This has shown both tor landforms and regolith-mantled surfaces at the summits have been eroding at relatively high rates. Similarly, the study of a blockslope indicated that material was being effectively transported away from the summit by slope processes. These results indicate that the summits were subject to intensive denudation over the Quaternary, with significant mass wasting and downslope transport of material (as suggested by Te Punga, 1957; and Palmer & Neilson, 1962). The Dartmoor landscape appears to have been heavily modified over successive glacial-interglacial climate cycles, although most of the present landforms appear to have developed during the Devensian glaciation (with the exception of some of the larger tors, which were still significantly modified during this interval).

It is the conclusion of this study that investigated summit tors are not transient landforms exposed as remnants of earlier deep weathering (two-stage model), but rather dynamic landforms generated over glacial-interglacial cycles of the Quaternary.

Catchment-Averaged Denudation:

The measurement of ^{10}Be concentrations in thirteen samples of alluvial sediment allowed for the calculation of spatially averaged denudation rates for catchments ranging in size from 3.1 to 77.2 km^2. The denudation rates derived were relatively consistent across the range of spatial scales and varying topography of the studied catchments, with typical rates of 20-40 mm ka^{-1}. However, the variability of results from the intensively sampled West Okement River catchment (34-70 mm ka^{-1}) highlights potential limitations with this approach in Dartmoor. In particular, there are likely to be problems with inadequate mixing of sediment leading to the violation of the models assumptions. This is especially likely when samples are collected from the coarse gravel bedload of small upland rivers. Consequently, while the results presented in this study provide a useful indication of landscape-wide denudation rates, there is limited scope for further interpretation of the data (e.g. catchment characteristics in Figure 5.19).

In conclusion, this research has demonstrated that, with careful interpretation, cosmogenic nuclide analysis can provide useful insights into the development of geomorphologically complex landforms and landscapes. In particular, the results presented in this study have provided key constraints on tor landform development, and in doing so, allowed for a re-evaluation of important models of landscape evolution.

References

Anderson R. S. (2002) Modeling the tor-dotted crests, bedrock edges, and parabolic profiles of high alpine surfaces of the Wind River Range, Wyoming. *Geomorphology* **46**(1-2), 35-58.

André M.-F. (2002) Rates of postglacial rock weathering on glacially scoured outcrops (Abisko-Riksgransen area, 68 degrees N). *Geografiska Annaler A, Physical Geography* **84A**, 139-150.

André M.-F. (2003) Do periglacial landscapes evolve under periglacial conditions? *Geomorphology* **52**, 149-164.

Balco G., Stone J. O., Lifton N. A., and Dunai T. J. (2008) A complete and easily accessible means of calculating surface exposure ages or erosion rates from 10Be and 26Al measurements. *Quaternary Geochronology* **3**(3), 174-195.

Barrows T. T., Stone J. O., and Fifield L. K. (2004) Exposure ages for Pleistocene periglacial deposits in Australia. *Quaternary Science Reviews* **23**, 697-708.

Bierman P. R. and Caffee M. (2001) Slow rates of rock surface erosion and sediment production across the Namib Desert and escarpment, southern Africa. *American Journal of Science* **301**(4-5), 326-358.

Bierman P. R. and Caffee M. (2002) Cosmogenic exposure and erosion history of Australian bedrock landforms. *Geological Society of America Bulletin* **114**(7), 787-803.

Bierman P. R., Caffee M., Davis P. T., Marsella K., Pavich M., Colgan P., Mickelson D., and Larsen J. (2002) Rates and timing of earth surface processes from in-situ-produced comsogenic 10Be. In *Reviews in Mineralogy, Vol. Beryllium : Mineralogy, Petrology, and Geochemistry* (ed. E. S. Grew), pp. 691. Mineralogical Society of America.

Bierman P. R., Marsella K. A., Patterson C., Davis P. T., and Caffee M. (1999) Mid-Pleistocene cosmogenic minimum-age limits for pre- Wisconsinan glacial surfaces in southwestern Minnesota and southern Baffin island: a multiple nuclide approach. *Geomorphology* **27**(1-2), 25-39.

Bierman P. R. and Nichols K. K. (2004) Rock to sediment - Slope to sea with Be-10 - Rates of landscape change. *Annual Review of Earth and Planetary Sciences* **32**, 215-255.

Bierman P. R. and Steig E. J. (1996) Estimating rates of denudation using cosmogenic nuclide isotope abundance in sediment. *Earth Surface Processes and Landforms* **21**, 125-139.

Bierman P. R. and Turner J. (1995) 10Be and 26Al evidence for exceptionally low rates of Australian bedrock erosion and the likely existence of pre-Pleistocene landscapes. *Quaternary Research* **44**, 378-382.

Binnie S. A. (2005) Edinburgh University Cosmogenic Laboratory Protocols. *Unpublished*.

Binnie S. A., Phillips W. M., Summerfield M. A., and Fifield L. K. (2006) Sediment mixing and basin-wide cosmogenic nuclide analysis in rapidly eroding mountainous environments. *Quaternary Geochronology* **1**, 4-14.

Binnie S. A., Phillips W. M., Summerfield M. A., and Fifield L. K. (2007) Tectonic uplift, threshold hillslopes, and denudation rates in a developing mountain range. *Geology* **35**(8), 743-746.

Boelhouwers J. (2004) New perspectives on autochthonous blockfield development. *Polar Geography* **28**(2), 133-146.

Briner J. P., Miller G. H., Davis P. T., Bierman P. R., and Caffee M. (2003) Last Glacial Maximum ice sheet dynamics in Arctic Canada inferred from young erratics perched on ancient tors. *Quaternary Science Reviews* **22**(5-7), 437-444.

Briner J. P., Miller G. H., Davis P. T., and Finkel R. (2006) Cosmogenic radionuclides from fiord landscapes support differential erosion by overriding ice sheets. *Geological Society of America Bulletin* **118**(3), 406-420.

Brown E. T., Bourles D. L., Colin F., Raisbeck G. M., Yiou F., and Desgarceaux S. (1995) Evidence for Muon-Induced Production of Be-10 in near-Surface Rocks from the Congo. *Geophysical Research Letters* **22**(6), 703-706.

Brown E. T., Colin F., and Bourlès D. L. (2003) Quantitative evaluation of soil processes using in situ-produced cosmogenic nuclides. *C.R. Geoscience* **335**, 1161-1171.

Brown E. T., Stallard R. F., Larsen M. C., Bourles D. L., Raisbeck G. M., and Yiou F. (1998) Determination of predevelopment denudation rates of an agricultural watershed (Cayaguas River, Puerto Rico) using in- situ-produced Be-10 in river-borne quartz. *Earth and Planetary Science Letters* **160**(3-4), 723-728.

Brown E. T., Stallard R. F., Larsen M. C., Raisbeck G. M., and Yiou F. (1995) Denudation Rates Determined from the Accumulation of in Situ- Produced Be-10 in the Luquillo Experimental Forest, Puerto-Rico. *Earth and Planetary Science Letters* **129**(1-4), 193-202.

Brunsden D. (1963) The denudation chronology of the River Dart. *Transactions and Papers (Institute of British Geographers)* **32**, 49-63.

Brunsden D. (1964) The origin of the decomposed granite on Dartmoor. In *Dartmoor Essays* (ed. I. G. Simmons), pp. 97-116. Devonshire Association.

Caine N. (1968) The fabric of periglacial blockfield material on Mt. Barrow, Tasmania. *Geografiska Annaler A, Physical Geography* **50**(4), 193-206.

Campbell S., Gerrard A. J., and Green C. P. (1998) Granite landforms and weathering products. In *Quaternary of South-West England*, Vol. 14 (ed. S. Campbell, J. D. Scourse, C. O. Hunt, D. H. Keen, and N. Stephens), pp. 439. Chapman and Hall.

Carson M. A. and Kirkby M. J. (1972) *Hillslope form and process*. Cambridge University Press.

Clapp E. M., Bierman P. R., Schick A. P., Lekach J., Enzel Y., and Caffee M. (2000) Sediment yield exceeds sediment production in arid region drainage basins. *Geology* **28**(11), 995-998.

Cockburn H. A. P., Seidl M. A., and Summerfield M. A. (1999) Quantifying denudation rates on inselbergs in the central Namib Desert using in situ-produced cosmogenic Be-10 and Al-26. *Geology* **27**(5), 399-402.

Codilean A. T. (2006) Calculation of the cosmogenic nuclide production topographic shielding scaling factor for large areas using DEMs. *Earth Surface Processes and Landforms*

Croot D. and Griffiths J. S. (2001) Engineering geological significance of relict periglacial activity in South and East Devon. *Quarterly Journal of Engineering Geology and Hydrogeology* **34**, 269-281.

Dangerfield J. and Hawkes J. R. (1981) The Variscan granites of South-West England: additional information. *Proceedings of the Ussher Society* **5**, 116-120.

Dearman W. R. and Baynes F. J. (1978) A field study of weathering patterns in the Dartmoor Granite. *Proceedings of the Ussher Society* **4**, 192-203.

Desilets D. and Zreda M. (2001) On scaling cosmogenic nuclide production rates for altitude and latitude using cosmic-ray measurements. *Earth and Planetary Science Letters* **193**(1-2), 213-225.

Desilets D. and Zreda M. (2003) Spatial and temporal distribution of secondary cosmic-ray nucleon intensities and applications to in situ cosmogenic dating. *Earth and Planetary Science Letters* **206**(1-2), 21-42.

Desilets D., Zreda M., and Prabu T. (2006) Extended scaling factors for in situ cosmogenic nuclides: New measurements at low latitude. *Earth and Planetary Science Letters* **246**(3-4), 265-276.

Dietrich W. E., Reiss R., Hsu M.-L., and Montgomery D. R. (1995) A process-based model for colluvial soil depth and shallow landsliding using digital elevation data. *Hydrological Processes* **9**, 383-400.

Doornkamp J. C. (1974) Tropical weathering and the ultra-microscopic characteristics of regolith quartz on Dartmoor. *Geografiska Annaler A, Physical Geography* **56**(1/2), 73-82.

Dunai T. J. (2000) Scaling factors for production rates of in situ produced cosmogenic nuclides: a critical reevaluation. *Earth and Planetary Science Letters* **176**(1), 157-169.

Dunai T. J. and Team C.-E. S. (2005) CRONUS-EU - Cosmic ray produced nuclide systematics – the European contribution. *Geochimica et Cosmochimica Acta* **69**(10), A165.

Dunne J., Elmore D., and Muzikar P. (1999) Scaling factors for the rates of production of cosmogenic nuclides for geometric shielding and attenuation at depth on sloped surfaces. *Geomorphology* **27**(1-2), 3-11.

Eden M. J. and Green C. P. (1971) Some aspects of granite weathering and tor formation on Dartmoor, England. *Geografiska Annaler A, Physical Geography* **53A**, 92-98.

Ehlen J. (1991) Significant geomorphic and petrographic relations with joint spacing in the Dartmoor Granite, Southwest England. *Zeitschrift für Geomorphologie* **35**(425-438).

Ehlen J. (1992) Analysis of spatial relationships among geomorphic, petrographic and structural characteristics of the Dartmoor tors. *Earth Surface Processes and Landforms* **17**, 53-67.

Ehlen J. (1994) Classification of Dartmoor tors. In *Rock Weathering and Landform Evolution* (ed. D. A. Robinson and R. B. G. Williams), pp. 3-20. Wiley.

Ehlen J. (2002) Some effects of weathering on joints in granitic rocks. *Catena* **49**, 91-109.

Exley C. S. and Stone M. (1964) The granite rocks of south-west England. In *Present views of some aspects of the geology of Cornwall and Devon* (ed. K. F. G. Hosking and G. J. Shrimpton), pp. 131-184. Geological Society of Cornwall.

Exley C. S. and Stone M. (1982) Hercynian intrusive rocks. In *Igneous rocks of the British Isles* (ed. D. S. Sutherland), pp. 287-320. Wiley.

Fabel D., Stroeven A. P., Harbor J., Kleman J., Elmore D., and Fink D. (2002) Landscape preservation under Fennoscandian ice sheets determined from in situ produced Be-10 and Al-26. *Earth and Planetary Science Letters* **201**(2), 397-406.

Fookes P. G., Dearman W. R., and Franklin J. A. (1971) Some engineering aspects of rock weathering with field examples from Dartmoor and elsewhere. *Quarterly Journal of Engineering Geology* **4**, 139-185.

Freeman S., Bishop P., Bryant C., Cook G., Dougans D., Ertunc T., Fallick A., Ganeshram R., Maden C., Naysmith P., Schnabel C., Scott M., Summerfield M. A., and Xu S. (2007) The SUERC AMS laboratory after 3 years. *Nuclear Instruments & Methods in Physics Research Section B- Beam Interactions with Materials and Atoms* **259**, 66-70.

Freeman S., Bishop P., Bryant C., Cook G., Fallick A., Harkness D., Metcalfe S., Scott M., Scott R., and Summerfield M. A. (2004) A new environmental sciences AMS laboratory in Scotland. *Nuclear Instruments & Methods in Physics Research Section B-Beam Interactions with Materials and Atoms* **223-24**, 31-34.

French H. M. (1996) *The periglacial environment*. Longman.

Gerrard A. J. (1974) The geomorphological importance of jointing in the Dartmoor granite. In *Progress in Geomorphology*, Vol. 7 (ed. E. H. Brown and R. S. Waters), pp. 39-50. Institute of British Geographers.

Gerrard A. J. (1978) Tors and granite landforms of Dartmoor and eastern Bodmin Moor. *Proceedings of the Ussher Society* **4**, 204-210.

Gerrard A. J. (1982) Granite structures and landforms. In *Papers in Earth Studies* (ed. B. A. Adlam, C. R. Fenn, and L. Morris). Geo Abstracts.

Gerrard A. J. (1984) Multiple working hypotheses and equifinality in geomorphology: comments on recent article by Haines-Young and Petch. *Transactions and Papers (Institute of British Geographers)* **NS 9**, 364-366.

Gerrard A. J. (1988) Periglacial modification of the Cox-Tor - Staple Tors area of western Dartmoor, England. *Physical Geography* **9**, 280-300.

Gerrard A. J. (1989) The nature of slope materials on the Dartmoor granite, England. *Zeitschrift für Geomorphologie* **33**(2), 179-188.

Gerrard A. J. (1993) Landscape sensitivity and change on Dartmoor. In *Landscape Sensitivity* (ed. D. S. G. Thomas and R. J. Allison), pp. 49-63. Wiley.

Gerrard A. J. (1994) Classics in physical geography revisited: the problem of tors. *Progress in Physical Geography* **18**, 559-563.

Gilbert G. K. (1877) *Report on the geology of the Henry Mountains*. U.S. Geographical and Geological Survey of the Rocky Mountain Region.

Gosse J. C. and Phillips F. M. (2001) Terrestrial in situ cosmogenic nuclides: theory and application. *Quaternary Science Reviews* **20**(14), 1475-1560.

Granger D. E., Fabel D., and Palmer A. N. (2001) Pliocene-Pleistocene incision of the Green River, Kentucky, determined from radioactive decay of cosmogenic Al-26 and Be-10 in Mammoth Cave sediments. *Geological Society of America Bulletin* **113**(7), 825-836.

Granger D. E., Kirchner J. W., and Finkel R. (1996) Spatially averaged long-term erosion rates measured from in situ-produced cosmogenic nuclides in alluvial sediment. *Journal of Geology* **104**(3), 249-257.

Granger D. E. and Muzikar P. F. (2001) Dating sediment burial with in situ-produced cosmogenic nuclides: theory, techniques, and limitations. *Earth and Planetary Science Letters* **188**(1-2), 269-281.

Granger D. E., Riebe C. S., Kirchner J. W., and Finkel R. C. (2001) Modulation of erosion on steep granitic slopes by boulder armoring, as revealed by cosmogenic Al-26 and Be-10. *Earth and Planetary Science Letters* **186**(2), 269-281.

Granger D. E. and Smith A. L. (2000) Dating buried sediments using radioactive decay and muogenic production of Al-26 and Be-10. *Nuclear Instruments & Methods in Physics Research Section B- Beam Interactions with Materials and Atoms* **172**, 822-826.

Green C. P. and Eden M. J. (1973) Slope deposits on the weathered Dartmoor granite, England. *Zeitschrift für Geomorphologie* **18**, 26-37.

Hall A. M. and Phillips W. (2006) Glacial modification of granite tors in the Cairngorms, Scotland. *Journal of Quaternary Science* **21**(8), 811-830.

Hall A. M. and Phillips W. M. (2006) Weathering pits as indicators of the relative age of granite surfaces in the Cairngorm Mountains, Scotland. *Geografiska Annaler A, Physical Geography* **88A**, 135-150.

Hall K., Thorn C. E., Matsuoka N., and Prick A. (2002) Weathering in cold regions: some thoughts and perspectives. *Progress in Physical Geography* **26**(4), 577-603.

Hancock G. S. and Kirwan M. (2007) Summit erosion rates deduced from 10Be: Implications for relief production in the central Appalachians. *Geology* **35**(1), 89-92.

Harrison S. (2001) Speculations on the glaciation of Dartmoor. *Quaternary Newsletter* **93**, 15-26.

Harrison S., Anderson E., and Passmore D. G. (2001) Further glacial tills on Exmoor, Southwest England; implications for small ice cap and valley glaciation. *Proceedings of the Geologists' Association* **112**, 1-5.

Hawkes J. R. (1982) The Dartmoor granite and later volcanic rocks. In *Geology of Devon* (ed. E. M. Durrance and D. J. C. Laming), pp. 85-116. University of Exeter.

Heimsath A. M., Chappell J., Dietrich W. E., Nishiizumi K., and Finkel R. C. (2000) Soil production on a retreating escarpment in southeastern Australia. *Geology* **28**(9), 787-790.

Heimsath A. M., Chappell J., Dietrich W. E., Nishiizumi K., and Finkel R. C. (2001) Late Quaternary erosion in southeastern Australia: a field example using cosmogenic nuclides. *Quaternary International* **83-5**, 169-185.

Heimsath A. M., Chappell J., Spooner N. A., and Questiaux D. G. (2002) Creeping soil. *Geology* **30**(2), 111-114.

Heimsath A. M., Dietrich W. E., Nishiizumi K., and Finkel R. C. (1997) The soil production function and landscape equilibrium. *Nature* **388**(6640), 358-361.

Heimsath A. M., Dietrich W. E., Nishiizumi K., and Finkel R. C. (1999) Cosmogenic nuclides, topography, and the spatial variation of soil depth. *Geomorphology* **27**(1-2), 151-172.

Heimsath A. M., Dietrich W. E., Nishiizumi K., and Finkel R. C. (2001) Stochastic processes of soil production and transport: Erosion rates, topographic variation and cosmogenic nuclides in the Oregon Coast Range. *Earth Surface Processes and Landforms* **26**(5), 531-552.

Heimsath A. M., Furbish D. J., and Dietrich W. E. (2005) The illusion of diffusion: Field evidence for depth-dependent sediment transport. *Geology* **33**(12), 949-952.

Heisinger B., Lal D., Jull A. J. T., Kubik P., Ivy-Ochs S., Knie K., and Nolte E. (2002) Production of selected cosmogenic radionuclides by muons: 2. Capture of negative muons. *Earth and Planetary Science Letters* **200**(3-4), 357-369.

Heisinger B., Lal D., Jull A. J. T., Kubik P., Ivy-Ochs S., Neumaier S., Knie K., Lazarev V., and Nolte E. (2002) Production of selected cosmogenic radionuclides by muons 1. Fast muons. *Earth and Planetary Science Letters* **200**(3-4), 345-355.

Heisinger B. and Nolte E. (2000) Cosmogenic in situ production of radionuclides: Exposure ages and erosion rates. *Nuclear Instruments & Methods in Physics Research Section B- Beam Interactions with Materials and Atoms* **172**, 790-795.

Hewawasam T., von Blanckenburg F., Schaller M., and Kubik P. (2003) Increase of human over natural erosion rates in tropical highlands constrained by cosmogenic nuclides. *Geology* **31**(7), 597-600.

Humphreys G. S. and Wilkinson M. T. (2007) The soil production function: A brief history and its rediscovery. *Geoderma* **139**, 73-78.

Johnston R. (2005) Pattern without a plan: rethinking the bronze age coaxial field systems on Dartmoor, South-West England. *Oxford Journal of Archaeology* **24**(1), 1-21.

Kirkbride M. P. (2006) Boulder edge-roundness as an indicator of relative age: a Lochnagar case study. *Scottish Geographical Journal* **121**, 219-236.

Kirkham F. W., Fowbert J. A., Parkin A. B., Darlaston M., and Glaves D. J. (2005) Moorland vegetation monitoring in the Dartmoor ESA 1994-2003. In *ADAS Report to the Department for Environment, Food and Rural Affairs.*

Kubik P. and Reuther A. U. (2007) Attenuation of cosmogenic 10Be production in the first 20 cm below a rock surface. *Nuclear Instruments & Methods in Physics Research Section B- Beam Interactions with Materials and Atoms* **259**, 616-624.

Lal D. (1988) In-situ produced cosmogenic isotopes in terrestrial rocks. *Annual Review of Earth and Planetary Sciences* **16**, 355-388.

Lal D. (1991) Cosmic ray labelling of erosion surfaces: in situ nuclides production rates and erosion models. *Earth and Planetary Science Letters* **104**, 424-439.

Lal D. (2000) Cosmogenic nuclide production rate systematics in terrestrial materials: Present knowledge, needs and future actions for improvement. *Nuclear Instruments & Methods in Physics Research Section B- Beam Interactions with Materials and Atoms* **172**, 772-781.

Lal D. and Arnold J. R. (1985) Tracing quartz through the environment. *Proceedings of the Indian Academy of Science, Earth and Planetary Science* **94**, 1-5.

Lal D. and Peters B. (1967) Cosmic ray produced radioactivity on the Earth. In *Handbuch der Physik*, Vol. 46/2 (ed. K. Sitte), pp. 551-612. Springer Verlag.

LeBoutllier. (2002) The Tectonics of Variscan Magmatism & Mineralisation in South West England.

Lifton N. A., Bieber J. W., Clem J. M., Duldig M. L., Evenson P., Humble J. E., and Pyle R. (2005) Addressing solar modulation and long-term uncertainties in scaling secondary cosmic rays for in situ cosmogenic nuclide applications. *Earth and Planetary Science Letters* **239**(1-2), 140-161.

Linton D. L. (1955) The problem of tors. *The Geographical Journal* **121**(4), 470-487.

Lowe J. J. and Walker M. J. C. (1997) *Reconstructing Quaternary Environments*. Longman.

Maden C., Anastasi P. A. F., Dougans A., Freeman S., Kitchen R., Klody G., Schnabel C., Sundquist M., Vanner K., and Xu S. (2007) SUERC AMS ion detection. *Nuclear Instruments & Methods in Physics Research Section B- Beam Interactions with Materials and Atoms* **259**, 131-139.

Masarik J. and Reedy R. C. (1995) Terrestrial cosmogenic-nuclide production systematics calculated from numerical simulations. *Earth and Planetary Science Letters* **136**(3-4), 381-395.

Masarik J. and Wieler R. (2003) Production rates of cosmogenic nuclides in boulders. *Earth and Planetary Science Letters* **216**(1-2), 201-208.

Matmon A., Bierman P. R., Larsen J., Southworth S., Pavich M., and Caffee M. (2003) Temporally and spatially uniform rates of erosion in the southern Appalachian Great Smoky Mountains. *Geology* **31**(2), 155-158.

Matsuoka N. (2001) Solifluction rates, processes and landforms: a global review. *Earth-Science Reviews* **55**, 107-134.

Nishiizumi K., Winterer E. L., Kohl C. P., Klein J., Middleton R., Lal D., and Arnold J. R. (1989) Cosmic ray production rates of 10Be and 26Al in quartz from glacially polished rocks. *Journal of Geophysical Research* **94**(17), 907-915.

Omerod G. W. (1859) On the rock basins in the granite of Dartmoor district, Devonshire. *Quarterly Journal of the Geological Society of London* **15**, 16-29.

Palmer J. (1956) Tor formation at the Bridestones in North-East Yorkshire and its significance in

relation to problems of valley-side development and regional glaciation. *Transactions and Papers (Institute of British Geographers)* **22**, 55-71.

Palmer J. and Neilson R. A. (1962) The origin of granite tors on Dartmoor, Devonshire. *Proceedings of the Yorkshire Geological Society* **33**(3/15), 315-340.

Palmer J. and Radley J. (1961) Gritstone tors of the English Pennines. *Zeitschrift für Geomorphologie* **5**, 37-52.

Phillips W. M., Hall A. M., Mottram R., Fifield L. K., and Sugden D. E. (2006) Cosmogenic Be-10 and Al-26 exposure ages of tors and erratics, Cairngorm Mountains, Scotland: Timescales for the development of a classic landscape of selective linear glacial erosion. *Geomorphology* **73**(3-4), 222-245.

Pigati J. S. and Lifton N. A. (2004) Geomagnetic effects on time-integrated cosmogenic nuclide production with emphasis on in situ C-14 and Be-10. *Earth and Planetary Science Letters* **226**(1-2), 193-205.

Quigley M., Sandiford M., Fifield K., and Alimanovic A. (2007) Bedrock erosion and relief production in the northern Flinders Ranges, Australia. *Earth Surface Processes and Landforms* **32**(6) 929-924.

Rapp A. (1960) Recent development of mountain slopes in Kärkevagge and surroundings, northern Scandinavia. *Geografiska Annaler* **42**, 65-200.

Rea B. R., Whalley W. B., Rainey M. M., and Gordon J. E. (1996) Blockfields, old or new? Evidence and implications from some plateaus in northern Norway. *Geomorphology* **15**, 109-121.

Reedy R. C., Arnold J. R., and Lal D. (1983) Cosmic-ray record in solar system matter. *Science* **219**(4581), 127-135.

Riebe C. S., Kirchner J. W., and Finkel R. C. (2003) Long-term rates of chemical weathering and physical erosion from cosmogenic nuclides and geochemical mass balance. *Geochimica Et Cosmochimica Acta* **67**(22), 4411-4427.

Riebe C. S., Kirchner J. W., and Finkel R. C. (2004) Erosional and climatic effects on long-term chemical weathering rates in granitic landscapes spanning diverse climate regimes. *Earth and Planetary Science Letters* **224**, 547-562.

Riebe C. S., Kirchner J. W., and Granger D. E. (2001) Quantifying quartz enrichment and its consequences for cosmogenic measurements of erosion rates from alluvial sediment and regolith. *Geomorphology* **40**(1-2), 15-19.

Riebe C. S., Kirchner J. W., Granger D. E., and Finkel R. C. (2000) Erosional equilibrium and disequilibrium in the Sierra Nevada, inferred from cosmogenic Al-26 and Be-10 in alluvial sediment. *Geology* **28**(9), 803-806.

Schaefer J. M. and Committee C.-E. S. (2005) The CRONUS-Earth (cosmic-ray produced nuclide systematics on earth) initiative. *Geochimica et Cosmochimica Acta* **69**(10), A167.

Schaller M., von Blanckenburg F., Hovius N., and Kubik P. W. (2001) Large-scale erosion rates from in situ-produced cosmogenic nuclides in European river sediments. *Earth and Planetary Science Letters* **188**(3-4), 441-458.

Schaller M., von Blanckenburg F., Veldkamp A., Tebbens L. A., Hovius N., and Kubik P. W. (2002) A 30 000 yr record of erosion rates from cosmogenic Be-10 in Middle European river terraces. *Earth and Planetary Science Letters* **204**(1-2), 307-320.

Schnabel C., Reinhardt L., Barrows T. T., Bishop P., Davidson A., Fifield L. K., Freeman S., Kim J. Y., Maden C., and Xu S. (2007) Inter-comparison in 10Be analysis starting from pre-purified quartz. *Nuclear Instruments & Methods in Physics Research Section B- Beam Interactions with Materials and Atoms* **259**, 571-575.

Small E. E., Anderson R. S., and Hancock G. S. (1999) Estimates of the rate of regolith production using Be-10 and Al-26 from an alpine hillslope. *Geomorphology* **27**(1-2), 131-150.

Small E. E., Anderson R. S., Repka J. L., and Finkel R. (1997) Erosion rates of alpine bedrock summit surfaces deduced from in situ Be-10 and Al-26. *Earth and Planetary Science Letters* **150**(3-4), 413-425.

Stone J. O. (2000) Air pressure and cosmogenic isotope production. *Journal of Geophysical Research-Solid Earth* **105**(B10), 23753-23759.

Stone J. O., Evans J. M., Fifield L. K., Allan G. L., and Cresswell R. G. (1998) Cosmogenic chlorine-36 production in calcite by muons. *Geochimica Et Cosmochimica Acta* **62**(3), 433-454.

Strudley M. W., Murray A. B., and Haff P. K. (2006) Emergence of pediments, tors, and piedmont junctions from a bedrock weathering–regolith thickness feedback. *Geology* **34**(10), 805-808.

Strudley M. W., Murray A. B., and Haff P. K. (2006) Regolith thickness instability and the formation of tors in arid environments. *Journal of Geophysical Research* **111**, F03010.

Te Punga M. T. (1957) Periglaciation in southern England. *Tijdschrift Koninklijk Nederlands Aardrijkskundig Genootschap* **74**, 400-412.

Thorn C. E., Darmody R. G., Dixon J. C., and Schlyter P. (2002) Weathering rates of buried machine-polished rock disks, Karkevagge, Swedish Lapland. *Earth Surface Processes and Landforms* **27**(8), 831-845.

Thorndycraft V. R., Pirrie D., and Brown A. G. (2004) Alluvial records of Medieval and prehistoric tin mining on Dartmoor, Southwest England. *Geoarchaeology: An International Journal* **19**(3), 219-236.

Tilley C., Hamilton S., Harrison S., and Anderson E. (2000) Nature, culture, clitter distinguishing between cultural and geomorphological landscapes; the case of hilltop tors in South-West England. *Journal of Material Culture* **5**(2), 197-224.

Tuniz C., Bird J. R., Fink D., and Herzog G. F. (1998) *Accelerator mass spectrometry, ultrasensitve analysis for global science*. CRC Press.

Twidale C. R. (2002) The two-stage concept of landform and landscape development involving etching: origin, development and implications of an idea. *Earth-Science Reviews* **57**, 37-74.

van Steijn H., Boelhouwers J., Harris S., and Hétu B. (2002) Recent research on the nature, origin and climatic relations of blocky and stratified slope deposits. *Progress in Physical Geography* **26**(4), 551-575.

Vermeesch P. (2007) CosmoCalc: an Excel add-in for cosmogenic nuclide calculations. *Geochemistry, Geophysics, Geosystems* **8**(8), Q08003.

von Blanckenburg F. (2005) The control mechanisms of erosion and weathering at basin scale from cosmogenic nuclides in river sediment. *Earth and Planetary Science Letters* **237**(3-4), 462-479.

von Blanckenburg F., Hewawasam T., and Kubik P. W. (2004) Cosmogenic nuclide evidence for low weathering and denudation in the wet, tropical highlands of Sri Lanka. *Journal of Geophysical Research-Earth Surface* **109**(F3).

Wakasa S., Matsuzaki H., Tanaka Y., and Matsukura Y. (2006) Estimation of episodic exfoliation rates of rock sheets on a granite dome in Korea from cosmogenic nuclide analysis. *Earth Surface Processes and Landforms* **31**(10), 1246-1256.

Waters R. S. (1957) Differential weathering and erosion on oldlands. *The Geographical Journal* **123**(4), 503-509.

Waters R. S. (1960) The bearing of superficial deposits on the age and origin of the upland plain of East Devon, West Dorset and South Somerset. *Transactions of the Institute of British Geographers* **28**, 89-97.

Waters R. S. (1964) The Pleistocene legacy to the geomorphology of Dartmoor. In *Dartmoor Essays* (ed. I. G. Simmons), pp. 73-96. Devonshire Association.

Watson E. (1977) The periglacial climate of Great Britain during the Devensian. *Philosophical Transactions of the Royal Society of London, Series B* **280**, 183-197.

Whalley W. B., Rea B. R., and Rainey M. M. (2004) Weathering, blockfields, and the implications for long-term landscape development: Some evidence from Lyngen and Øksfordjøkelen mountain areas in north Norway. *Polar Geography* **28**(2), 93-119.

White S. E. (1976) Is frost action really only hydration shattering? A review. *Arctic and Alpine Research* **8**(1), 1-6.

White S. E. (1981) Alpine mass movement forms (noncatastrophic): classification, description, and significance. *Arctic and Alpine Research* **13**(2), 127-137.

Wilkinson M. T. and Humphreys G. S. (2005) Exploring pedogenesis via nuclide-based soil production rates and OSL-based bioturbation rates. *Australian Journal of Soil Research* **43**(6), 767-779.

Williams A. G., Ternan L., and Kent M. (1984) Hydrochemical characteristics of a Dartmoor hillslope. In *Catchment Experiments in Fluvial Geomorphology* (ed. D. E. Walling and T. P. Burt), pp. 379-398. GeoBooks.

Williams A. G., Ternan L., and Kent M. (1986) Some observations on the chemical weathering of the Dartmoor granite. *Earth Surface Processes and Landforms* **11**, 557-574.

Williams R. B. G. (1975) The British climate during the last Glaciation; an interpretation based on periglacial phenomena. In *Ice Ages - Ancient and Modern* (ed. A. E. Wright and F. Mosely), pp. 95-120. Seele House.

Woolridge S. W., Hollingworth S. E., Linton D. L., Lewis W. V., Palmer J., Waters R. S., Warwick G. T., Steers J. A., and Stamp D. (1955) The problem of tors: discussion. *The Geographical Journal* **121**(4), 482-486.

Ziegler J. F. (1996) Terrestrial cosmic rays. *IBM Journal of Reseach and Development* **40**(1), 19-39.

Appendix I - Sample Acquisition and Laboratory Processing

Field Sampling

The collection of samples for cosmogenic nuclide analysis was undertaken during visits to Dartmoor in November 2004, May 2005, November 2005, and July 2006. Three different types of samples were collected: (i) *unweathered* granite from bedrock outcrops and boulders; (ii) samples of regolith; and (iii) alluvial samples from streams and rivers. This section describes the practical aspects of sample collection. The rationale for the various approaches is discussed in the relevant results section.

Bedrock Samples

These samples of unweathered granite were taken from the surfaces of tor outcrops, exposed bedrock surfaces, and boulders. Samples were removed from surfaces using a hammer and chisel. The granite is difficult to remove without exploiting existing weaknesses within the rock. For the tors and bedrock samples taken in the north-west of Dartmoor, this meant exploiting the horizontal jointing present in the rocks to remove samples as sheets of rock between 2 and 5 cm thickness. Fortunately, this thickness is useful as it minimises the need to correct for sample thickness due to the attenuation of cosmic rays with depth. The need to find existing weakness meant that randomisation of sample locations on surfaces was not possible. However, in most cases samples were able to be taken from towards the middle of surface, minimising the potential for shape effects to influence the accumulation of cosmogenic nuclides in the rock. Samples from tors and bedrock surface typically weighed between 400 and 1200 g of granite. The samples taken from a blockslope on the slopes of Yes Tor were smaller than those taken from tors. For these smaller pieces of rock (~ 100 g) were taken from the uppermost edge of the boulders by striking with a hammer. Once removed from the surface samples, for those that were still largely intact, had their upper surface marked with indelible ink marker. Samples were assigned a unique ID code and placed in labelled canvas sack for transport back to Edinburgh. Field notes included the dimensions of the sample and the characteristics of the surface required for the calculation of site-specific scaling factors (e.g. shielding, slope, and outcrop/surface dimensions). Photographs were taken of the sample and surface.

GPS was used in combination with maps and aerial photography to locate the sampling site.

Regolith Samples

Samples of regolith were taken from the vicinity of Yes Tor and the High Willhays in north-west Dartmoor. There were two types of samples taken of the regolith. The first were surface samples, which simply required the shovelling of surface material into labelled bags. Alternatively, regolith was collected from pits. From these sediment was extracted from the walls of the pit, with the range of depth from which they were taken recorded. The location of the sampling site was recorded with GPS in combination with maps and aerial photos.

Alluvial Samples

The sampling of alluvial sediments was relatively straightforward. As little sand-sized material was available in most river beds, the sampling location was usually a bar or lag deposit. Most sediment was coarse-sand or larger. Sediment was shovelled from the bed and stored in sealed and labelled plastic bags. The sample location was recorded with GPS and identified on ordinance survey maps of Dartmoor.

Laboratory Procedures

This section describes the procedures followed in the preparation of samples for analysis of ^{10}Be concentrations by AMS. All such work was conducted at the University of Edinburgh's Cosmogenic Nuclide Laboratory during the period 2004-2006. As such, it is based on the laboratory protocols described by Binnie (2005); these are available from the laboratory. These protocols are largely an adaptation of protocols developed by Kohl & Nishiizumi (1992) and Bierman *et al.* (2002). While the processing of samples undertaken for this research broadly follows the procedures laid out in the laboratory protocols (Binnie, 2005), as is typical for cosmogenic nuclide laboratory work, some deviations and adaptations were necessary to deal with the particular physical and lithological characteristics of the samples.

Physical Preparation of Samples

The first stage of sample preparation is to produce sediment with a grain size appropriate for the process of quartz purification; typically 250-710 μm. As there were three different types of samples (rock, regolith, and alluvium) each required different procedures to produce material for the chemical stages of preparation.

Rock - samples were broken into smaller pieces of rock (< 5cm) using a either a hammer or rock-splitter. These were then fed into a jaw crusher which pulverised the sample producing sand-sized material. This was then sieved using 250 and 1000 μm pans. Material > 1000 μm was feed back into the jaw crusher, and this was repeated until a sufficient quantity of 250-710 μm grains were acquired. Each size fraction (<250, 250-1000, and >1000 μm) was separately bagged. Further sieving of the 250-1000 μm material was undertaken using a stack of dry sieves on a shaker and size fractions within the range 250-710 μm obtained from most samples.

Regolith – samples of regolith contained varying abundances of organic material, this must be removed before chemical processing. The first stage was wet sieving of the samples in a stack of sieve pans with varying mesh sizes between 250 and 2000 μm. This effectively removed much of the finer organic material from the sample. Where large amounts of organic material were still present in the 250-710 μm fraction, an additional step was included in which samples were placed in 4 L bottles with several hundred ml of H_2O_2 and left on a shaker table overnight. These samples were then rinsed and dried in an oven.

Alluvium – samples of alluvium were first oven dried, then dry sieved using a stack of sieves ranging in mesh size from 250 μm to 2 cm. For most samples the 250-710 μm size fraction was taken for quartz purification.

Quartz Separation

The aim of these procedures is to take a sample of sediment and extract from it a sample of pure quartz. This is achieved through the etching of the sample in dilute HF. As most silicate minerals dissolve more rapidly that quartz they can be etched

away leaving only quartz grains. In addition, the quartz grains are partially etched thus removing atmospheric ^{10}Be which may have been adsorbed by the surface.

HCl Wash – this is the first step of the cleaning procedure. Approximately 200 g of sample are placed in a 1 L bottle. This sample is then rinsed and decanted repeatedly to remove finer material that may still be present in the sample following dry sieving. At least 100 ml of concentrated HCl (35% analytical reagent grade) was then added to the bottles. In many cases the samples reacted strongly to the addition of HCl, and more was added. The sample was left overnight before being rinsed and decanted.

Junk Etch – this step is intended to remove easily dissolved minerals prior to the more intensive clean etching steps. In the earlier period of lab work (2004-2005) dilute HF (1%) and HNO3 (1%) was added to the 1 L bottles. Following a change in procedure (in 2005) the HF was replaced by the addition of ~200 ml of concentrated H_2SiF_6 (35%). Either way, samples were placed on a shaker table overnight then rinsed multiple times. Depending on the sample the junk etch may be repeated until samples appear sufficiently quartz-rich. Finally, samples are dried in an oven and bagged.

Magnetic Separation – this step was introduced to sample preparation in 2006 due to the presence of a significant quantity of mafic minerals that were time consuming to remove through LST (heavy liquid) separation (see below). The sample was spread over a large sheet of paper and a powerful hand magnet was run over it. This collected most of the mafic minerals present.

Quartz Etch – this step preferentially dissolves non-quartz minerals and etches the surface of quartz grains. Between 40 and 60 g of sample was added to bottles of either 2.5 or 4 L capacity (the amount of sample in proportion to the volume). This was then filled with a solution of dilute HF (40% GPR grade at 22.5 ml / litre) and HNO3 (70% analytical reagent grade at 12.5 ml / litre). Samples were then placed in ultrasonic baths for between 24-72 hours (increasing time with number of etches). Samples are then rinsed in 15 MΩ H_2O and etching repeated until only quartz is

apparent in the sample (some mafic minerals may still be present), after which it is dried in the oven.

Heavy Liquid (LST) Separation – this step separates quartz from remaining mafic and other minerals that have a greater density. The sample is added to centrifuge tubes which are then filled with sodium heteropolytungstate solution (LST) which has a density of 2.90 g ml^{-1}. The tube is then placed in a centrifuge and the quartz floats to the surface. This is extracted and the rinsed clean with 18.2 MΩ H_2O. The samples processed from Dartmoor contained a significant component of mafic minerals and it was often necessary to repeat the LST separation.

Final Etch – this is the final step in producing a quartz separate, with as few other minerals remaining as possible. The sample was transferred to a 2.5 or 4L bottle that had been rinsed in 18 MΩ H_2O. This time the etch is in only HF (48% certified grade at 20 ml / litre) and dilution is with 18 MΩ H_2O. The sample is oven dried, following which it is ready for ^{10}Be extraction.

^{10}Be Target Preparation

The aim of these procedures is to extract beryllium and prepare a target for AMS analysis. This involves the dissolution of the sample and a series of steps to remove contaminants and then produce BeO.

Dissolution – Each sample is transferred into a savillex jar, with the weight of the sample recorded, before the jar walls are washed down with 18 MΩ H_2O. A lab blank jar is also included in the sample batch. The samples are then transferred to the fume cupboard, where ~0.25 ml of ^{9}Be carrier solution is added to each sample with a digital pipette, the weight of the carrier added is also recorded. Each jar is then filled with undiluted HF (~48% analytical reagent grade) and hotplate is set to 90°C. The samples can take several days to completely dissolve, with further HF added as necessary.

Perchloric Fume – Following dissolution, the desiccated samples were transferred to another fumehood for perchloric fuming. This stage converts insoluble fluorides to

soluble perchlorates reducing the boron content. 1.0 ml of $HClO_4$ is added to each jar, which is then placed on a hotplate set to 200ºC. Further $HClO_4$ is added as the supply is exhausted, until 4 fumes have been completed. The jars walls are then rinsed in 18 MΩ H_2O and left to dry-down.

Anion Columns – this step removes Fe from the sample by selective adsorption of anions to resin beads, the ^{10}Be is able to pass through the 20 ml exchange columns. The sample is dissolved in HCl and passed into the columns in a series of elutions at varying molarity of HCl (60 ml : 9M → 5 ml : 9M → 40 ml : 9M → 80 ml : 0.5M → 60 ml : 18 MΩ H_2O), the sample is preserved from the 2nd and 3rd elulants.

Titanium Precipitation – involves adjusting the pH of a solution to precipitate Ti and other contaminants. The samples are taken into solution in HCl and transferred to centrifuge tubes. Addition of NH_4OH to lower the solution to pH 3.8-4.0, then centrifuged at 3000 rpm, the supernatant contains Be, while the Ti is in the precipitate. Supernatants are decanted into another centrifuge tube and the solution is adjusted to pH 8-9 by addition of further NH_4OH, with a flocculent containing the Be forming which is left overnight. The precipitates are retained, rinsed in 18 MΩ H_2O, and then taken back into solution with HCl.

Cation Columns – the cation exchange separates the Be fraction of the sample. Cations are adsorbed onto resin beads and selectively desorbed through the addition of varying molarity HCl solutions. Each sample is taken into solution with HCl and passed with a series of elutions through the columns (60 ml : 9M → 60ml : 4.5M → 60 ml : 1M → 60 ml : 1M → 160 ml : 1M → 80 ml : 1M → 80 ml : 1M → 60 ml 18 MΩ H_2O), with the Be retained during the 160 ml elution. The solution is then dried down.

Final Fume – this is a repeat of the perchloric fume as described above with the aim of minimising boron in the sample.

Hydroxide Precipitation – is the stage at which a $Be(OH)_2$ is precipitated as a gel. The samples are taken into solution in HCl and transferred to a centrifuge tube. The solution is adjusted to pH 9 through the addition of NH_4OH, and the sample centrifuged at 3000 rpm for 10 minutes. The supernatants are decanted, reserving the gel containing the Be, this is repeated, before the samples are left overnight. A final precipitation in centrifuge, then the gel is dried down for firing.

Firing and Target Pressing – the sample is now a small pellet of $Be(OH)_2$ material which is raised to high temperature to convert to BeO. This was done with an open butane-propane flame (prior to 2006) and in a high-temperature furnace (from 2006). The sample is then crushed and mixed to a BeO:Nb ratio of ~1/5 appropriate for SUERC analysis. It is then pressed into a target cathode ready for analysis.

Appendix II - GIS Methods

The compilation and processing of a digital elevation model (DEM) was necessary for the delineation of catchment boundaries upstream of alluvial sediment sampling sites. This allowed for variables to be determined for input into the CRONUS-Earth online calculator to derive denudation rates for samples. It also provided useful morphological characteristics for the catchment and the landscape.

These software packages and tool sets were used:

- ArcGIS 9.2
- Spatial Analyst
- Arc Hydro Tools 1.2
- ApFramework

Construction of DEM

The digital terrain model (DTM) was produced by the Ordinance Survey and obtained from the Digimap online service. This data was from the 'OS Land-Form PROFILE DTM, 1:10000', it has a 10 m horizontal grid interval and 1 m height resolution and an accuracy of 2.5-5 m, although this can be less in mountainous and moorland regions. This data was provided in NTF file format. It was necessary to convert the data to a GRID format DEM for use in the ArcGIS 9.2 environment. In addition, the data was provided in numerous coverages corresponding to OS map tiles, a composite of these was created to provide a single DEM for the entire Dartmoor area.

Catchment Delineation

Arc Hydro is a geospatial and temporal data model developed for water resources applications and designed to operate within ArcGIS. Usefully for the purposes of this research, it allows for the delineation of watershed boundaries based on a DEM. It is also able to determine the catchment feeding into any point in the drainage network, so these can be defined for each drainage site. Further details of the Arc Hydro

model can be found on the Centre for Research in Water Resources website (www.crwr.utexas.edu/gis). This research used the Arc Hydro Tools 1.2 toolset developed for ArcGIS 9.2 and available for download from the ESRI website (www.support.esri.com). The ApFramework was also installed, this is required by the Arc Hydro model and comes bundled with the download.
The following is a brief description of the steps involved in deriving a catchment models and associated coverages used in this research. For further details the operation of each function the user documentation should be consulted.

Preparation of the DEM – some pre-processing of the digital elevation model is necessary to allow the functions to operate correctly. The *fill sinks* function was used to find any cells completely surrounded by cells of higher elevation (a hydrological sink) and modify these so that flow is maintained across the DEM. This creates a DEM used for subsequent processing, although the original model is used at the end when elevation data is acquired.

Flow Characterisation – the Arc Hydro model is based on the calculation of flow paths through the DEM. The first step is to run the *flow direction* function, which for each cell determines its lowest elevation neighbour. Utilising the flow direction grid, the *flow accumulation* function then computes for each cell the accumulated number of cells upstream. The result of this is a grid coverage in which each cell has a value reflecting the number of cells that flow into that location.

Stream Identification – the next task is to produce a stream network that can be used to identify catchments. The *stream definition* function takes the flow accumulation grid and defines as a stream all cells that have a minimum number of upstream cells. This minimum threshold is user defined and its selection is a decision based on what effectively represents the drainage network for the study area while not creating too many streams and complicating catchment delineation at later stages. For the Dartmoor DEM a variety of cell threshold values were tested and a value of 5000 cells upstream was used to define a stream, this represents a catchment area of 0.5 km^2. The cells that have been identified as streams are grouped using the *stream*

segmentation function that gives each segment a unique identification value. A new segment begins when two or more neighbouring cells flow into a cell, rather than a single upstream cell. Each segment therefore represents a reach of stream between junctions. The *Drainage Line Processing* function is used to convert the streams into a line feature class.

Catchment Boundaries – the next step is to determine the catchment of each stream segment. The *Catchment Grid Delineation* function assigns the unique stream segment value to each cell in the segments catchment. This grid is then processed using the *Catchment Polygon Processing* function with creates a polygon feature class for each unique catchment. The *Adjoint Catchment Processing* function is then used to generate a feature class that creates aggregate catchments that include all upstream catchments of the one being processed. Finally, the *Drainage Point Processing* function creates a point feature class that identifies the outflow drainage point for each catchment.

Catchment Delineation for Study Sites – the coverages that have been generated up to this stage allow for the utilisation of the *Point Delineation* tool. This allows the user to click on any cell within the stream network and the model generates a catchment polygon that covers all cells that flow into that point. For this study catchments were generated for all sampling sites with the point determined by the GPS coordinates recorded in the field. In addition, catchments were derived for Meldon Valley (at the weir) and for the Dart River upstream of Dartmeet. The output from using the *Point Delineation* tool is a polygon coverage of the catchment area.

Creation of Catchment DEMs – to derive data useful for this research individual DEMs are required for each catchment. These are created using the Spatial Analyst Toolset included with ArcGIS 9.2. The catchment polygons were exported as shapefiles. These were then converted to a raster format with the same properties as the original Dartmoor DEM grid. The *Raster Calculator* function was then used to create a DEM that only included cells within the catchment area.

Output from GIS

From each individual DEM produced (i.e. each sampling site) the characteristics of the catchment can be derived. These include the mean, standard deviation, minimum and maximum of elevation values of cells in the grid. The area of each catchment is also available. A range of further hydrological parameters can be readily determined using ArcHydro Tools.

The main outputs from GIS were: (i) average catchment elevation for denudation rate calculations; (ii) catchment morphological characteristics (Table 5.2); and (iii) as a base elevation map and drainage network throughout.

Appendix III – Sample Data, AMS Results and Calculations

Figure A3.1 – Sample Data and AMS Measurements – Tors and Blockslopes

Figure A3.2 – Sample Data and AMS Measurements – Regolith and Alluvium

Figure A3.3 – Calculated Exposure Age and Erosion Rates – Tors and Blockslopes

Figure A3.4 – Calculated Exposure Age and Erosion Rates – Regolith and Alluvium

Table A3.1 Sample laboratory and AMS analysis details - Tor and Blockslope

Sample ID	Latitude	Longitude	Elevation (m)	Thickness (cm)	Shielding Correction	Quartz Mass (g)	Carrier Mass (g)	Blank Carrier Mass (g)	$^{10}Be/^{9}Be$ Sample	σ $^{10}Be/^{9}Be$ Sample	$^{10}Be/^{9}Be$ Blank	σ $^{10}Be/^{9}Be$ Blank	$N^{10}Be$ (atoms g^{-1})	σ $N^{10}Be$ (atoms g^{-1})
HW1A	50.68752	-4.01158	610	2	1	36.562	0.0002610	0.0002574	4.5508E-13	1.6850E-14	1.7277E-14	4.6360E-15	2.0895E+05	9.3933E+03
HW1B	50.68752	-4.01158	610	2	1	25.259	0.0002571	0.0002552	5.3100E-13	2.1210E-14	1.6646E-14	2.4550E-15	3.4991E+05	1.6219E+04
HW1G(2)	50.68752	-4.01158	608	3	0.9	48.855	0.0002550	0.0002543	6.6790E-13	1.8990E-14	8.2155E-14	4.9850E-15	2.0437E+05	8.3009E+03
HW1G(4)	50.68752	-4.01158	607	3	0.8	48.469	0.0002543	0.0002543	6.3826E-13	1.9640E-14	8.2155E-14	4.9850E-15	1.9496E+05	8.4157E+03
HW2B	50.68718	-4.01095	617	1	1	30.058	0.0002554	0.0002552	4.0498E-13	1.1550E-14	1.6646E-14	2.4550E-15	2.2049E+05	8.1320E+03
HW5D	50.68458	-4.01000	621	1	1	42.371	0.0002570	0.0002574	5.3489E-13	1.4150E-14	1.7277E-14	4.6360E-15	2.0978E+05	7.4330E+03
HW5F	50.68458	-4.01000	621	1	1	32.172	0.0002598	0.0002574	5.9796E-13	1.5700E-14	1.7277E-14	4.6360E-15	3.1343E+05	1.0936E+04
HWBS1	50.68777	-4.01128	600	1	1	28.180	0.0002539	0.0002552	3.9274E-13	1.5180E-14	1.6646E-14	2.4550E-15	2.2638E+05	1.0399E+04
HWBS2	50.68713	-4.01102	614	3	1	41.024	0.0002589	0.0002574	3.7803E-13	1.0680E-14	1.7277E-14	4.6360E-15	1.5217E+05	5.8522E+03
BT2D	50.68632	-4.02868	470	2	1	25.219	0.0002489	0.0002552	4.9331E-13	1.4510E-14	1.6646E-14	2.4550E-15	3.1407E+05	1.1692E+04
LT03	50.66949	-3.97608	496	2	1	28.404	0.0002552	0.0002540	4.0375E-13	1.3620E-14	3.5492E-14	2.7980E-15	2.2119E+05	9.6612E+03
DT01	50.67554	-4.00210	550	2	1	31.242	0.0002542	0.0002540	2.9798E-13	9.7950E-15	3.5492E-14	2.7980E-15	1.4273E+05	6.4280E+03
SAT02	50.67439	-3.97608	540	2	1	19.026	0.0002576	0.0002595	4.3049E-13	1.6390E-14	1.1429E-14	2.1220E-15	3.7906E+05	1.6863E+04
SAT03	50.67439	-3.97608	540	2	1	34.822	0.0002536	0.0002540	7.8731E-13	2.1710E-14	3.5492E-14	2.7980E-15	3.6584E+05	1.3127E+04
GLT1a	50.66245	-4.05192	587	2	1	36.660	0.0002562	0.0002574	4.3921E-13	1.3110E-14	1.7277E-14	4.6360E-15	3.1491E+05	1.1617E+04
GLT1b	50.66245	-4.05192	580	4	0.5	37.841	0.0002620	0.0002574	6.9764E-13	2.0370E-14	1.7277E-14	4.6360E-15	1.9700E+05	7.6853E+03
GLT2	50.66251	-4.05141	586	2	1	29.896	0.0002550	0.0002540	4.4218E-13	1.2390E-14	3.5492E-14	2.7980E-15	2.3187E+05	8.8295E+03
GLT3	50.66234	-4.05113	580	2	1	23.508	0.0002542	0.0002540	5.0048E-13	1.3560E-14	3.5492E-14	2.7980E-15	3.3600E+05	1.2355E+04
GLT4	50.66232	-4.05048	576	2	1	34.587	0.0002550	0.0002540	6.1452E-13	1.7890E-14	3.5492E-14	2.7980E-15	2.8533E+05	1.0786E+04
GLT5	50.66241	-4.04959	569	2	1	29.220	0.0002560	0.0002540	7.8827E-13	1.6870E-14	3.5492E-14	2.7980E-15	4.4085E+05	1.3621E+04
BF1(1)	50.69409	-4.01322	588	3.0	1	26.941	0.0002545	0.0002581	3.4134E-13	2.3420E-14	2.1210E-14	3.3540E-15	2.0188E+05	1.5550E+04
BF1(2)	50.69409	-4.01322	588	3.0	1	25.710	0.0002675	0.0002581	2.8959E-13	2.2020E-14	2.1210E-14	3.3540E-15	1.8710E+05	1.5991E+04
BF2(1)	50.69423	-4.01372	577	3.0	1	20.631	0.0002583	0.0002581	3.3345E-13	1.4320E-14	2.1210E-14	3.3540E-15	2.6123E+05	1.3514E+04
BF2(2)	50.69423	-4.01372	577	3	1	23.927	0.0002569	0.0002581	3.2501E-13	3.0230E-14	2.1210E-14	3.3540E-15	2.1789E+05	2.2318E+04
BF2(3)	50.69423	-4.01372	577	3	1	30.226	0.0002590	0.0002531	3.5048E-13	1.0410E-14	2.5275E-14	3.2600E-15	1.8653E+05	7.4192E+03
BF3(1)	50.69446	-4.01540	549	3	1	25.655	0.0002591	0.0002581	5.4603E-13	1.6490E-14	2.1210E-14	3.3540E-15	3.5423E+05	1.3539E+04
BF3(2)	50.69446	-4.01540	549	3	1	27.270	0.0002585	0.0002581	5.8003E-13	2.1030E-14	2.1210E-14	3.3540E-15	3.5398E+05	1.5362E+04

Table A3.2 Sample laboratory and AMS analysis details - Regolith and Alluvium

Sample ID	Latitude	Longitude	Elevation (m)	Thickness (cm)	Shielding Correction	Quartz Mass (g)	Carrier Mass (g)	Blank Carrier Mass (g)	$^{10}Be/^{9}Be$ Sample	σ $^{10}Be/^{9}Be$ Sample	$^{10}Be/^{9}Be$ Blank	σ $^{10}Be/^{9}Be$ Blank	$N^{10}Be$ (atoms g^{-1})	σ $N^{10}Be$ (atoms g^{-1})
R1	50.68808	-4.01261	608	-	1	39.607	0.0002534	0.0002531	3.9030E-13	1.5850E-14	2.5275E-14	3.2600E-15	1.5606E+05	7.6834E+03
R2	50.68692	-4.01145	614	-	1	38.011	0.0002543	0.0002543	3.7388E-13	1.3010E-14	8.2155E-14	4.9850E-15	1.3041E+05	7.1068E+03
R3	50.68491	-4.01121	618	-	1	36.599	0.0002541	0.0002543	3.2610E-13	1.1360E-14	8.2155E-14	4.9850E-15	1.1314E+05	6.5474E+03
HWPIT2	50.68794	-4.01243	608	-	1	37.959	0.0002542	0.0002543	3.6463E-13	1.2760E-14	8.2155E-14	4.9850E-15	1.2639E+05	6.9837E+03
HWPIT3	50.68794	-4.01243	608	-	1	35.651	0.0002531	0.0002531	2.7347E-13	1.0240E-14	2.5275E-14	3.2600E-15	1.1774E+05	5.7252E+03
HWPIT4	50.68794	-4.01243	608	-	1	34.991	0.0002601	0.0002531	3.8474E-13	1.0930E-14	2.5275E-14	3.2600E-15	1.7888E+05	6.8281E+03
M0(250)	50.68473	-4.03043	509	-	1	10.834	0.0002539	0.0002595	1.1413E-13	1.8520E-14	1.1429E-14	2.1220E-15	1.6044E+05	2.9421E+04
M0(710)	50.68473	-4.03043	509	-	1	25.312	0.0002570	0.0002595	2.8152E-13	1.5530E-14	1.1429E-14	2.1220E-15	1.8317E+05	1.1303E+04
ED-01	50.54433	-3.87565	411	-	1	24.574	0.0002564	0.0002595	2.8160E-13	1.2540E-14	1.1429E-14	2.1220E-15	1.8827E+05	9.7018E+03
TB-01	50.55858	-3.96587	473	-	1	24.911	0.0002563	0.0002595	4.1989E-13	1.4570E-14	1.1429E-14	2.1220E-15	2.8071E+05	1.1656E+04
M5	50.66345	-4.00209	529	-	1	15.608	0.0002547	0.0002595	1.2645E-13	6.1310E-15	1.1429E-14	2.1220E-15	1.2518E+05	7.6105E+03
UCB-01	50.57667	-3.93032	425	-	1	18.823	0.0002589	0.0002595	1.8826E-13	6.5570E-15	1.1429E-14	2.1220E-15	1.6250E+05	7.2221E+03
WD-01	50.54251	-3.87699	407	-	1	19.977	0.0002596	0.0002595	2.5780E-13	7.3980E-15	1.1429E-14	2.1220E-15	2.1394E+05	8.0465E+03
SM-01	50.51867	-3.95450	406	-	1	15.728	0.0002584	0.0002595	1.8635E-13	8.2200E-15	1.1429E-14	2.1220E-15	1.9198E+05	1.0184E+04
EO-01	50.73328	-3.97608	419	-	1	18.653	0.0002580	0.0002595	2.4854E-13	9.7460E-15	1.1429E-14	2.1220E-15	2.1909E+05	1.0305E+04
WB-01	50.53003	-4.05711	389	-	1	22.973	0.0002591	0.0002595	3.7151E-13	1.9330E-14	1.1429E-14	2.1220E-15	2.7135E+05	1.5690E+04
M1	50.68512	-4.03424	511	-	1	21.030	0.0002536	0.0002531	2.1721E-13	1.0210E-14	2.5275E-14	3.2600E-15	1.5470E+05	9.3261E+03
M2	50.67942	-4.02681	512	-	1	31.734	0.0002559	0.0002543	2.1114E-13	8.0820E-15	8.2155E-14	4.9850E-15	6.9779E+04	5.6606E+03
M3	50.67345	-4.01895	515	-	1	29.480	0.0002552	0.0002543	2.4187E-13	8.5910E-15	8.2155E-14	4.9850E-15	9.2554E+04	6.4559E+03

Table A3.3 Calculated Exposure Age and Erosion Rates from CRONUS-Earth Online Calculator (v2.0) - Tors and Blockslopes

Sample ID	Production Rate (atoms g^{-1} a^{-1})		Internal Uncertainty (%)	Exposure Age (ka)[b]				Erosion Rate (mm ka^{-1})[c]			
	Spallation[a]	Muonic		Stone (2000)	Desilets *et al.* (2003; 2006)	Dunai (2001)	Lifton *et al.* (2005)	Stone (2000)	Desilets *et al.* (2003; 2006)	Dunai (2001)	Lifton *et al.* (2005)
HW1A	8.71	0.24	4.52%	23.46 ± 2.30	24.95 ± 3.09	25.21 ± 3.11	24.04 ± 2.57	33.86 ± 2.84	32.20 ± 3.27	31.97 ± 3.23	33.24 ± 2.99
HW1B	8.71	0.24	4.68%	39.43 ± 3.91	41.81 ± 5.22	42.03 ± 5.23	39.99 ± 4.32	19.55 ± 1.70	18.60 ± 1.97	18.49 ± 1.95	19.29 ± 1.80
HW1G(2)	7.76	0.24	4.09%	25.68 ± 2.47	27.28 ± 3.34	27.55 ± 3.36	26.26 ± 2.77	31.65 ± 2.55	30.14 ± 2.96	29.93 ± 2.92	31.11 ± 2.69
HW1G(4)	6.89	0.24	4.34%	27.49 ± 2.68	29.19 ± 3.60	29.45 ± 3.62	28.07 ± 2.99	30.38 ± 2.47	28.97 ± 2.83	28.78 ± 2.80	29.88 ± 2.59
HW2B	8.84	0.24	3.71%	24.42 ± 2.31	25.96 ± 3.15	26.22 ± 3.17	25.00 ± 2.60	32.36 ± 2.58	30.78 ± 3.03	30.56 ± 2.99	31.79 ± 2.74
HW5D	8.87	0.25	3.56%	23.14 ± 2.18	24.61 ± 2.97	24.87 ± 2.99	23.72 ± 2.45	34.21 ± 2.70	32.54 ± 3.17	32.30 ± 3.13	33.60 ± 2.86
HW5F	8.87	0.25	3.52%	34.67 ± 3.27	36.78 ± 4.45	37.03 ± 4.46	35.23 ± 3.64	22.34 ± 1.80	21.25 ± 2.12	21.12 ± 2.10	22.02 ± 1.92
HWBS1	8.70	0.24	4.62%	25.45 ± 2.51	27.05 ± 3.37	27.32 ± 3.39	26.04 ± 2.80	31.08 ± 2.63	29.56 ± 3.03	29.35 ± 2.99	30.53 ± 2.77
HWBS2	8.67	0.24	3.86%	17.14 ± 1.63	18.27 ± 2.22	18.50 ± 2.24	17.69 ± 1.85	47.10 ± 3.72	44.78 ± 4.33	44.40 ± 4.27	46.10 ± 3.92
BT2D	7.68	0.23	3.76%	40.05 ± 3.81	42.50 ± 5.18	42.74 ± 5.19	40.72 ± 4.25	19.70 ± 1.60	18.74 ± 1.88	18.63 ± 1.86	19.40 ± 1.70
LT03	7.87	0.23	4.40%	27.48 ± 2.69	29.22 ± 3.61	29.50 ± 3.63	28.13 ± 3.00	29.27 ± 2.43	27.85 ± 2.80	27.65 ± 2.77	28.73 ± 2.56
DT01	8.26	0.24	4.52%	16.87 ± 1.65	18.00 ± 2.23	18.22 ± 2.25	17.44 ± 1.87	48.39 ± 3.98	46.01 ± 4.55	45.61 ± 4.49	47.31 ± 4.16
SAT02	8.18	0.24	4.50%	45.49 ± 4.48	48.23 ± 6.00	48.47 ± 6.01	46.11 ± 4.95	16.98 ± 1.47	16.15 ± 1.70	16.06 ± 1.69	16.75 ± 1.56
SAT03	8.18	0.24	3.63%	43.89 ± 4.16	46.54 ± 5.66	46.77 ± 5.66	44.50 ± 4.63	17.65 ± 1.44	16.78 ± 1.70	16.69 ± 1.68	17.40 ± 1.54
GLT1a	8.53	0.24	3.72%	36.18 ± 3.44	38.39 ± 4.67	38.64 ± 4.68	36.77 ± 3.83	21.51 ± 1.75	20.45 ± 2.06	20.33 ± 2.04	21.19 ± 1.86
GLT1b	4.17	0.24	3.94%	45.11 ± 4.33	47.74 ± 5.85	47.96 ± 5.86	45.67 ± 4.80	20.85 ± 1.60	19.99 ± 1.82	19.89 ± 1.80	20.59 ± 1.68
GLT2	8.53	0.24	3.83%	26.61 ± 2.54	28.28 ± 3.44	28.55 ± 3.46	27.21 ± 2.84	29.78 ± 2.40	28.33 ± 2.80	28.13 ± 2.77	29.26 ± 2.54
GLT3	8.48	0.24	3.71%	38.87 ± 3.69	41.23 ± 5.02	41.46 ± 5.03	39.46 ± 4.11	19.95 ± 1.63	18.98 ± 1.92	18.87 ± 1.90	19.67 ± 1.74
GLT4	8.45	0.24	3.81%	33.08 ± 3.15	35.11 ± 4.28	35.38 ± 4.29	33.68 ± 3.52	23.70 ± 1.93	22.54 ± 2.26	22.40 ± 2.23	23.33 ± 2.05
GLT5	8.40	0.24	3.13%	51.64 ± 4.81	54.78 ± 6.59	55.07 ± 6.60	52.34 ± 5.37	14.76 ± 1.19	14.03 ± 1.42	13.96 ± 1.41	14.57 ± 1.28
BF1(1)	8.37	0.24	7.75%	23.59 ± 2.83	25.04 ± 3.66	25.30 ± 3.69	24.18 ± 3.12	33.95 ± 3.67	32.35 ± 4.04	32.11 ± 4.00	33.33 ± 3.79
BF1(2)	8.37	0.24	8.59%	21.85 ± 2.74	23.21 ± 3.50	23.47 ± 3.53	22.45 ± 3.01	36.80 ± 4.21	35.06 ± 4.57	34.79 ± 4.52	36.10 ± 4.32
BF2(1)	8.28	0.24	5.21%	30.86 ± 3.26	32.71 ± 4.40	32.99 ± 4.43	31.46 ± 3.64	25.61 ± 2.34	24.41 ± 2.72	24.25 ± 2.70	25.20 ± 2.48
BF2(2)	8.28	0.24	10.30%	25.71 ± 3.55	27.28 ± 4.40	27.55 ± 4.43	26.31 ± 3.84	31.07 ± 4.03	29.60 ± 4.27	29.39 ± 4.23	30.52 ± 4.10
BF2(3)	8.28	0.24	4.00%	21.99 ± 2.20	23.37 ± 3.04	23.62 ± 3.06	22.59 ± 2.50	36.62 ± 3.04	34.89 ± 3.62	34.62 ± 3.57	35.92 ± 3.24
BF3(1)	8.08	0.24	3.86%	43.00 ± 4.29	45.51 ± 5.93	45.74 ± 5.94	43.60 ± 4.82	18.09 ± 1.55	17.23 ± 1.86	17.13 ± 1.84	17.83 ± 1.67
BF3(2)	8.08	0.24	4.38%	42.97 ± 4.38	45.48 ± 6.00	45.70 ± 6.01	43.57 ± 4.90	18.10 ± 1.60	17.24 ± 1.90	17.15 ± 1.88	17.85 ± 1.71

[a] from exposure age model results

[b] exposure age at $\varepsilon = 0$ mm ka-1; external uncertainty reported

[c] external uncertainty reported

Table A3.4 Calculated Exposure Age and Erosion Rates from CRONUS-Earth Online Calculator (v2.0) - Regolith and Alluvium

Sample ID	Production Rate (atoms g^{-1} a^{-1})		Internal Uncertainty (%)	Exposure Age (ka)[b]				Erosion Rate (mm ka^{-1})[c]			
	Spallation[a]	Muonic		Stone (2000)	Desilets *et al.* (2003; 2006)	Dunai (2001)	Lifton *et al.* (2005)	Stone (2000)	Desilets *et al.* (2003; 2006)	Dunai (2001)	Lifton *et al.* (2005)
R1	8.84	0.24	4.94%	17.25 ± 1.73	18.40 ± 2.31	18.62 ± 2.33	17.81 ± 1.94	46.56 ± 3.97	44.26 ± 4.52	43.88 ± 4.46	45.57 ± 4.15
R2	8.89	0.24	5.47%	14.33 ± 1.47	15.31 ± 1.95	15.52 ± 1.97	14.87 ± 1.65	56.42 ± 4.97	53.61 ± 5.58	53.11 ± 5.50	55.12 ± 5.15
R3	8.92	0.25	5.81%	12.39 ± 1.30	13.25 ± 1.71	13.44 ± 1.73	12.89 ± 1.45	65.59 ± 5.90	62.30 ± 6.56	61.68 ± 6.47	63.99 ± 6.09
HWPIT2	8.84	0.24	5.54%	13.96 ± 1.44	14.92 ± 1.91	15.12 ± 1.93	14.49 ± 1.62	58.04 ± 5.14	55.14 ± 5.75	54.62 ± 5.67	56.68 ± 5.32
HWPIT3	8.84	0.24	4.88%	13.00 ± 1.30	13.91 ± 1.74	14.10 ± 1.76	13.52 ± 1.47	62.49 ± 5.25	59.36 ± 5.96	58.78 ± 5.88	60.98 ± 5.46
HWPIT4	8.84	0.24	3.84%	19.79 ± 1.88	21.07 ± 2.56	21.32 ± 2.58	20.37 ± 2.12	40.35 ± 3.21	38.36 ± 3.74	38.06 ± 3.70	39.55 ± 3.39
M0(250)	7.99	0.24	18.42%	19.59 ± 4.03	20.84 ± 4.63	21.08 ± 4.68	20.20 ± 4.26	41.67 ± 8.66	39.69 ± 8.61	39.37 ± 8.53	40.79 ± 8.60
M0(710)	7.99	0.24	6.20%	22.38 ± 2.48	23.78 ± 3.29	24.04 ± 3.32	23.00 ± 2.77	36.23 ± 3.49	34.52 ± 3.95	34.25 ± 3.90	35.51 ± 3.64
ED-01	7.31	0.23	5.18%	25.11 ± 2.64	26.67 ± 3.58	26.95 ± 3.61	25.79 ± 2.98	32.72 ± 2.92	31.20 ± 3.38	30.96 ± 3.34	32.07 ± 3.07
TB-01	7.74	0.23	4.19%	35.52 ± 3.59	37.65 ± 4.94	37.92 ± 4.96	36.19 ± 4.03	22.36 ± 1.92	21.30 ± 2.28	21.17 ± 2.26	21.99 ± 2.05
M5	8.14	0.24	6.10%	15.01 ± 1.65	16.01 ± 2.21	16.22 ± 2.23	15.57 ± 1.86	54.85 ± 5.17	52.21 ± 5.83	51.73 ± 5.75	53.55 ± 5.36
UCB-01	7.41	0.23	4.47%	21.39 ± 2.18	22.73 ± 2.99	23.00 ± 3.02	22.04 ± 2.47	38.66 ± 3.27	36.85 ± 3.82	36.55 ± 3.78	37.84 ± 3.45
WD-01	7.29	0.23	3.79%	28.66 ± 2.84	30.41 ± 3.94	30.70 ± 3.97	29.35 ± 3.22	28.46 ± 2.34	27.14 ± 2.79	26.94 ± 2.76	27.92 ± 2.49
SM-01	7.28	0.23	5.34%	25.73 ± 2.73	27.31 ± 3.69	27.60 ± 3.71	26.41 ± 3.07	31.93 ± 2.89	30.44 ± 3.32	30.21 ± 3.28	31.29 ± 3.03
EO-01	7.37	0.23	4.74%	29.02 ± 3.00	30.77 ± 4.09	31.05 ± 4.11	29.67 ± 3.37	28.02 ± 2.45	26.72 ± 2.86	26.54 ± 2.83	27.52 ± 2.59
WB-01	7.17	0.23	5.83%	37.01 ± 4.03	39.20 ± 5.38	39.48 ± 5.40	37.71 ± 4.47	21.75 ± 2.07	20.74 ± 2.38	20.61 ± 2.35	21.38 ± 2.18
M1	8.01	0.24	6.05%	18.85 ± 2.07	20.06 ± 2.76	20.30 ± 2.79	19.45 ± 2.32	43.36 ± 4.10	41.31 ± 4.64	40.96 ± 4.59	42.43 ± 4.27
M2	8.01	0.24	8.13%	8.48 ± 1.04	9.08 ± 1.34	9.24 ± 1.36	8.83 ± 1.16	99.48 ± 10.71	94.55 ± 11.55	93.47 ± 11.38	96.63 ± 10.87
M3	8.04	0.24	7.00%	11.22 ± 1.29	12.00 ± 1.70	12.18 ± 1.72	11.71 ± 1.46	74.41 ± 7.41	70.78 ± 8.18	70.04 ± 8.07	72.44 ± 7.61

[a] from exposure age model results

[b] exposure age at $\varepsilon = 0$ mm ka-1; external uncertainty reported

[c] external uncertainty reported